

SIMULATION OF DRIVE TRAINS WITH
MULTIPLE CLEARANCES

By

THOMAS A. COOK

Bachelor of Science
Massachusetts Institute of Technology
Cambridge, Massachusetts
1959

Master of Science
University of Arkansas
Fayetteville, Arkansas
1981

Submitted to the Faculty of the Graduate College
of the Oklahoma State University
in partial fulfillment of the requirements
for the Degree of
DOCTOR OF PHILOSOPHY
July, 1989

Thesis
1989 D
07715
cop. 2

SIMULATION OF DRIVE TRAINS WITH
MULTIPLE CLEARANCES

Thesis Approved:

R. L. Lowrey

Thesis Advisor

J. F. Lord

Ray E. Young

J. J. Whitlock

A. Kelly

Norman N. Durham

Dean of the Graduate College

PREFACE

This work was undertaken to provide a tool for the analysis and design of solar tracking drive trains. It is specifically designed to allow the study of impact loads within drive trains due to intermittent input motion and loading torque.

A FORTRAN program (TRAIN) was developed which takes as input a block diagram-like description of a drive train and, after specification of loading and initial conditions, uses a fourth-order Runge-Kutta numerical integration technique to solve the nonlinear state equations.

Aside from the coding of the simulation shell, the bulk of the work consisted in developing realistic, nonlinear models of system elements. The two elements receiving the most attention were the spur/helical gear pair and the keyed joint.

Various models have been used to validate the code. These show good agreement with theory and, to some extent, with experimental results. Use of TRAIN has shown it to be flexible and that it does offer a simple, expeditious means to analyze mechanical systems such as those found in solar trackers.

I wish to express my sincere gratitude to all the people who assisted me in this work and during my stay at Oklahoma State University. In particular, I am especially indebted to my major advisor, Dr. Richard L. Lowery, for his willingness to take me as his advisee and for agreeing to this project.

I am also thankful to the other committee members, Dr. James K.

Good, Dr. Lawrence L. Hoberock, Dr. Allen E. Kelly, and Dr. Gary Young, for their advisement in the course of this work.

The financial support of Sandia National Laboratories (Contract 95-4188) is acknowledged. Special thanks are due to Mr. Alexander Maish of Sandia for his encouragement and support of the project.

Finally, my deepest appreciation to my wife, Ruth, without whose support and encouragement I could not have completed this work.

TABLE OF CONTENTS

Chapter	Page
I. INTRODUCTION.	1
II. SUMMARY OF PAST AND PRESENT WORK.	3
2.1. Systems Studies.	3
2.2. Element Studies.	5
2.3. Impact	7
2.4. Compliance in Elements	11
2.5. Damping and Friction	12
III. SPUR GEAR MODEL	13
3.1. Physical System.	13
3.1.1. Model Description	13
3.1.2. Meshing Action.	13
3.1.3. Tooth Stiffness	18
3.1.4. Damping	22
3.2. Analytic Approaches.	26
3.2.1. Mathematical Model.	26
3.2.2. Elastic Contact Force	28
3.2.3. Damping Contact Force	28
3.2.4. Perturbation Solution	31
3.3. Simulation	33
IV. KEYED JOINT MODEL	47
4.1. Physical System.	47
4.1.1. Conventional Model.	47
4.1.2. Rigid Body Model With Clearances.	49
4.2. Stiffness Models	56
4.2.1. Analytic Model.	56
4.2.2. Finite Element Model.	64
4.2.3. Dynamic Model	102
V. SYSTEM MODEL.	108
5.1. Digital Simulation Program	108
5.1.1. Preprocessor.	109
5.1.2. Solution Processor.	112
5.1.3. Postprocessor	113
5.2. Verification Models.	113
5.2.1. Integration	114
5.2.2. Ideal Gear Pair	114

Chapter	Page
5.2.3. Spur Gear Pair With Backlash.	114
5.2.4. Keyed Joint	115
5.2.5. Comparison With Experiment.	115
VI. OTHER ELEMENT MODELS.	132
6.1. Shaft Model.	132
6.2. Helical Gear Model	132
VII. SIMULATION OF A MULTI-CLEARANCE TRAIN	135
7.1. Description of System.	135
7.2. Simulation Conditions.	138
7.3. Simulation Results	139
VIII. SUMMARY, CONCLUSIONS, AND RECOMMENDATIONS	144
8.1. Summary.	144
8.2. Conclusions.	145
8.3. Recommendations.	145
BIBLIOGRAPHY	147
APPENDICES	152
APPENDIX A - TOOTH MESH CONTACT ZONES	152
APPENDIX B - GEAR TOOTH DEFLECTION.	155
APPENDIX C - PERTURBATION SOLUTION.	158
APPENDIX D - DELTA SOLUTION	165
APPENDIX E - GEAR DIMENSION	168
APPENDIX F - PROGRAM DESCRIPTION FOR NUMERICAL SOLUTION TO SPUR GEAR MODEL.	171
APPENDIX G - NODE LIBRARY	178
APPENDIX H - ELEMENT LIBRARY.	181
APPENDIX I - ADDING AN ELEMENT OR NODE.	189

LIST OF TABLES

Table	Page
3.1. The Number of Teeth in Contact and the Tooth Face Given by Coefficient C.	30
4.1. Contact Stiffness as a Function of Applied Load	62
4.2. AGMA 9002-A86 (1986) Shaft/Hub Fits	68
4.3. Clearance/Interference for Keyed Joint Analysis	69
4.4. Position Data for 1.000 Inch Diameter, Tight Fit Run Used to Calculate Rotation of Hub.	72
4.5. Calculated Hub Rotation Angles 1.000 Inch Diameter, Tight Fit Load Steps 1 and 8.	72
5.1. Input for Verification of Integration Method.	117
5.2. Input for Verification of Ideal Gear Pair	119
5.3.. Input for Verification of Spur Gear Pair with Backlash.	121
5.4. Input for Verification of Keyed Joint	123
5.5. Input for Verification of Gregory, Harris and Munro Test.	126
7.1. Input for Multi-Clearance Simulation.	136

LIST OF FIGURES

Figure	Page
2.1. Impact-Pair	5
2.2. Gear Impact-Pair Force-Approach Curve	10
3.1. Physical System	14
3.2. Contact Angles.	15
3.3. Number of Teeth in Contact.	17
3.4. Equivalent Tooth Model.	21
3.5. Friction Forces During Single Pair Contact.	24
3.6. Friction Forces During Two Pair Contact	25
3.7. Normalized Friction Torque.	26
3.8. Individual and Single Pair Tooth Stiffness.	29
3.9. Tooth Stiffness for One and Two Pair Contact.	29
3.10. Coefficient of Restitution.	31
3.11. Solutions to Gear Tooth Impact Equation	34
3.12. Relative Displacement vs Time (Case I).	36
3.13. Relative Velocity vs Time (Case I).	37
3.14. Phase Plane (Case I).	38
3.15. Contact Force vs Time (Case I).	39
3.16. Relative Displacement vs Time (Case II)	41
3.17. Phase Plane (Case II)	42
3.18. Relative Displacement vs Time (Case II)	43
3.19. Relative Velocity vs Time (Case III).	44
3.20. Phase Plane (Case III).	45

Figure	Page
3.21. Contact Force vs Time (Case III).	46
4.1. Simplified Model for Key Stress	47
4.2. Cantilever Beam Model for Key Stiffness	48
4.3. Layout of Shaft, Key and Hub.	50
4.4. Geometry for Contact Point A.	52
4.5. Key/Shaft Geometry.	54
4.6. Relative Shaft/Hub Reaction Position.	55
4.7. Relative Shaft/Hub Reaction Magnitude	57
4.8. Generalized Loading on Keyed Joint.	58
4.9. Key Loading in Shear.	59
4.10. Shaft Support for Key	63
4.11. Finite Element Mesh	65
4.12. Tight Fit Mesh.	66
4.13. Loose Fit Mesh.	66
4.14. Location of Nodes Used for Hub Rotation Calculation	70
4.15. Stiffness vs Deflection, Tight Fits	73
4.16. Stiffness vs Deflection, Loose Fits	74
4.17. Stiffness vs Deflection, 1.000 Inch Diameter.	75
4.18. Key and Hub Force Distribution, Tight Fit, 150 lb-in.	77
4.19. Key and Hub Force Distribution, Tight Fit, 450 lb-in.	78
4.20. Key and Hub Force Distribution, Tight Fit, 750 lb-in.	79
4.21. Key and Hub Force Distribution, Tight Fit, 1500 lb-in	80
4.22. Key and Hub Force Distribution, Tight Fit, 2250 lb-in	81
4.23. Key and Hub Force Distribution, Tight Fit, 3000 lb-in	82
4.24. Key and Hub Force Distribution, Tight Fit, 4500 lb-in	83
4.25. Key and Hub Force Distribution, Tight Fit, 7500 lb-in	84

Figure	Page
4.26. Key and Hub Force Distribution, Tight Fit, 11250 lb-in. . . .	85
4.27. Key and Hub Force Distribution, Tight Fit, 15000 lb-in. . . .	86
4.28. Key and Hub Force Distribution, Tight Fit, 22500 lb-in. . . .	87
4.29. Key and Hub Force Distribution, Tight Fit, 30000 lb-in. . . .	88
4.30. Key and Hub Force Distribution, Loose Fit, 150 lb-in.	89
4.31. Key and Hub Force Distribution, Loose Fit, 450 lb-in.	90
4.32. Key and Hub Force Distribution, Loose Fit, 750 lb-in.	91
4.33. Key and Hub Force Distribution, Loose Fit, 1500 lb-in	92
4.34. Key and Hub Force Distribution, Loose Fit, 2250 lb-in	93
4.35. Key and Hub Force Distribution, Loose Fit, 3000 lb-in	94
4.36. Key and Hub Force Distribution, Loose Fit, 4500 lb-in	95
4.37. Key and Hub Force Distribution, Loose Fit, 7500 lb-in	96
4.38. Key and Hub Force Distribution, Loose Fit, 11250 lb-in.	97
4.39. Key and Hub Force Distribution, Loose Fit, 15000 lb-in.	98
4.40. Key and Hub Force Distribution, Loose Fit, 22500 lb-in.	99
4.41. Key and Hub Force Distribution, Loose Fit, 30000 lb-in.	100
4.42. Key Stiffness Equations vs FEM Results.	103
4.43. Friction Force on Hub, No Contact at Key.	105
4.44. Key Stiffness vs Deflection	107
5.1. Action Diagram of TRAIN	109
5.2. Action Diagram of the Preprocessor.	110
5.3. Linear Shaft Element Definition	111
5.4. Action Diagram of Processor and Postprocessor	112
5.5. Integration Method Verification Problem	113
5.6. Output of Integration Verification Problem.	118
5.7. Output of Ideal Gear Pair Verification.	120

Figure	Page
5.8. Output of Spur Gear Pair with Backlash Verification	122
5.9. Output of Keyed Joint Verification.	124
5.10. Gregory, Harris and Munro Experiment.	125
5.11. Comparison Between TRAIN Results and Experiment	125
5.12. System Response, 285 Teeth/s.	128
5.13. System Response, 485 Teeth/s.	129
5.14. System Response, 550 Teeth/s.	130
6.1. The Plane of Action	133
7.1. Multi-Clearance System Diagram.	135
7.2. Transmission Error, Nodes 2 & 3, 260 Teeth/Sec.	140
7.3. Transmission Error, Nodes 4 & 5, 260 Teeth/Sec.	140
7.4. Torque on Shaft EL3, 260 Teeth/Sec.	141
7.5. Transmission Error, Nodes 2 & 3, 400 Teeth/Sec.	141
7.6. Peak-To-Peak Transmission Error vs Mesh Frequency	143
7.7. Torque on Shaft EL3 vs Mesh Frequency	143
A.1. Number of Teeth in Contact.	153
D.1. Graphical Interpretation of Equation (D.9).	166
G.1. Passive Inertia	179
G.2. DC Motor.	180
H.1. Shaft Element	181
H.2. Keyed Joint Element	183
H.3. Ideal Gear Pair Element	184
H.4. Spur Gear Pair with Backlash Element.	185

CHAPTER I

INTRODUCTION

When geared systems with clearances are driven continuously they experience a dynamic load that is generated by manufacturing errors in the gear teeth and by the continuous change in number of pairs of teeth in contact. The magnitude of this dynamic load is a function of speed, average load, and amount of backlash. This type of dynamic loading has been studied extensively and is accounted for in gear rating methods. Many, if not most, geared systems are driven continuously and are, therefore, subject to this dynamic loading. However, some geared systems are used to position large inertial loads in systems that are operated in a repeated start-stop mode. In this situation the gears and other components (with clearance) in the drive-train are subjected to repeated impact loading in two directions. The magnitude of the dynamic load in this case is a function of the initial conditions, external load history, the system physical properties, and the amount of backlash. This transient, vibro-impact mode of operation for geared systems has not previously been investigated. As a result, we find unexpected failures in systems that were thought to have been designed with adequate safety margins.

The purpose of this investigation is to develop a method for determining the dynamic loads present in geared systems with multiple clearances that are driven in a repeated start-stop mode.

This investigation is different from other investigations of geared systems with backlash in the following ways:

1. It considers the transient response to arbitrary initial conditions as opposed to the steady-state response of a continuously rotating system.
2. It considers multiple clearances as opposed to a single gear-pair with a single clearance (backlash).
3. It considers the loads in other system elements such as shaft-couplings, and key/keyway interfaces.
4. It considers the effects of external loading.
5. A rotational model is used rather than an equivalent rectilinear model.

CHAPTER II

SUMMARY OF PAST AND PRESENT WORK

2.1. Systems Studies

Geared systems have been the subject of several doctoral dissertations since the late 1950's. All of the early work, such as Richardson's (1958) and Kasuba's (1962), is based on a one-dimensional, rectilinear model that rotates continuously. The interest was in a steady-state solution for the lightly loaded and/or the heavily loaded cases when manufacturing errors and clearances are present. Hahn (1969) was the first to consider the effects of other drive train elements on the tooth engagement phenomenon. He also expanded the model to include more than one dimension. In a more recent study, Azar (1974) investigated the impact phenomenon in geared systems that consisted of a motor, a spur gear pair and an inertial load. He was interested in the lightly loaded, continuously rotating system and its behavior under a variety of parameter changes.

One of the earliest studies of a large, nonlinear mechanical system was done by Kashay, et al. (1972). They studied the dynamic response of a steel rolling mill station both experimentally and through a computer model. Their experimental work, in which backlash was a parameter, showed that transient torque variations of up to 3.5 times the steady-state torque occurred when the station was subjected to sudden load changes. They used a rather simple mathematical model with a fourth

order Runge-Kutta integration method. To avoid instabilities in the solution they combined high natural frequency elements with lower frequency elements.

Wang and Morse (1972) defined a method of decomposing a gear train system into what they called spans and joints. The spans are any continuous member of the system that can be described by a lumped mass system. The joints are the ends of the spans. Transfer matrix techniques were used to solve for the static and dynamic torsional response. They validated their model by comparing it with the results from an experimental set-up. Although the model included nonlinearities due to gear backlash and gear-tooth loading, the experimental work was not specifically set up to measure the effects of backlash, but rather the dependence of tooth compliance on frequency.

Allen (1979) reported on a technique using bond graph multiport models to represent gear power transmissions. Although the bond graph is basically a kinematic tool he has added dissipative, compliance and inertial effects to it to model the dynamic effects of the system. Although nonlinearities are permitted, he does not seem to address the question of clearances in the system. His results focus on steady-state frequency response.

The most recent study to include system dynamics with gear-pair element dynamics was done by Bahgat, et al. (1983). Although they apparently did not consider backlash in the gear mesh and they considered only steady, unidirectional motion, their study is interesting because of the solution method employed. A harmonic series expansion was used as the assumed solution to the (linear) dynamic equations.

2.2. Element Studies

The seminal work in the area of impact models was done by Dubowsky and Freudenstein (1971). Until this time most impact models were based on a coefficient of restitution which was first developed by Newton. But Dubowsky and Freudenstein pointed out that such models omitted dynamic coupling, stresses, and time duration of contact. This, in turn, affects the frequency of oscillations and the nature of the impacts, whether bilateral or unilateral. Their basic model is shown in Figure 2.1(a) and a qualitative model of the contact force is shown in Figure 2.1(b). Although the model was conceived for use in revolute and spherical joints, it can be applied to gear pairs as well. They found that for ball and pin joints the nonlinearity of the Hertzian contact can be replaced with a linear spring rate without significantly

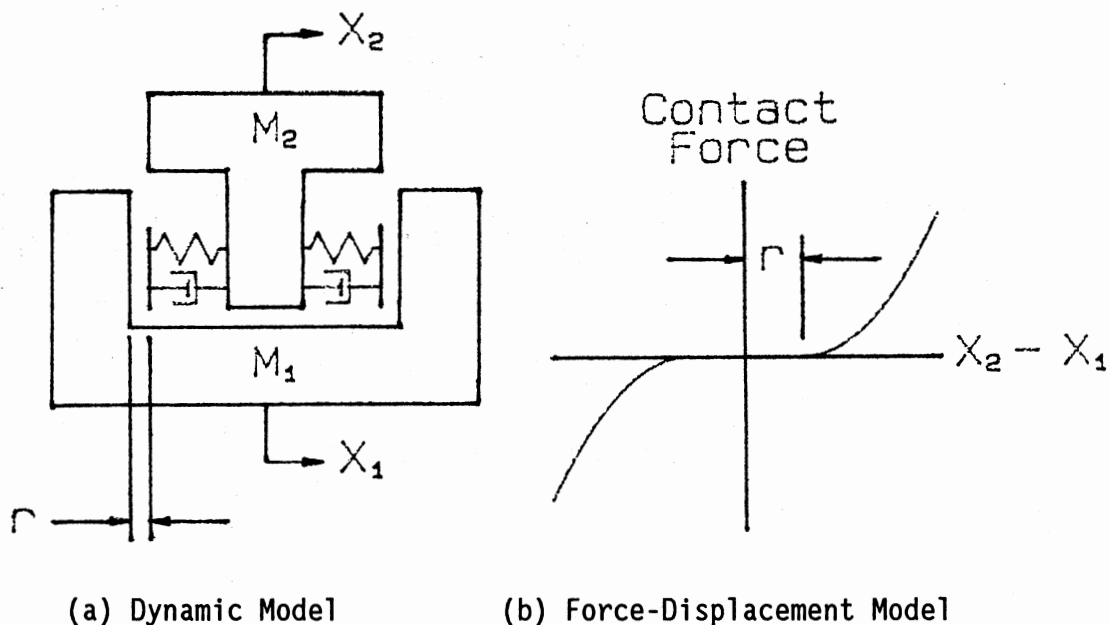


Figure 2.1. Impact-Pair

affecting dynamic response. Dubowsky and Gardner (1975) extended the impact model to an impact beam model for use in studying the interactions of link elasticity and clearance in planar mechanisms. They showed that, while clearances increase the bearing forces, increasingly flexible links can reduce the bearing forces at the expense of increased stress in the links.

Azar and Crossley (1977) extended the impact model to incorporate a gear-pair model that includes the inertia of the gears, loss of contact (backlash), stiffness variation, frictional effects, and profile errors of gear teeth. The dynamic equations were solved using a fourth order Runge-Kutta method and a set of logical functions to determine the various contact regimes which occur in vibroimpact systems. They obtained good correlation between the experimental and simulated results.

Benton and Seireg (1978) did experimental and simulation work on resonances and instability conditions in pinion-gear systems. They used phase-plane methods and digital filtering to predict amplitude ratio vs. frequency. Unfortunately, they only worked with steady loads and did not simulate conditions where loss of contact between the teeth occurs.

Yang and Sun (1985) combined and extended the work of Dubowsky and Freudenstein (1971) and of Azar and Crossley (1977) by devising an impact model for gearing that was based on a rotary, rather than rectilinear, model. The model includes backlash, material compliance, and energy dissipation. They demonstrated the behavior of the model by giving the results of a digital simulation of a gear pair. This model forms the basis of the spur gear pair element used in this study and is further described in Chapter 3. Later, Yang and Lin (1986) added tooth

friction and bending elasticity to the model.

Models of other system elements are not as numerous in the literature. Orthwein (1979) reviews the literature concerning stresses in shafts with keyways and analyzes some existing data along with some new data that he has generated. He is able to predict where the points of greatest stress are in the shaft and gives design guides for reducing the stress. The stiffness of keyed joints is mentioned briefly by Mancuso (1986) and by Wang and Morse (1972). In both cases the treatment is superficial.

2.3. Impact

Impact occurs in drive trains, when clearances are present, under a variety of circumstances. For lightly loaded systems, impact can occur whenever there are sudden disturbances in the input or load. For heavily loaded systems impact is less likely to occur, even with sudden changes in input or load, unless the system is operating near a dynamic resonance point. In this case severe damage can be done to the system elements that absorb the resulting impacts. In this project we are interested in the former class of problems, that is, those in which the loading is either light or non-steady and for which there are sudden changes in input.

Classical impact theory, as developed by Newton, treated the impacting bodies as rigid and developed the relationship between the relative velocities of the approaching and receding bodies. Unfortunately, this method gives us no information about local deformations, stresses, or duration of contact. Hertz and others have attempted to develop a theory that does account for these other factors

that are so important from the machine design standpoint. There has been a substantial amount of work done in the last 15 years to develop useful models of impact in machine elements.

Dubowsky and Freudenstein (1971), who first proposed the impact model now widely used in mechanism simulation, found that clearances in the model did not affect the amplitudes of free vibrations of the model. However, under forced vibration significant stress amplification due to clearance was found. Their analysis assumed that the frequency of the elastic waves in the bodies are much higher than the free or forced vibration frequencies. One result of clearance coupling in a system is that it will not have a single characteristic or natural frequency, but a continuum of oscillating frequencies, which depend on time and initial conditions. Under constant load operation they found that not only did bilateral impact occur, but also multiple impacts on one side of the clearance. The results of the constant load operation can be divided into three forms. The first mode has successive impacts on alternate sides of the clearance and looks much like the free vibration motion. This will decay into the second mode where the pair exhibits impacts on only one side of the clearance. In the lowest-energy mode the relative velocity of the elements is not sufficient to cause separation and there is continuous, oscillating contact on one side of the clearance similar to a linear system. This type of multiple-mode behavior is what lightly loaded systems will exhibit on startup or on sudden change of load.

Azar and Crossley (1975) performed an experimental study of impact phenomenon in lightly loaded and heavily loaded spur gear systems. They found that the magnitude of backlash is significant in lightly loaded systems but, as the load is increased, the effect of backlash becomes

less significant. One important finding was that there is significant amplification at the tooth mesh frequency and that, even for heavily loaded systems, if this frequency approaches as much as half the system's lowest resonant frequency, oscillations could occur that would be of the same magnitude as those that would occur at resonance.

Seireg, et al. (1975) also investigated impacts in lightly loaded gear systems. They tested a pair of lightly loaded gears by driving the pinion with a shaker while coupling the gear to ground with a soft spring. They found that maximum gear shaft torque increased linearly with shaker amplitude until tooth separation occurred, after which it increased linearly at a much higher rate until impact occurred on the back side of the tooth at which point the rate dropped off nonlinearly. This experimental work proved that the presence of backlash caused stress amplification in system elements and that the magnitude of the amplification depended on the amount of backlash, although no qualitative information was given relating the amplification to the backlash.

A force approach law was used by Azar and Crossley (1977) for use with the impact model of Dubowsky and Freudentein. In previous experimental work they found that surface compliance and damping were highly nonlinear. The Hertzian "spring constant" is represented by a $1/2$ -power function of penetration but, only by including a viscous damping coefficient which included a $3/2$ -power of the penetration was it possible to corroborate the one-sided multiple impacts obtained experimentally. A qualitative plot of the impact pair force-approach law is shown in Figure 2.2.

In a study of impact forces in elastic, mechanical systems Dubowsky

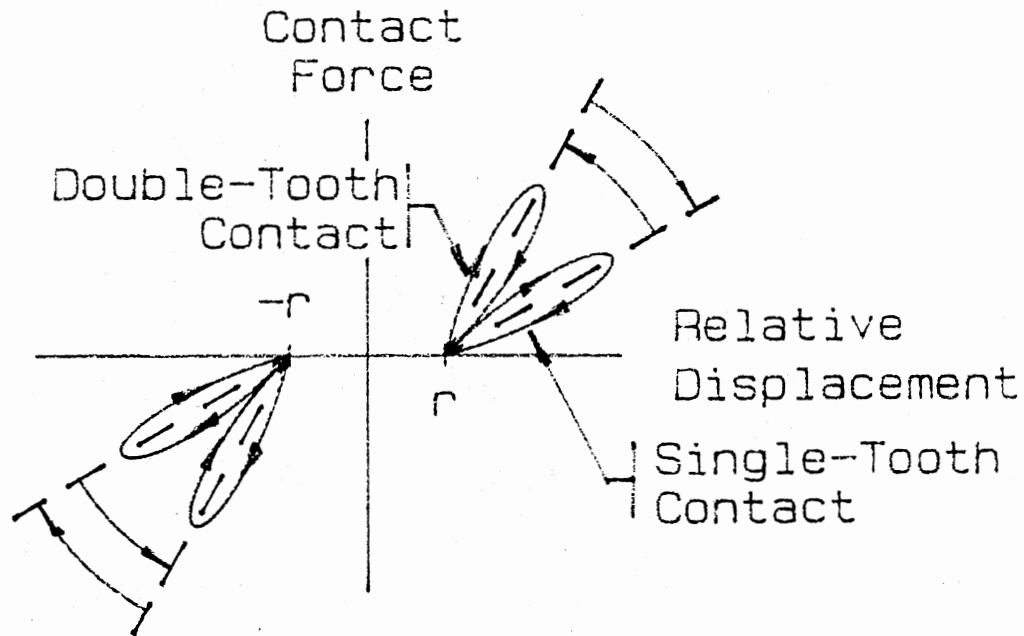


Figure 2.2 Gear Impact-Pair Force-Approach Curve

and Moening (1978) found that, for the scotch-yoke analyzed and tested, flexibility in the linkage (as opposed to a rigid link) reduced the maximum impact force by as much as a factor of two. This is only significant in a geared system to the extent that the designer has the ability to reduce the stiffness of the connecting elements in the train.

Despite the work that had been done up to this point using Hertzian contact models, C.C. Wang (1981) did an extensive experimental and analytical investigation of rotational vibration with backlash (of lightly loaded gears running at high speed) using a Newtonian impact model with an assumed coefficient of restitution of 0.5. He considered a two- and a three-mass model in which the inertia of the driving gear was very much larger than that of the driven gear. One result of the

comparison of the simulation results with the experimental results was the realization by the author that the zero-time-of-impact assumption (a result of using Newton's approach) was not realistic. In any event, his experimental work showed clearly the nature of the motion of the impact driven gear.

Haines (1980), in a critical survey of the literature on 2-dimensional motion and impact in revolute joints, says that the most consistent finding (relative to impact and the motion across the clearance) is that the level of impact, by a variety of measures, increases at an increasing rate with the magnitude of the clearance.

2.4. Compliance in Elements

Early work by Dubowsky and Freudenstein (1971) in modeling pin and ball joints showed that linearizing the force-deflection relationship over the elastic range of deflection was satisfactory. They concluded that Hertzian-type contact could be linearized so that the error in the transient deflection amplitude is less than two percent.

Wang and Morse (1972) found that an exact mathematical model of key deflection was not available, but they have supplied an approximation. Using two-dimensional elasticity theory, they also give the compliance of a constant thickness gear web. The authors summarize the work of Weber (1949) in defining a gear-tooth compliance that includes local, Hertzian deflection, tooth beam-like deflection, and the number of teeth in contact. The final result is piece-wise linear over the range of each constant number of teeth in contact.

Cornell (1981) has done an extensive evaluation of spur gear tooth-pair compliance. He compared four different methods of characterizing

the local contact compliance and concluded that the closed-form expression of Weber was the most accurate. He then combined this compliance with detailed predictions of beam and foundation bending to come up with over-all tooth-pair compliance for several tooth forms.

Working at the same time as Cornell, Kasuba and Evans (1981) also report on gear tooth compliance models and the numerical techniques that they used to evaluate them for given gear geometry and materials.

2.5. Damping and Friction

Some viscous damping can be expected to be present in the class of drive-trains under investigation. However, the amount will be small and will be associated largely with structural losses. It can also be expected that friction is present, particularly near the load end of the train. Predicting values of damping coefficients and friction coefficients will be difficult. However, sensitivity studies can be undertaken to determine the degree to which the certain knowledge of the values is necessary.

Dubowsky and Freudenstein (1971) used a value for damping ratio in their impact-pair of less than ten percent. They state that values of between one and five percent can be expected. Azar and Crossley (1977) found from experiment that the damping ratio in the gear-pair that they were testing was about 1.5 percent which is consistent with structural damping rates.

CHAPTER III

SPUR GEAR MODEL

3.1 Physical System

3.1.1. Model Description

The physical system, based on the Yang and Sun (1985) model, is shown in Fig. 3.1. It consists of two gears with one or two pairs of teeth in mesh, the number depending on the contact ratio and the position of the gears with respect to an arbitrary datum. In the figure, the clearance is greatly magnified with respect to the dimensions of the gear teeth. Typically, the clearance will vary from about 0.01 times the tooth thickness to almost nothing. The initial position of the system is, as shown in the figure, taken such that the clearance (2b) is equally divided on each side of the driving gear tooth when its centerline is coincident with the line of centers of the gear pair. In this model, clearance (backlash) is measured along the line of action rather than along the pitch circle, as is more commonly done.

3.1.2. Meshing Action

Fig. 3.2 shows a pair of gears in mesh, with the upper gear (the driver) turning counter-clockwise. The left tooth on the driver has just made contact with a tooth on the driven gear at point "A". It will remain in contact with that tooth until the point "B" is reached. The

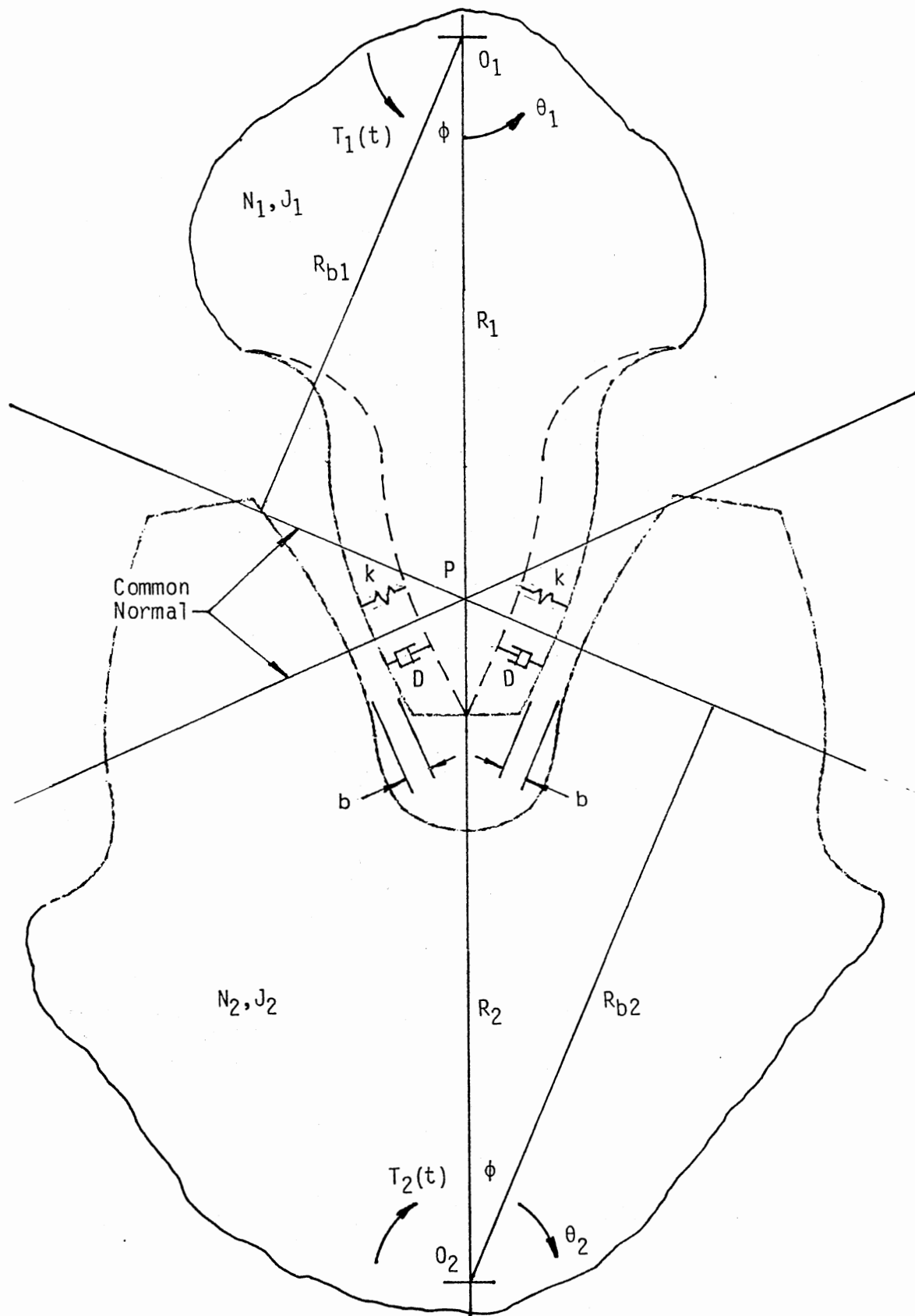


Fig. 3.1. Physical System (from Yang and Sun, 1985)

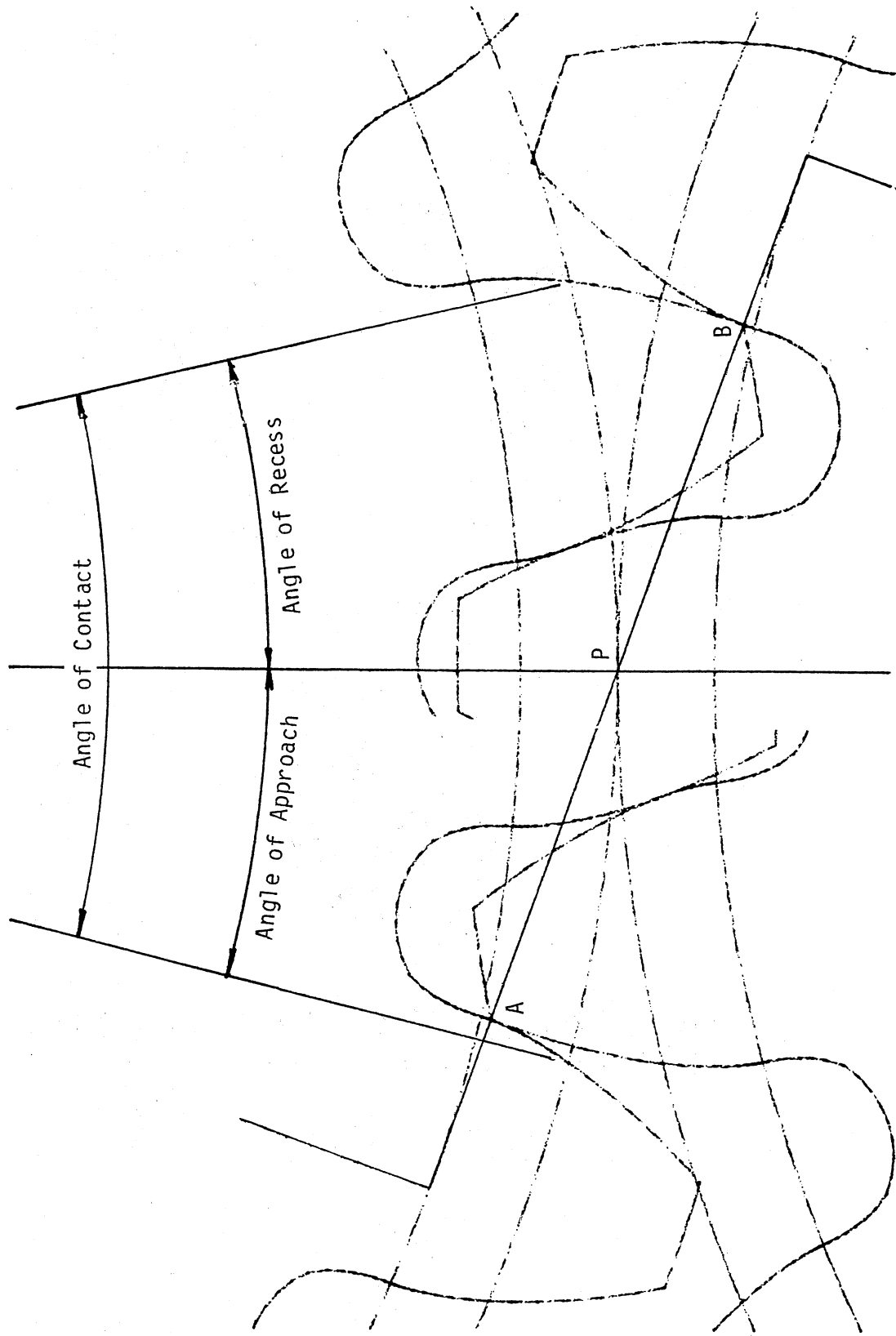


Fig. 3.2. Contact Angles

angle through which the driver travels during this contact is defined as the angle of contact. To measure the contact angle a polar coordinate system is established with center coincident with the center of the driving gear and with the zero angle reference line from that center through the pitch point of the gear tooth as it just makes contact at point "A". If we imagine a line on the gear through its center and pitch point, we can determine the rotation of the gear by measuring the angle between this line and the zero reference line. The angle of contact is the sum of two angles, the angle of approach and the angle of recess. The angle of approach is the angle made by the tooth as it moves from the initial point of contact to contact at the line of centers of the meshing pair. The contact angle is given by the ratio of the length AB to the base circle radius of the gear. Similarly, the angle of approach is given by the ratio of AP to the base circle radius. These angles are used in determining the transition from two-to-one pair contact and the transition from one-to-two pair contact.

For gear pairs with a contact ratio of less than two (which covers most cases), at any given instant there will be either two pair of teeth in contact or one pair. Fig. 3.3 shows a schematic representation of the number of teeth in contact vs. the rotation angle of one of the two gears in mesh. The arbitrary reference condition for this figure is taken when the centerline of a tooth on the driver is coincident with the line of centers. As we saw from the discussion of contact angle, this differs from the reference line for the contact angle which is a line through the pitch point of the tooth. The difference between these two reference lines is one half the tooth thickness which is (nominally) $\pi/2N$. The relationships shown in the figure are referred also to the

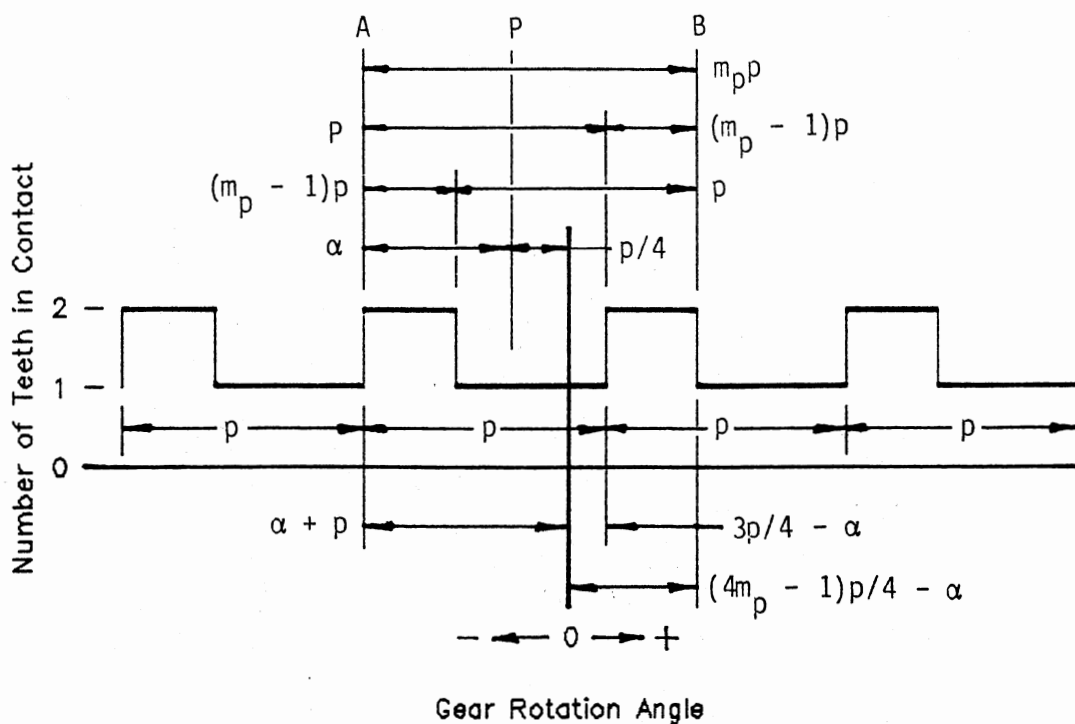


Fig. 3.3. Number of Teeth in Contact

point where a tooth on the driver has just come into contact with the driven gear. At this instant two pair of teeth are in contact. As the driving gear continues its motion the tooth ahead of the reference tooth comes out of contact, reducing the number of pairs in contact to one. This condition continues until the tooth just behind the reference tooth comes into contact, thereby increasing the number of teeth in contact to two again. The angles of two-tooth and single-tooth contact are shown in the figure as functions of the contact ratio m_p and the number of teeth N . The approach angle, alpha, is also shown in the figure such that if the gear-pair were in the initial position used in the model, the number of teeth in contact would be one pair. This is arbitrary. Whether or not one or two pair would be in contact at the initial

position depends on the attributes of the particular gears being modeled. The zones of one-pair and two-pair contact are derived in Appendix A.

3.1.3. Tooth Stiffness

Dudley (1984) reports that "the stiffness constants for mesh deflection of teeth have never been known with certainty." However, he, and others, take the force-deflection relationship to be constant over the range of tooth contact. The accepted value of elastic stiffness for steel gears is $2.9E06$ lb/in per inch of face width. Various attempts have been made to predict tooth pair stiffness, some for contact at a single point along the path of contact while others have developed equations covering the entire range of contact.

Yang and Sun (1985), in their paper describing the basic impact model for spur gears, have developed a model of the contact deflection which does not include bending or shear. Starting with the Hertzian formulation of two cylindrical bodies in contact, they develop the following close approximation to the deflection due to a normal contact force, W

$$\delta_c = \frac{4(1-\mu^2)W}{\pi EF} \quad (3.1)$$

where μ , E and F are Poisson's ratio, Young's modulus, and the face width of the two gears, respectively. The total deflection of a pair of gear teeth in contact will include bending and shear components as well. Kozesnick (as given by Shigley and Mitchell, 1983) has developed equations for these two components. They are, for bending

$$\delta_b = \frac{W_t b^3}{3EI} \quad (3.2)$$

and for shear

$$\delta_s = \frac{W_t b}{0.833GA} \quad (3.3)$$

where

$$I = Ft^3/12$$

$$A = Ft$$

and W_t , b , t , and G are the tangential component of the load on the tooth, dedendum, tooth thickness at the pitch circle, and modulus of rigidity, respectively. Adding these two components and substituting for I and A gives

$$\delta_{bs} = \frac{W_t b}{Ft} \left[\frac{4b^2}{Et^2} + \frac{1.2}{G} \right] \quad (3.4)$$

To get an estimate of the total deflection we need to add equations (3.1) and (3.4). But before this can be done we must convert the tangential force, W_t , to an equivalent normal force, W . The relationship is

$$W_t = W \cos \phi \quad (3.5)$$

where ϕ is the gear pressure angle. Substituting equation (3.5) into (3.4) and adding the result to (3.1) gives

$$\delta = \frac{4(1-\nu^2)W}{\pi EF} + \frac{4b^3 W \cos \phi}{EFt^3} + \frac{1.2bW \cos \phi}{Gft} \quad (3.6)$$

if $G = E/[2(1+\mu)]$ is substituted into equation (3.6) the result is

$$\delta = \frac{4W}{EF} \left[\frac{1-\nu^2}{\pi} + \frac{b^3 \cos \phi}{t^3} + \frac{0.6b(1+\mu) \cos \phi}{t} \right] \quad (3.7)$$

The first term in the brackets in this equation is independent of tooth

size while the remaining two are apparently not. However, for standard tooth dimensions, we can take $b = 1.25/P$ and $t = \pi/2P$, where P is the diametral pitch, so that $b/t = 2.5/\pi$. Making this substitution, equation (3.7) can be rewritten as

$$\delta = \frac{4W}{EF} \left[\frac{1-\nu^2}{\pi} + \left(\frac{2.5}{\pi} \right)^3 \cos \phi + 0.477(1+\nu) \cos \phi \right] \quad (3.8)$$

For steel gears this reduces to

$$\delta = W(0.39 + 1.49 \cos \phi) (10)^{-7} / F \quad (3.9)$$

If the pressure angle is 20° (a common value) this becomes

$$\delta = 1.78W(10)^{-7} / F$$

or

$$K = \frac{W}{\delta F} = 5.60(10)^6 \frac{lb}{in^2}$$

which is about twice the value given above by Dudley.

An experimental evaluation of tooth deflection was done by Furrow and Mabie (1970). Using an acrylic plastic material cut into the shape of 20° , full-depth involute teeth, they were able to carefully measure the deflection of a single tooth at points along the path of action for various combinations of numbers of pinion and gear teeth. They found that the data fit the Timoshenko and Baud (1926) deflection equation well, provided certain terms in the equation were interpreted in a way that they defined. Referring to figure 3.4 for a definition of the geometric terms, the Timoshenko and Baud equation for the bending and shear deflection of a single tooth is

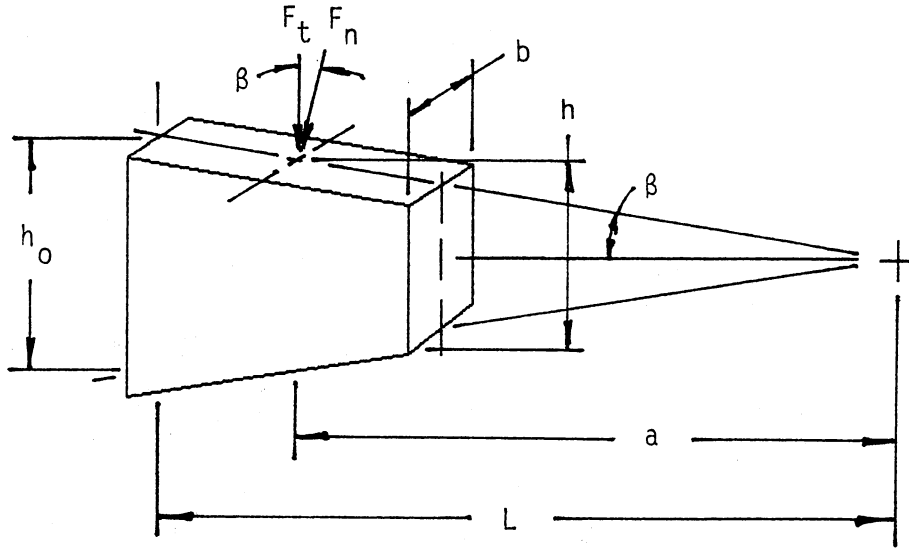


Fig. 3.4. Equivalent Tooth Model

$$\delta_{bs} = \frac{4W \cos \beta}{EF} \left\{ 3 \left[\frac{L}{h_0} \right]^3 \left[\frac{\left(3 - \frac{a}{L} \right) \left(\frac{a}{L} - 1 \right)}{2} + \ln \left(\frac{L}{a} \right) \right] + \frac{(1+\nu)(L-a)}{h_0(1+a/L)} \right\} \quad (3.10)$$

where the independent variable, a , is determined by the position of the normal load, W , along the tooth profile. In addition to the bending and shear deflection, they also added a contact deflection which they cite as having come from Timoshenko and Baud as modified by Caldwell. It is

$$\delta_c = \frac{2(1-\nu^2)W}{\pi E b} \left[\frac{2}{3} + \ln \left[\frac{1.731 E b C \sin \phi}{W} \right] \right] \quad (3.11)$$

where C is the center distance between the gears and the other terms are as defined above. The total deflection of a pair of gears in mesh would be the sum of the deflections found by applying equation (3.10) to each tooth of the mesh and by adding the result to the contact deflection found from equation (3.11). The exact method for doing this is given in

Appendix B.

3.1.4. Damping

An interesting damping model for impacting gear teeth has been developed by Yang and Sun (1985) based on earlier work by Lee and Wang (1982). Starting with the hypothesis that the damping force is proportional to the product of the penetration and the penetration velocity (where penetration is the amount by which remote points on each of the gears approach each other during contact), they develop the requirements for the constant of proportionality, D . They give this as

$$D = \frac{6(1-e)K}{[(2e-1)^2 + 3]V_i} \quad (3.12)$$

where e , K , and V_i are the coefficient of restitution, tooth pair stiffness, and relative approach velocity, respectively. For the coefficient of restitution Yang and Sun used a curve fit to Goldsmith's (1960) data which gives values that range from about 0.9 to 0.99 for steel. However, Smith (1984) has reported considerably lower values for the coefficient of restitution, based on experimental evidence. He found that, in fact, the coefficient of restitution for impacting steel gear teeth ranged from about 0.22 to 0.33, depending on velocity at impact. Through a simple model he shows that the limiting value should be $1/3$, provided that the time between impacts is much longer than the time of contact. When this is not the case, values of about 0.9 are more reasonable.

Friction forces that are developed as a result of sliding between gear teeth in contact also contribute to system damping. The magnitude of the friction force depends upon the transmitted normal force and the

coefficient of friction (which usually is quite low) while its sense depends upon the sign of the relative velocity. The sign of the relative velocity changes abruptly as each pair of teeth pass through the pitch point. Figure 3.5 shows the contact and friction forces on a gear tooth during single pair contact, while Figure 3.6 shows the forces on two teeth during two pair contact. Two pair contact will, in general, occur when the contact points are on either side of the pitch point. Single pair contact occurs as the contact point is moving through the pitch point. The friction torque (opposing the rotation) on the gear during single pair contact is

$$T_1 = fWr [\text{sign}(V_s)] \quad (3.13)$$

where f , r , and V_s are the coefficient of friction, radius of curvature, and sliding velocity, respectively. Interestingly, during approach action the friction torque reduces the torque due to the load (WR_b) while during recess action it increases the load torque. The friction torque during two pair contact is constant and is

$$T_2 = \frac{fWp_b}{2} \quad (3.14)$$

where p_b is the base pitch. Figure 3.7 shows the normalized friction torque through the meshing cycle of one pair of teeth. The highest torques occur during single pair contact, but the net energy lost during this period is approximately zero due to the sign change of the sliding velocity. The actual friction model will be developed in section 3.2.3, below.

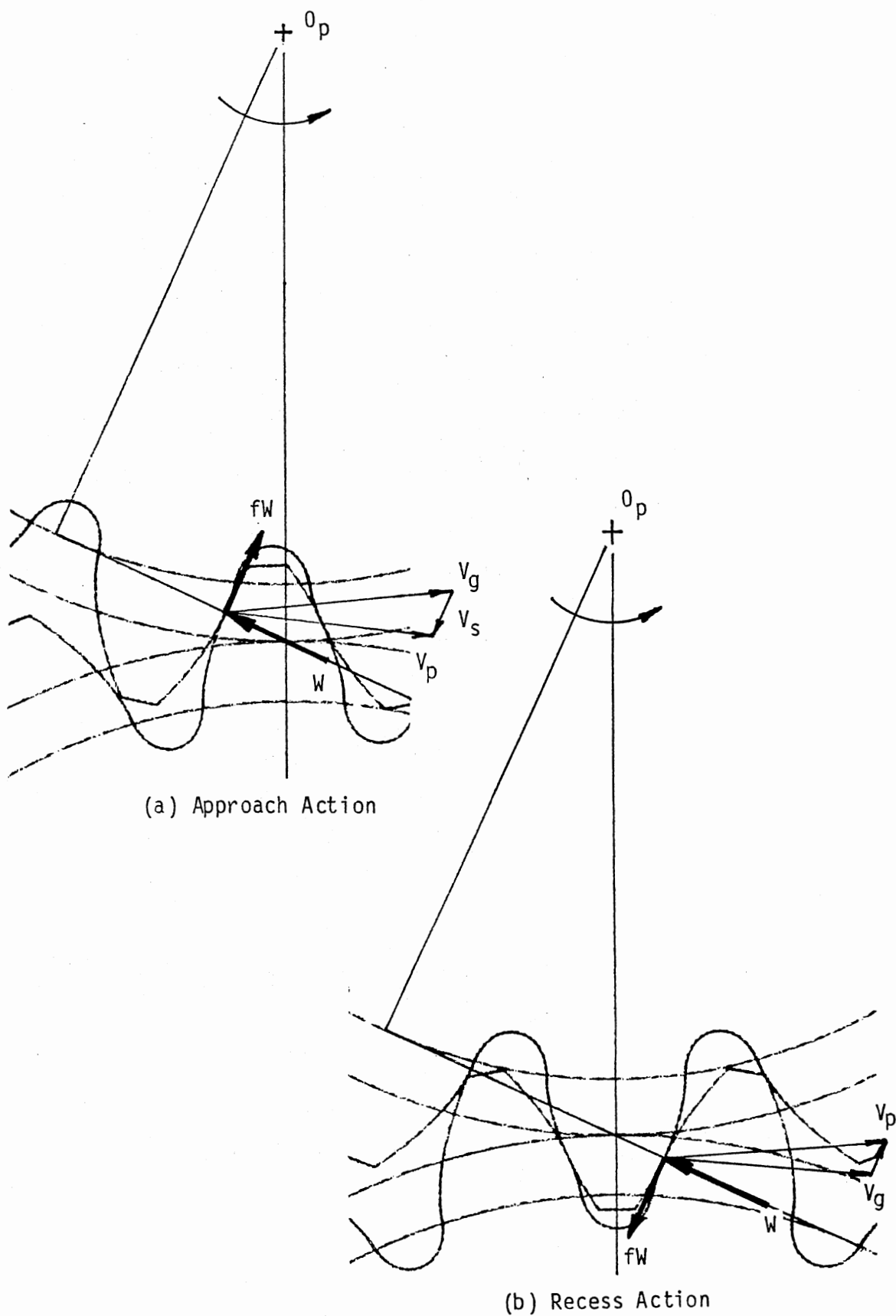


Fig. 3.5. Friction Forces During Single Pair Contact

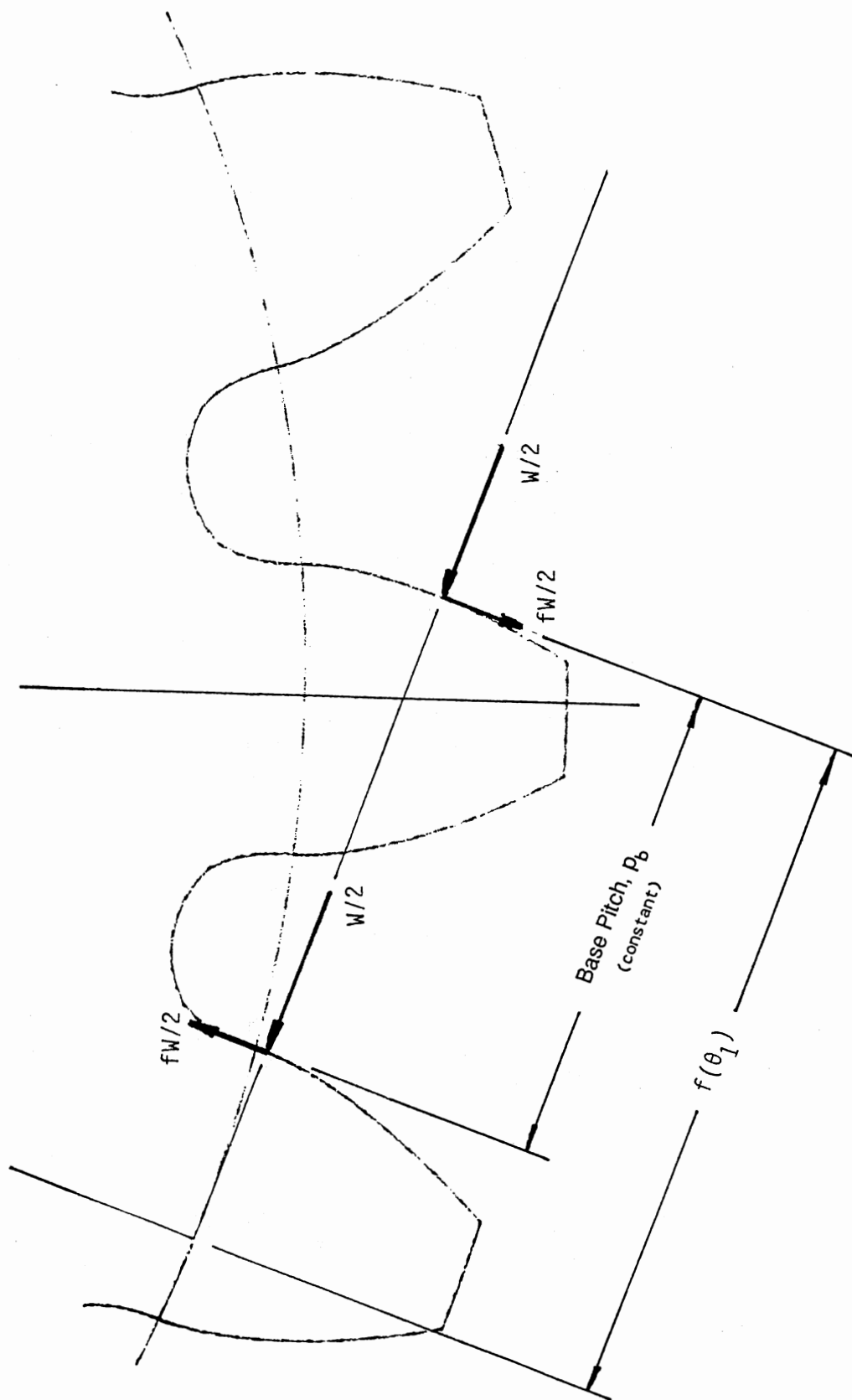


Fig. 3.6. Friction Forces During Two Pair Contact

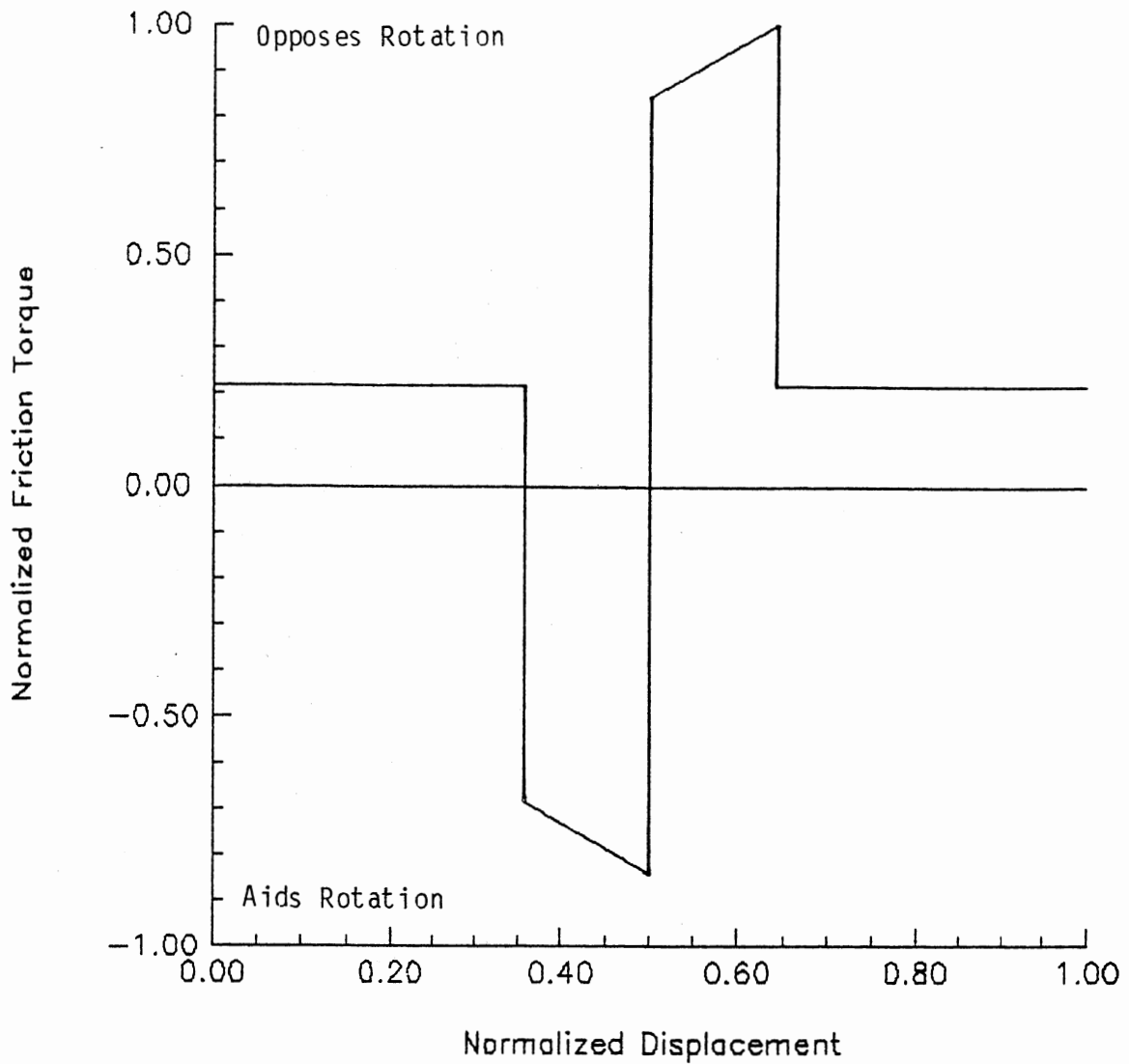


Fig. 3.7. Normalized Friction Torque

3.2 Analytic Approaches

The system will always be in one of three distinct states. They are defined as (i) contact on the front faces of the contacting teeth, (ii) no contact between the gears, and (iii) contact on the rear faces of the contacting teeth. In addition, when the gears are in contact,

there may be either two or one pair of teeth contacting. These conditions are all accounted for in the model.

3.2.1. Mathematical Model

Contact is determined by comparing the relative position of the two gears with the initial clearance. The system equations are given below for each of the three contact states described above:

$$\begin{aligned}
 & \text{(i)} \\
 & R_{b1}\theta_1 - R_{b2}\theta_2 > b, \\
 & J_1\ddot{\theta}_1 = T_1(t) - [F(t) + G(t)]R_{b1} \\
 & J_2\ddot{\theta}_2 = T_2(t) + [F(t) + G(t)]R_{b2} \qquad \qquad \qquad (3.15)
 \end{aligned}$$

$$\begin{aligned}
 & \text{(ii)} \\
 & |R_{b1}\theta_1 - R_{b2}\theta_2| < b, \\
 & J_1\ddot{\theta}_1 = T_1(t) \\
 & J_2\ddot{\theta}_2 = T_2(t) \qquad \qquad \qquad (3.16)
 \end{aligned}$$

$$\begin{aligned}
 & \text{(iii)} \\
 & R_{b1}\theta_1 - R_{b2}\theta_2 \geq b, \\
 & J_1\ddot{\theta}_1 = T_1(t) + [F(t) + G(t)]R_{b1} \\
 & J_2\ddot{\theta}_2 = T_2(t) - [F(t) + G(t)]R_{b2} \qquad \qquad \qquad (3.17)
 \end{aligned}$$

where

$T_1(t)$ and $T_2(t)$ are external torques applied to gears 1 and 2, respectively;

$F(t)$ is the elastic component of the contact force; and,

$G(t)$ is the damping component of the contact force.

Note that $F(t)$ is defined in such a way that it is always positive, i.e., it is always compressive. $G(t)$, on the other hand, may be positive or negative, depending on the sign of the relative velocity between the teeth in contact.

3.2.2. Elastic Contact Force

As explained in section 3.1.2, the stiffness of a meshing tooth pair varies along the path of contact. A representative plot of tooth-pair stiffness is shown in Figure 3.8. Notice that the stiffness is a maximum near the pitch point and is lowest at the beginning and end of contact. Figure 3.9 shows the superposition of stiffness profiles for two teeth to give the over all stiffness when two pair of teeth are in contact. Although there is some variation over the length of contact, the stiffness function is modeled quite well by a square wave as shown. Note however, that the magnitude during two pair contact is not twice the single pair stiffness. This is because the two pair contact takes place near the ends of the contact path while single pair contact takes place near the pitch point.

In this model the elastic coefficient is a constant for each pair of teeth in contact but, because the number of tooth pairs in contact varies, the elastic contact force becomes a nonlinear term in the system equations. The elastic contact force equation used is:

$$F(t) = cK(\delta - b) \quad (3.18)$$

where

$$c = 0, \pm 1, \text{ or } \pm 1.8 \text{ as given in table 3.1}$$

and

$$\delta = R_{b1}\theta_1 - R_{b2}\theta_2$$

3.2.3. Damping Contact Force

Following Yang and Sun (1985) a nonlinear damping force is assumed. It is proportional to the relative penetration of the contacting gear teeth times the relative velocity of the gears. The coefficient of the

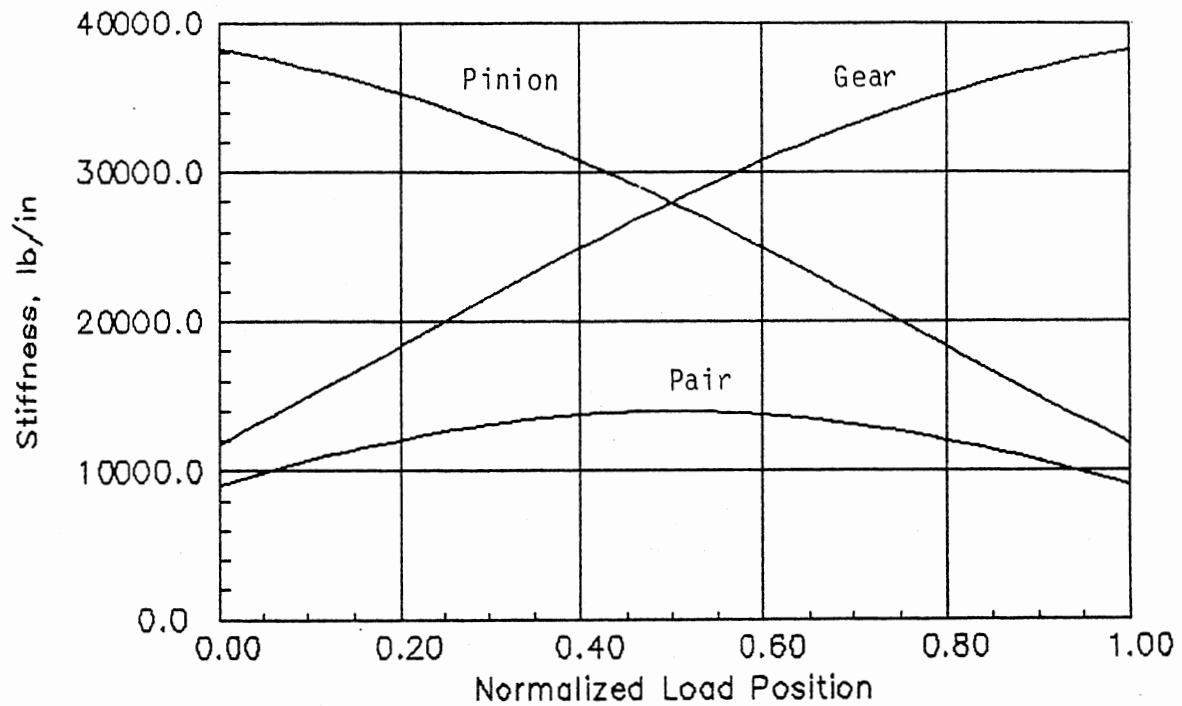


Fig. 3.8. Individual and Single Pair Tooth Stiffness

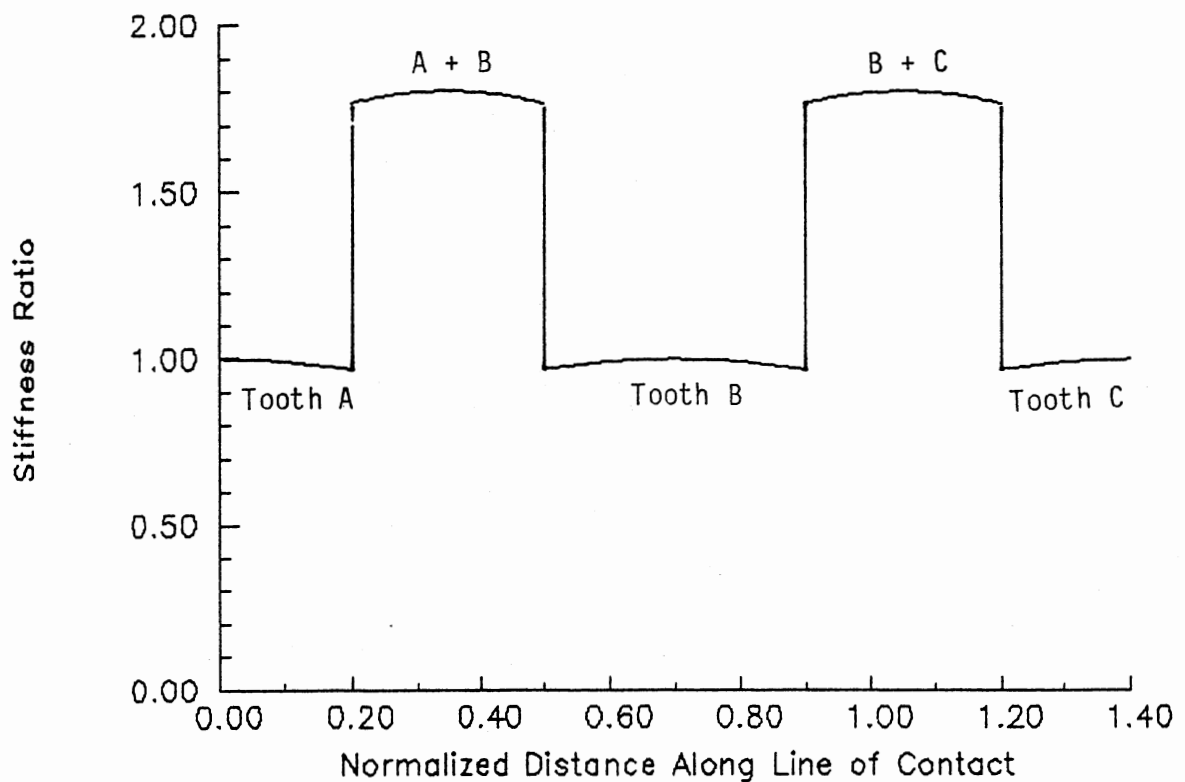


Fig. 3.9. Tooth Stiffness for One and Two Pair Contact

damping term is constant throughout the impact event, but is a function of the impact velocity. The damping contact force equation is:

$$G(t) = cD|\delta - b|\delta \quad (3.19)$$

where c , K and δ are defined as above and D is defined in equation (3.12). Using a curve fit to the data of Smith (1984) the coefficient of restitution, as used in equation (3.12) is (see Figure 3.10)

$$e = \frac{1 - \exp[-0.0263V_1]}{3} \quad (3.20)$$

TABLE 3.1
THE NUMBER OF TEETH IN CONTACT
AND THE TOOTH FACE GIVEN BY
COEFFICIENT C

Condition on θ_1	$\delta \geq b$	$-b < \delta < b$	$\delta \leq -b$
$2\pi(n-2+m_p)/N_1 - \alpha$ $< \theta_1 <$ $2\pi n/N_1 - \alpha$	1	0	-1
Otherwise	1.8	0	-1.8

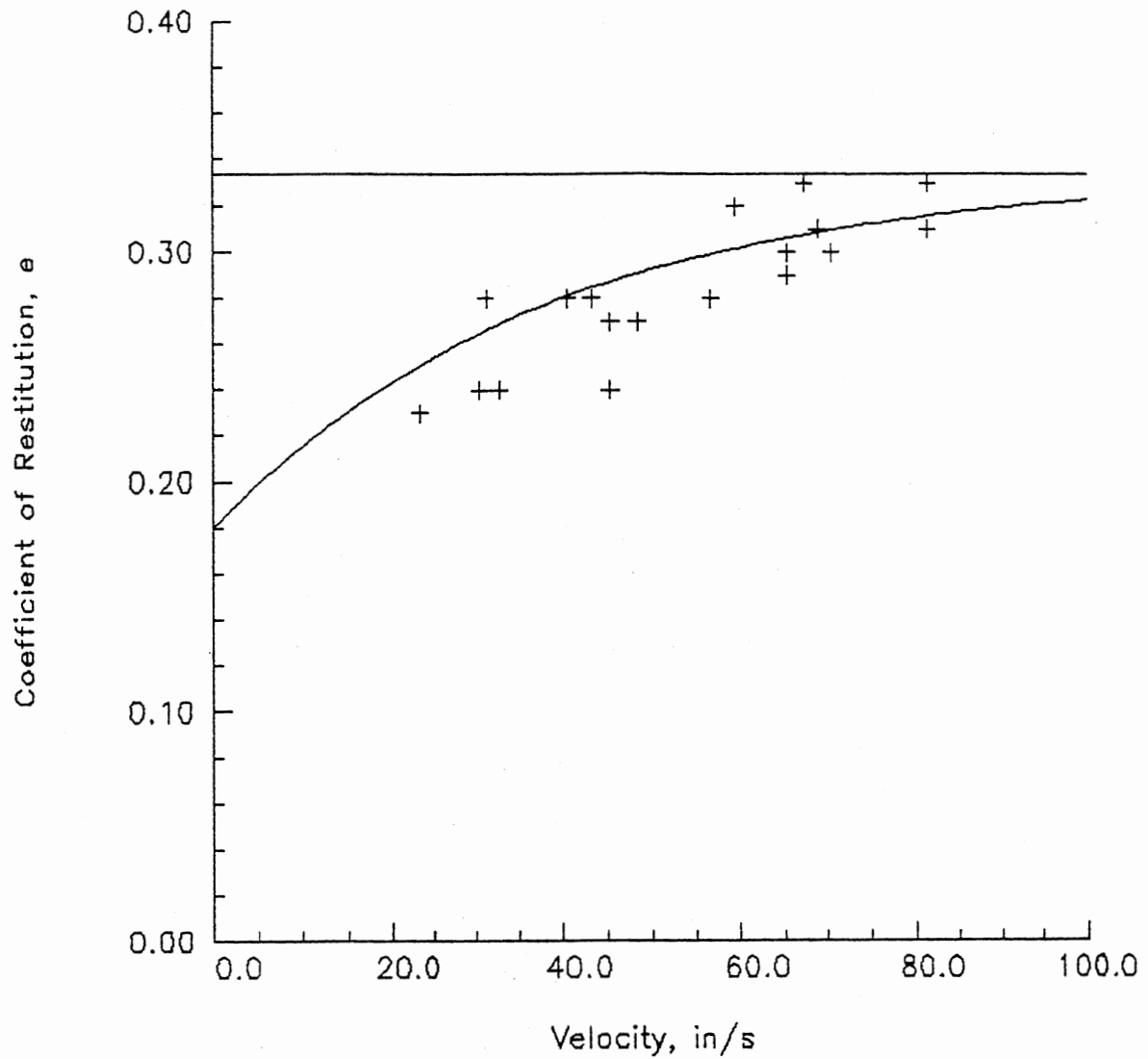


Fig. 3.10. Coefficient of Restitution

3.2.4. Perturbation Solution

A perturbation solution for the impact phase of the motion is possible, under certain conditions, since this phase can be described with just one state variable. During contact on the front faces of the teeth, let

$$\delta = R_{b1}\theta_1 - R_{b2}\theta_2 - b \quad (3.21)$$

and

$$\dot{\delta} = R_{b1}\dot{\theta}_1 - R_{b2}\dot{\theta}_2 \quad (3.22)$$

$$\ddot{\delta} = R_{b1}\ddot{\theta}_1 - R_{b2}\ddot{\theta}_2 \quad (3.23)$$

but, from the system equations we have

$$\ddot{\theta}_1 = \frac{T_1}{J_1} - \frac{R_{b1}}{J_1}[F(t) + G(t)] \quad (3.24)$$

and

$$\ddot{\theta}_2 = \frac{T_2}{J_2} - \frac{R_{b2}}{J_2}[F(t) + G(t)] \quad (3.25)$$

Substituting, we have the system equations in terms of delta:

$$\ddot{\delta} = \frac{R_{b1}T_1}{J_1} - \frac{R_{b2}T_2}{J_2} - \left[\frac{R_{b1}^2}{J_1} + \frac{R_{b2}^2}{J_2} \right] [F(t) + G(t)] \quad (3.26)$$

where $F(t)$, $G(t)$, c , K , and D are defined above. Rearranging equation (3.26), we have

$$\ddot{\delta} + cD \left[\frac{R_{b1}^2}{J_1} + \frac{R_{b2}^2}{J_2} \right] \dot{\delta} + ck \left[\frac{R_{b1}^2}{J_1} + \frac{R_{b2}^2}{J_2} \right] \delta = \frac{R_{b1}T_1}{J_1} - \frac{R_{b2}T_2}{J_2} \quad (3.27)$$

If we let

$$\frac{R_{b1}^2}{J_1} + \frac{R_{b2}^2}{J_2} = \epsilon$$

then we can rewrite equation (3.27) as

$$\ddot{\delta} + c\epsilon(D\dot{\delta} + k)\delta = 0 ; \quad T_1 = T_2 = 0 \quad (3.28)$$

The perturbation solution for this equation is derived in Appendix C,

and is:

$$x(T) = V \sin T + \epsilon \frac{V^2}{6} (-2 \sin T + \sin 2T) + \\ \epsilon^2 \frac{V^2}{288} (37 \sin T - 32 \sin 2T + 9 \sin 3T) + \dots$$

where

$$T = \omega\tau, \quad \tau = \omega_{\infty}t, \quad \text{and} \quad \omega = 1 - \frac{v^2}{24}$$

but

$$V = \frac{\delta(0)}{b\omega \left[k \left(\frac{R_{G1}^2}{J_1} + \frac{R_{G2}^2}{J_2} \right) \right]^{0.5}} = \frac{\delta(0)}{b\omega\omega_{\infty}} = \frac{c_1}{\omega}$$

so that

$$\omega^3 - \omega^2 + c_1 = 0$$

In addition to the perturbation solution, equation (3.28) has been solved using a graphical technique known as the Delta Method (see Appendix D). The Delta Method solution and the one-term and two-term perturbation solutions have been plotted in Figure 3.11. The Delta solution and two-term perturbation solution appear to fall on the same curve.

3.3 Simulation

A simulation program, using a fourth-order Runge-Kutta numerical integration technique, was developed to investigate the behavior of the following subsystem:

Number of teeth (both gears) = 28

Diametral Pitch = 8

Pressure angle = 20 degrees

Face width = 0.700 in.

Mass added to gear 2 to bring its natural frequency down to 350 hertz.

The derived gear dimensions are given in Appendix E, and the simulation program is described and listed in Appendix F.

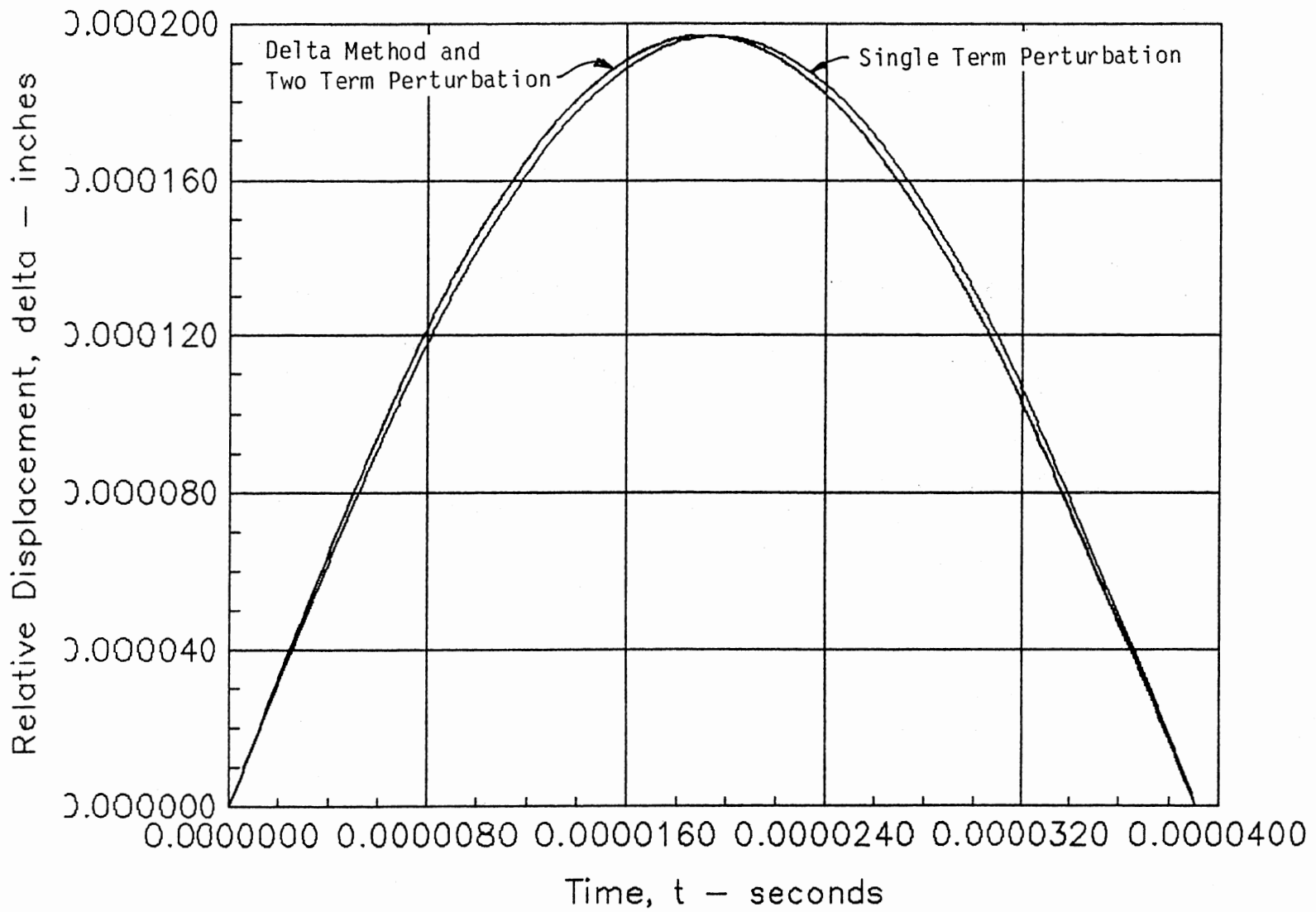


Fig. 3.11. Solutions to Gear Tooth Impact Equations

The state equations used in the simulation are:

$$\begin{aligned}x_1 &= \theta_1, \quad x_2 = \dot{\theta}_1, \quad x_3 = \theta_2, \quad x_4 = \dot{\theta}_2, \quad R_{b1} = R_{b2} = R_b \\ \dot{x}_1 &= x_2 \\ \dot{x}_2 &= \frac{T_1 - ckR_b \left[R_b |x_1 - x_3| - b \right] - cDR_b^2 |x_2 - x_4| \left[R_b |x_1 - x_3| - b \right]}{J_1} \\ \dot{x}_3 &= x_4 \\ \dot{x}_4 &= \frac{T_2 + ckR_b \left[R_b |x_1 - x_3| - b \right] + cDR_b^2 |x_2 - x_4| \left[R_b |x_1 - x_3| - b \right]}{J_2}\end{aligned}$$

Three cases were run with the simulation program. They were:

- I - Free vibration, induced by an initial velocity of gear 1 of 10 rad/sec.
- II - Both gears loaded with equal and opposite torques of 1000 lb.-in.
- III - An external load on gear 1 only of 1000 lb.-in.

Figures 3.12 through 3.15 give the results for Case I. The non-linear frequency is obvious in figure 3.12 which shows displacement of gear 1 (and, because gear 2 is not moving, relative gear displacement) as a function of time. The dashed lines in figure 3.12 represent the clearance, b . Any excursion above or below these lines represents deflection in the gear teeth. The phase-plane plot of figure 3.14 clearly shows that the system will reach a stable equilibrium somewhere on the zero-velocity axis.

Figures 3.16 and 3.17 show the results from Case II. Notice, in figure 3.16, that there is no impact on the rear face of the teeth in this case. After impact on the front faces the teeth separate but return to impact again on the same faces. After nine impacts the system

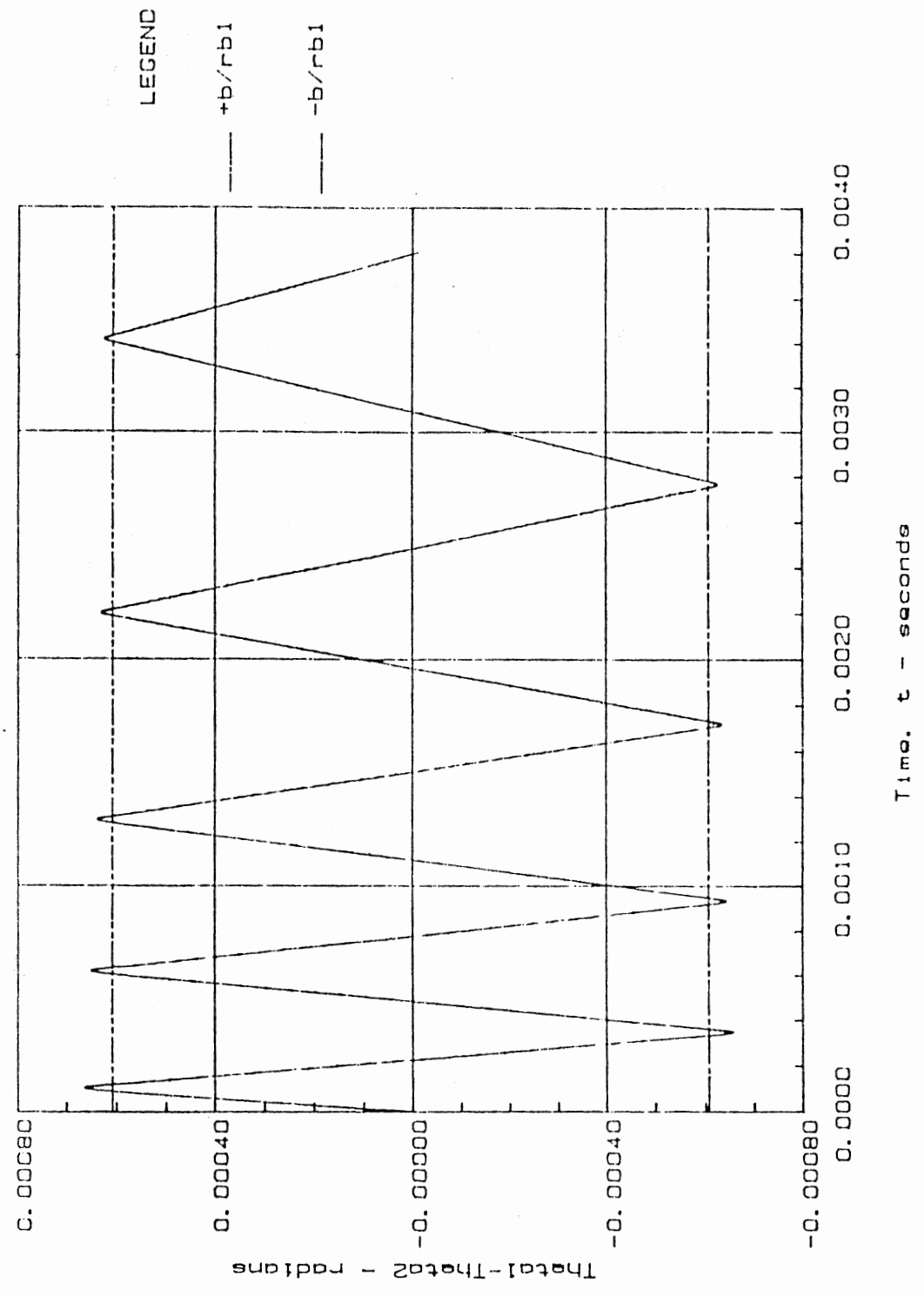


Fig. 3.12. Relative Displacement vs Time (Case I)

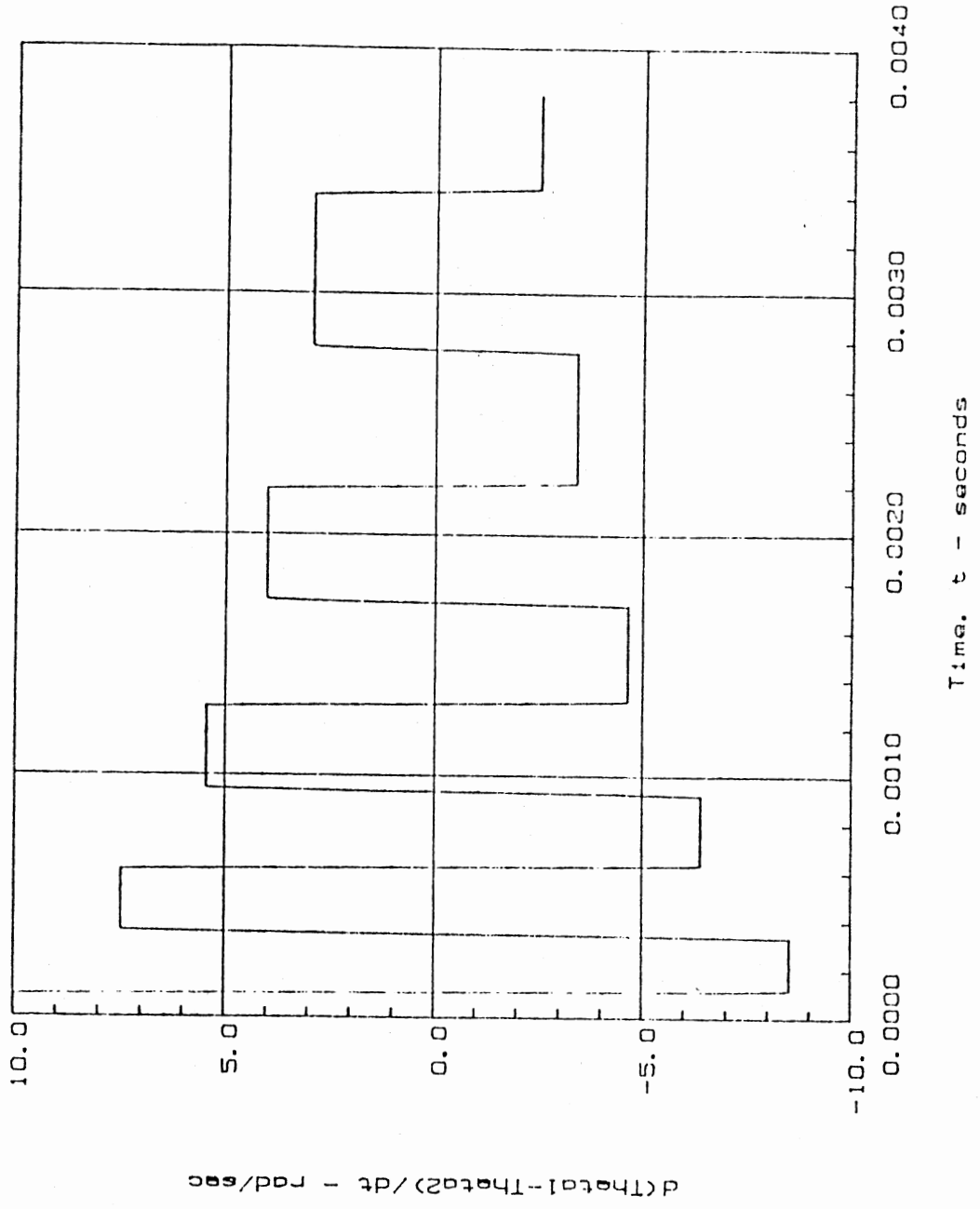


Fig. 3.13. Relative Velocity vs Time (Case I)

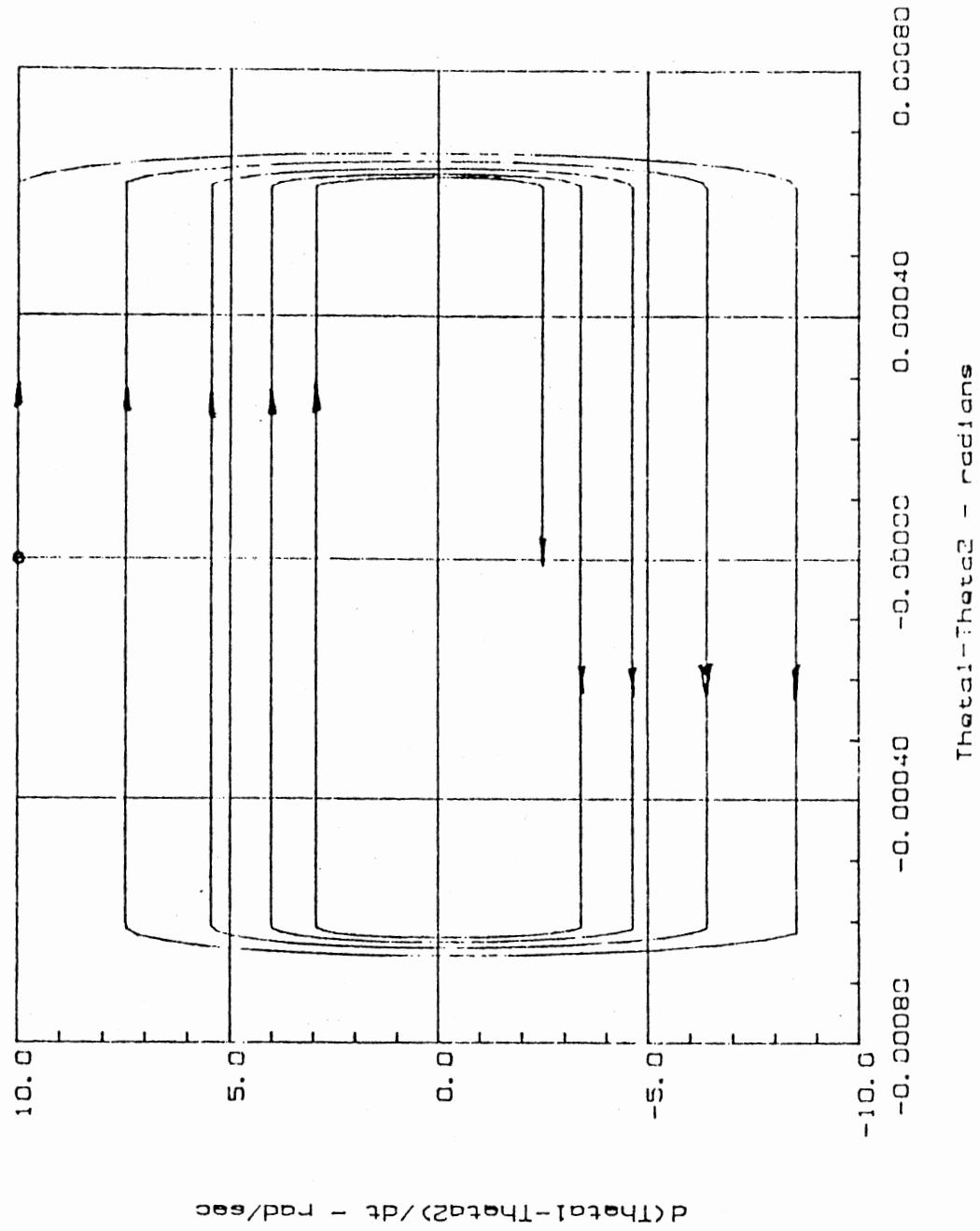


Fig. 3.14. Phase Plane (Case I)

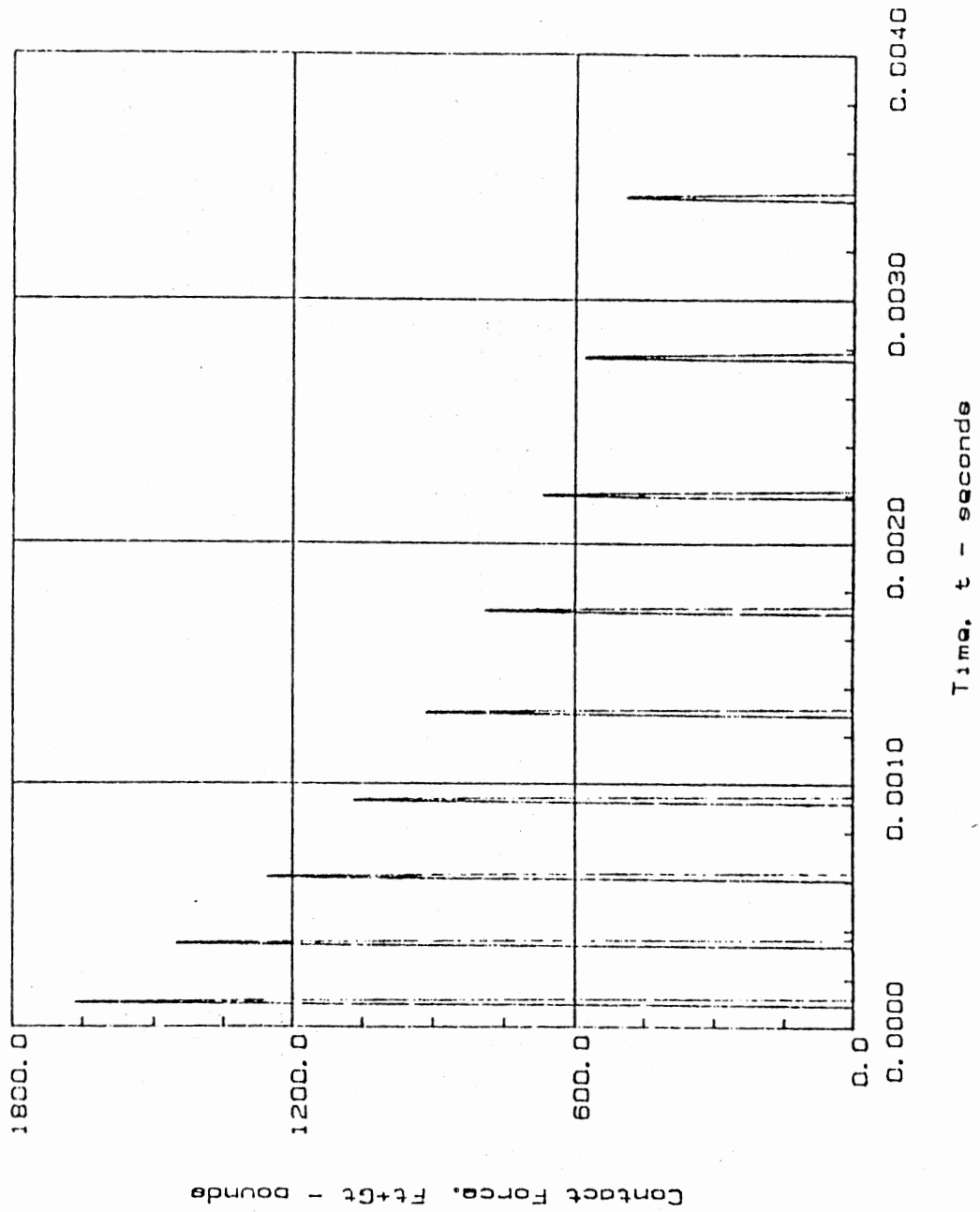


Fig. 3.15. Contact Force vs Time (Case I)

continues to oscillate, but without further separation of the teeth. Figure 3.17 shows the stable equilibrium point to be the teeth in contact.

Figures 3.18 through 3.21 show the results from Case III. The results here are similar to Case II except that gear 2 now has some detectable motion. In the phase-plane (figure 3.12) we see that there is no equilibrium position because the system will continue in motion indefinitely under the influence of the driving torque on gear 1.

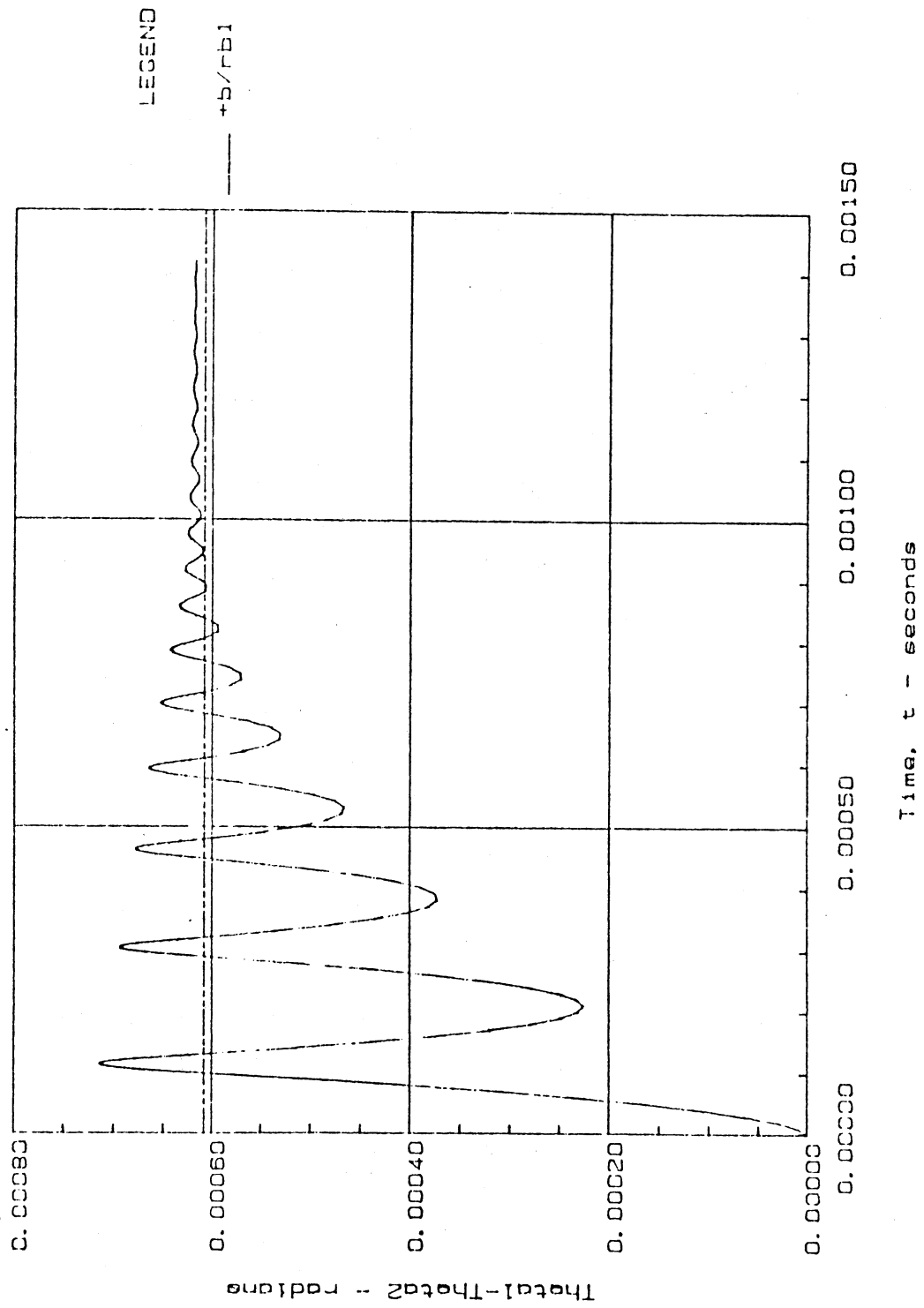


Fig. 3.16. Relative Displacement vs Time (Case II)

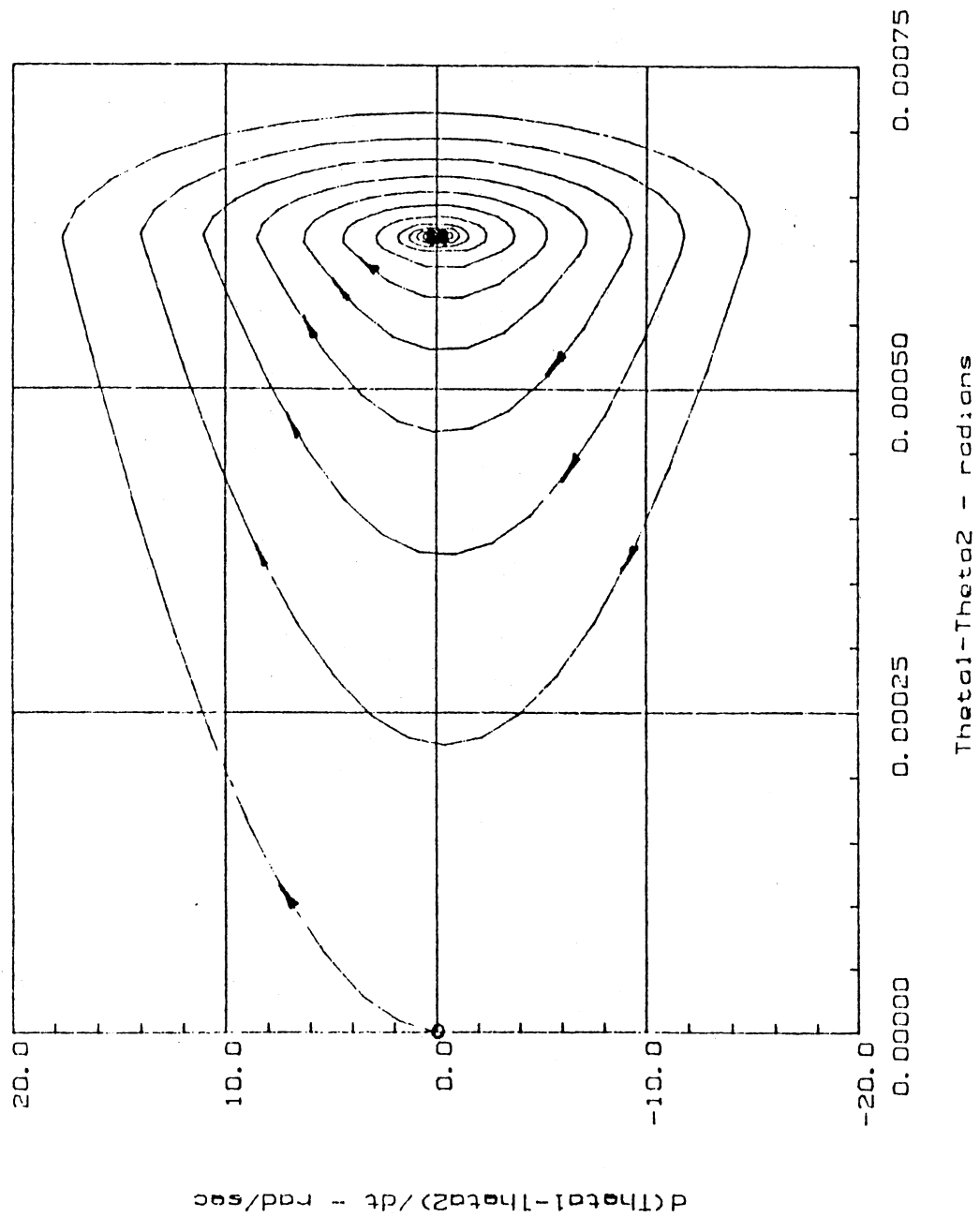


Fig. 3.17. Phase Plane (Case II)

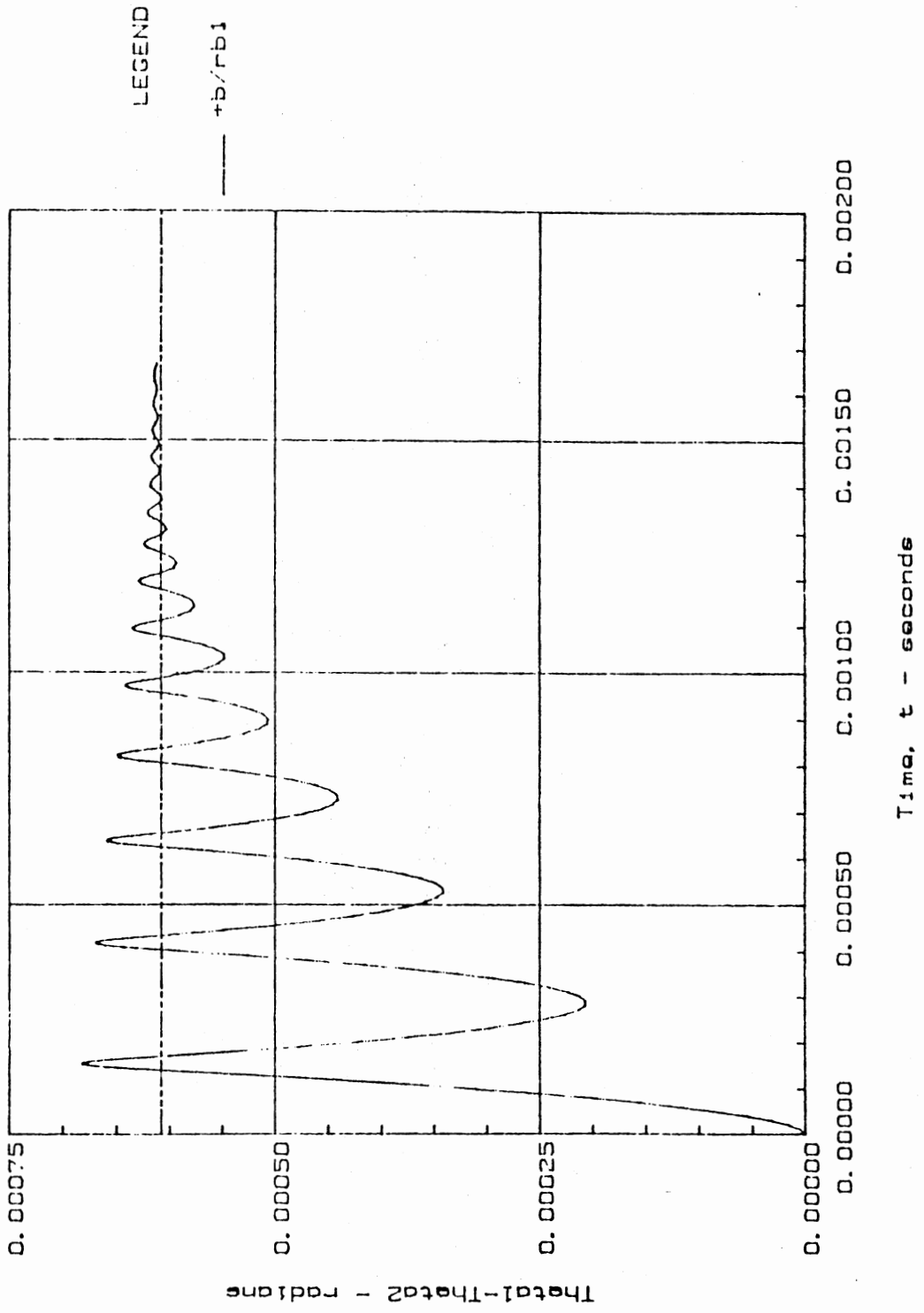


Fig. 3.18. Relative Displacement vs Time (Case III)

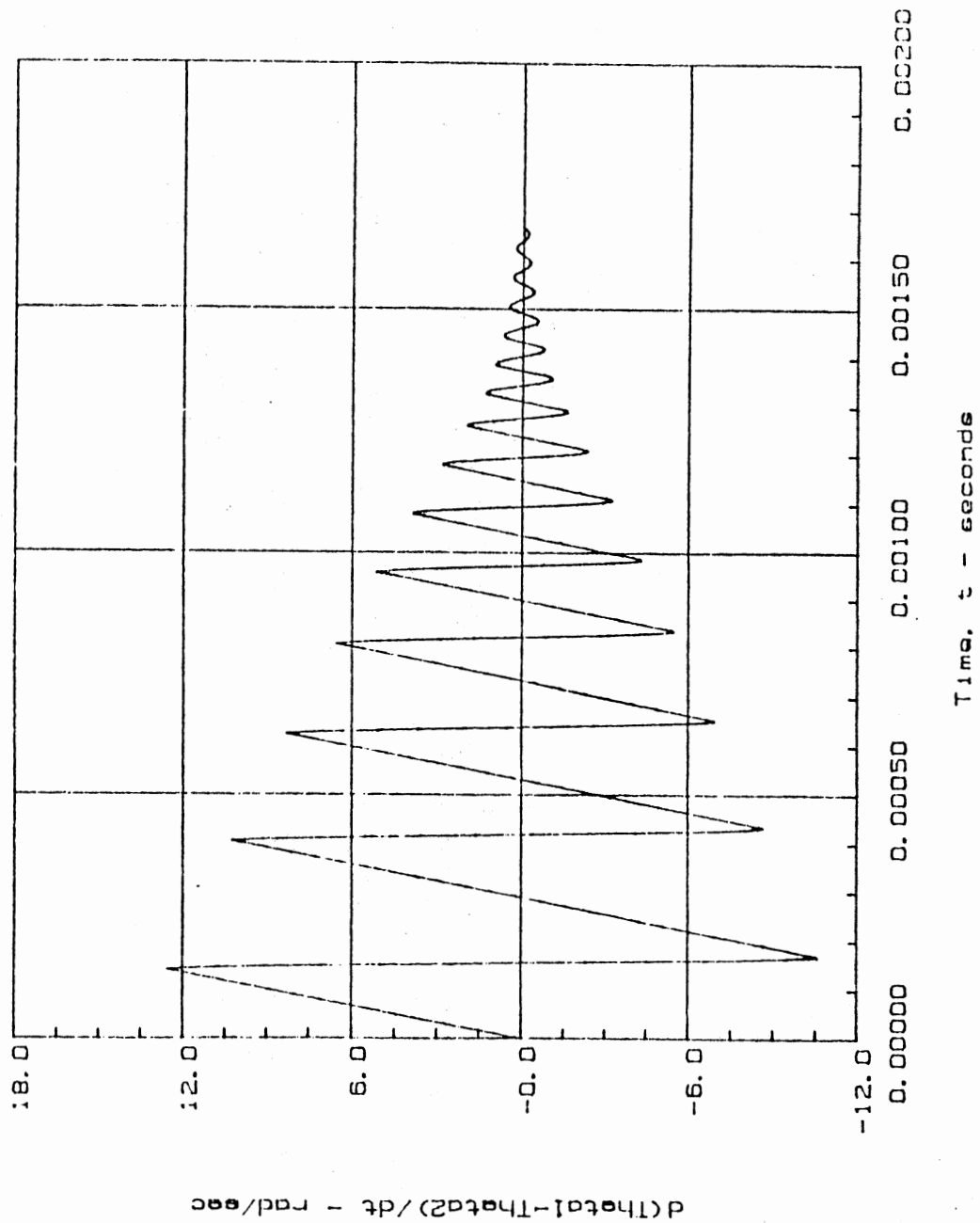


Fig. 3.19. Relative Velocity vs Time (Case III)

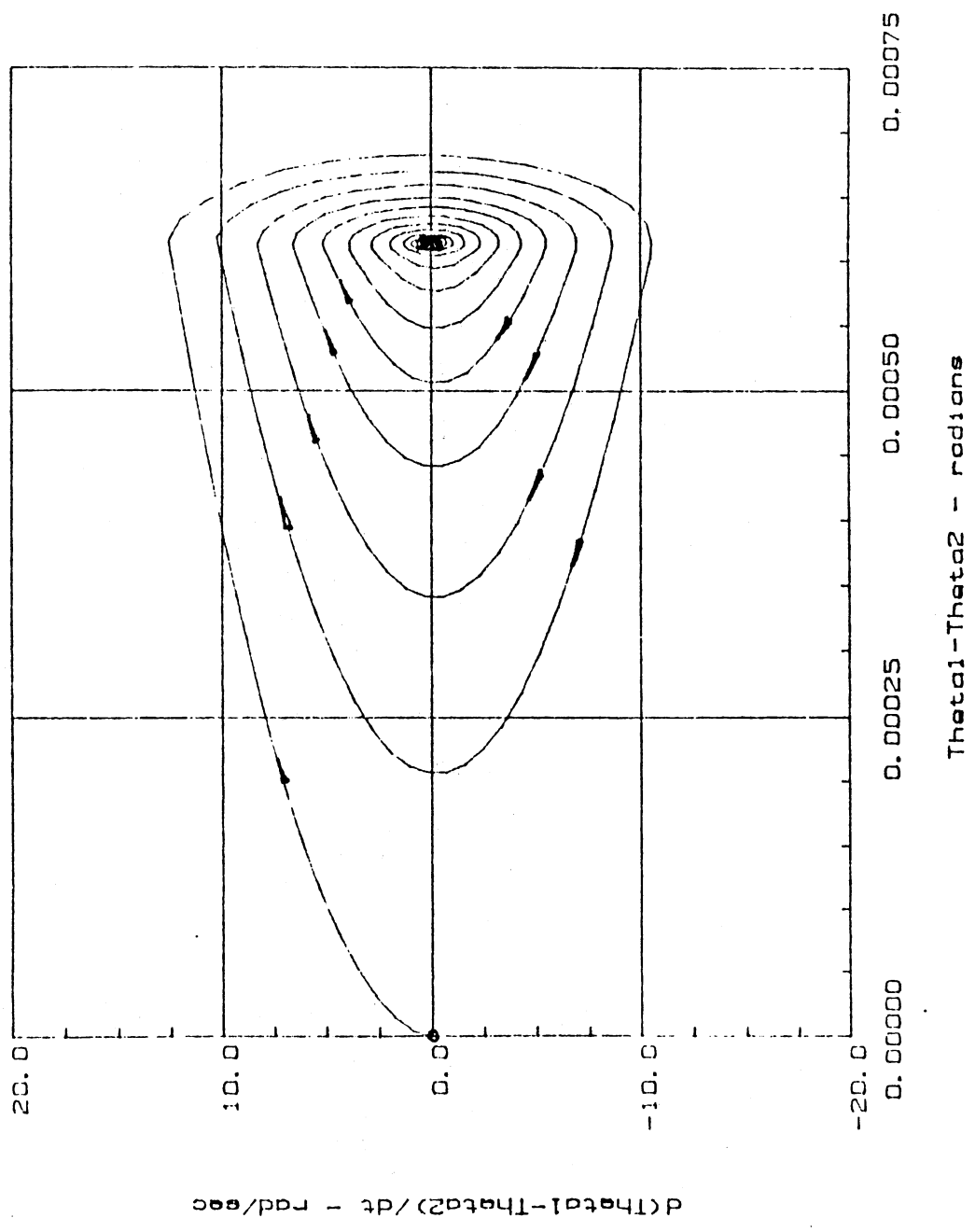


Fig. 3.20. Phase Plane (case III)

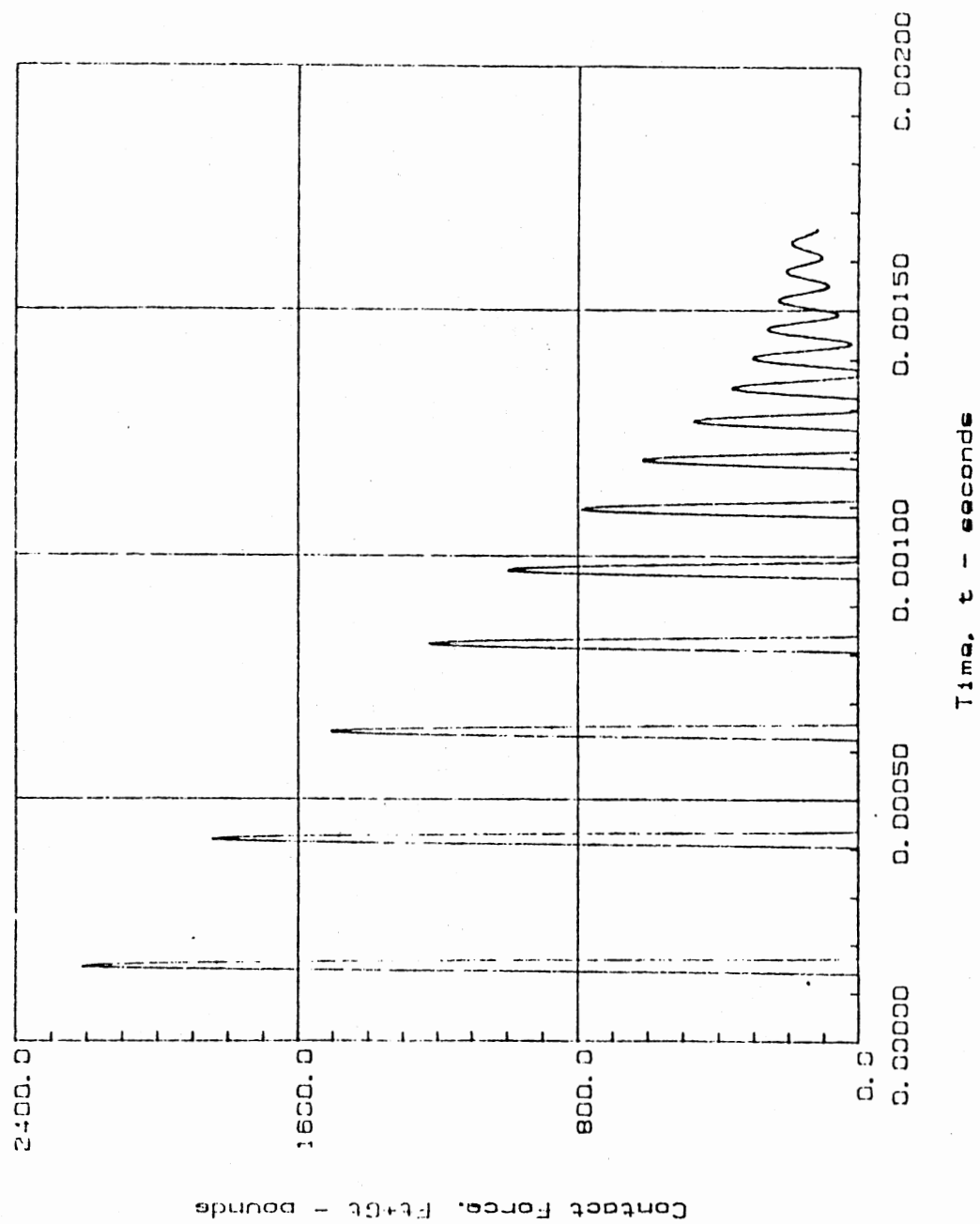


Fig. 3.21. Contact Force vs Time (Case III)

CHAPTER IV

KEYED JOINT MODEL

4.1 Physical System

The keyed joint consists of three parts: a shaft, key, and a hub. There are many different key shapes in use but this study is restricted to square (cross-section) keys in either sled-runner or milled keyseats. It is further assumed that the cross-section dimension of the key is equal to one-fourth of the shaft diameter. The key may be of any length.

4.1.1 Conventional Model

The analysis of key and keyway stresses is usually done by assuming a very simple model (see Figure 4.1). Shigley and Mitchell (1983) and others give the (average) shear stress in the key as F/A , where F is the force on the face of the key and A is the area found by multiplying the width by the length of the key. In this model, the force is found by dividing the torque applied to the joint by the radius of the shaft/hub interface (one-half the shaft diameter).

Keyed joints are usually ignored in deflection analysis. For this reason there is very little published information on the elastic behavior of a keyed joint. Wang and Morse (1972) developed a very simplistic model for use in dynamic modeling of gear train systems. They assumed that the key was a short cantilever beam subjected to a distributed load

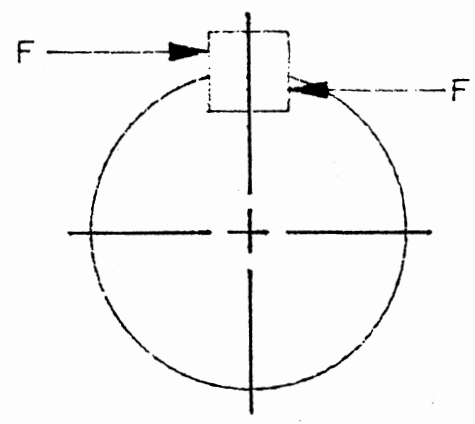


Fig. 4.1. Simplified Model for Key Stress

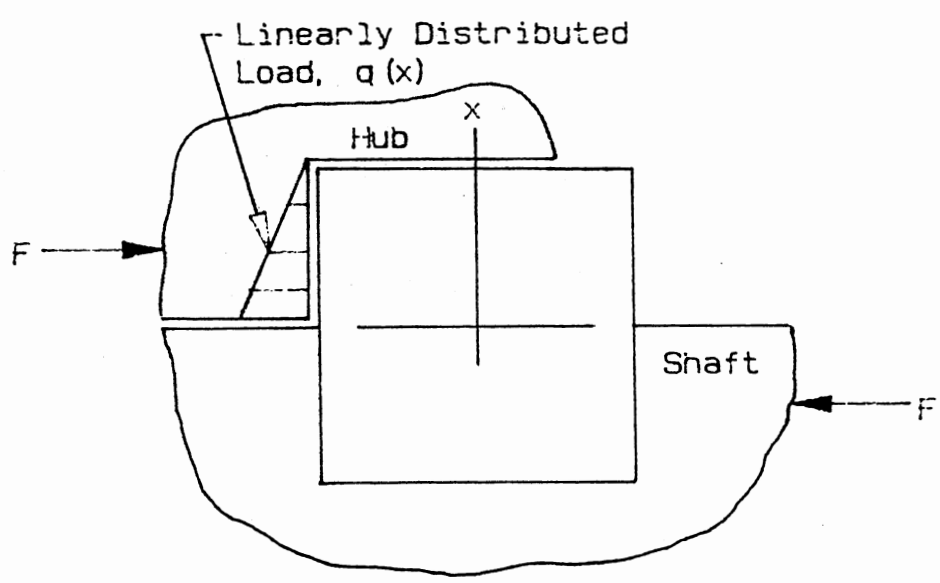


Fig. 4.2. Cantilever Beam Model for Key Stiffness

along its length (see Figure 4.2). Further assumptions were that (1) the key is force fit in the shaft and is a slide fit in the hub, (2) deflection in the key is due solely to shear, (3) the concave corner of the hub keyway is not deformed, and (4) the convex corner of the hub keyway is locally flexible. This leads to the conclusion that (for a square key of width $d/4$) the lateral stiffness is independent of diameter and is given by

$$k = 2Gb \quad \text{lb/in}$$

where G is the Modulus of Rupture (shear Modulus) and b is the length of the key. This can be converted to an angular stiffness by multiplying by the square of half of the shaft diameter, or

$$k' = d^2Gb/2 \quad \text{lb-in/rad}$$

For a steel key, this model predicts a linear stiffness of 23×10^6 lb/in/in of length. This compares with a value of 2.9×10^6 for steel spur gear teeth in contact.

4.1.2 Rigid Body Model With Clearances

There will be clearance between the hub and shaft diameters, and between the hub keyway and the key. The key will be either a snug fit in the shaft or an interference fit.

Assume that a force F acts on the hub (Figure 4.3) at the point P and that this point is stationary in space while the hub/shaft rotate at constant velocity. A stationary Cartesian coordinate frame, fixed in space, has its origin at the center of the hub and its y -axis through the point P . The centerline of the hub keyway will be at an arbitrary angle α with respect to the x -axis. The hub and shaft will contact at two points, A and B , at which there will be hub reaction forces R_k and

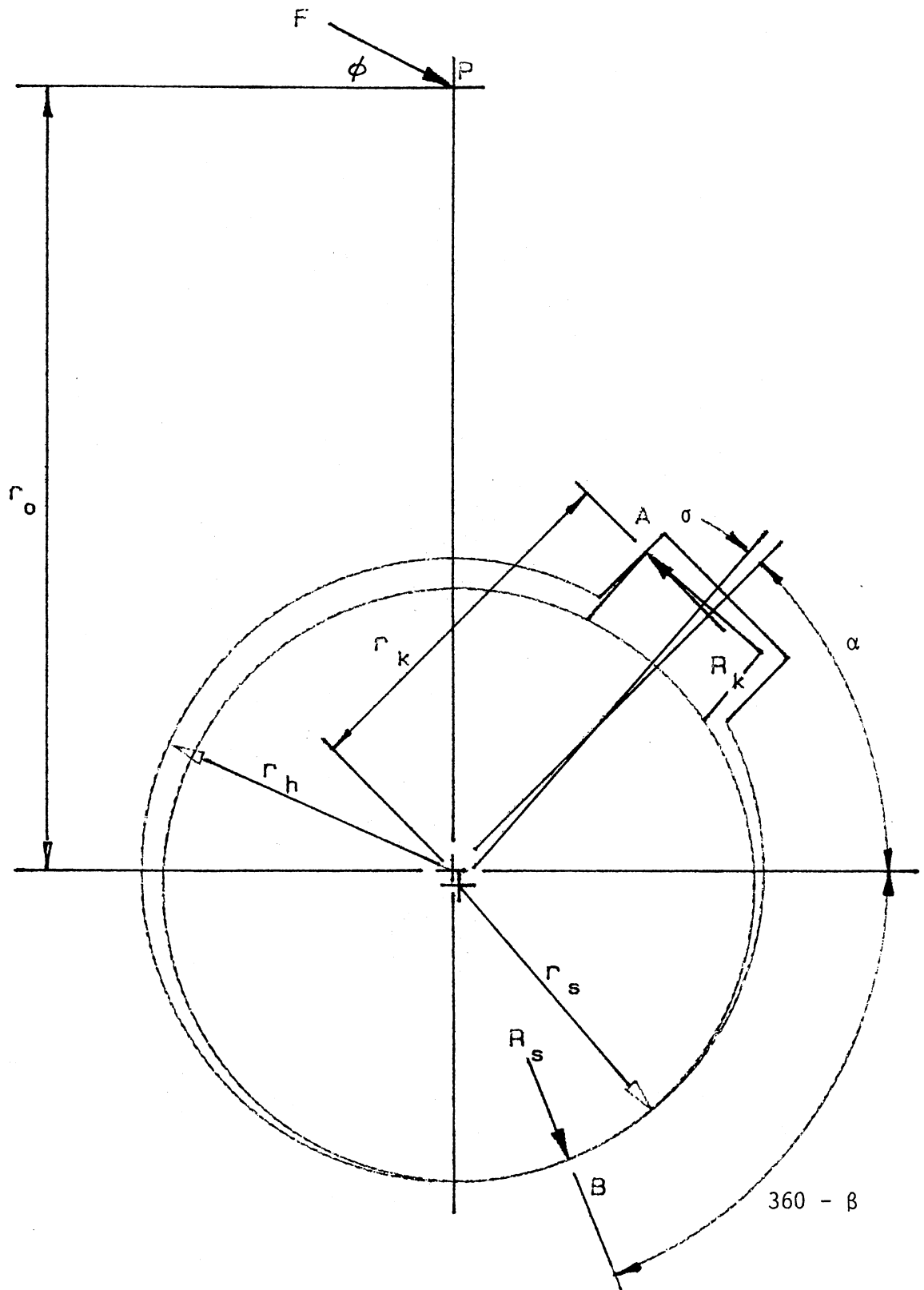


Fig. 4.3. Layout of Shaft, Key and Hub

R_s , respectively. The angle from the x-axis to the point B is β . The shaft and hub centers will be offset an amount c which is equal to the radial clearance between the hub and shaft. The distance along the hub keyway centerline to the extension of the reaction force at A is r_k and the angle between the key centerline and the hub keyway centerline is σ . Taking the hub as a free body, we can write the following three equilibrium equations:

$$\sum M_O = 0: (F \cos \phi) r_o - R_k r_k = 0 \quad (4.1)$$

$$\sum F_x = 0: F \cos \phi - R_k \sin \alpha + R_s \cos \beta = 0 \quad (4.2)$$

$$\sum F_y = 0: -F \sin \phi + R_k \cos \alpha - [-R_s \sin \beta] = 0 \quad (4.3)$$

In these equations R_k , R_s , r_k , and β are the dependent variables and F , ϕ , α , and r_o are independent. Since there are four unknowns we need one more equation for solution. The additional equation is provided by the geometric constraints associated with the points A and B. That is, the point A lies on both the key (assumed fixed to the shaft) and the hub, and the center of the shaft lies on the line OB at a distance c from O. Assuming for the moment that r_a (distance O'B) and δ are known (from shaft/key dimensions), then the point A is at the intersection of the line (Figure 4.4)

$$y = x \tan \alpha + \frac{w_h}{2 \cos \alpha} \quad (4.4)$$

and the circle

$$\left[x - x_{O'} \right]^2 + \left[y - y_{O'} \right]^2 = r_a^2 \quad (4.5)$$

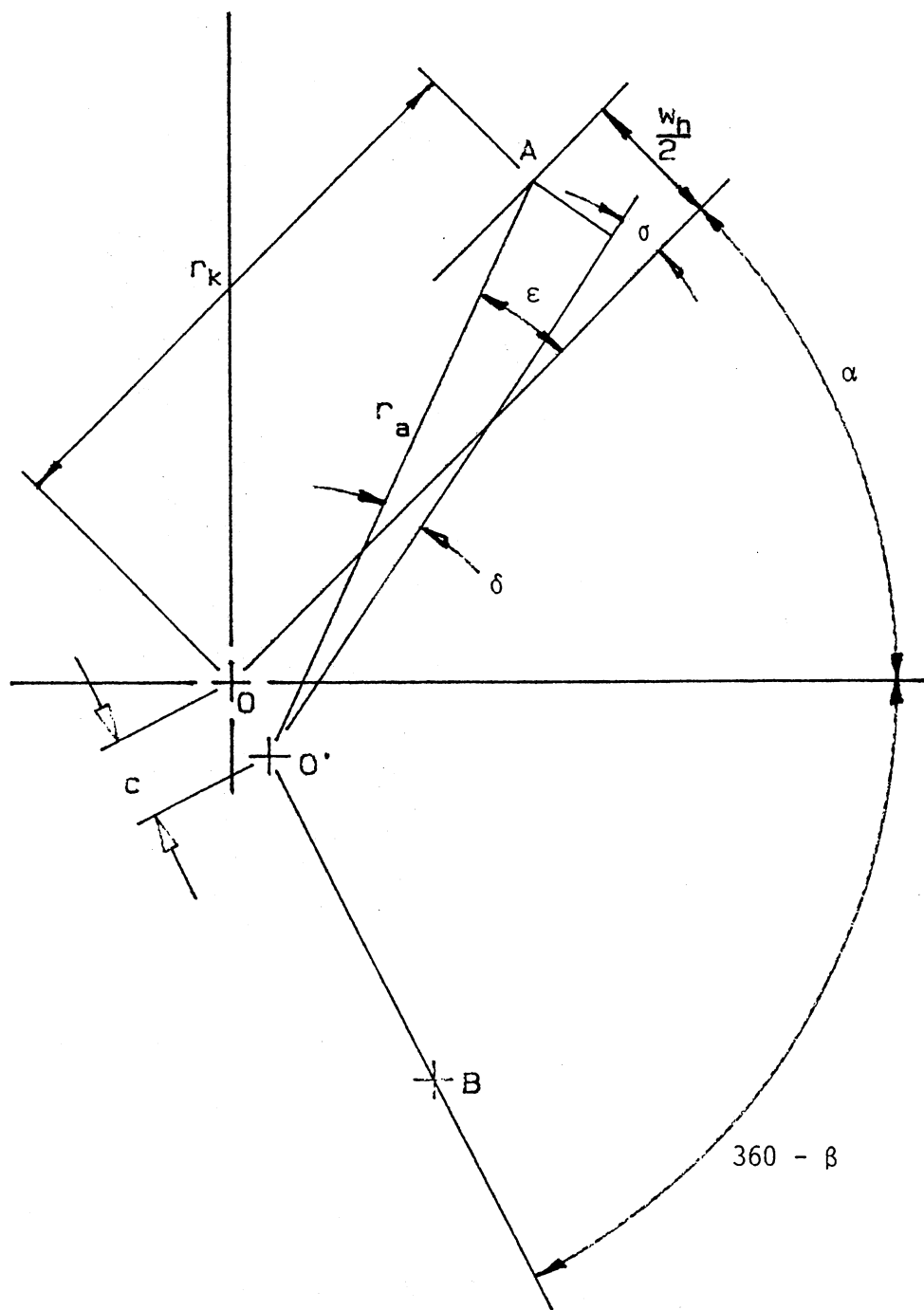


Fig. 4.4. Geometry for Contact Point A

where

$$x_{O'} = c \cos \beta$$

$$y_{O'} = c \sin \beta$$

$$c = r_h - r_s$$

then

$$r_k = \sqrt{x_A^2 + y_A^2} \quad (4.6)$$

where x_A and y_A are the coordinates of the point A and are found by solving equations (4.4) and (4.5) simultaneously. Unfortunately, to solve these two equations the angle β must be known. An iterative solution can be employed by first guessing a value for β then solving equations (4.4), (4.5), and (4.6) for r_k . Using the calculated value of r_k and the guessed value of β , equations (4.1), (4.2) and (4.3) can be solved for R_k , R_s , and β . If the calculated β does not agree with the guessed value it is substituted for it and the process is repeated until the two agree.

The quantities r_a and δ are found as follows (see Figure 4.5):

$$r_a = \left[\left(\frac{w_k}{2} \right)^2 + h_s^2 \right]^{0.5} \quad (4.7)$$

$$\delta = \arctan \left[\frac{w_k}{2h_s} \right] \quad (4.8)$$

where

w_k = key width, in.

h_s = distance from top of key to center of shaft

It is interesting to look at the relative position and relative magnitude of the shaft/hub contact force R_s . The above equations were solved for the following case:

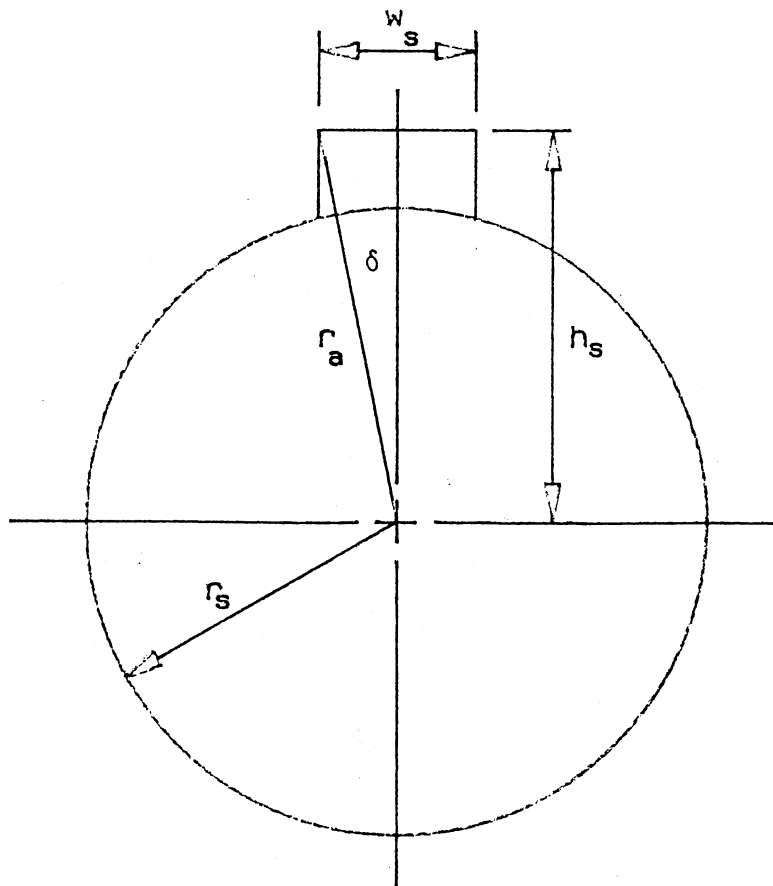


Fig. 4.5. Key/Shaft Geometry

Shaft radius, $R_s = 0.995$ in.
 Hub radius, $R_h = 1.000$ in.
 Hub keyway width, $w_h = 0.510$ in.
 Key width, $w_s = 0.500$ in.
 Pressure angle, $\phi = 20^\circ$
 Pitch radius, $r_o = 2.5$ and 10 in.

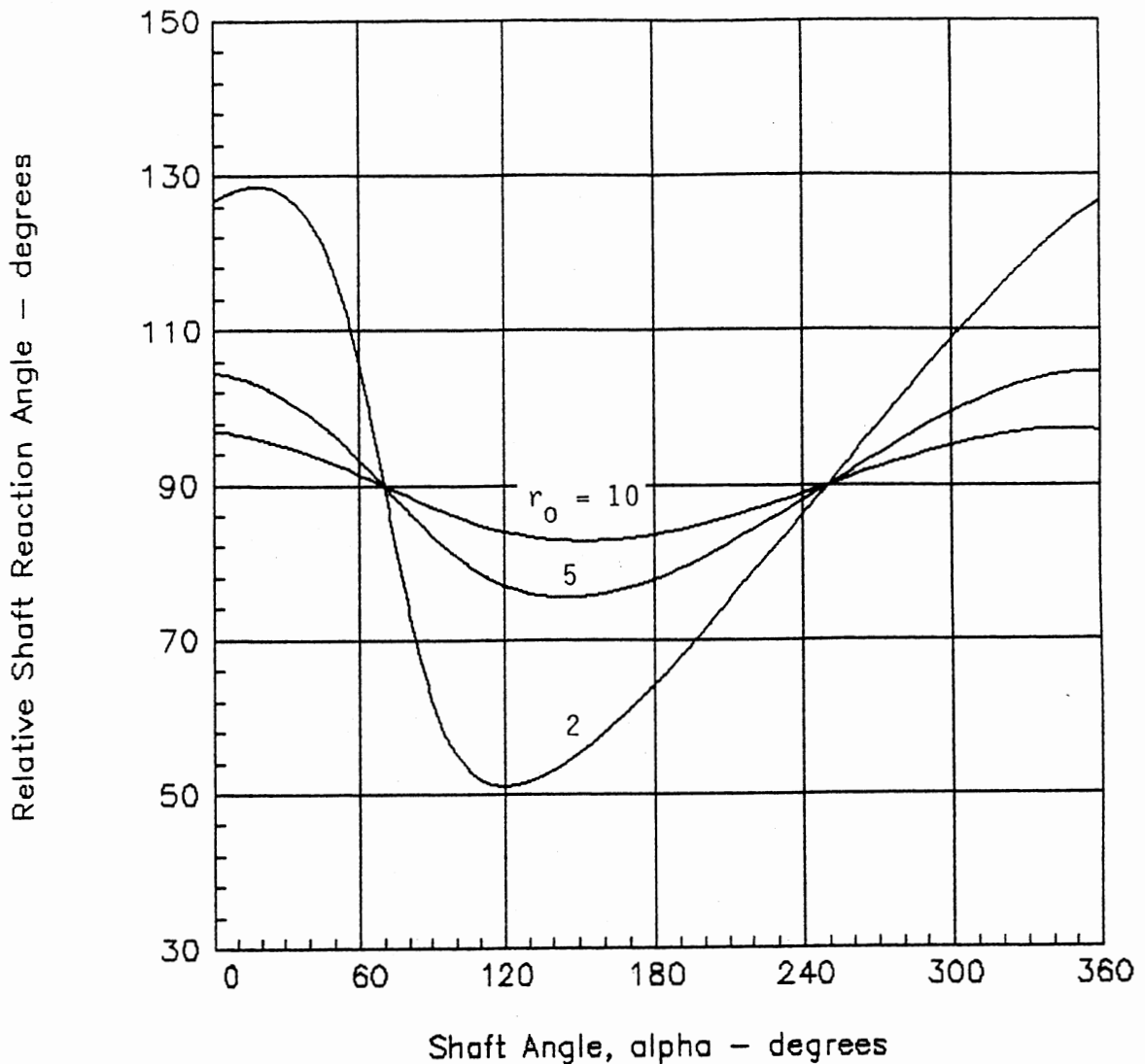


Fig. 4.6. Relative Shaft/Hub Reaction Position

Figure 4.6 shows the relative position of R_s with respect to the centerline of the keyway as the shaft and hub turn through the angle α . Notice that, as the pitch radius (distance from the center of rotation to the application of the driving load F) decreases, there is considerable relative motion between the shaft and hub. On the other hand, as the pitch point gets further from the center of rotation the position

of the shaft/hub reaction with respect to the shaft rotation angle tends to stabilize at 90° behind the rotation angle.

The relative magnitude of the shaft/hub reaction is shown in Figure 4.7. As in the case of the position, the magnitude fluctuation is greater as the ratio of pitch radius to hub radius decreases. As the pitch radius tends to infinity the magnitude of the shaft/hub reaction will tend toward equality with the force between the key and the hub.

It is clear from this analysis that the shaft/hub contact force must be taken into account when estimating the joint stiffness. One way to do this is to analyze a finite element model of the entire shaft, key and hub.

4.2 Stiffness Models

4.2.1 Analytic Model

In the preceding section it was assumed that the key is held firmly by the keyseat with half of its depth protruding from the shaft and deflections on the bearing surfaces were not considered. In fact, the keyseat only partially supports the key and, because of clearance between the shaft and the hub, contact deflections allow some relative motion between the shaft and hub. A more generalized approach to modeling the keyed joint is shown in Figure 4.8.

The total deflection of the system has the following components: 1) shear deflection of the key, 2) contact between key and hub, 3) contact between key and shaft, 4) contact between shaft and hub, and 5) shear deflection of shaft support (lip). A model will be developed below that considers components 1), 4), and 5) with concentrated loading.

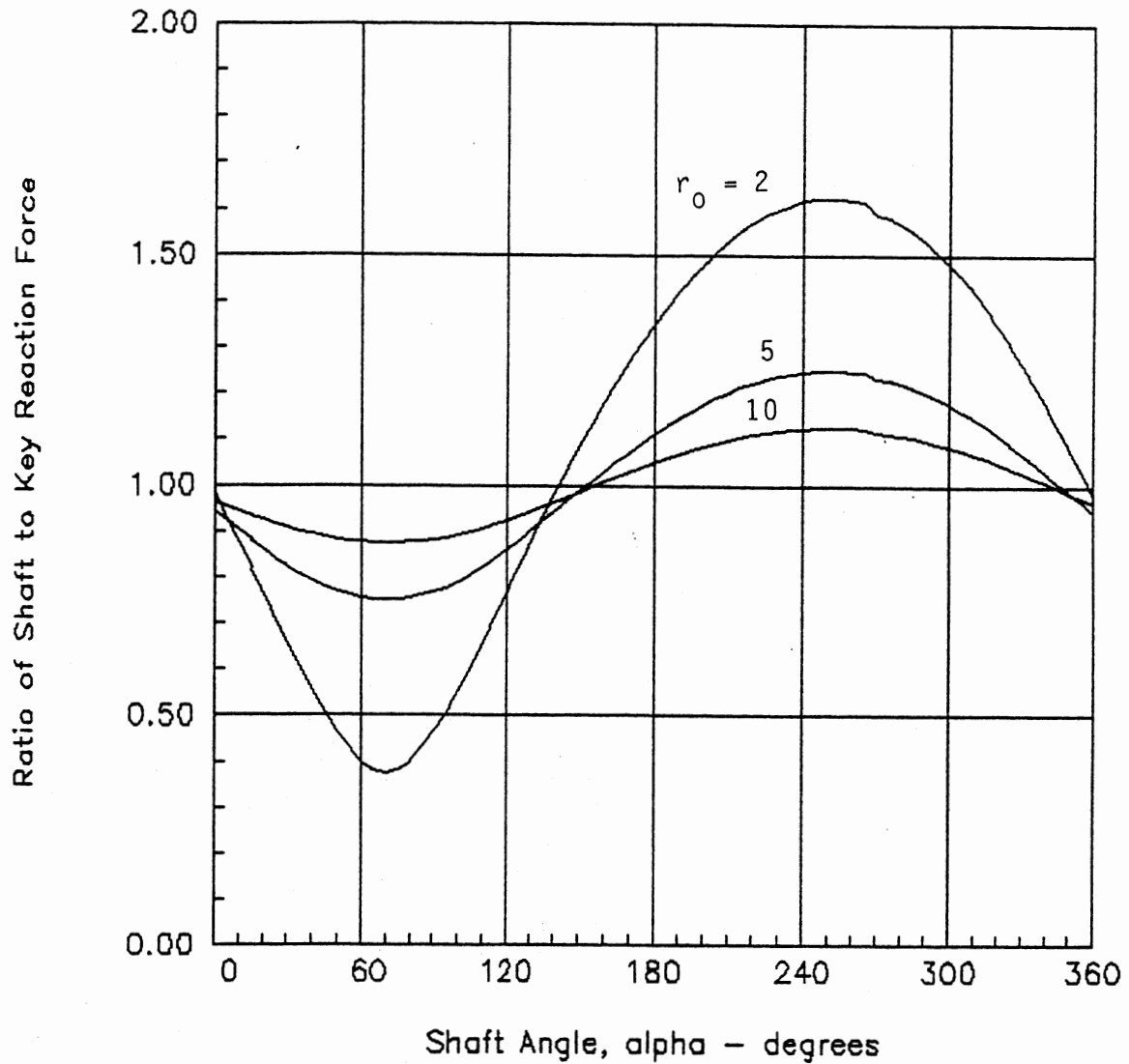


Fig. 4.7. Relative Shaft/Hub Reaction Magnitude

4.2.1.1 Shear deflection of Key. By Castigliano's first theorem, the deflection at $x=0$ (Fig. 4.9) is

$$\delta_0 = \partial U_s / \partial P \quad (4.9)$$

where U_s is the shear strain energy for a rectangular cross-section and is given by (Budynas, 1977)

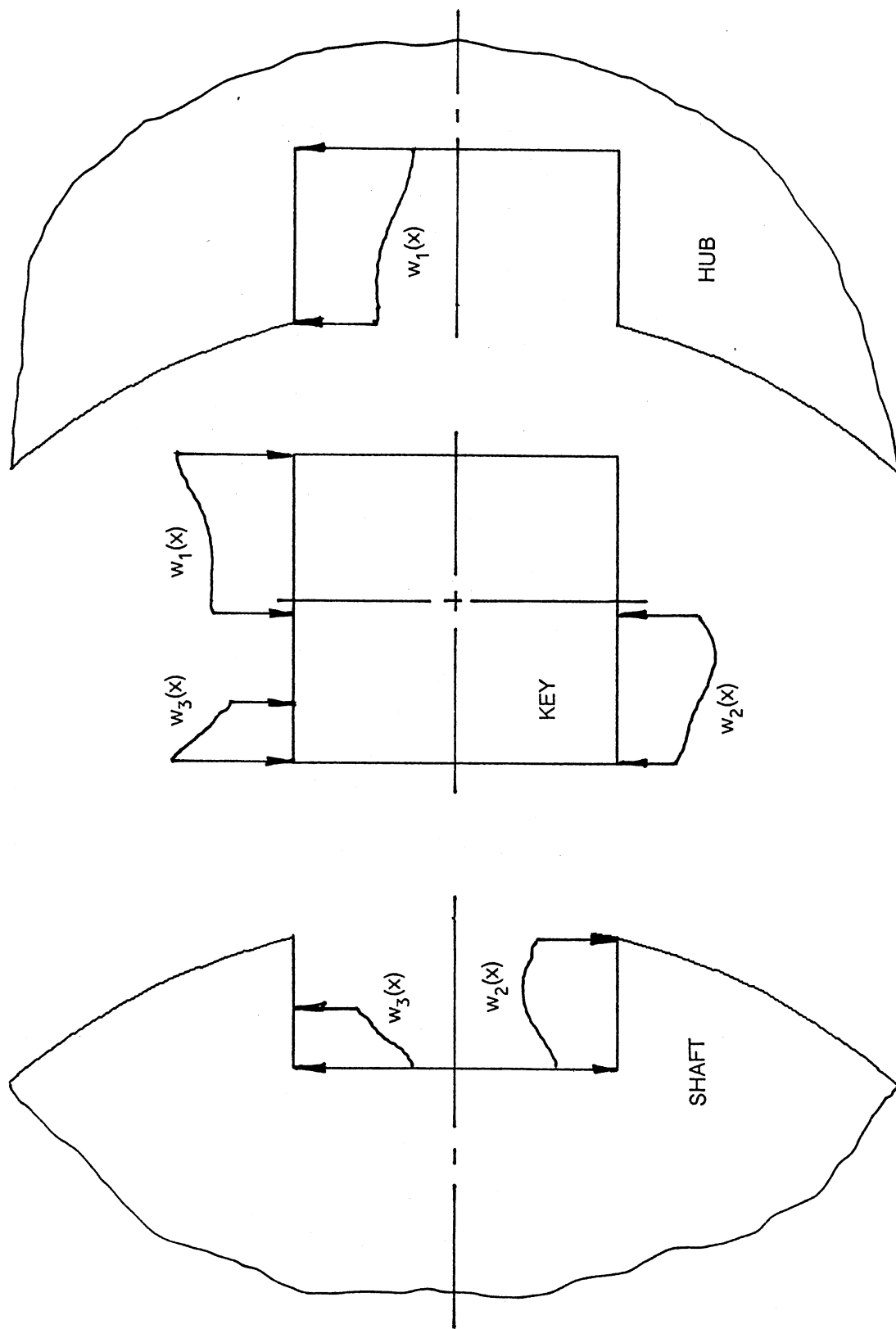


Fig. 4.8 Generalized Key Loading Model

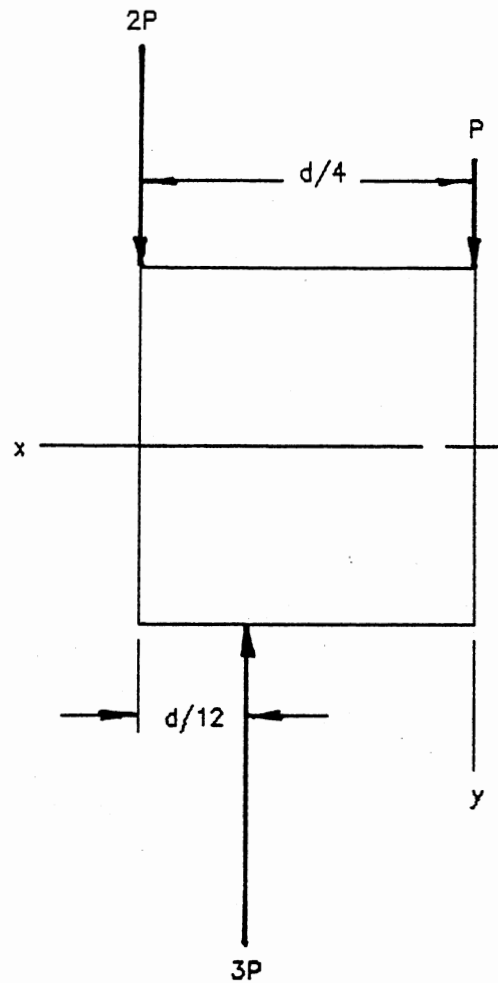


Figure 4.9. Key Loading in Shear

$$U_s = \frac{12(1 + \nu)}{5Eb(d/8)} \int_0^{d/4} v^2 dx \quad (4.10)$$

and

$$v^2 = \begin{cases} P^2, & 0 \leq x \leq d/6 \\ 4P^2, & d/6 \leq x \leq d/4 \end{cases} \quad (4.11)$$

Combining equations (4.10) and (4.11) and integrating yields

$$U_s = \frac{48(1 + \nu)P^2}{5Eb} \quad (4.12)$$

Substituting equation (4.12) into (4.9) and differentiating gives the displacement

$$\delta_o = \frac{96(1 + \nu)P}{5Eb} \quad (4.13)$$

which is independent of diameter, d . The stiffness per unit length of key is

$$\frac{k}{b} = \frac{P}{\delta_o b} = \frac{5E}{96(1 + \nu)} = 1.20(10)^6 \quad (4.14)$$

for steel.

4.2.1.2. Contact Between Key and Shaft. Assuming that the shaft and hub have slightly different diameters and that the force P acts on a line through the center of the shaft and parallel to the force system on the key, Roark and Young (1975) give the surface contact deflection as

$$\delta = \frac{2P(1 - \nu^2)}{\pi Eb} \left[\frac{2}{3} + \ln \left(\frac{2d_h}{c} \right) + \ln \left(\frac{2d_s}{c} \right) \right] \quad (4.15)$$

where

$$c = 2.15\sqrt{PK_d/Eb} \quad (4.16)$$

and

$$K_d = \frac{d_h d_s}{d_h - d_s} \quad (4.17)$$

The constant c is the half-width of the contact zone (a rectangle in the case of two cylinders in contact). Thus, this formulation will only be accurate for values of c that are reasonably small compared with the diameter, d . Letting

$$D = d_h - d_s$$

and

$$d^2 = d_h d_s$$

then

$$K_d = d^2/D \quad (4.18)$$

and

$$c = 2.15d\sqrt{P/EbD}, \quad c^2 = 4.62d^2P/EbD \quad (4.19)$$

also, the term in the square brackets in equation (4.15) becomes

$$\ln \left[\frac{4d^2}{c^2} \right] = \ln \left[\frac{EbD}{1.16P} \right] \quad (4.20)$$

Substituting equations (4.18), (4.19) and (4.20) into (4.15) gives, for the stiffness per unit length of key $P/\delta b$,

$$k = \frac{\pi E}{2[1 - \nu^2] \left[\frac{2}{3} + \ln \left[\frac{EbD}{1.16P} \right] \right]} \quad (4.21)$$

Note that this result is also independent of diameter, d , but that it does depend on the load, P . Some values of stiffness are listed in Table 4.1 for a relatively tight fit between shaft and hub ($D = 0.0025$ in.).

4.2.1.3. Shear deflection of Shaft Support. The keyseat can be modeled as a cantilever beam with variable depth (Fig. 4.10). The area moment of inertia will be a function of distance along the beam, or

$$I(x) = b[h(x)]^3/12 \quad (4.22)$$

$$\text{where } h(x) = Cx^2 \quad (4.23)$$

The constant, C , can be evaluated by inserting the boundary conditions at $x = d/8$ in equation (4.23). Thus,

$$C = \frac{\sqrt{7} d/8}{(d/8)^2} = \frac{\sqrt{7}}{d/8} \quad (4.24)$$

TABLE 4.1
CONTACT STIFFNESS AS A FUNCTION
OF APPLIED LOAD

<u>Load per Unit Length, lb./in.</u>	<u>Stiffness per Unit Length, lb./in./in.</u>
100	7 250 000
300	8 570 000
500	9 370 000
1000	10 700 000
1500	11 690 000
2000	12 500 000

Substituting equation (4.24) into (4.22) gives

$$I(x) = 1.543bx^6/(d/8)^3 \quad (4.25)$$

The shear energy is given by

$$U_s = \frac{16(1+\mu)(d/8)^5}{15E} \int \left[\frac{V}{I} \right]^2 dx \quad (4.26)$$

where

$$V/I = 3P(d/8)^3/(1.543bx^6) \quad (4.27)$$

over the interval $(d/6) \leq x \leq (d/4)$.

Substituting equation (4.27) into (4.26) and integrating yields

$$U_s = 1.85(1+\mu)P^2/Eb \quad (4.28)$$

deflection under the 3P load is

$$\delta = \partial U_s / \partial P = 3.70(1+\mu)P/Eb \quad (4.29)$$

The stiffness per unit length of key is

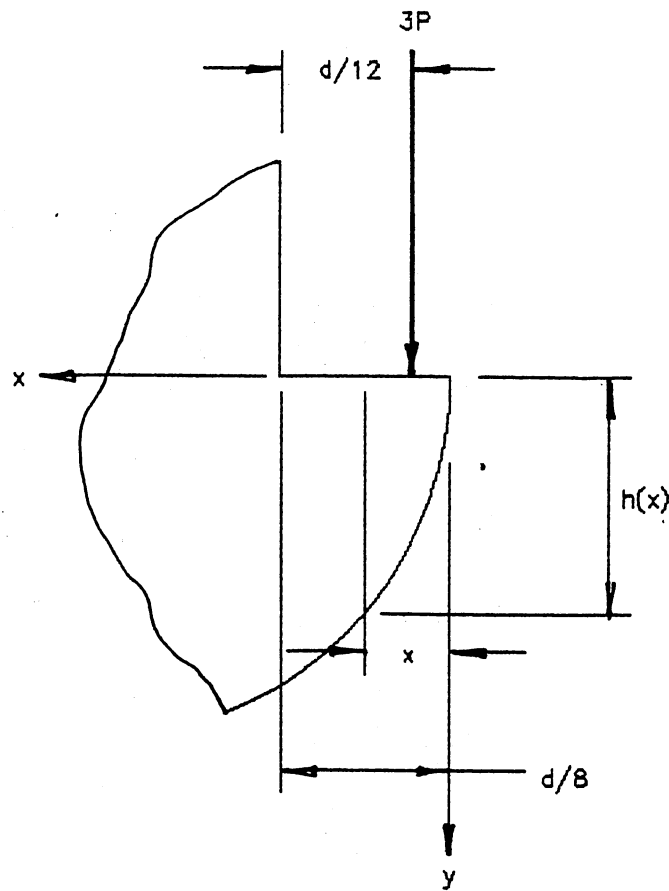


Figure 4.10. Shaft Support for Key

$$k/b = P/\delta b = E/[3.70(1+\mu)] \quad (4.30)$$

which, for steel, is $6.22(10)^6$.

4.2.1.4. Analytic Model Stiffness. Two of the stiffnesses derived above are independent of load while one depends on the load. They are combined by adding the reciprocals of the individual stiffnesses. Thus,

$$1/K_t = 1/K_1 + 1/K_2 + 1/K_3 \quad (4.31)$$

As an example of the total stiffness, assume a load of 500 lb, then

$$(10)^6/k_t = 1/1.2 + 1/9.37 + 1/6.22$$

and

$$k_t = 0.908(10)^9 \text{ lb/in/in}$$

This is approximately twenty times smaller than the stiffness predicted by the model of Section 4.1.1.

4.2.2 Finite Element Model

A two-dimensional finite element model of the shaft, key and hub has been developed. The element mesh is shown in Figure 4.11. Two kinds of elements were used; 2-dimensional isoparametric and 2-dimensional interface or gap elements. The hub, key and shaft are modeled with the isoparametric elements and are connected only by the interface elements. Although the gap elements are capable of modeling a transverse friction force, the analysis would not converge when a non-zero coefficient of friction was used. The initial condition for the model has all clearances equal. Thus, when first loaded, some rigid body motion takes place until the clearances are taken up. This is possible because the gap elements, which normally transmit only compressive forces, can be set to have a very small stiffness in the tensile direction.

Four shaft diameters were modeled: 0.750, 1.000, 1.500, and 2.000 inch. For each diameter there was a tight fit model and a loose fit model for a total of eight different models. Each of the eight models was loaded with thirteen different load steps. The loads applied to each model were the same regardless of size or fit. They were: 10, 100, 300, 500, 1000, 1500, 2000, 3000, 5000, 10000, 15000, 20000, and 30000 lb. The rigid body motion takes place during the first load step of 10 lb.

There are 62 interface elements between the shaft and hub. The

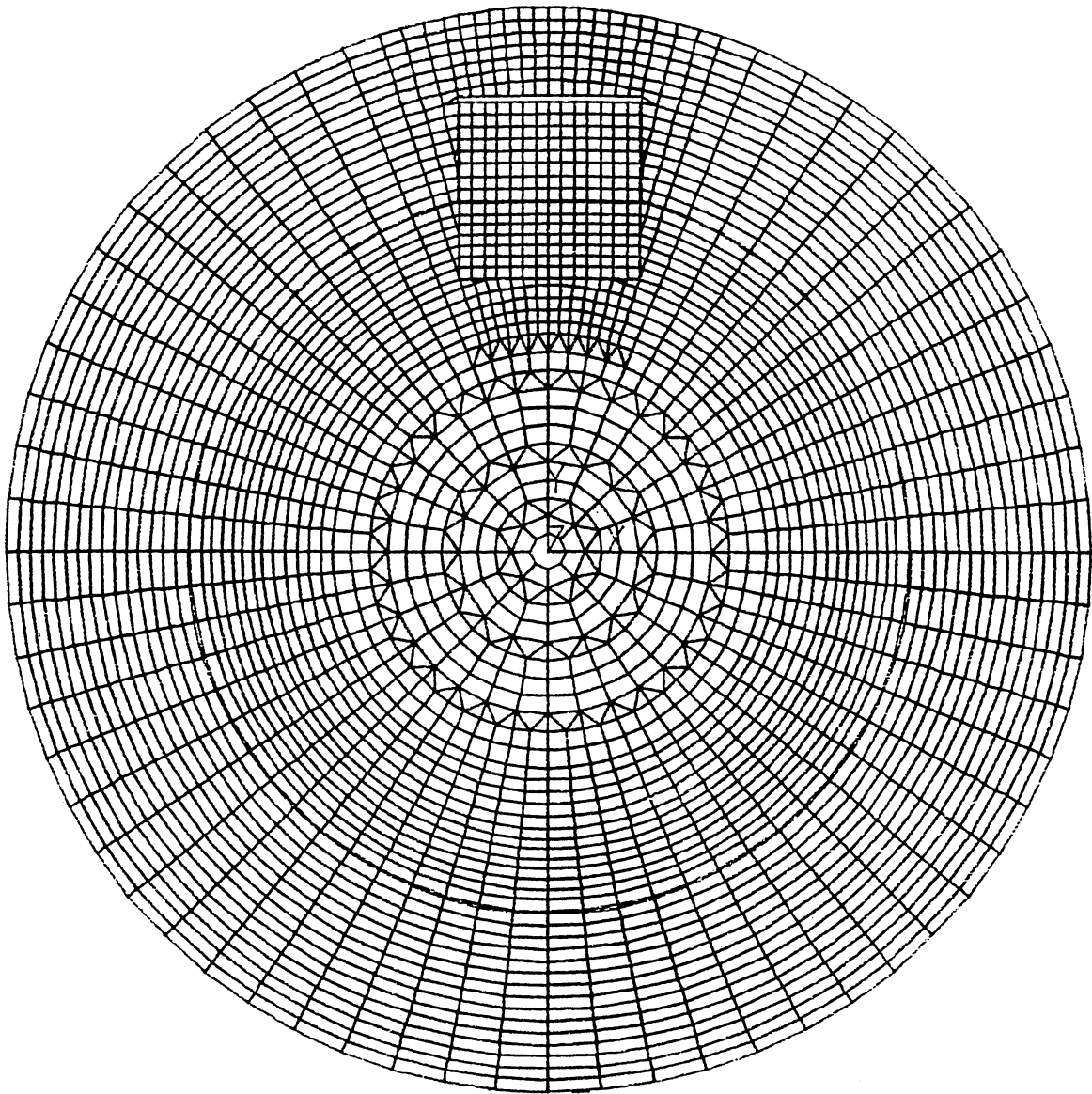


Fig. 4.11. Finite Element Mesh

keyshaft interface has eight interface elements on each side and 14 elements along the bottom. The key-hub interface has nine elements on each side, and 14 elements along the top. Figures 4.12 and 4.13 show an enlargement of the mesh in the key area. Figure 4.12 shows the tight

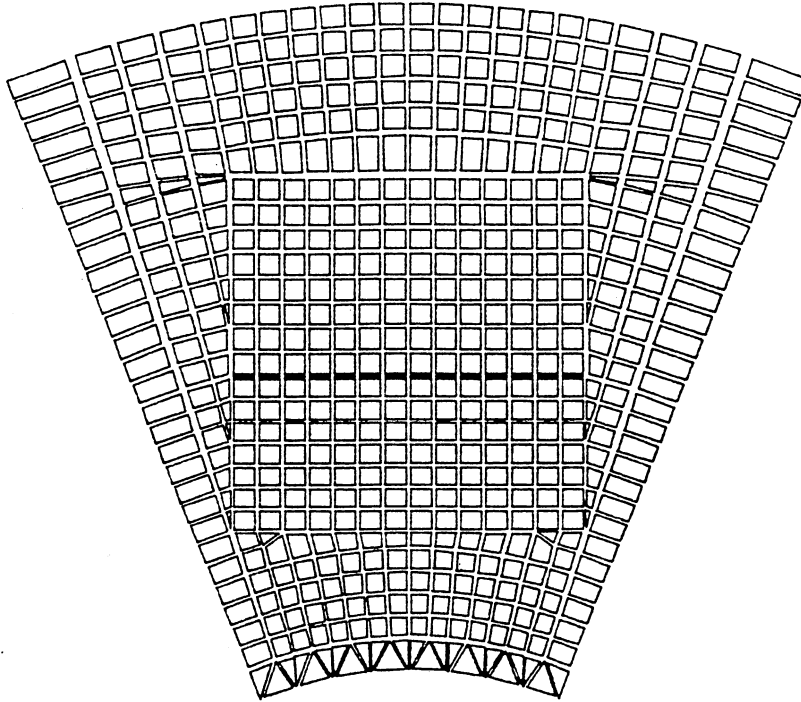


Fig. 4.12. Tight Fit Mesh

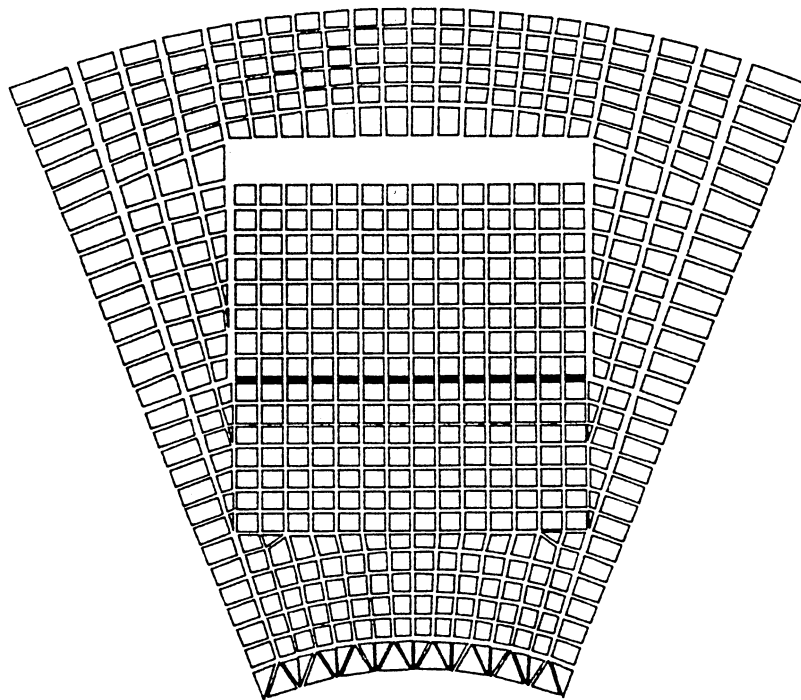


Fig. 4.13. Loose Fit Mesh

Fit and Figure 4.13 shows the loose fit.

The fits represent the extremes that resulted from analysis of the American Gear Manufacturers Association Standard 9002-A86 (1986). The standard covers fits between shaft and hub and between key and hub for keyed flexible couplings. Dimensional data from the standard is summarized in Table 4.2. Although the standard does give tolerances for the key and the keyway in the hub, it does not cover fits between the key and keyseat in the shaft. It was assumed that for the tight fit there would be a total interference between key and keyseat of 0.002 in. and a snug fit for the loose case. The various fit dimensions used are given in Table 4.3.

Torques were applied to the model by putting equal and opposite forces on the two nodes on the hub outside diameter that are on the plus and minus x-axis. The shaft was prevented from rotating by fixing all of the nodes on the smallest inside circle on the shaft (which is, in fact, hollow at that point). The first load-step of 10 lb. was introduced to take up the gaps and bring the assembly to a position of static equilibrium.

4.2.2.1 Hub Rotation. Hub rotation for each run and load step was determined from the deflections of the seven nodes on the hub that are just above the key on the positive y-axis. The nodes were on a straight line before loading and, essentially, stayed on a straight but rotated line after loading. The calculated angle of rotation is the angle between the rotated line made by these seven nodes and the y-axis (see Fig. 4.14). The rigid body rotation angle was calculated for each run from the results of load step number one. This value was then subtracted from the angle calculated for each load step (2 through 13)

TABLE 4.2
AGMA 9002-A86 (1986)
SHAFT/HUB FITS

Nominal Shaft Diameter	Shaft Tolerance (Minus)	Bore Tolerance (Plus)	
		Class I	Class II
0.750	0.0005	0.0010	0.0020
1.000	0.0005	0.0010	0.0020
1.500	0.0005	0.0010	0.0020
2.000	0.0010	0.0010	0.0020

KEY/KEYWAY FITS

Nominal Shaft Diameter	Square Key Size	Key Tolerance (Width and Height)		Keyway Width Tolerance
		Commercial	Precision	
0.750	0.1875	+0.000/-0.002	+0.001/-0.000	+0.0030
1.000	0.2500	+0.000/-0.002	+0.001/-0.000	+0.0030
1.500	0.3750	+0.000/-0.002	+0.001/-0.000	+0.0035
2.000	0.5000	+0.000/-0.002	+0.001/-0.000	+0.0040

TABLE 4.3
CLEARANCE/INTERFERENCE FOR KEYED JOINT ANALYSIS

<u>Run No.</u>	<u>Shaft Dia.</u>	<u>Shaft/Hub Clearance (Radial)</u>	<u>Hub/Key Clearance (per side)</u>	<u>Key Top Clearance (Total)</u>	<u>Shaft/Key Interference (Total)</u>
0751	0.750	0.00075	0.0010	0.001	0.002
0752	0.750	0.00125	0.0025	0.023	0.000
1001	1.000	0.00075	0.0010	0.001	0.002
1002	1.000	0.00125	0.0025	0.023	0.000
1501	1.500	0.00075	0.0010	0.001	0.002
1502	1.500	0.00125	0.0028	0.023	0.000
2001	2.000	0.00100	0.0010	0.001	0.002
2002	2.000	0.00150	0.0030	0.023	0.000

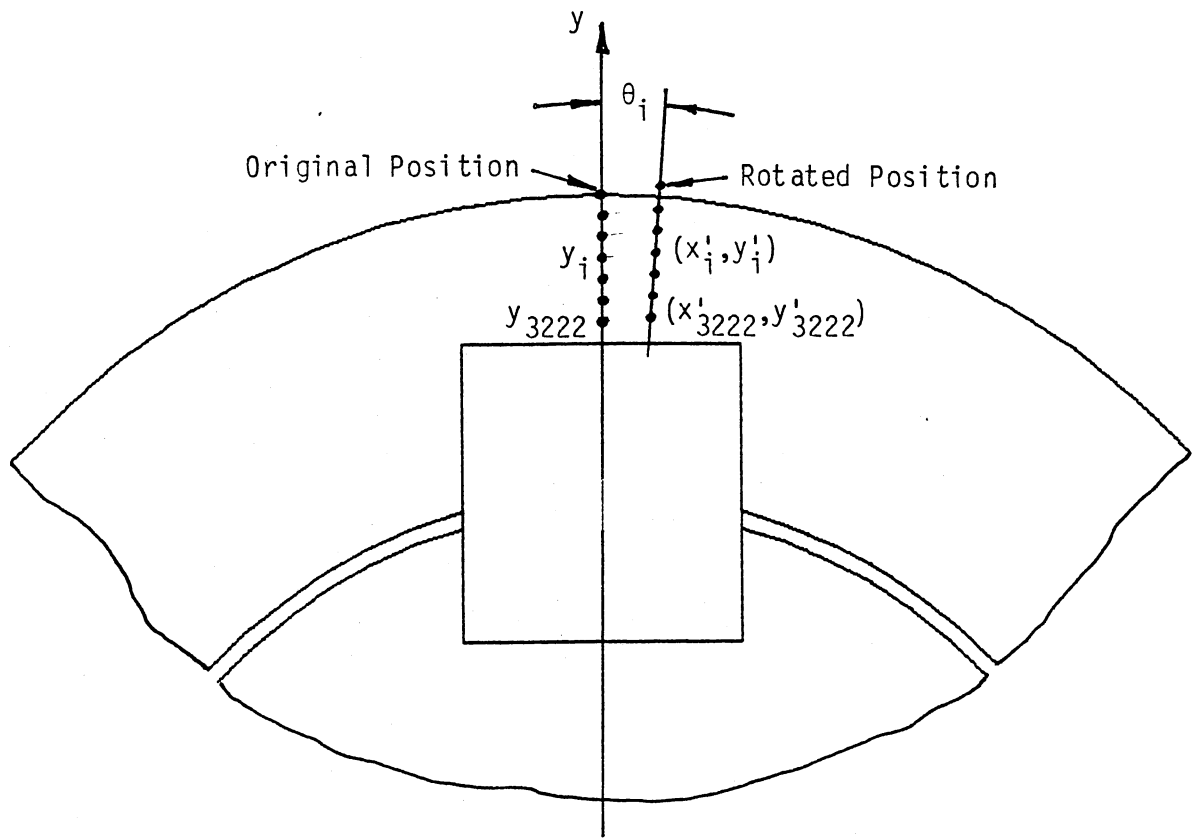


Fig. 4.14. Location of Nodes Used for Hub Rotation Calculation

for that run (diameter and fit condition). The average value of the calculated angles was used to calculate the stiffness for the load step. Using the symbols in Fig. 4.14, the procedure for calculating the rigid body angle is:

1. Read the deflections for the seven nodes from load step 1.
2. Add the original y components to the y deflections to determine the new position coordinates for the seven points.

3. Starting with the second point, calculate the angle that the line through the i th point and the first point makes with the y -axis.
4. The average of these six angles is the rigid body rotation angle.

Mathematically,

$$\theta_i = \arctan \left(\frac{x_i - x_{3222}}{y_i - y_{3222}} \right) \quad (4.32)$$

and

$$\theta_{\text{rigid}} = (1/6) \sum \theta_i \quad (4.33)$$

The procedure for finding the rotation due to loading is similar except that, in step three above, the rigid body angle for that run is subtracted from the calculated angle before the angles are averaged. Table 4.4 gives the x, y coordinates for the seven nodes of run 1001 for the following three conditions: 1) initial (before any loading), 2) after rigid body rotation (load step one), and 3) after a load of 3000 lb (4500 lb-in, load step 8). Table 4.5 shows the calculated angles of step three above for the same run. Similar data was analyzed for each of the 96 different load runs.

4.2.2.2 Joint Stiffness. The angular stiffness for each run was calculated by dividing the applied torque by the average rotation angle. A lineal stiffness was then calculated by dividing the angular stiffness by the square of the nominal shaft radius. Lineal stiffness has been plotted as a function of nominal shear load (torque divided by shaft radius) on the key in Figures 4.15, 4.16 and 4.17. Figure 4.15 shows the results of the tight fits for all diameters, while Figure 4.16 shows the results for all of the loose fits. Figure 4.17 gives a comparison

TABLE 4.4

POSITION DATA FOR 1.000 IN DIAMETER, TIGHT FIT RUN
USED TO CALCULATE ROTATION OF HUB

Node	Initial		After Rigid Body Rot.*		Loaded**	
	X	Y	X	Y	X	Y
3222	0.0	0.62600	1.02343E-03	0.626015	0.03674	0.62724
3243	0.0	0.65713	1.09483E-03	0.657145	0.03885	0.65834
3264	0.0	0.67570	1.13741E-03	0.675715	0.04009	0.67690
3285	0.0	0.69428	1.17999E-03	0.694295	0.04134	0.69546
3306	0.0	0.71285	1.22251E-03	0.712865	0.04259	0.71402
3327	0.0	0.73143	1.26514E-03	0.731445	0.04384	0.73259
3348	0.0	0.75000	1.30773E-03	0.750015	0.04509	0.75116

All dimensions are inches

* 15 lb-in load

** 4500 lb-in load

TABLE 4.5

CALCULATED HUB ROTATION ANGLES 1.000 IN DIAMETER
TIGHT FIT LOAD STEPS 1 AND 8 (RADIAN)

Node	Rigid Body	4500 lb-in
3243	0.0022936	0.06536
3264	0.0022934	0.06517
3285	0.0022928	0.06506
3306	0.0022928	0.06500
3327	0.0022926	0.06499
3348	0.0022927	0.06503
Average	0.0022930	0.06510

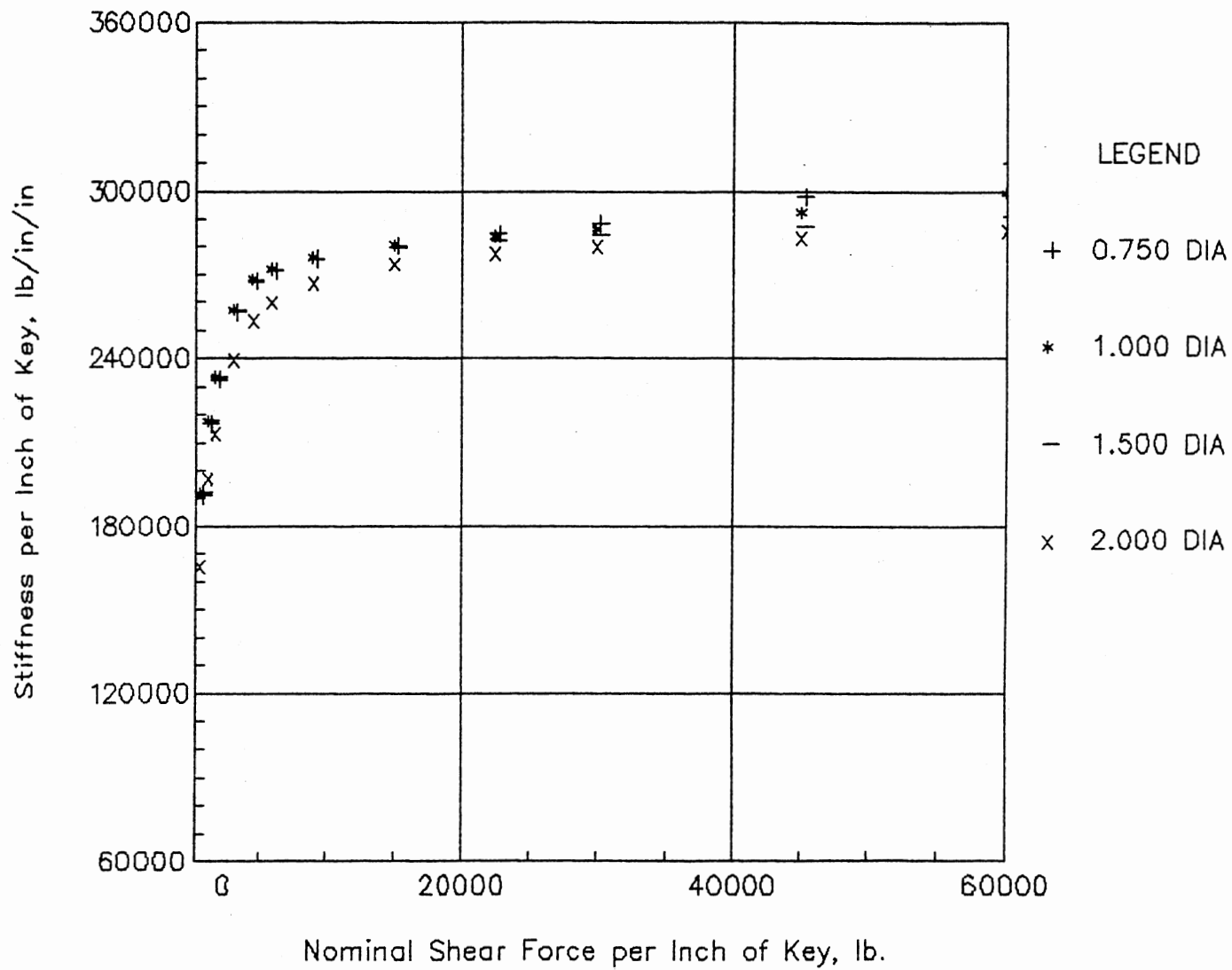


Fig. 4.15. Stiffness vs. Deflection, Tight Fits

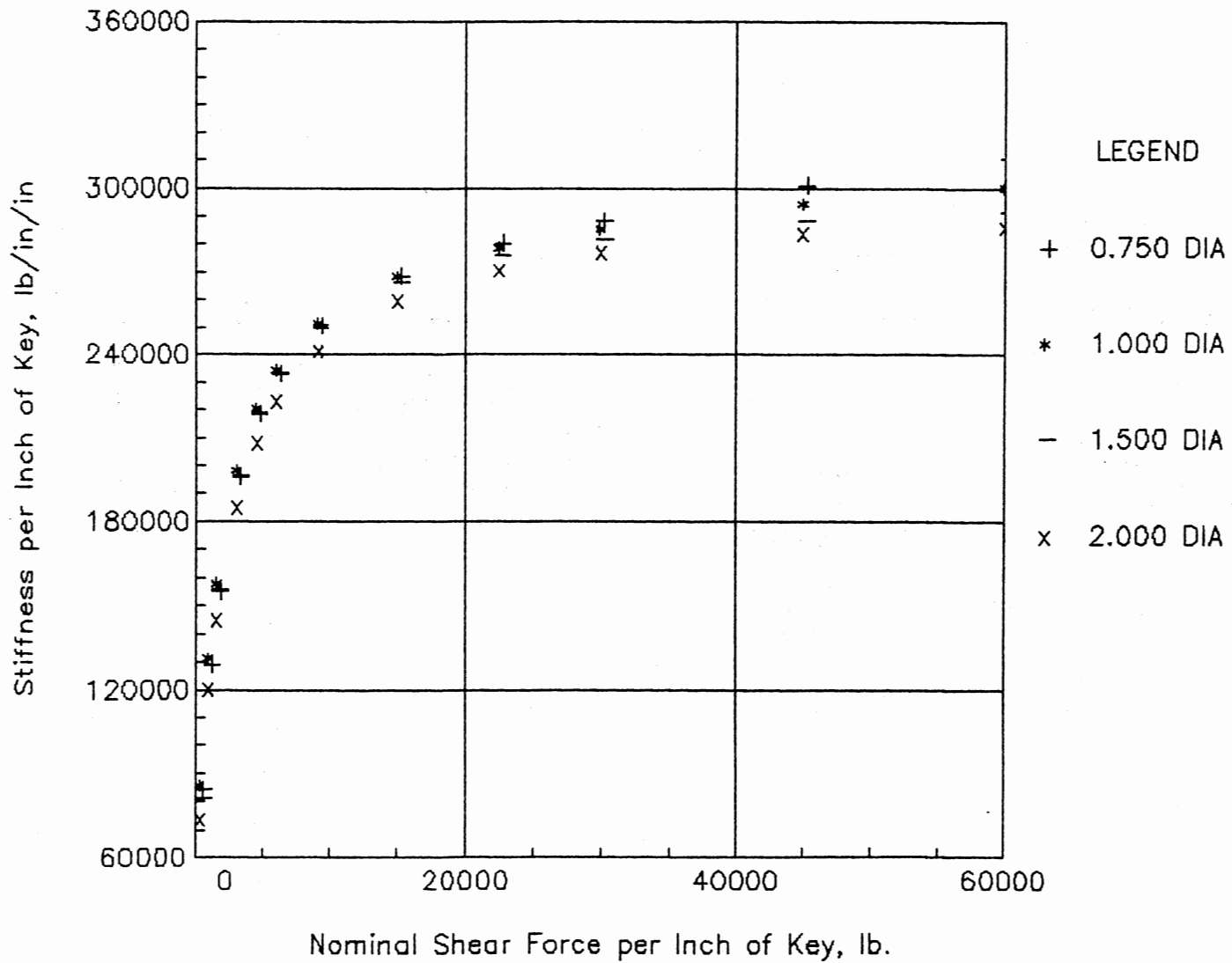


Fig. 4.16. Stiffness vs. Deflection, Loose Fits

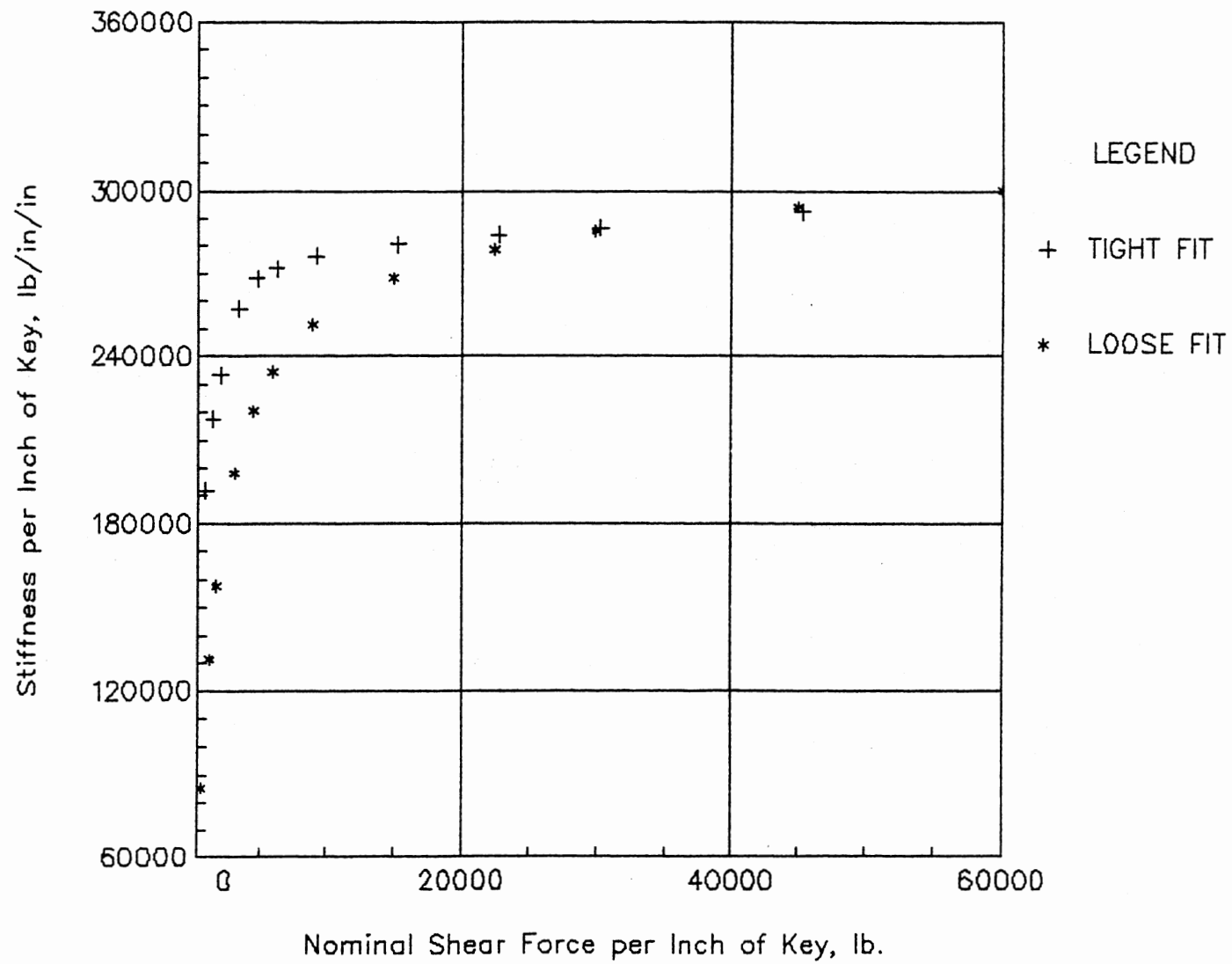


Fig. 4.17. Stiffness vs. Deflection, 1.000 in Diameter

of the tight and loose fit for a 1.000 in diameter shaft.

The stiffnesses predicted by this model are about one third of those predicted in Section 4.2.1 above. On the one hand, you might expect a finite element model to give a stiffer response than the actual structure modeled. On the other hand, the analytic model was obviously lacking in detail and did not account for all of the deflection components. The analytic model did predict a load dependent component as well as a constant term. The finite element results clearly show this. The difference between the tight and loose fit results seems to be that in the loose case some motion of the key takes place that doesn't occur in the tight case. Both cases appear to converge on the same value at high load. The results are based on a completely elastic response of the components to the applied loads. There will, however, be local plastic deformation under the high loads, especially at the lower end of the diameter range. An attempt was made to allow for a nonlinear stress-strain relationship but the analysis would not converge when this complexity was added.

That the key does rotate under load can be seen by inspection of Figures 4.18 through 4.41. These figures show, graphically, the force distribution on the key and on the inside surface of the hub. Note that the drawing scale for the key and hub are the same for all 24 figures, but the force scale is not. These figures summarize the force data, taken from the interface elements, from each of the load cases for the 1.000 in diameter, tight and loose cases. Recall, from Table 4.3, that the clearance above the key was 0.001 in for the tight case and 0.023 in for the loose case. Now, looking at Figures 4.18 through 4.29 (the tight case loading), you can see that a substantial reaction develops

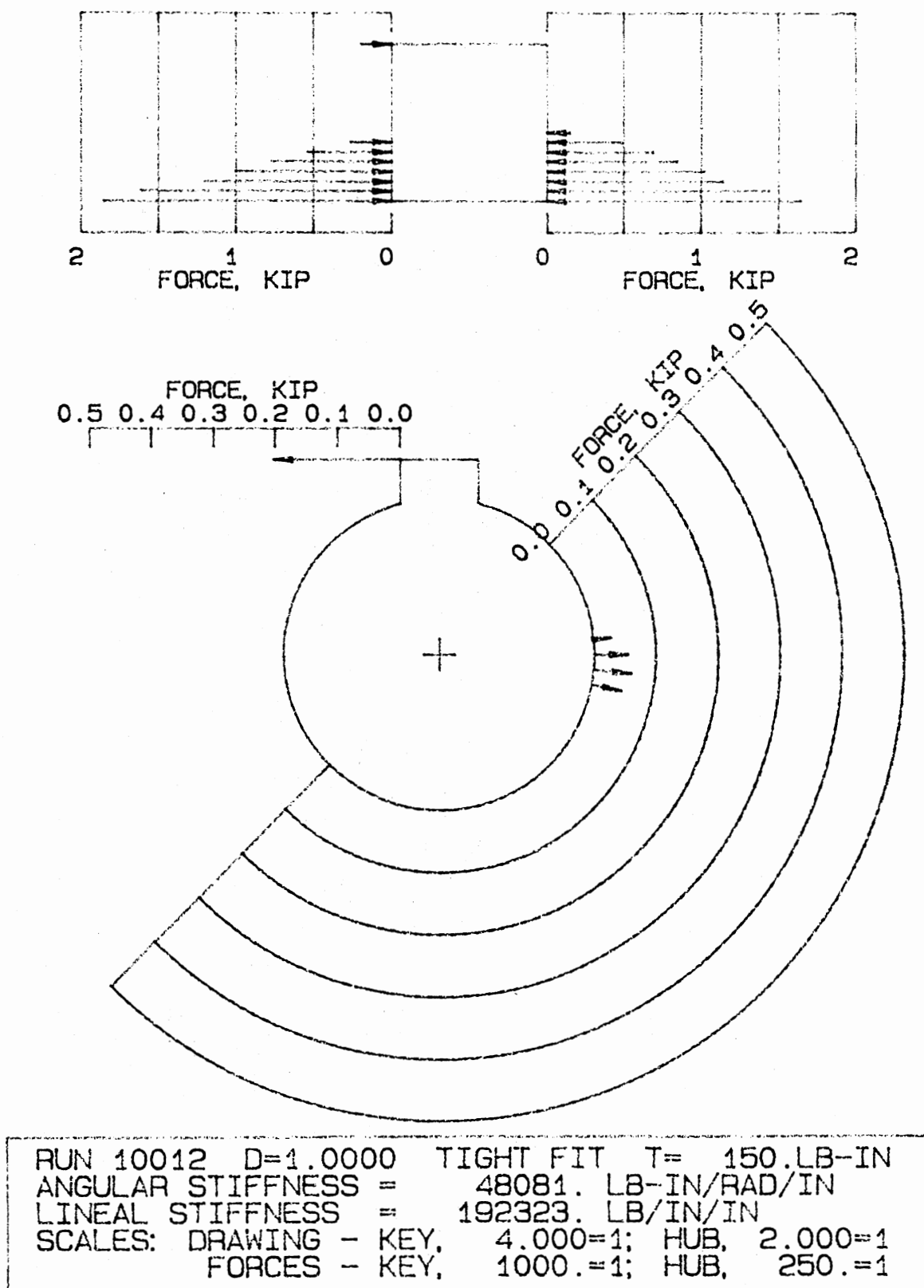
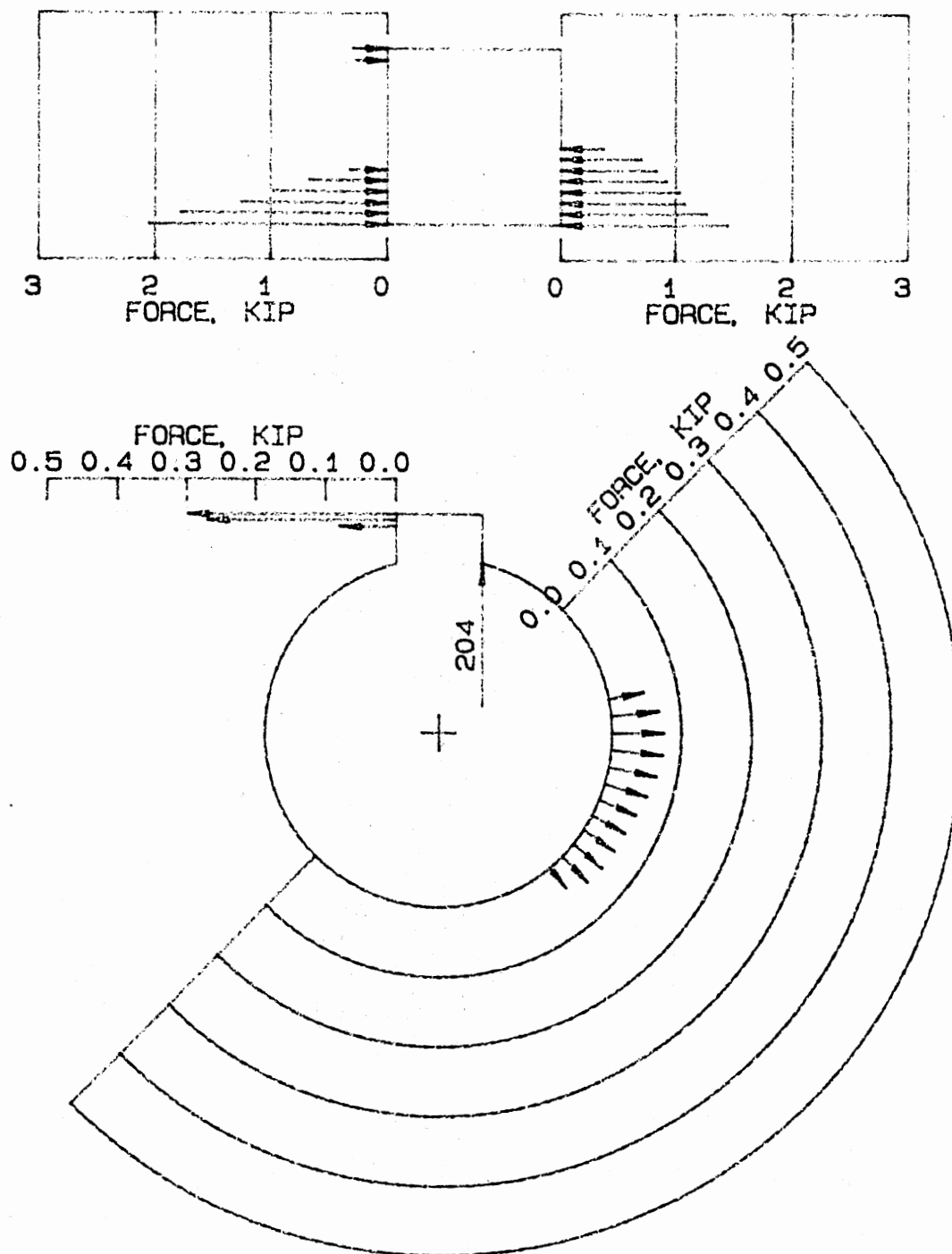
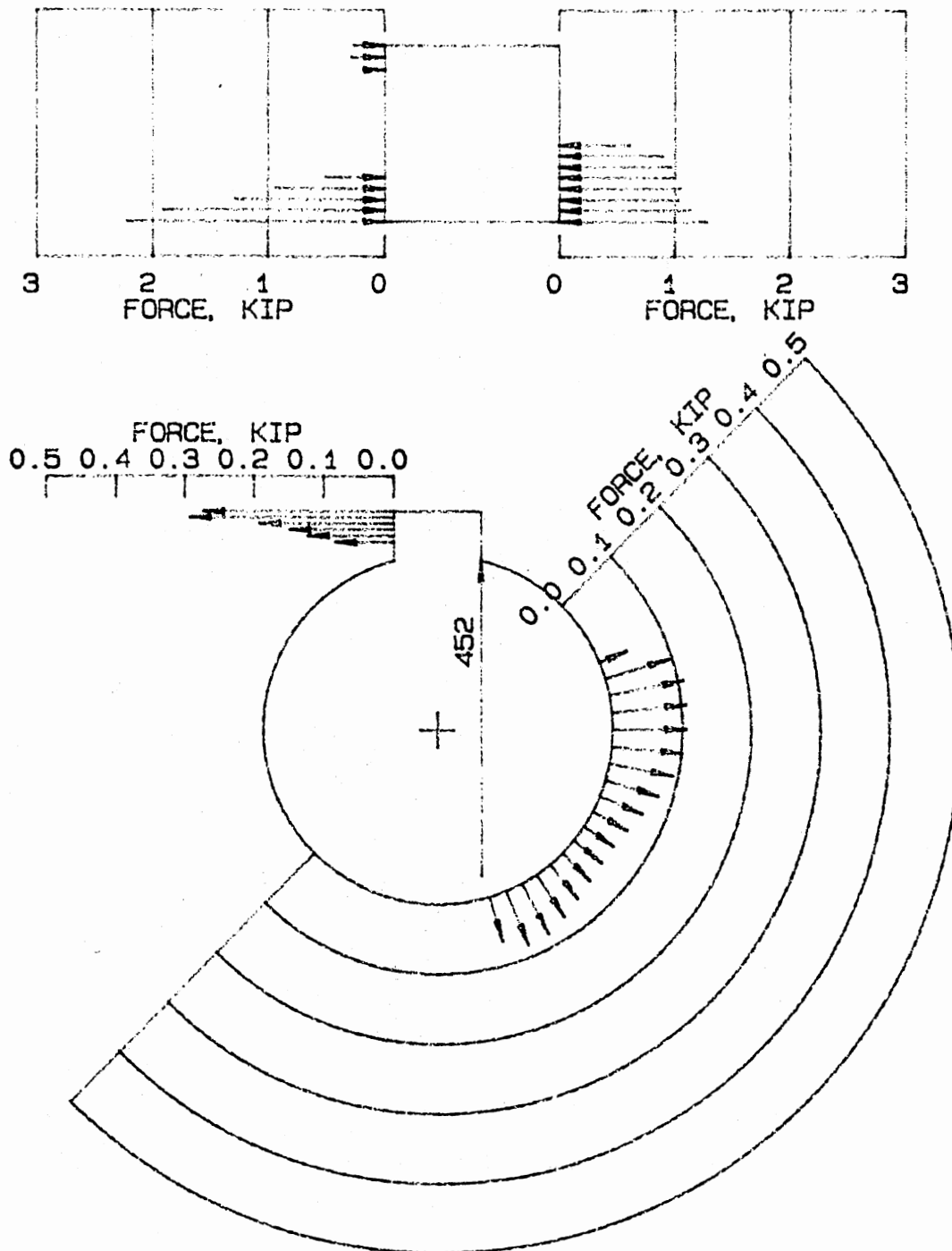


Fig. 4.18. Key and Hub Force Distribution, Tight Fit, 150 lb-in



RUN 10013 D=1.0000 TIGHT FIT T= 450.LB-IN
 ANGULAR STIFFNESS = 54509. LB-IN/RAD/IN
 LINEAL STIFFNESS = 218035. LB/IN/IN
 SCALES: DRAWING - KEY, 4.000=1; HUB, 2.000=1
 FORCES - KEY, 1500.=1; HUB, 250.=1

Fig. 4.19. Key and Hub Force Distribution, Tight Fit, 450 lb-in



RUN 10014 D=1.0000 TIGHT FIT T= 750.LB-IN
 ANGULAR STIFFNESS = 58412. LB-IN/RAD/IN
 LINEAL STIFFNESS = 233650. LB/IN/IN
 SCALES: DRAWING - KEY, 4.000=1; HUB, 2.000=1
 FORCES - KEY, 1500.=1; HUB, 250.=1

Fig. 4.20. Key and Hub Force Distribution, Tight Fit, 750 lb-in

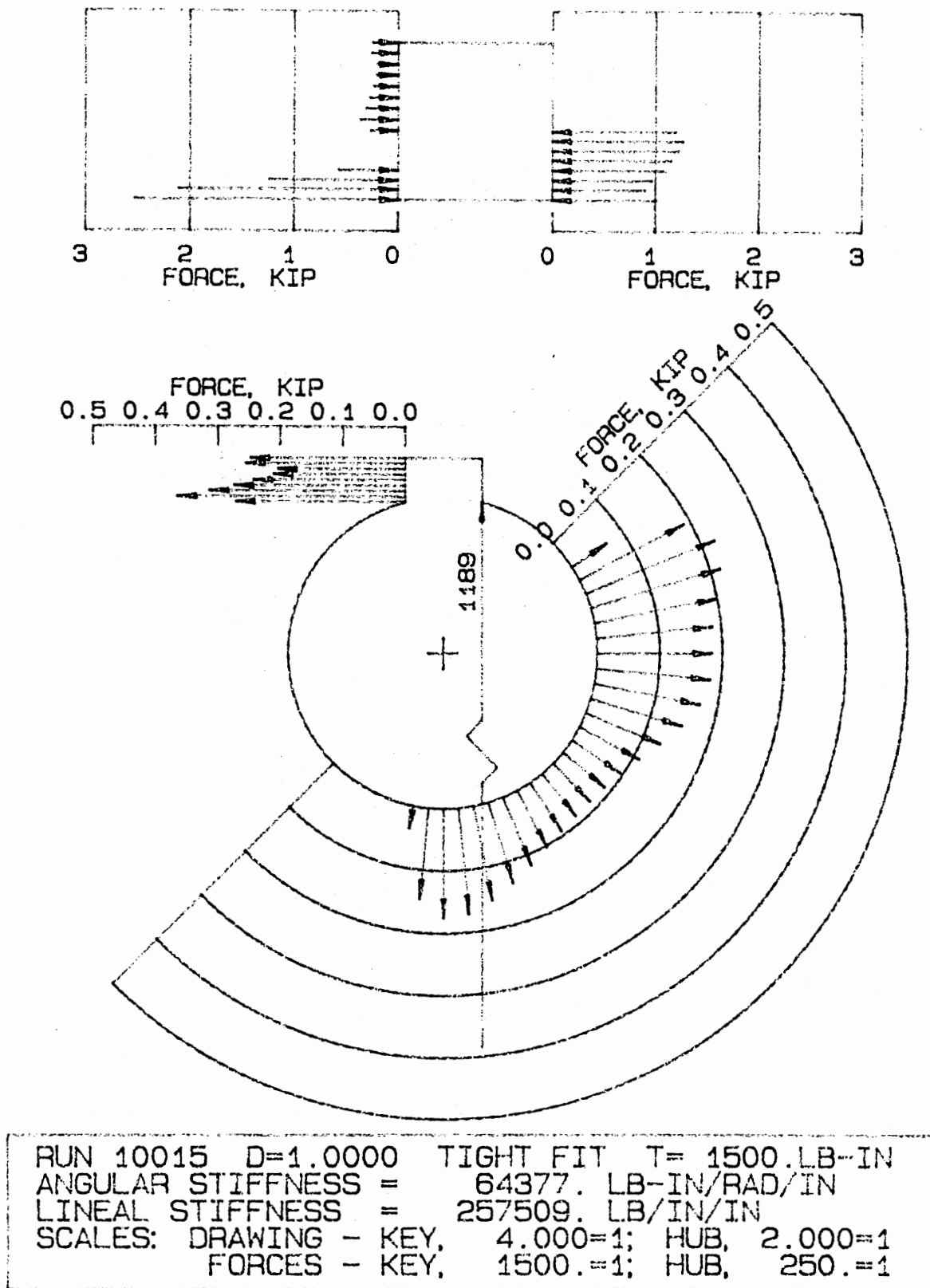
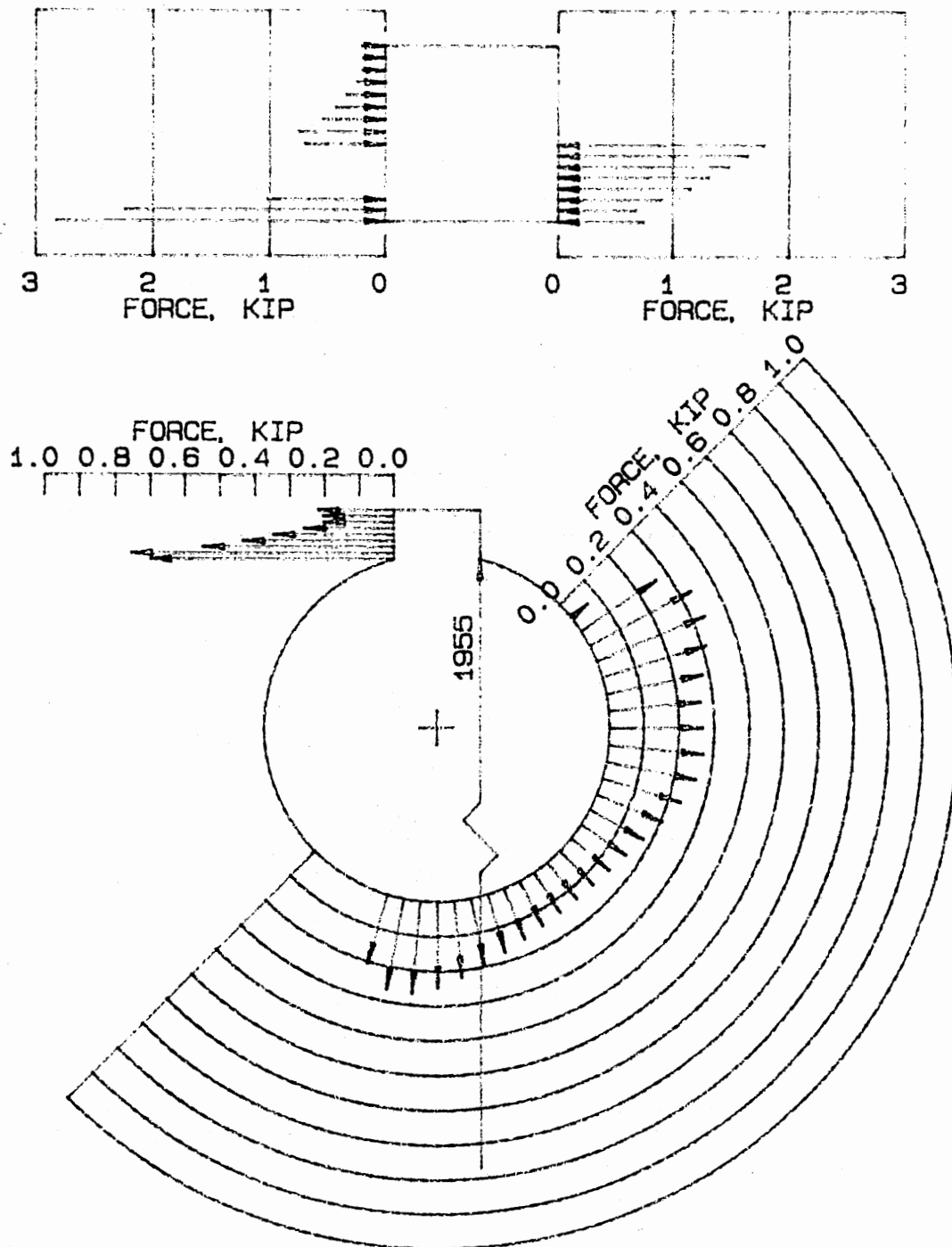
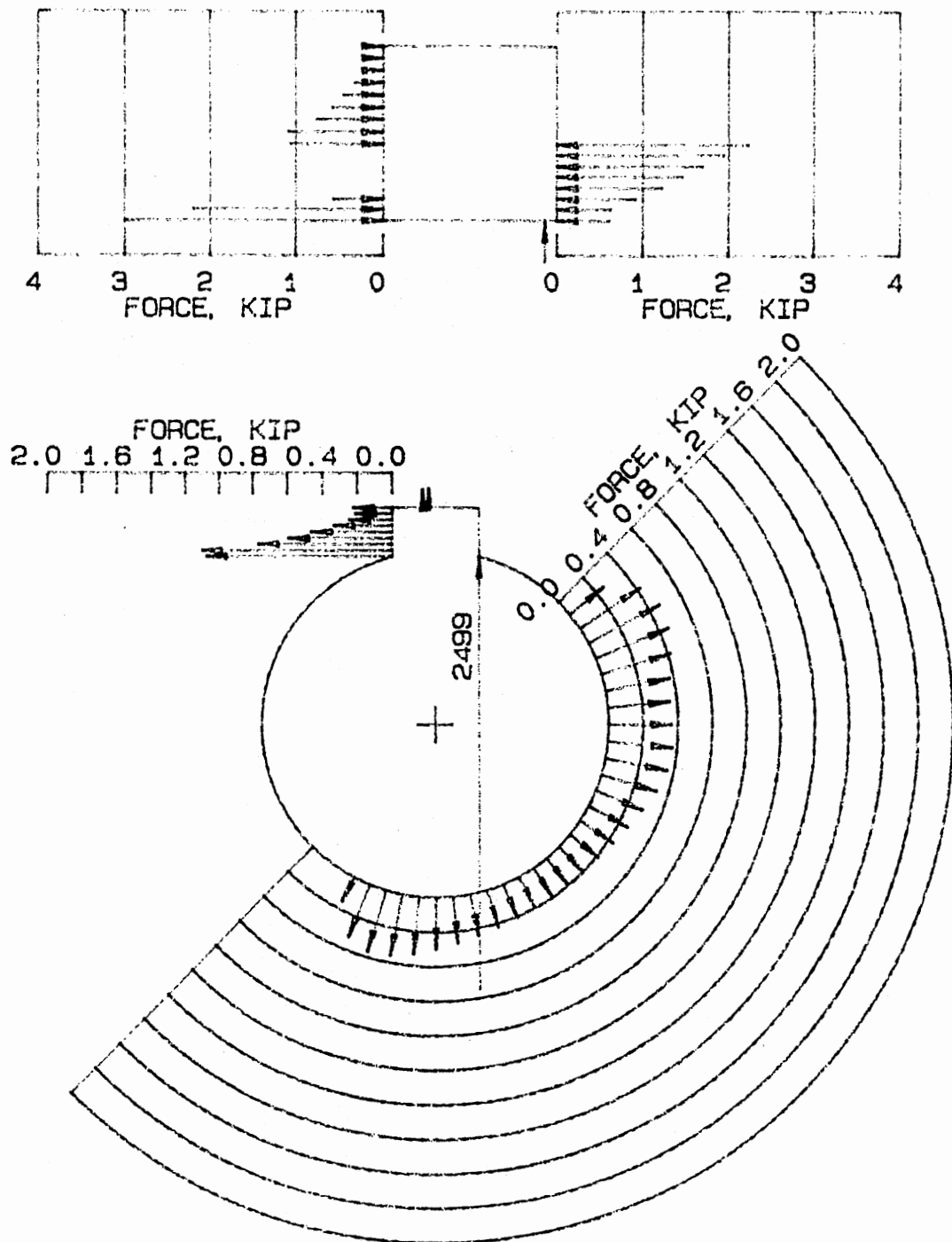


Fig. 4.21. Key and Hub Force Distribution, Tight Fit, 1500 lb-in



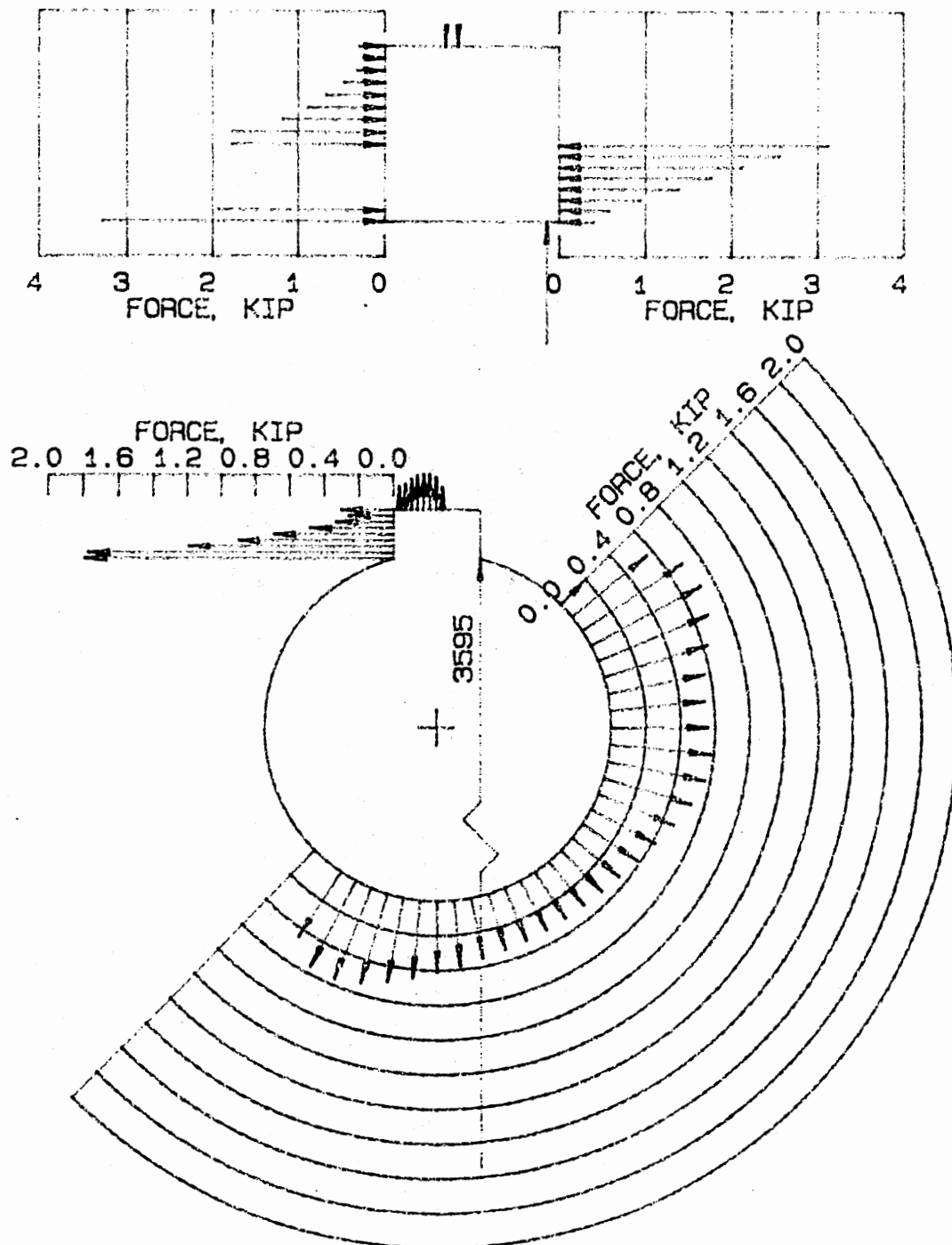
RUN 10016 D=1.0000 TIGHT FIT T= 2250.LB-IN
 ANGULAR STIFFNESS = 67145. LB-IN/RAD/IN
 LINEAL STIFFNESS = 268579. LB/IN/IN
 SCALES: DRAWING - KEY, 4.000=1; HUB, 2.000=1
 FORCES - KEY, 1500.=1; HUB, 500.=1

Fig. 4.22. Key and Hub Force Distribution, Tight Fit, 2250 lb-in



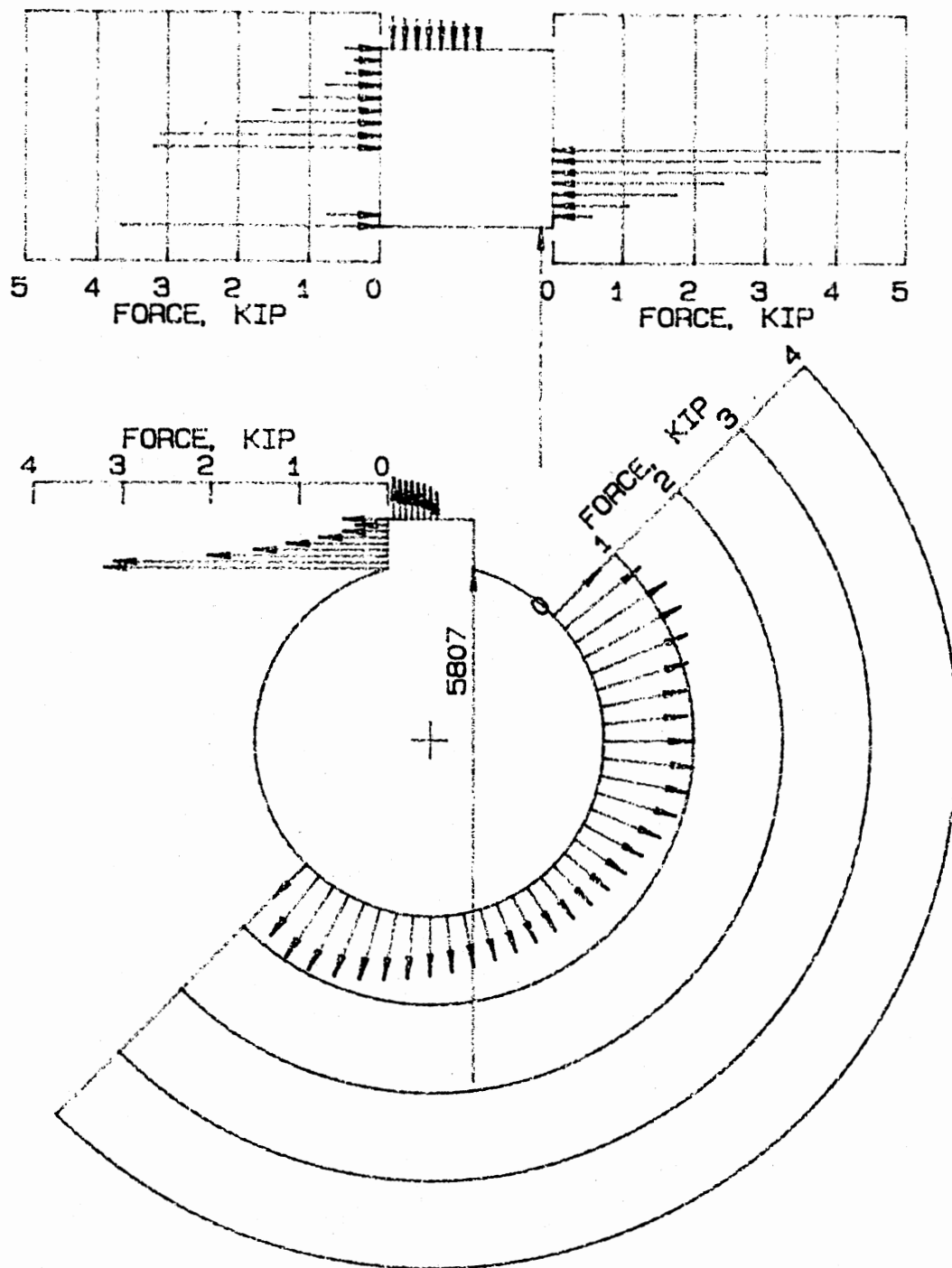
RUN 10017 D=1.0000 TIGHT FIT T= 3000.LB-IN
 ANGULAR STIFFNESS = 68053. LB-IN/RAD/IN
 LINEAL STIFFNESS = 272211. LB/IN/IN
 SCALES: DRAWING -- KEY, 4.000=1; HUB, 2.000=1
 FORCES -- KEY, 2000.=1; HUB, 1000.=1

Fig. 4.23. Key and Hub Force Distribution, Tight Fit, 3000 lb-in



RUN 10018 D=1.0000 TIGHT FIT T= 4500.LB-IN
 ANGULAR STIFFNESS = 69125. LB-IN/RAD/IN
 LINEAL STIFFNESS = 276498. LB/IN/IN
 SCALES: DRAWING - KEY, 4.000=1; HUB, 2.000=1
 FORCES - KEY, 2000.=1; HUB, 1000.=1

Fig. 4.24. Key and Hub Force Distribution, Tight Fit, 4500 lb-in



RUN 10019 D=1.0000 TIGHT FIT T= 7500.LB-IN
 ANGULAR STIFFNESS = 70226. LB-IN/RAD/IN
 LINEAL STIFFNESS = 280903. LB/IN/IN
 SCALES: DRAWING - KEY, 4.000=1; HUB, 2.000=1
 FORCES - KEY, 2500.=1; HUB, 2000.=1

Fig. 4.25. Key and Hub Force Distribution, Tight Fit, 7500 lb-in

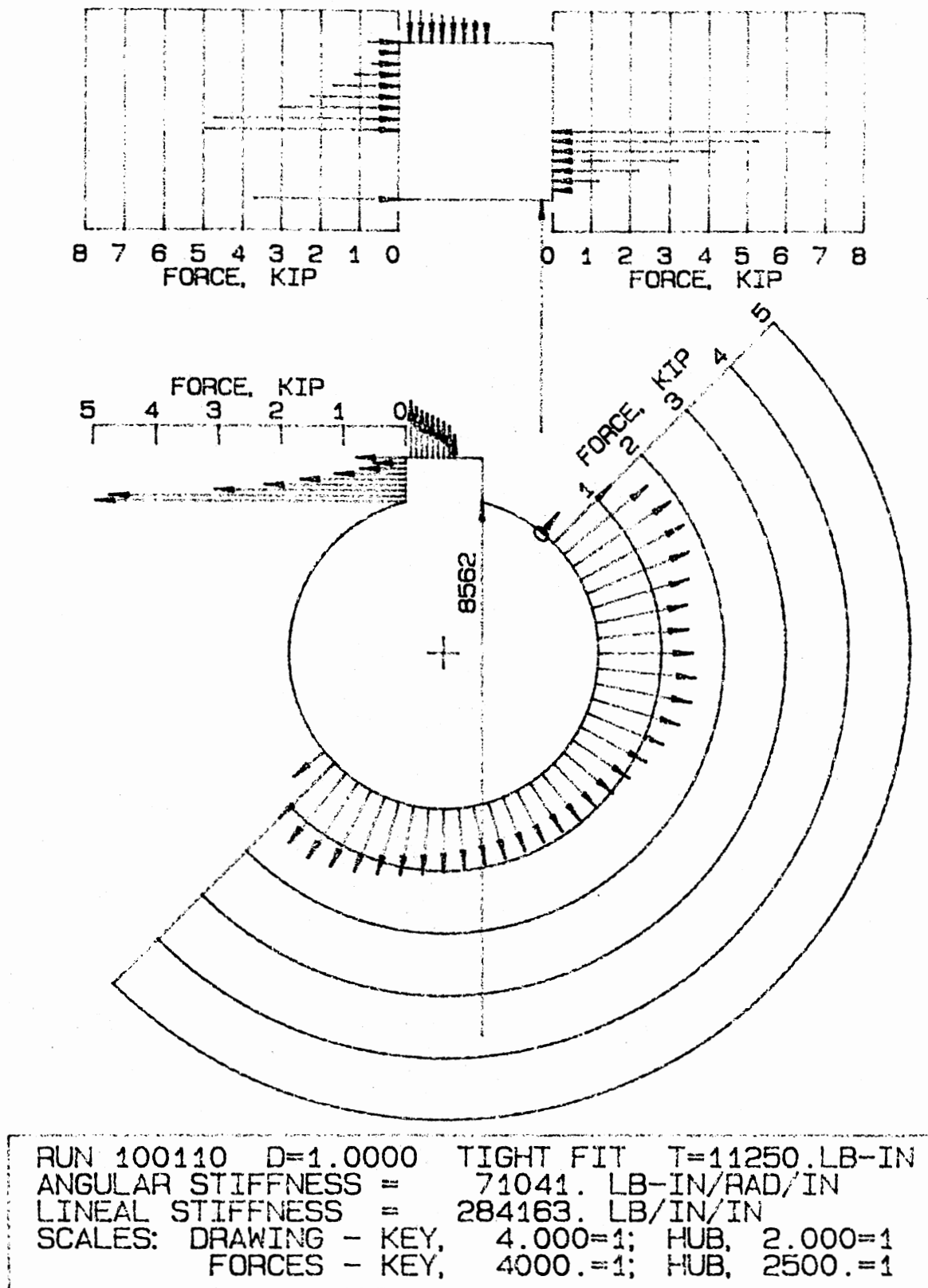


Fig. 4.26. Key and Hub Force Distribution, Tight Fit, 11250 lb-in

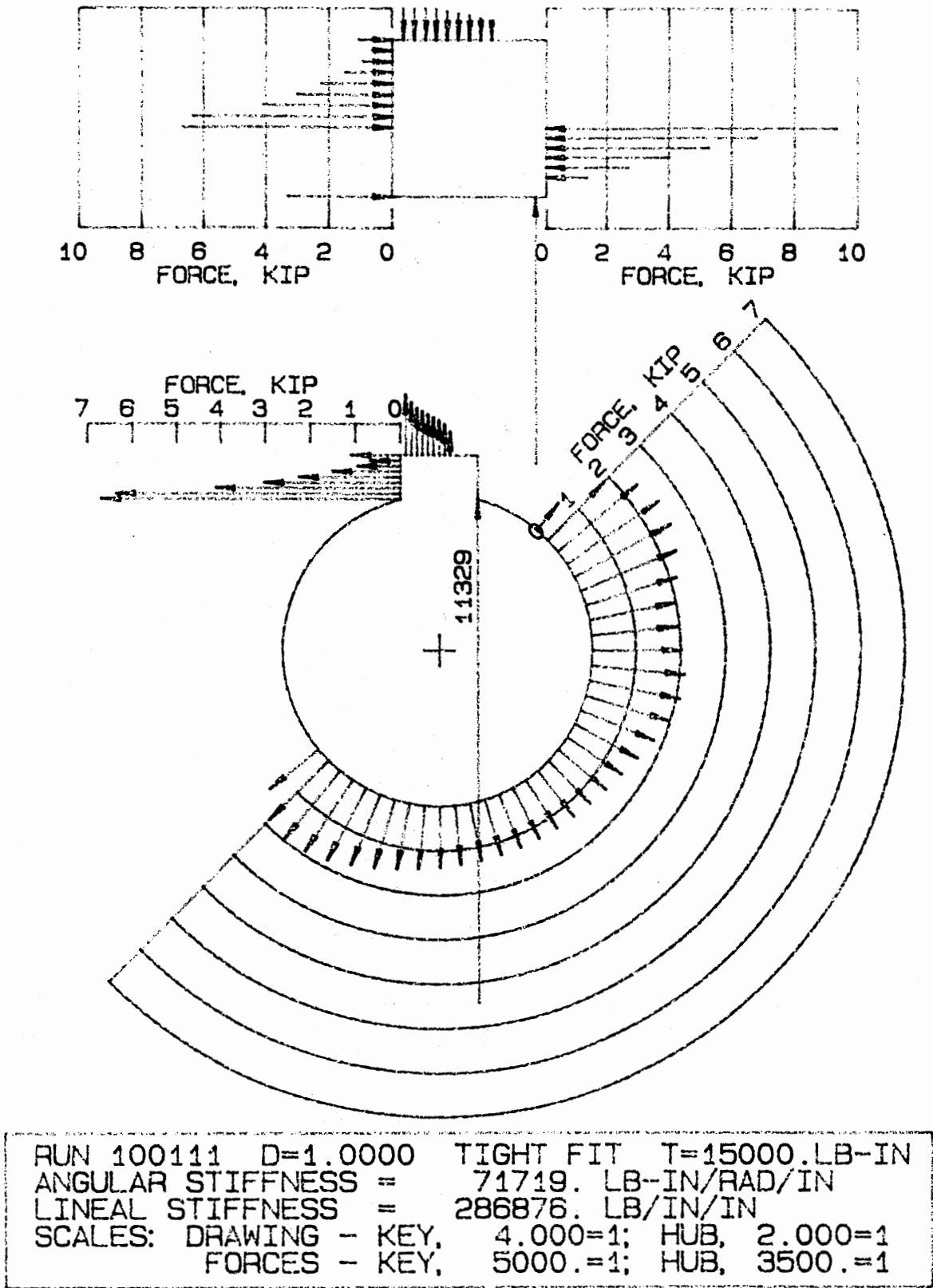
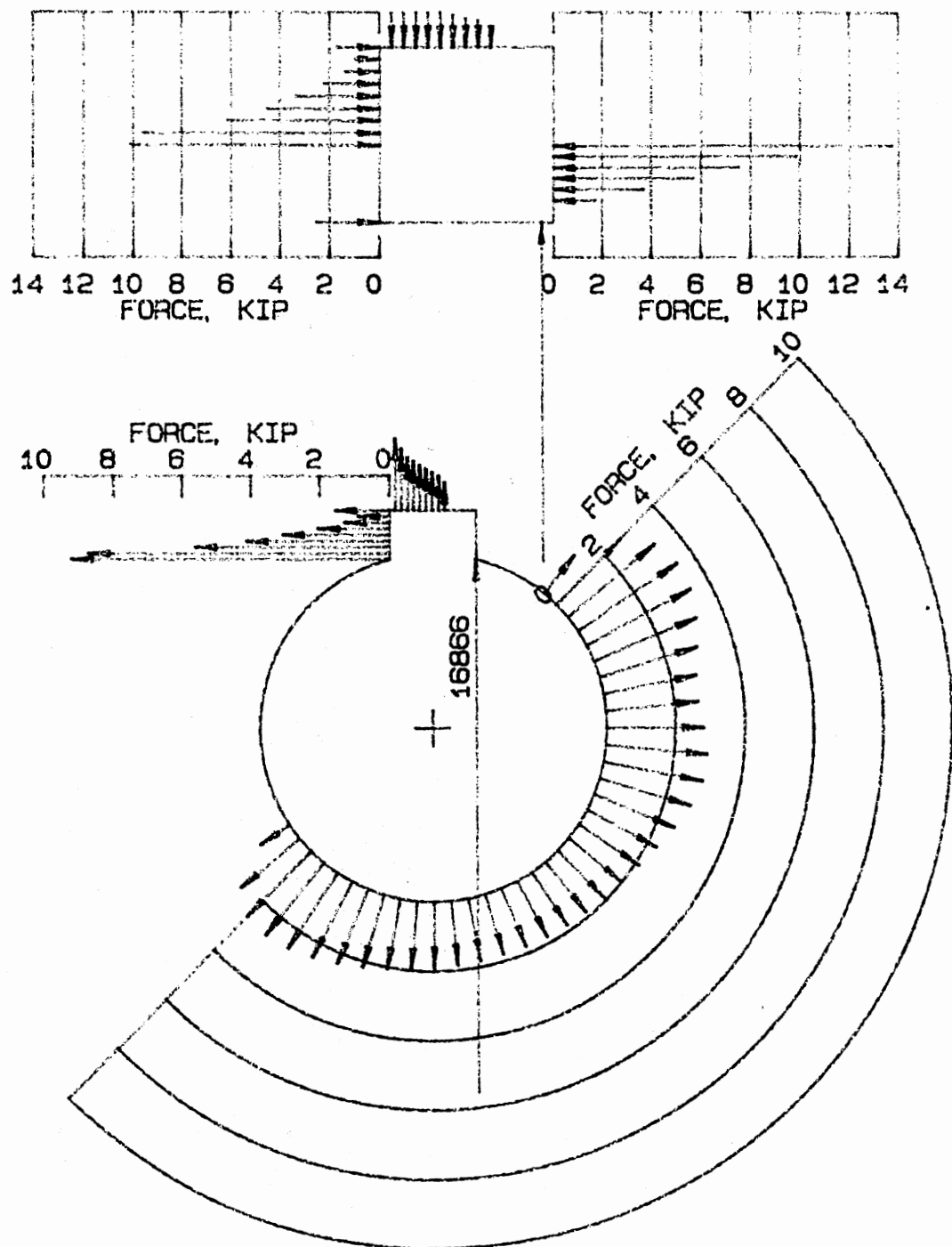
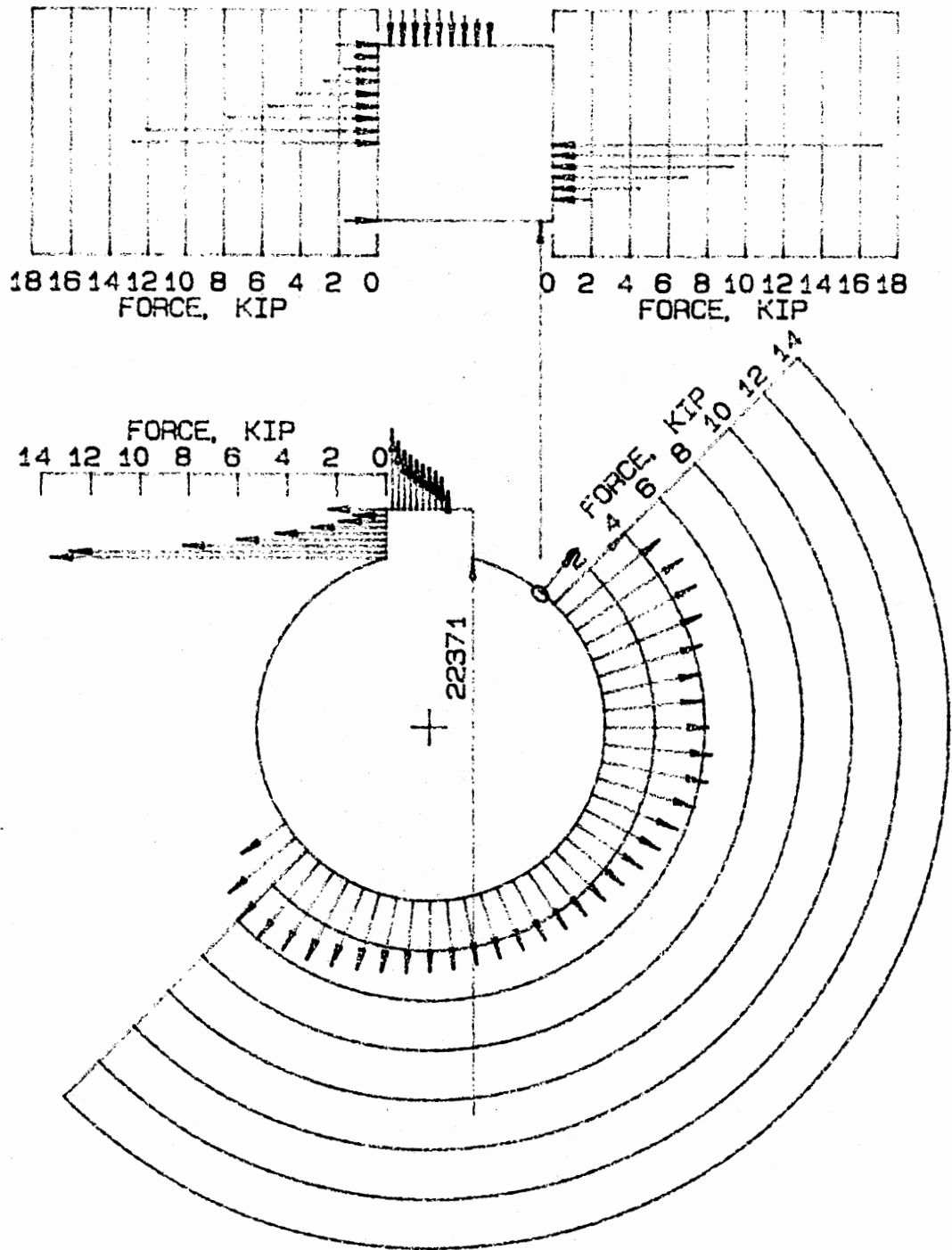


Fig. 4.27. Key and Hub Force Distribution, Tight Fit, 15000 lb-in



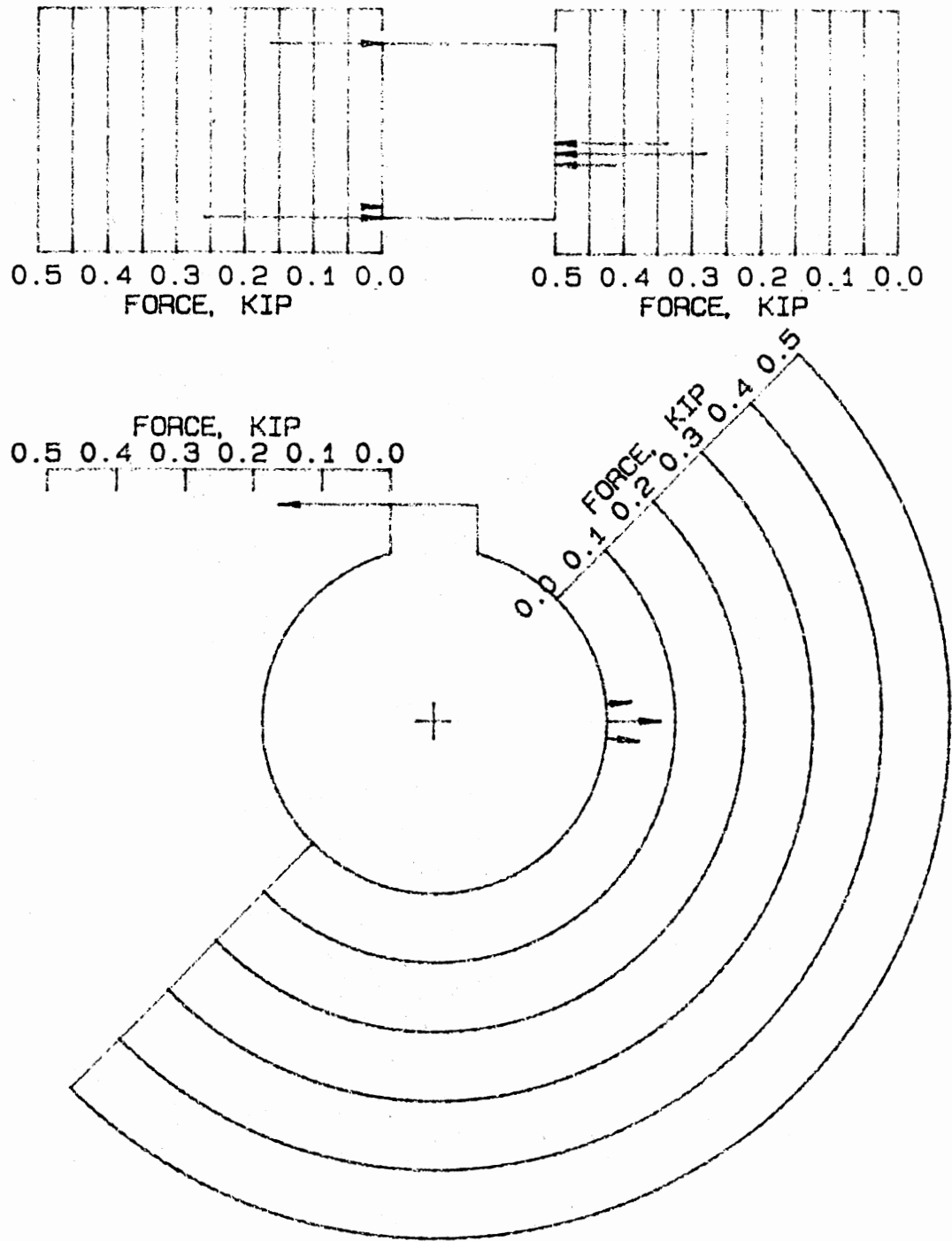
RUN 100112 D=1.0000 TIGHT FIT T=22500.LB-IN
 ANGULAR STIFFNESS = 73182. LB-IN/RAD/IN
 LINEAL STIFFNESS = 292727. LB/IN/IN
 SCALES: DRAWING - KEY, 4.000=1; HUB, 2.000=1
 FORCES - KEY, 7000.=1; HUB, 5500.=1

Fig. 4.28. Key and Hub Force Distribution, Tight Fit, 22500 lb-in



RUN 100113 D=1.0000 TIGHT FIT T=30000.LB-IN
 ANGULAR STIFFNESS = 74944. LB-IN/RAD/IN
 LINEAL STIFFNESS = 299778. LB/IN/IN
 SCALES: DRAWING - KEY, 4.000=1; HUB, 2.000=1
 FORCES - KEY, 9500.=1; HUB, 7000.=1

Fig. 4.29. Key and Hub Force Distribution, Tight Fit, 30000 lb-in



RUN 10022 D=1.0000 LOOSE FIT T= 150.LB-IN
 ANGULAR STIFFNESS = 21448. LB-IN/RAD/IN
 LINEAL STIFFNESS = 85792. LB/IN/IN
 SCALES: DRAWING - KEY, 4.000=1; HUB, 2.000=1
 FORCES - KEY, 250.=1; HUB, 250.=1

Fig. 4.30. Key and Hub Force Distribution, Loose Fit, 150 lb-in

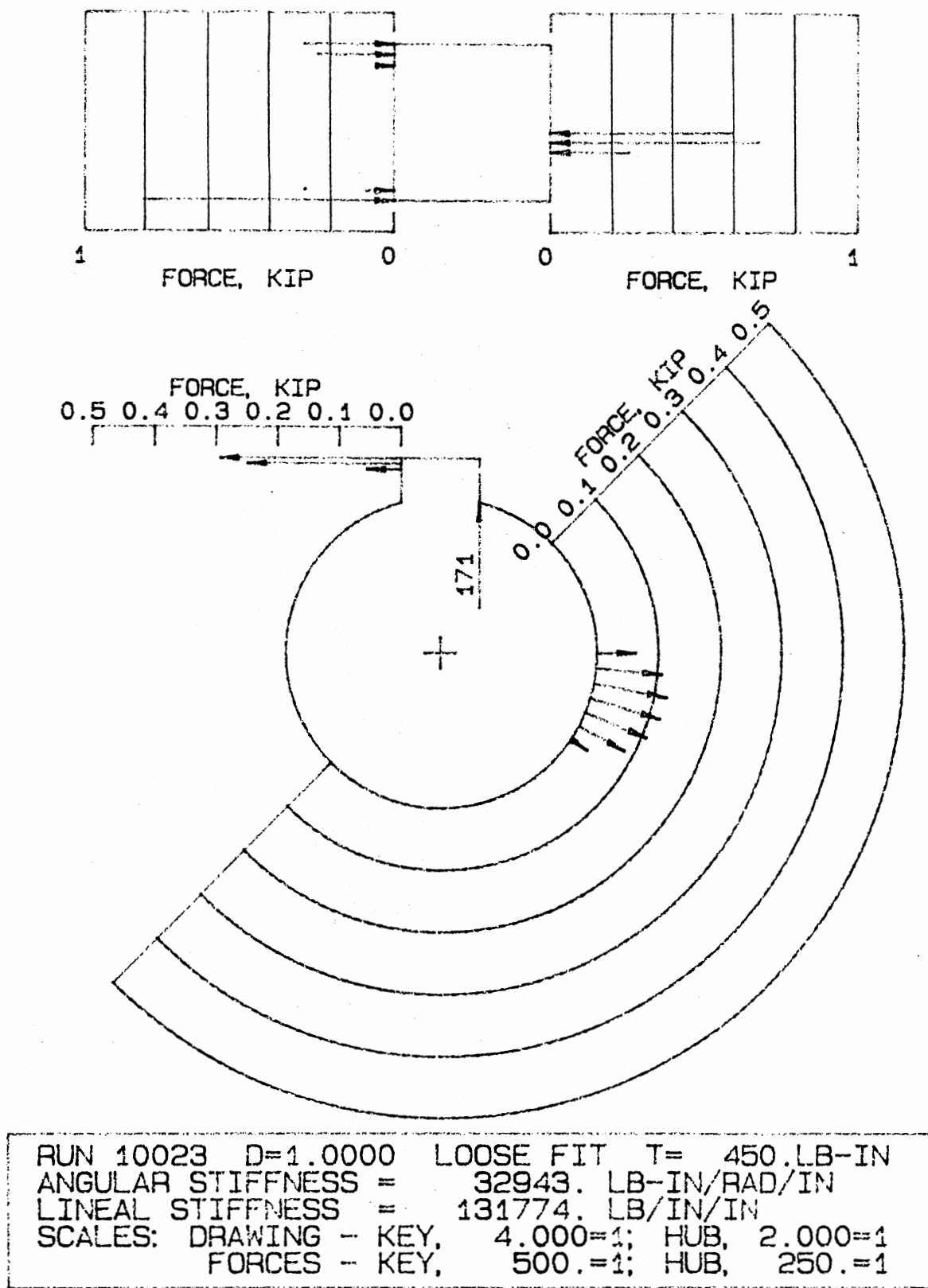
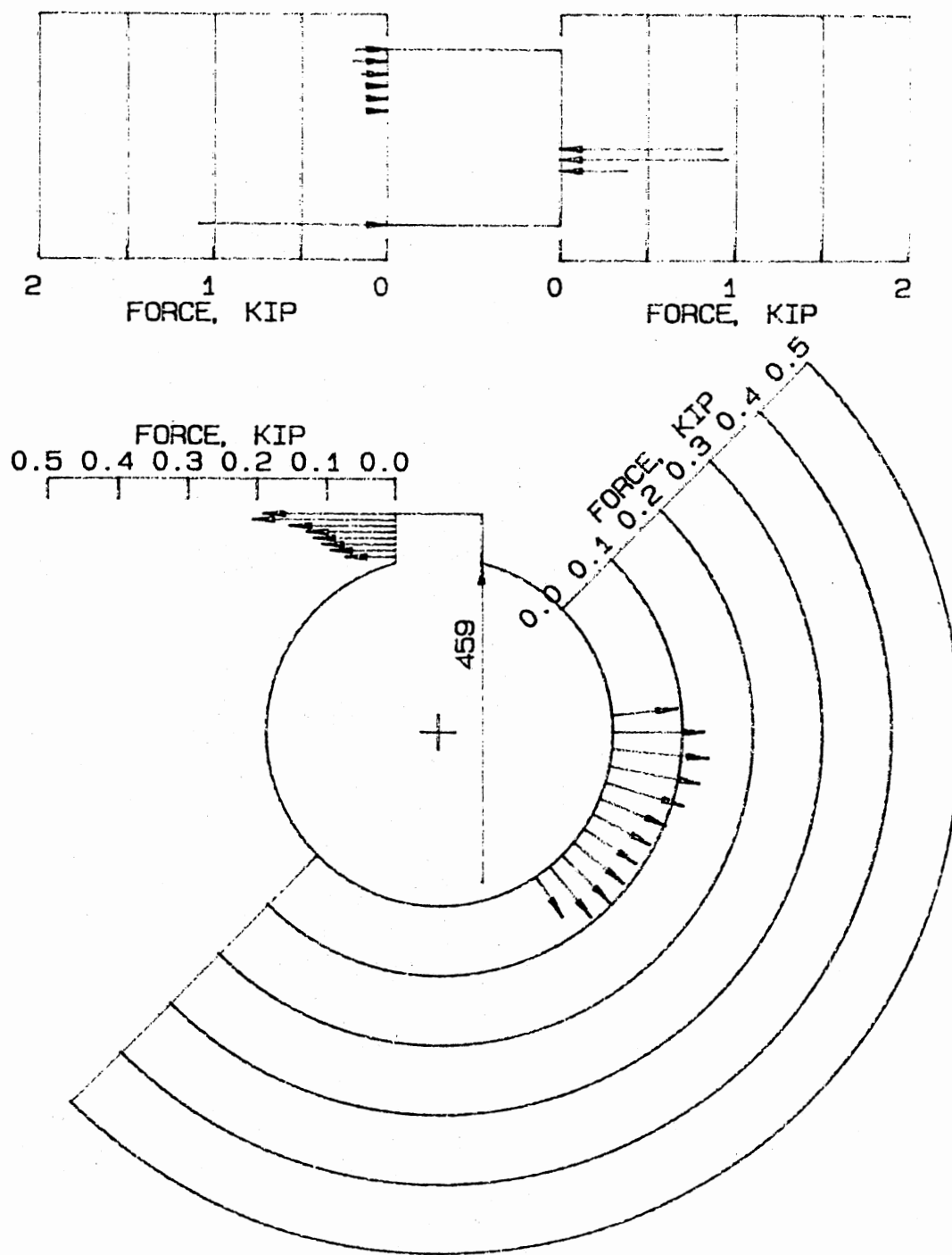
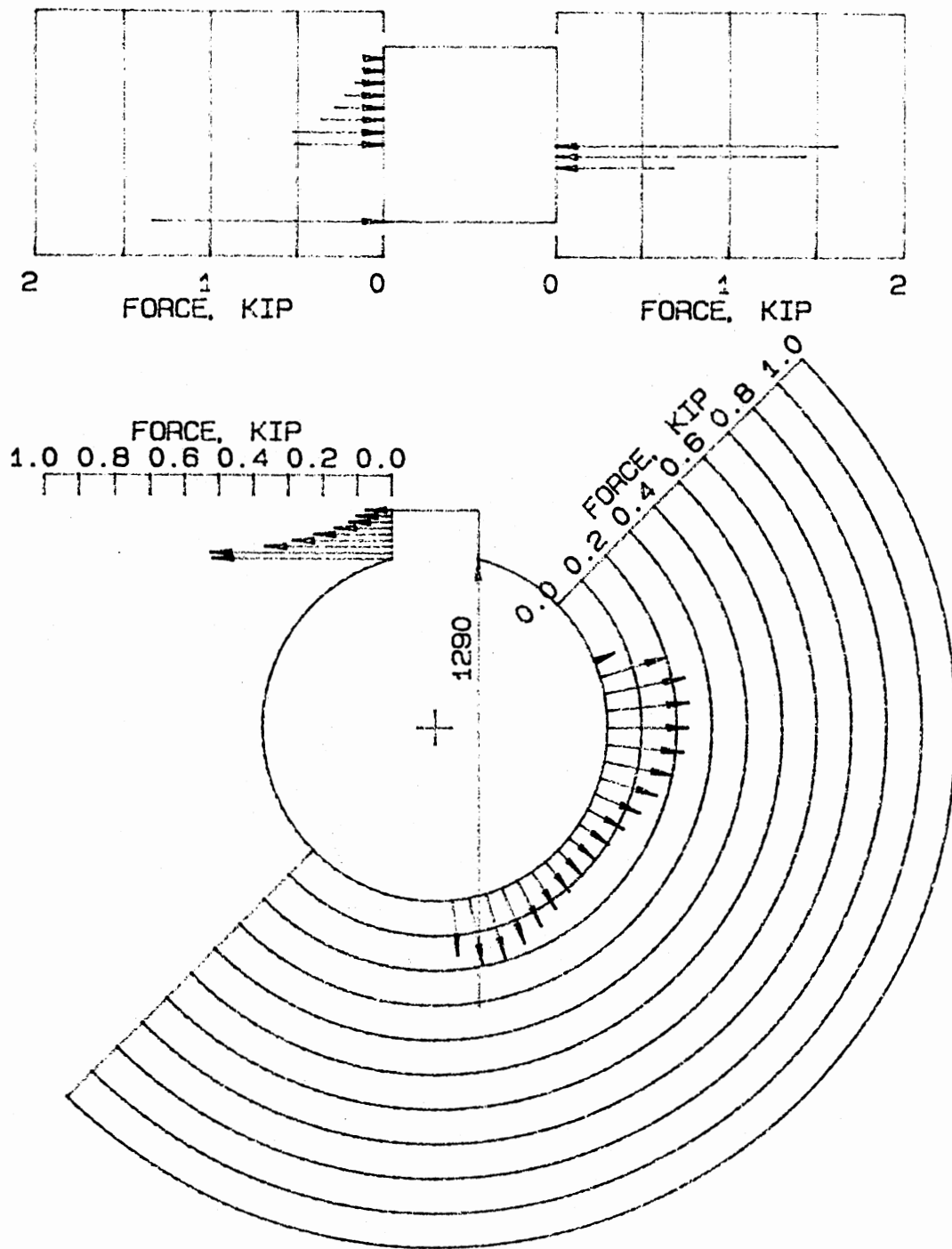


Fig. 4.31. Key and Hub Force Distribution, Loose Fit, 450 lb-in



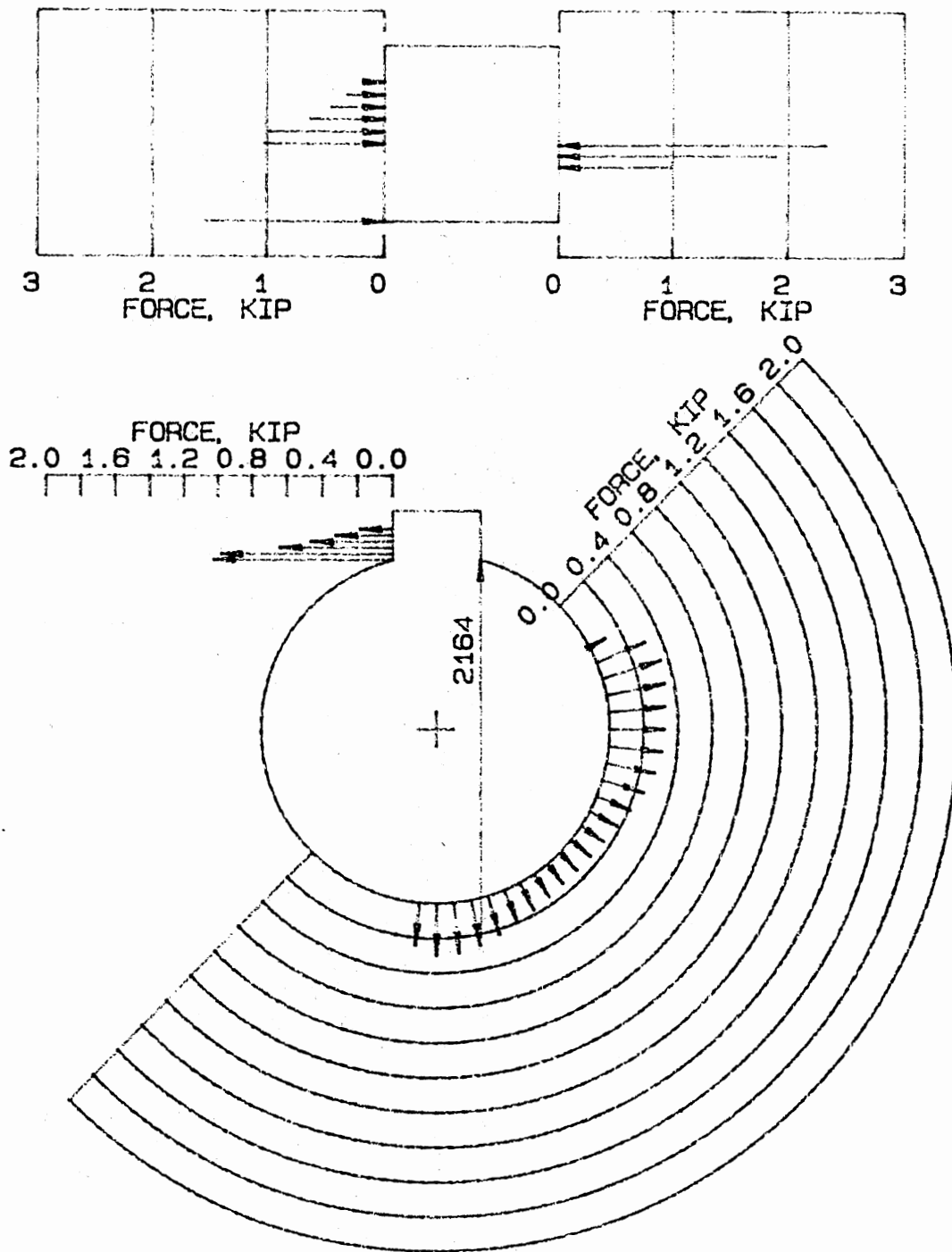
RUN 10024 D=1.0000 LOOSE FIT T= 750.LB-IN
 ANGULAR STIFFNESS = 39515. LB-IN/RAD/IN
 LINEAL STIFFNESS = 158062. LB/IN/IN
 SCALES: DRAWING - KEY, 4.000=1; HUB, 2.000=1
 FORCES - KEY, 1000.=1; HUB, 250.=1

Fig. 4.32. Key and Hub Force Distribution, Loose Fit, 750 lb-in



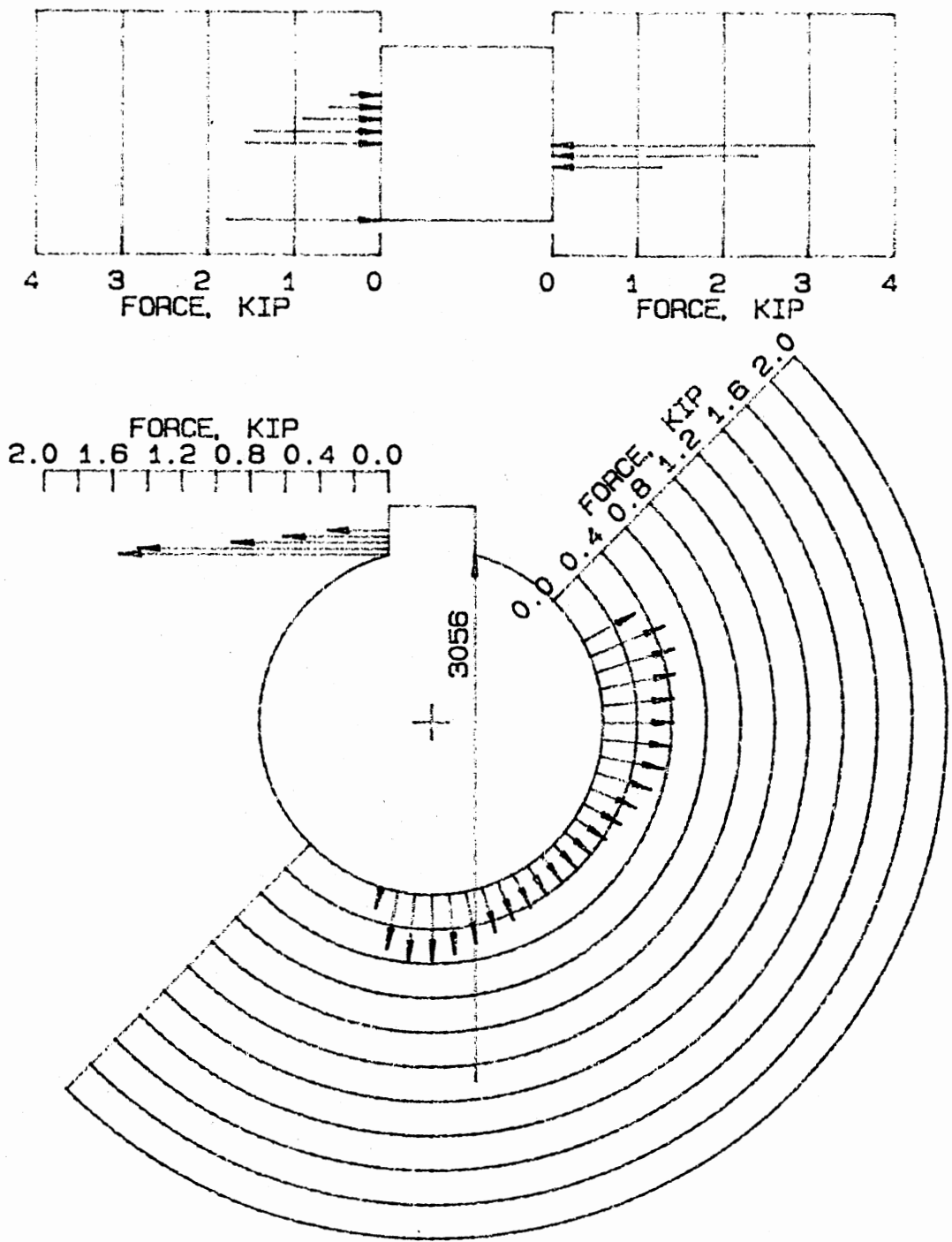
RUN 10025 D=1.0000 LOOSE FIT T= 1500.LB-IN
 ANGULAR STIFFNESS = 49640. LB-IN/RAD/IN
 LINEAL STIFFNESS = 198560. LB/IN/IN
 SCALES: DRAWING - KEY, 4.000=1; HUB, 2.000=1
 FORCES - KEY, 1000.=1; HUB, 500.=1

Fig. 4.33. Key and Hub Force Distribution, Loose Fit, 1500 lb-in



RUN 10026 D=1.0000 LOOSE FIT T= 2250.LB-IN
 ANGULAR STIFFNESS = 55191. LB-IN/RAD/IN
 LINEAL STIFFNESS = 220766. LB/IN/IN
 SCALES: DRAWING - KEY, 4.000=1; HUB, 2.000=1
 FORCES - KEY, 1500.=1; HUB, 1000.=1

Fig. 4.34. Key and Hub Force Distribution, Loose Fit, 2250 lb-in



RUN 10027 D=1.0000 LOOSE FIT T= 3000.LB-IN
 ANGULAR STIFFNESS = 58699. LB-IN/RAD/IN
 LINEAL STIFFNESS = 234797. LB/IN/IN
 SCALES: DRAWING - KEY, 4.000=1; HUB, 2.000=1
 FORCES - KEY, 2000.=1; HUB, 1000.=1

Fig. 4.35. Key and Hub Force Distribution, Loose Fit, 3000 lb-in

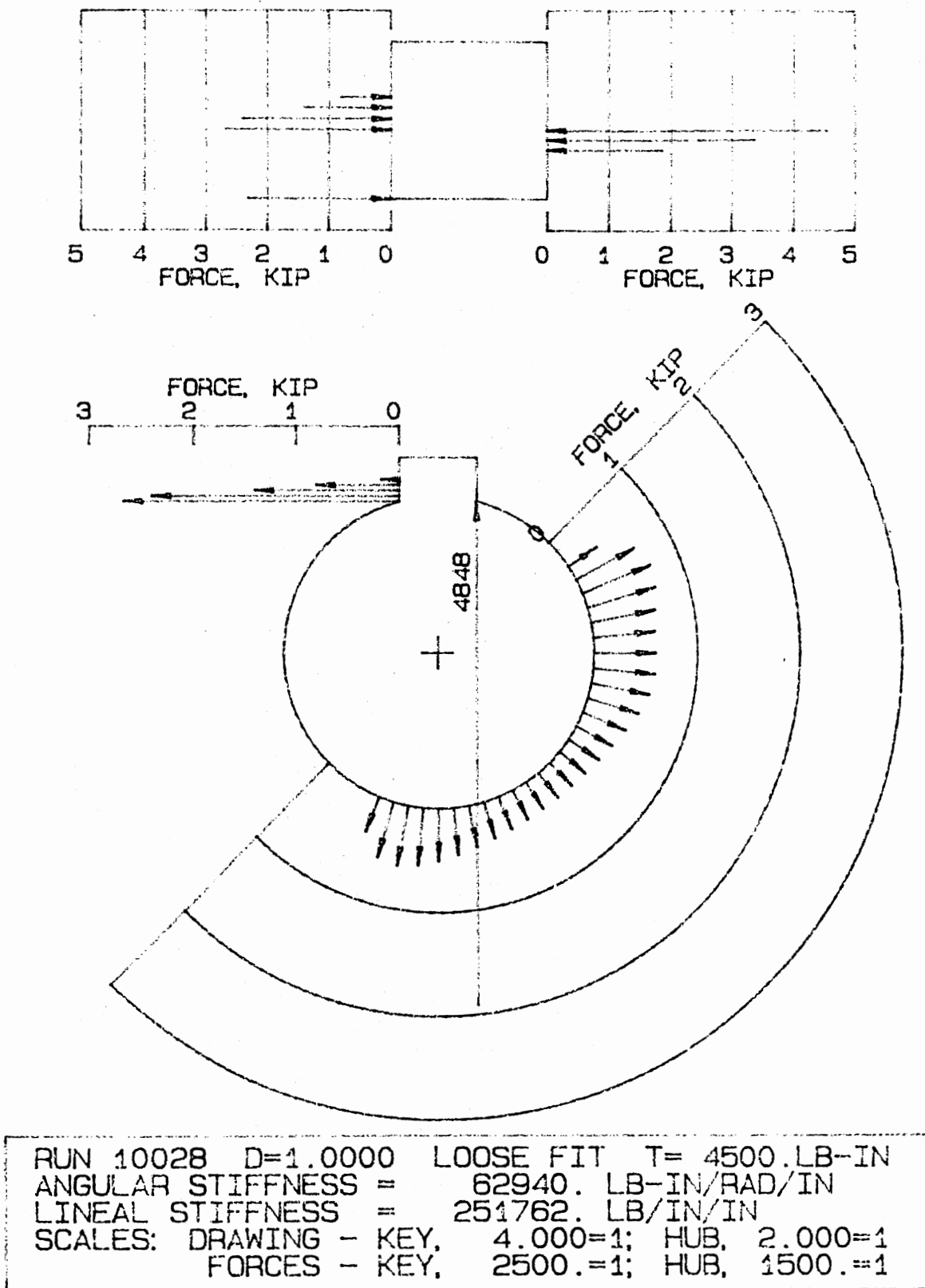
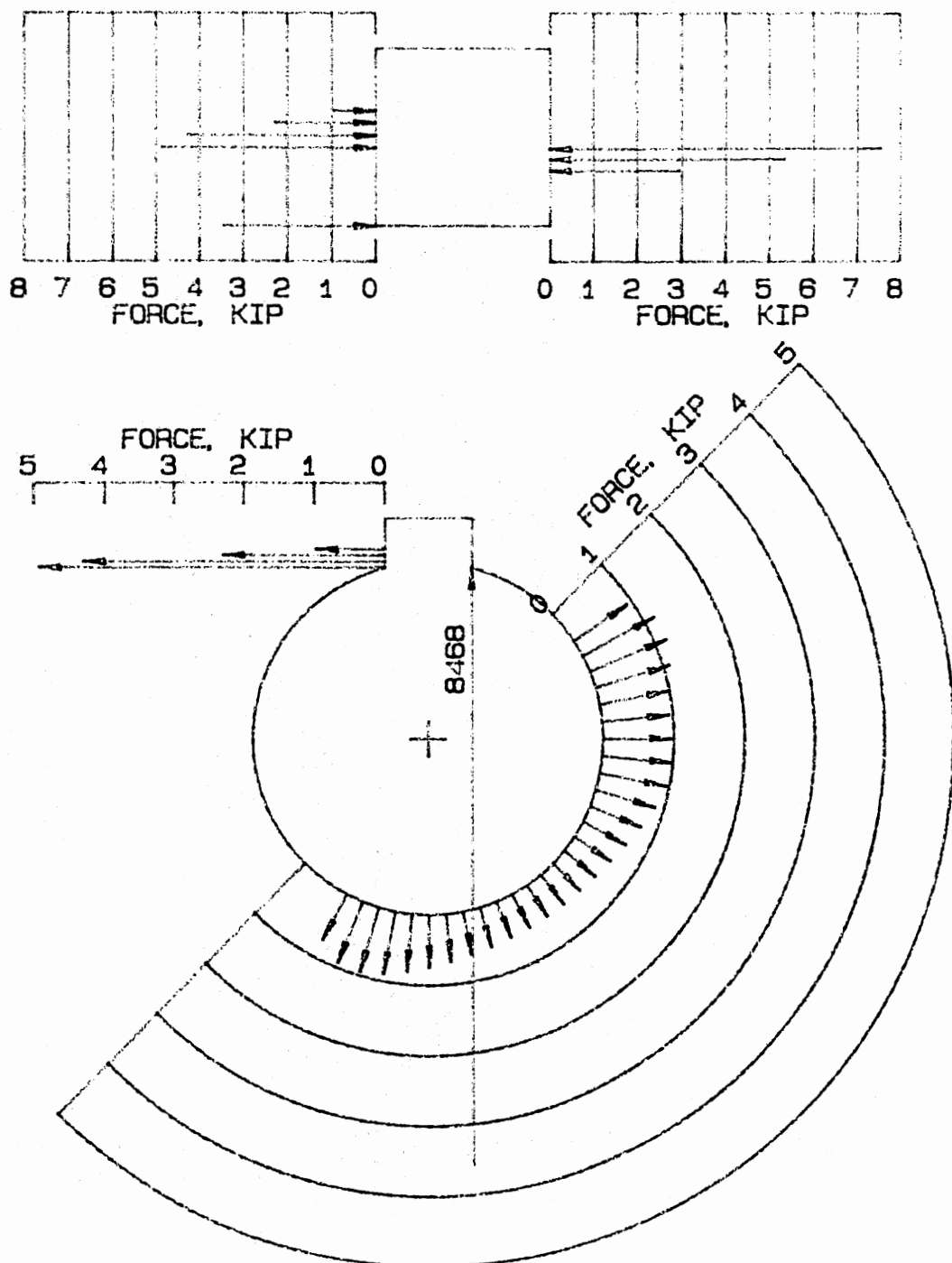
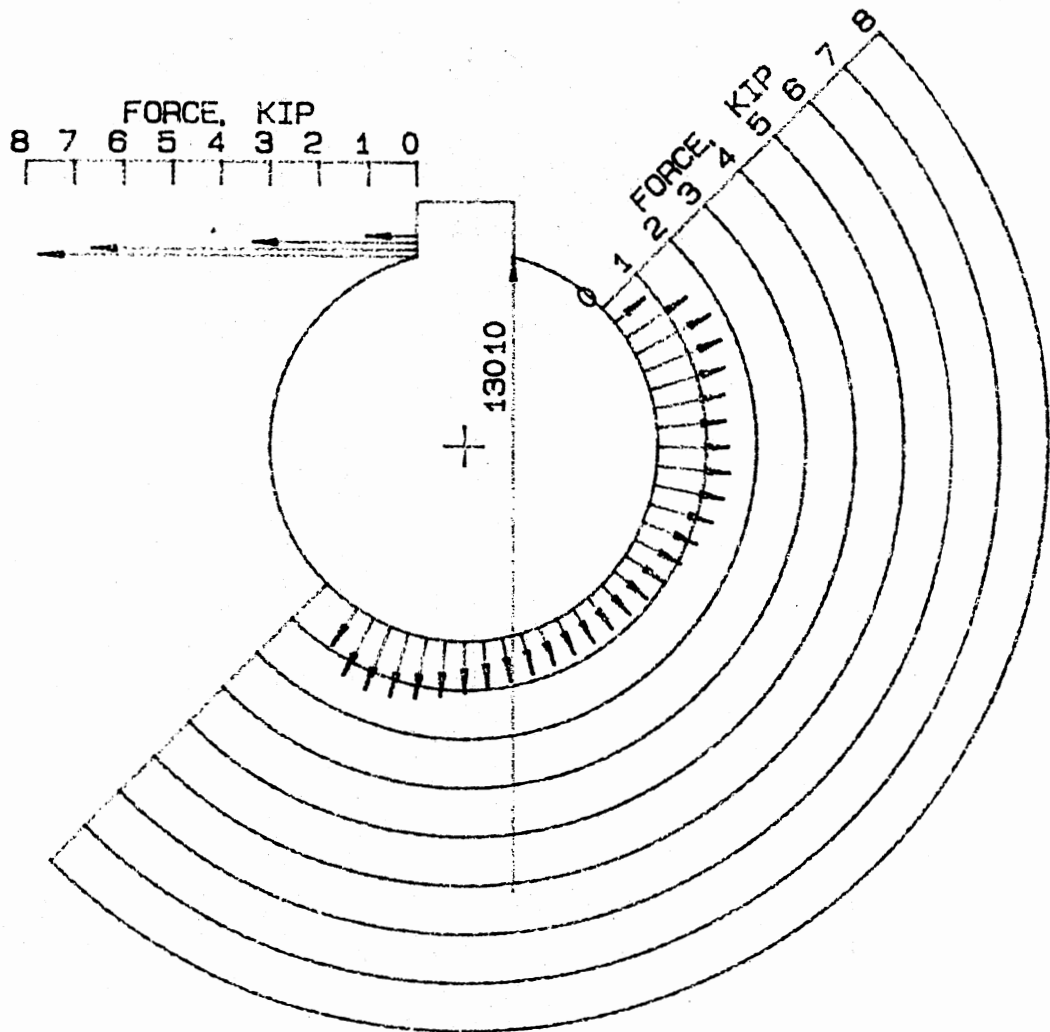
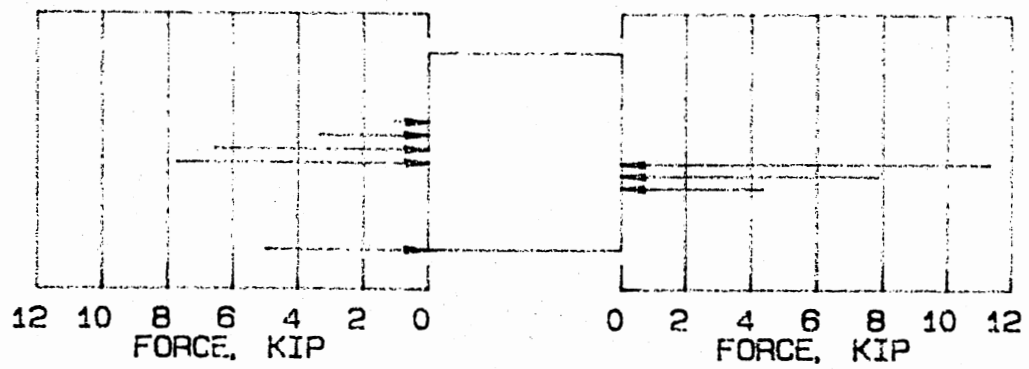


Fig. 4.36. Key and Hub Force Distribution, Loose Fit, 4500 lb-in



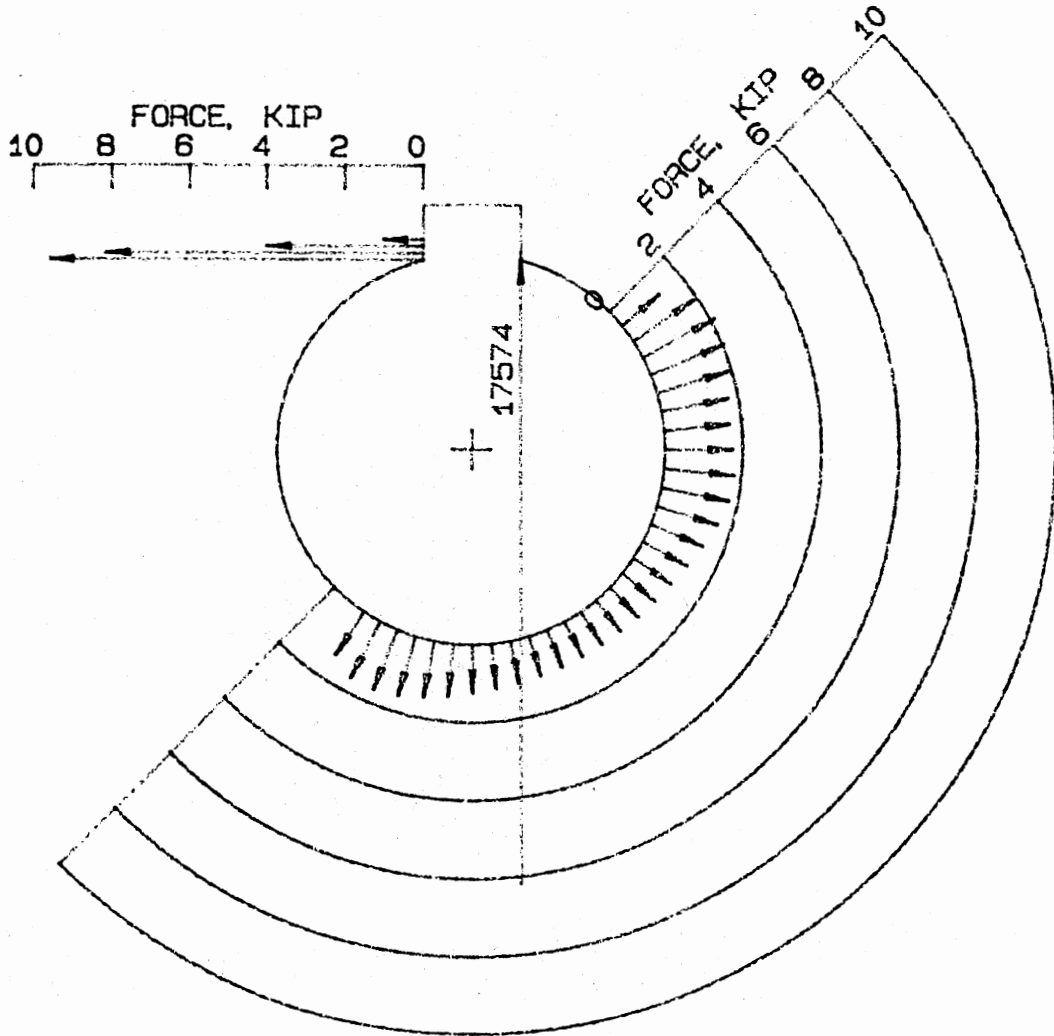
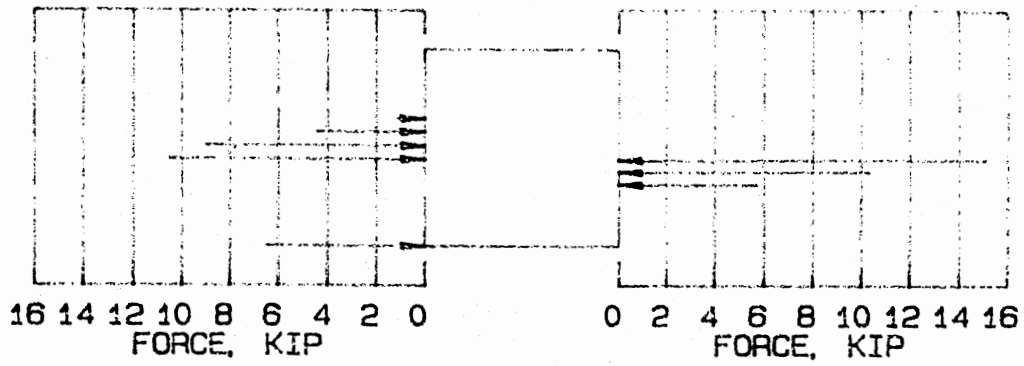
RUN 10029 D=1.0000 LOOSE FIT T= 7500.LB-IN
 ANGULAR STIFFNESS = 67139. LB-IN/RAD/IN
 LINEAL STIFFNESS = 268556. LB/IN/IN
 SCALES: DRAWING - KEY, 4.000=1; HUB, 2.000=1
 FORCES - KEY, 4000.=1; HUB, 2500.=1

Fig. 4.37. Key and Hub Force Distribution, Loose Fit, 7500 lb-in



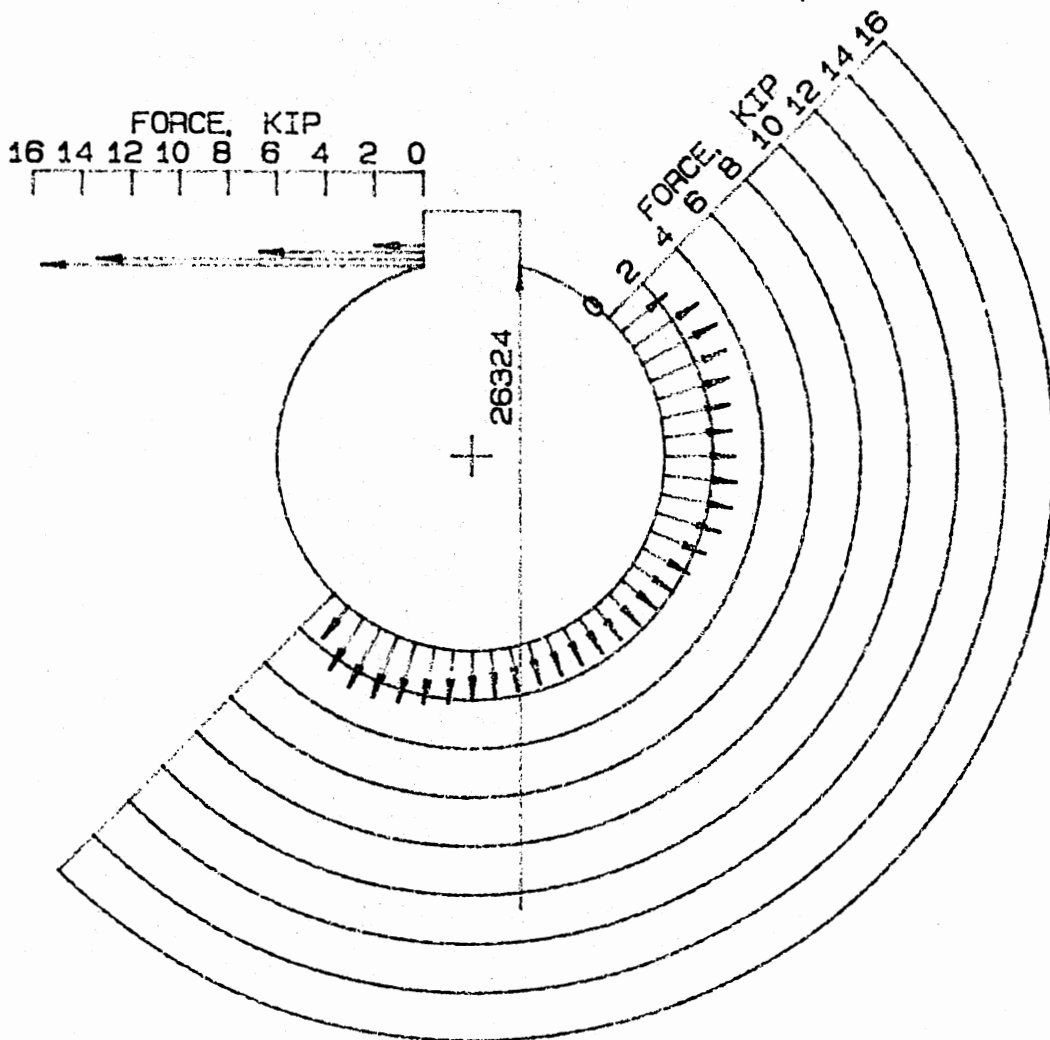
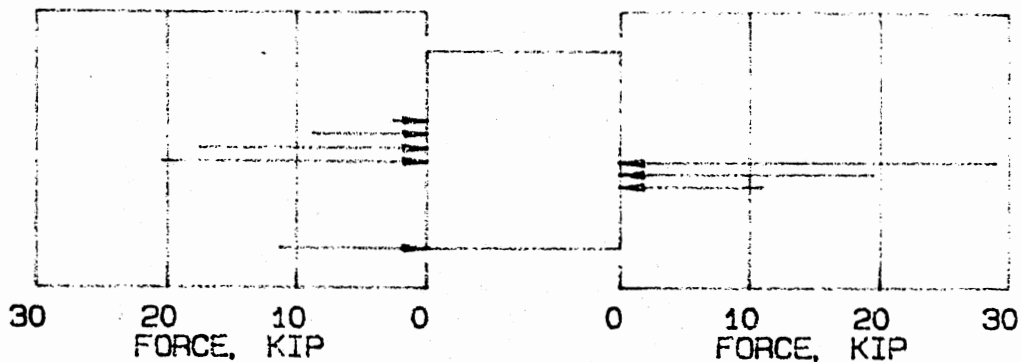
RUN 100210 D=1.0000 LOOSE FIT T=11250.LB-IN
 ANGULAR STIFFNESS = 69762. LB-IN/RAD/IN
 LINEAL STIFFNESS = 279049. LB/IN/IN
 SCALES: DRAWING - KEY, 4.000=1; HUB, 2.000=1
 FORCES - KEY, 6000.=1; HUB, 4000.=1

Fig. 4.38. Key and Hub Force Distribution, Loose Fit, 11250 lb-in



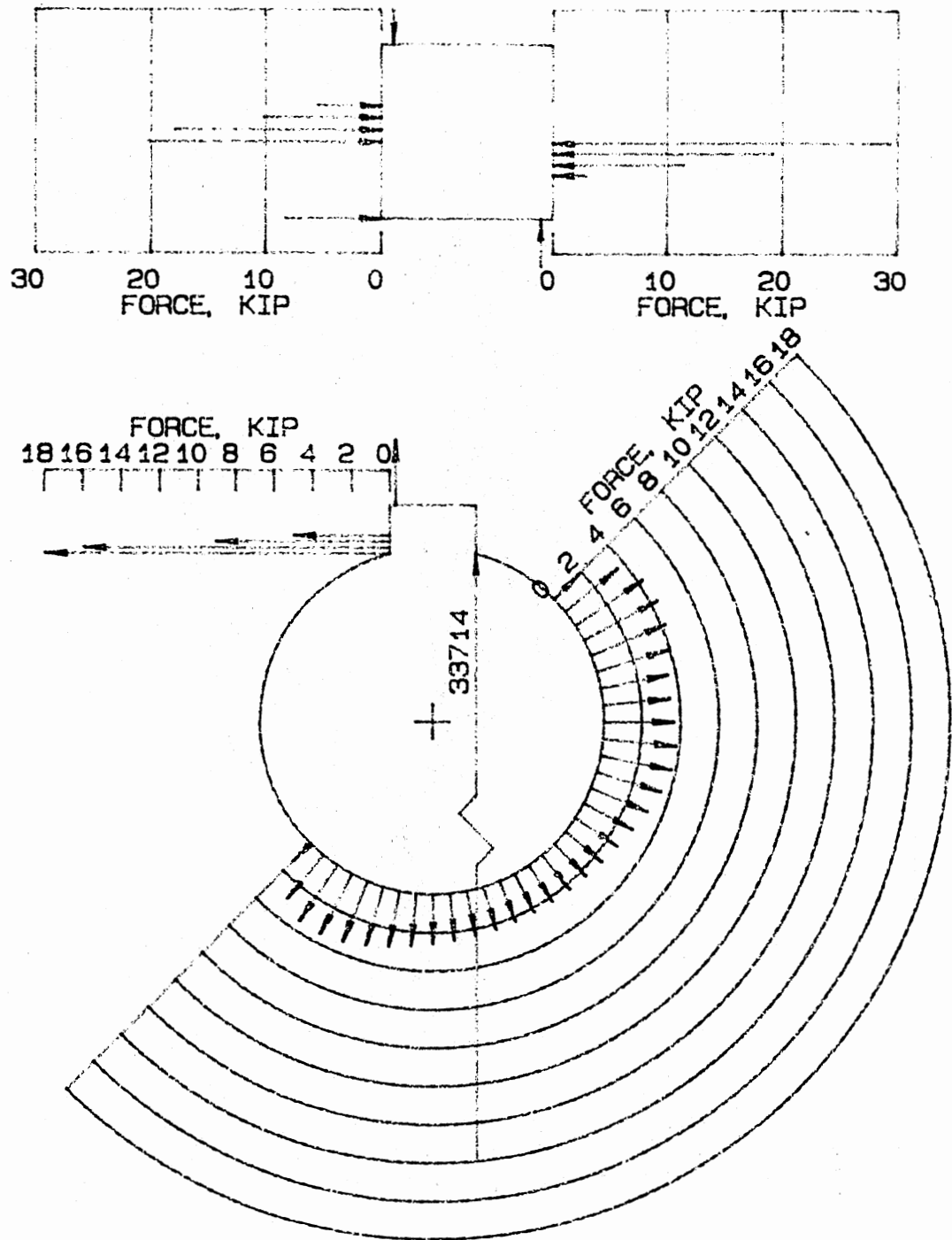
RUN 100211 D=1.0000 LOOSE FIT T=15000.LB-IN
 ANGULAR STIFFNESS = 71432. LB-IN/RAD/IN
 LINEAL STIFFNESS = 285729. LB/IN/IN
 SCALES: DRAWING - KEY, 4.000=1; HUB, 2.000=1
 FORCES - KEY, 8000.=1; HUB, 5500.=1

Fig. 4.39. Key and Hub Force Distribution, Loose Fit, 15000 lb-in



RUN 100212 D=1.0000 LOOSE FIT T=22500.LB-IN
 ANGULAR STIFFNESS = 73665. LB-IN/RAD/IN
 LINEAL STIFFNESS = 294661. LB/IN/IN
 SCALES: DRAWING - KEY, 4.000=1; HUB, 2.000=1
 FORCES - KEY, 11500.=1; HUB, 8000.=1

Fig. 4.40. Key and Hub Force Distribution, Loose Fit, 22500 lb-in



RUN 100213 D=1.0000 LOOSE FIT T=30000.LB-IN
 ANGULAR STIFFNESS = 75111. LB-IN/RAD/IN
 LINEAL STIFFNESS = 300444. LB/IN/IN
 SCALES: DRAWING - KEY, 4.000=1; HUB, 2.000=1
 FORCES - KEY, 14000.=1; HUB, 9500.=1

Fig. 4.41. Key and Hub Force Distribution, Loose Fit, 30000 lb-in

along the top surface of the key as the load is increased. No such load is present in Figures 4.30 through 4.41 (the loose case loading). This top surface loading, in fact, accounts for different stiffness models for the tight and loose case over a portion of the loading range as will be explained below.

4.2.2.3 Static Stiffness Model. The analytic model suggested that a mathematical fit to the stiffness data represented in Figures 4.15, 16 and 17 should be of the form

$$k = a/[1+b \ln(1/P)] + cP \quad (4.34)$$

There are three coefficients to be determined in this equation, thus, a curve drawn using it can be made to pass through three data points. A procedure was developed to solve for the coefficients a, b, and c given three sets of k and P from the reduced finite element data. The results are

$$k = \begin{cases} \frac{98800}{1 + 0.0846 \ln(1/P)} - 17.1P, & 100 \leq P \leq 9000 \\ 0.46P + 272400, & 9000 \leq P \leq 60000 \end{cases} \quad (4.35)$$

for the tight fit cases, and

$$k = \frac{85800}{1 + 0.0774 \ln(1/P)} - 4.62P \quad (4.36)$$

for the loose fit cases. It is interesting to note that the general equation given in (4.35) would not fit the tight data over the entire range while it did fit over the full range for the loose case. The difference can be explained by the difference in clearance on the top of the key between the two cases. For loads up to about 4500 lb-in in the tight case there is no appreciable reaction on top of the key. For the loose case there is no reaction except at the 30,000 lb-in load step.

To get a model for a general case (neither tight nor loose) the data from the 1.000 in diameter model was averaged for each load step. The resulting curve fit to this average is

$$k = \begin{cases} \frac{99500}{1 + 0.073 \ln(1/P)} - 4.05P, & 100 \leq P \leq 22500 \\ 0.46P + 272400, & 22500 \leq P \leq 60000 \end{cases} \quad (4.37)$$

The curves defined by equations (4.35), (4.36) and (4.37) are drawn in Figure 4.42 superimposed over the data from the 1.000 in diameter load steps. In the figure the upper curve is for the tight case, the lower curve is for the loose case, and the center curve fits the average data.

The stiffness predicted from the finite element analysis seem reasonable, however, at best it is a two dimensional model that neglects end effects. Depending on the shape of the keyseat (milled or sled-runner, for instance) there will be some additional stiffening at the ends of the key if the key length is approximately the same as the keyseat length.

4.2.3 Dynamic Model

The derivation of the equations of motion for the keyed joint is similar to the derivation for the spur gear pair given in Chapter III with the exception of the condition when the key is not in contact with the hub. In fact, with a few changes in terms equations (3.15) and (3.17) apply directly to the keyed joint for the cases of contact on each side of the key (the keyed joint can be thought of as a gear pair with one external tooth and one internal tooth). During the period when the key is not in contact there will be relative motion between the hub and shaft that will produce a friction torque that opposes the motion.

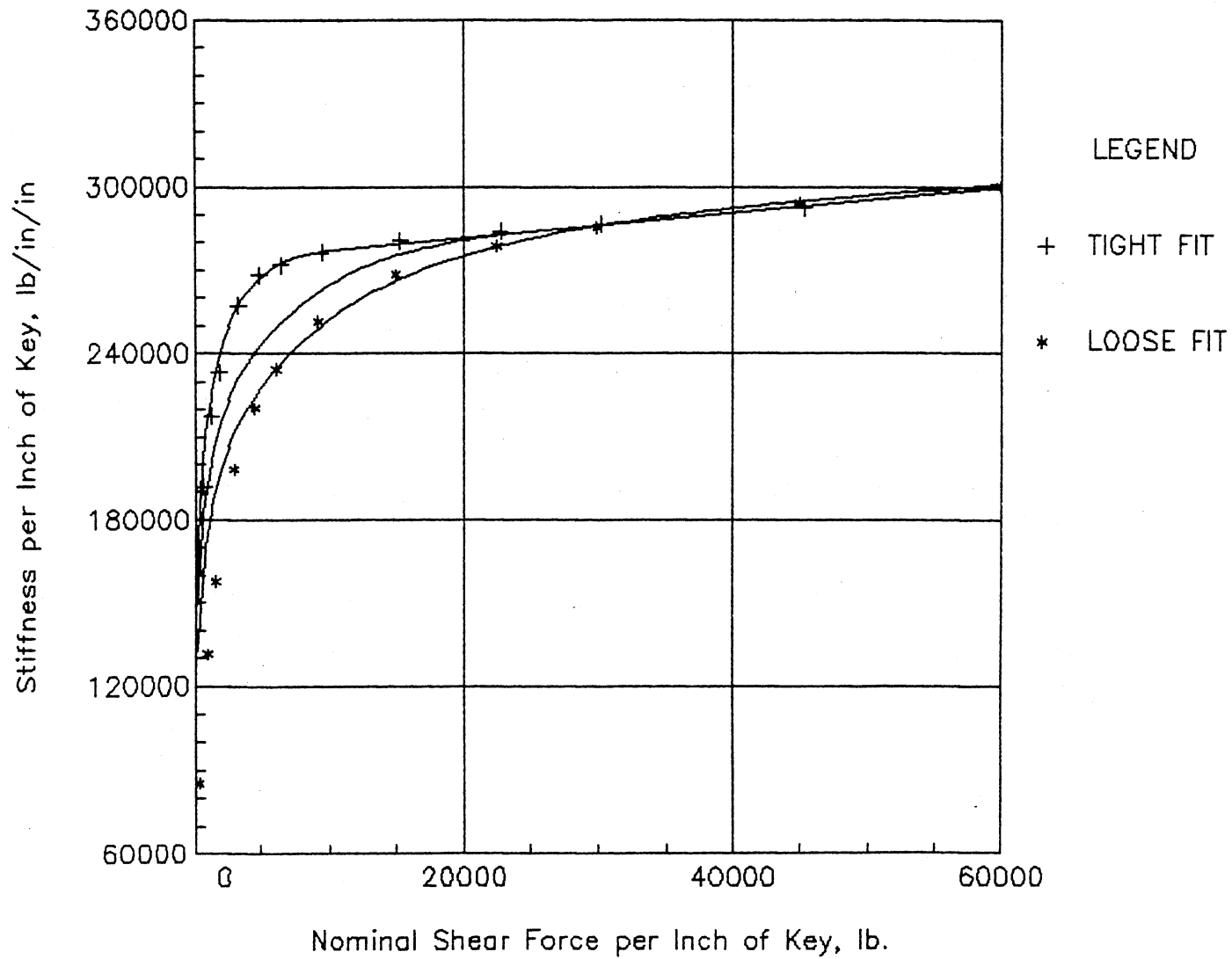


Fig. 4.42. Key Stiffness Equations vs. FEM Results

With respect to Figure 4.43, summing the horizontal and vertical forces and the moments to zero gives

$$-F^T + F_n \sin \alpha + \mu F_n \cos \alpha = 0 \quad (4.38)$$

$$-F^R - \mu F_n \sin \alpha + F_n \cos \alpha = 0 \quad (4.39)$$

$$F^T R - \mu F_n r = 0 \quad (4.40)$$

Eliminating F_n from equations (4.38) and (4.39) yields

$$\frac{F^T}{F^R} = \frac{\sin \alpha + \mu \cos \alpha}{\cos \alpha - \mu \sin \alpha} \quad (4.41)$$

which, in turn, can be solved for α ,

$$\tan \alpha = \frac{1 - \mu (F^R/F^T)}{(F^R/F^T) - \mu} \quad (4.42)$$

If we define $\tan \phi = F^R/F^T$,

$$\tan \alpha = \frac{1 - \mu \tan \phi}{\tan \phi - \mu} \quad (4.43)$$

With this definition of the angle α we can write the equations of motion for the hub and shaft during the period when the key is not in contact as

$$\left. \begin{aligned} I_1 \ddot{\theta}_1 &= [1 - \mu r R (\sin \alpha + \mu \cos \alpha)] T_1 \\ I_2 \ddot{\theta}_2 &= \left[T_2 - \frac{\mu r T_1}{R (\sin \alpha + \mu \cos \alpha)} \right] \end{aligned} \right\} \quad (4.44)$$

The equations for the contact cases, as adapted from the spur gear pair are

$$\left. \begin{aligned} I_1 \ddot{\theta}_1 + [F(t) + G(t)] r &= T_1 \\ I_2 \ddot{\theta}_2 - [F(t) + G(t)] r &= T_2 \end{aligned} \right\} \quad (4.45)$$

and

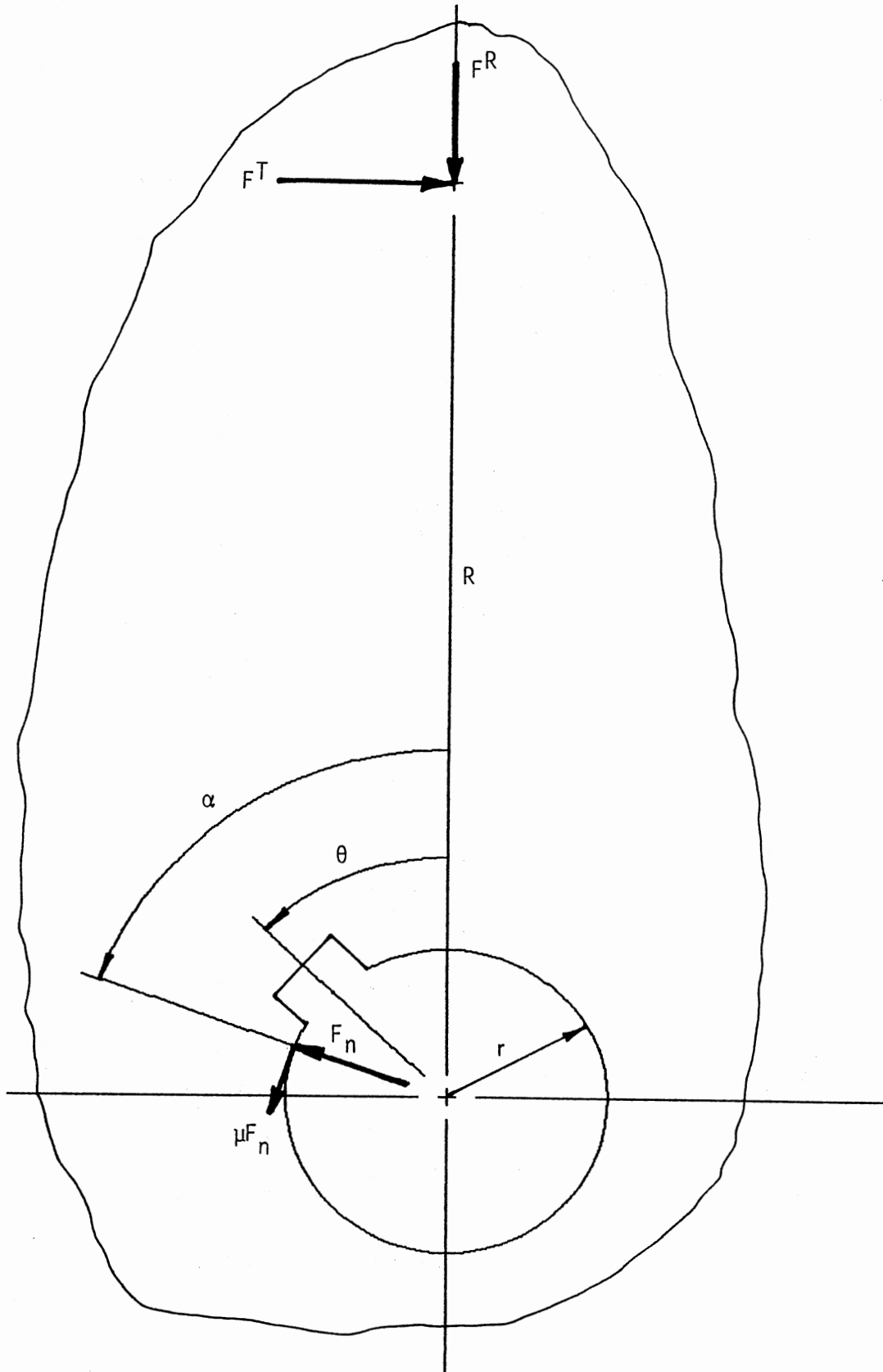


Fig. 4.43. Friction Force on Hub, No Contact at Key

$$\left. \begin{aligned} I_1 \ddot{\theta}_1 - [F(t) + G(t)]r &= T_1 \\ I_2 \ddot{\theta}_2 + [F(t) + G(t)]r &= T_2 \end{aligned} \right\} \quad (4.46)$$

Equations (4.44) along with equations (4.45) and (4.46) describe the motion of the keyed joint. As in the case of the spur gear pair, the forces $F(t)$ and $G(t)$ are defined as

$$F(t) = k(x) \cdot s \quad (4.47)$$

and

$$G(t) = D|s|\dot{s} \quad (4.48)$$

The stiffness $k(x)$ is derived from the finite element model described in the section above in the following manner. The stiffnesses for the tight and loose cases were averaged and then divided into the nominal shear force yielding a deflection, x . The results were then plotted as stiffness vs deflection and are shown in Figure 4.44. A curve fit to the average data is shown in the figure and is

$$k(x) = \begin{cases} \left[\frac{3.184}{2.98 \ln(1/x)} - 2.584x \right] (10)^6, & x \leq 0.1 \\ (1.49x + 2.70) \cdot (10)^6, & 0.1 < x \end{cases} \quad (4.49)$$

The damping coefficient, D , is defined exactly as it was for the spur gear pair.

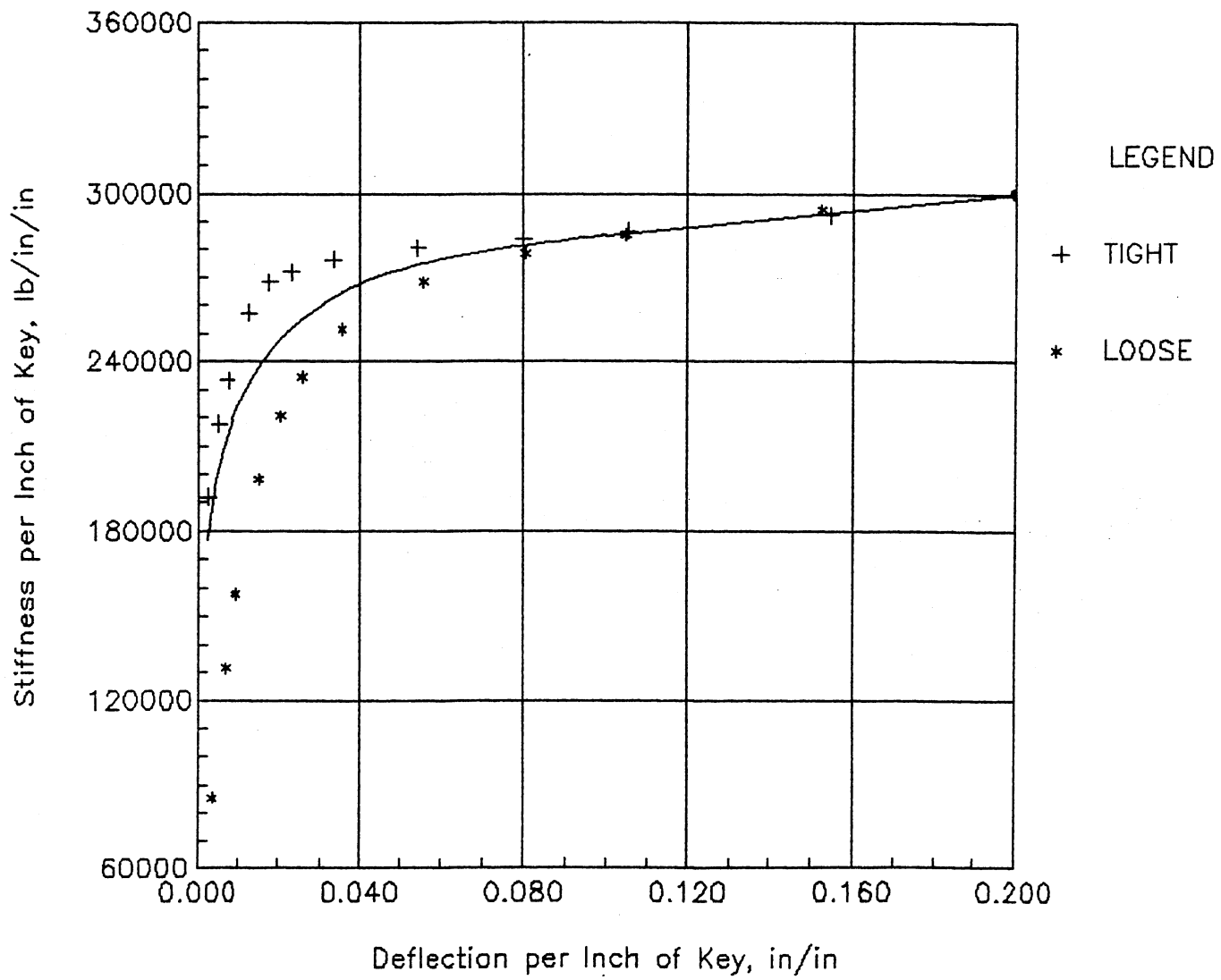


Fig. 4.44. Key Stiffness vs. Deflection

CHAPTER V
SYSTEM MODEL

5.1. Digital Simulation Program

A general-purpose, dynamic simulation program for drive trains has been developed to assist in this study. The program is named TRAIN and consists of three main modules: A preprocessor, a processor, and a postprocessor (see Fig. 5.1). The particular drive-train to be studied is defined while in the preprocessor. Once this phase is complete, the program automatically moves into the solution phase in the processor. The output of the processor is written to a file that is read by the postprocessor. The user can get both printed and plotted data on the response of the drive-train while in the postprocessor.

The user starts by building a system block diagram, interactively at the terminal, from a menu of predefined nodes and elements in any order that is desired. The user is then prompted to input the numerical constants that are used in the state equations for the elements that are to be used in the simulation. Next, the user is prompted to choose the type of external load conditions that are to be applied to the model. Finally, the user is prompted to define the start and run times and the solution time step for the simulation. The program then goes into the processing module.

The simulation is accomplished by numerically integrating the state equations using a fourth-order Runge-Kutta procedure. For each time

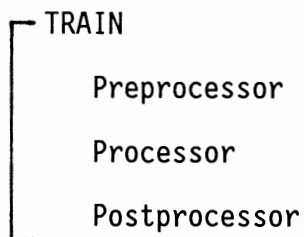


Fig. 5.1. Action Diagram of TRAIN

step the relevant state equations are chosen from a subprogram in the order that was specified by the user when the model was created. As the solution proceeds, the values of the state variables are written to a file which will be read later by the postprocessor.

The user may choose printed output, plotted output or both. After making a menu choice of one of these two, additional menus are presented to the user to further define the output desired. A small graphics library is included with the program for the plot output. Drivers are included for Tektronix 4014 and 4115 terminals.

5.1.1. Preprocessor

An action diagram of the preprocessor is shown in Fig. 5.2. Options are presented on the first menu in the preprocessor to define a completely new model, modify an existing model, or processes an existing model.

5.1.1.1. Nodes and Elements. The real physical system is modeled by a lumped mass system. The user may choose to subdivide the physical system in any way. The lumped masses are concentrated at nodes that are connected by visco-elastic elements. Elements consist of shafts,

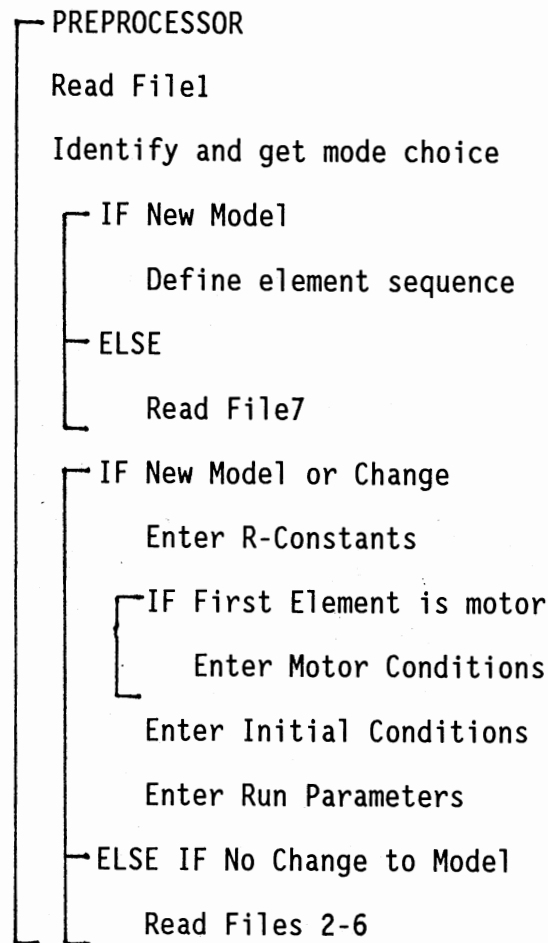


Fig. 5.2. Action Diagram of the Preprocessor

couplings, gear pairs, etc. The nodes and elements are defined in libraries (Appendix G and H, respectively). The procedure for adding a new element to the source code is given in Appendix I.

Equations of state are written for each node type in terms of its state variables and the external torques on the node. A method similar to that used in the development of transfer matrices is used to derive the external torques. Except at the beginning and ends of the train, each node is connected to two elements, one on the left and one on the right. The element to the right has the same sequence number as the

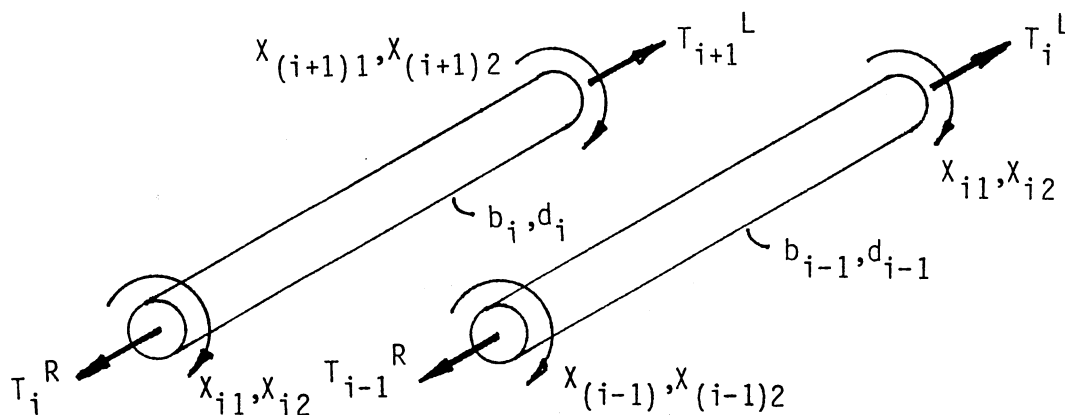


Fig. 5.3. Linear Shaft Element Definition

node, while the one on the left has a sequence number that is one less. Thus, two torque equations are written for each element, one for use when considering the node on the left and one when considering the node on the right. An example, the linear shaft element, is shown and described in Fig. 5.3. The state variables are displacement and speed for the passive nodes.

5.1.1.2. Physical Constants. The physical system constants are called R-constants in this program. Each node has some number of RN-constants, while those associated with elements are RE-constants. The number and definition are given in the node or element definition in the libraries (Appendix G or H). Referring to Fig. 5.3, there are two RE-constants for the linear shaft, they are: (1) the shaft stiffness, b_i , and (2) the internal damping coefficient, d_i , for the shaft (RE_{i1} and RE_{i2} , respectively).

5.1.1.3. External Loads. External loads can be applied to the drive-train at the two ends only. Generally speaking, the user has a

choice of no load, a steady load, or a time-varying load. Once one of these choices is made, the user is prompted to input further specifications as to magnitude and time parameters.

5.1.1.4. Initial Conditions. Each state variable must be given an initial value to start the numerical integration. The user is prompted to give each state variable for each element an initial value. A default value of zero is used for all state variables.

5.1.1.5. Run Conditions. The user is prompted to enter the start time and the stop time for the simulation as well as the integration step interval. Some trial and error may be necessary to find a step interval that results in a stable solution.

5.1.2. Solution Processor

The processor calls the subroutine RK4 (see Fig. 5.4(a)) which, in turn, invokes the function F. This function contains the state equations for the complete element library. RK4 is a fourth-order

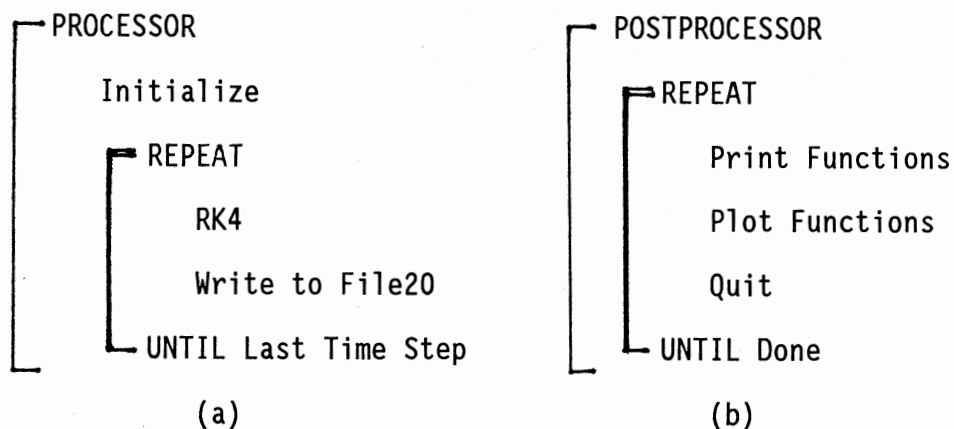


Fig. 5.4. Action Diagram of (a) Processor, and (b) Postprocessor

Runge-Kutta numerical integration procedure.

5.1.3. Postprocessor

In the postprocessor (see Fig. 5.4(b)) it is possible to extract information about each state variable as a function of time or as a function of another state variable. In addition, information on one state variable relative to another or on the torque on any given element is available. This can either be printed out to a file or plotted to the terminal screen (if the user is logged on to a graphics terminal supported by TRAIN).

5.2. Verification Models

A series of verification problems have been devised and executed to provide assurance that the simulation provides correct answers to known problems. Generally speaking, only one feature of the program is verified at a time.

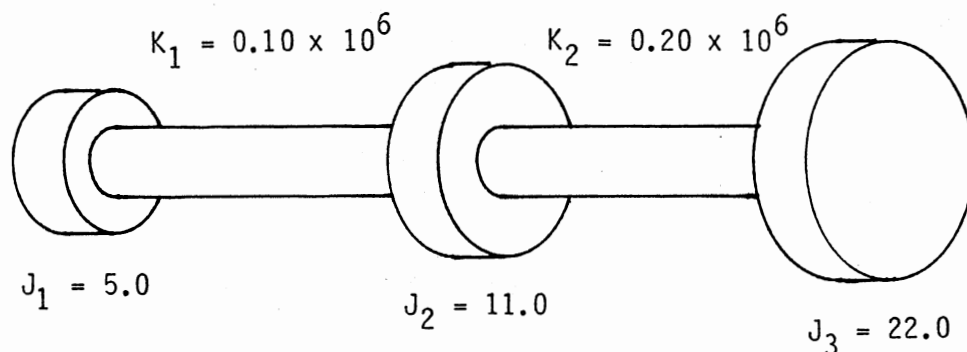


Figure 5.5. Integration Method Verification Problem

5.2.1. Integration

This problem utilizes passive node and linear elastic elements to solve a simple torsional problem. The problem is solved in Thomson (1981) and is defined in Figure 5.5. Using the Holzer method, the fundamental frequency for the system is found to be 19.68 hz, with a corresponding mode shape giving relative angular deflections of 1.0, 0.2353, and -0.3449 radians, respectively, at each of the three disks. The input to TRAIN for this problem is given in Table 5.1, and the output is shown in Figure 5.6. As seen from Table 5.1, the system is given an initial displacement equivalent to the mode shape of the fundamental frequency. The expected response is a cosine function with amplitude equal to the initial displacement and period equal to $1/19.68$ s.

5.2.2. Ideal Gear Pair

This is a test of the ideal gear pair. It consists of a pair of gears only with no external torques and demonstrates the kinematic property of velocity ratio. The input is given in Table 5.2 and the output is shown in Figure 5.7. The expected result is that both initial speeds remain constant.

5.2.3. Spur Gear Pair With Backlash

This is a test of the gear model developed in Chapter III. It consists of the same pair of gears for which the perturbation and delta method solutions (see 3.2.4.) were developed. The input is given in Table 5.3 and the output is shown in Figure 5.8. The expected result is the response predicted by the perturbation and delta method solutions.

5.2.4. Keyed Joint

This is a test of the keyed joint developed in Chapter IV. It consists of two nodes connected by a keyed joint element. The input is given in Table 5.4 and the output is shown in Figure 5.9. The expected result is a response similar to a spur gear with backlash.

5.2.5. Comparison With Experimental Results

A series of 27 runs of TRAIN have been made using the gear dimensions given in Gregory, et al. (1962). The experimental observations were made on a back-to-back gear test rig in order to show that large vibrations can occur in a pair of spur gears without any manufacturing errors and without any external excitation. The test gears (Figure 5.10) were 4-pitch, 20° pressure angle, 32 teeth, and had a 0.5 in face width. No information was given as to the gear materials, but from force and deflection information given it was deduced that they had a single pair mesh stiffness of 234500 lb/in. The tooth profile was modified to eliminate tooth interference under a load of 1700 lb/in of face width. This resulted in tip relief of 0.001 in. Since there is no way of modeling tip relief in TRAIN, only the results of loading at 425 lb/in was simulated.

Using a linear model, calculations of natural frequency for the gear pair can be made. When there are one pair of teeth in contact the natural frequency (in the TRAIN model) is 412 Hz. During two-pair contact it is 553 Hz. The weighted average natural frequency is 510 Hz. We expect the nonlinear system to have a critical response somewhere in this range of frequencies and also at their harmonics and subharmonics.

The TRAIN input is given in Table 5.5. The results of the 27 runs of TRAIN are compared with the experimental results in Figure 5.11. The experimental results are the average peak-to-peak errors over a seven tooth interval. The TRAIN results are the average peak-to-peak errors over the time period from the first peak to the last full peak on the response plots. The TRAIN results are indicated by a continuous curve through points marked with "+". The experimental results are shown in two curves. The curve through the points marked "x" are for increasing velocity and the curve through the points marked "o" are for decreasing velocity. A jump, which is characteristic of a nonlinear system, is exhibited at 447 teeth/s on increasing speed and at 380 teeth/s on decreasing speed. In the TRAIN simulation it is not possible to get the response while the speed is changing. Each response is determined at a constant speed and it will be the same regardless of the speed of a previous run. In the experiment, tooth separation occurred at all speeds above 447 teeth/s for decreasing speed and at 380 teeth/s for increasing speed. In the TRAIN results tooth separation first occurred at 460 teeth/s and continued for increasing speed up to about 500 teeth/s.

Examples of response curves are shown in Figures 5.12, 5.13, and 5.14. The difference between the angular displacements of the gears (transmission error) is plotted as a function of time for a given mesh frequency. The square wave shown at the top of each plot is the number of pairs of teeth in contact, either two or one (number of pair of teeth in contact scale is on the right at the top). The horizontal line at the ordinate value of 0.00133 rad is the threshold of contact. When the relative displacement drops below this line there is a loss of contact

TABLE 5.1
 INPUT FOR VERIFICATION OF
 INTEGRATION METHOD

Number of nodes: 3

Node and element description:

Node 1 - N01, Passive
 Elem 1 - E11, Shaft
 Node 2 - N01, Passive
 Elem 2 - E11, Shaft
 Node 3 - N01, Passive

R-constants:

Node 1 $RN_{11} = 5.0$
 $RN_{12} = 0.0$
 Elem 1 $RE_{11} = 100000$
 $RE_{12} = 0.0$
 Node 2 $RN_{21} = 11.0$
 $RN_{22} = 0.0$
 Elem 2 $RE_{21} = 200000$
 $RE_{22} = 0.0$
 Node 3 $RN_{31} = 22.0$
 $RN_{32} = 0.0$

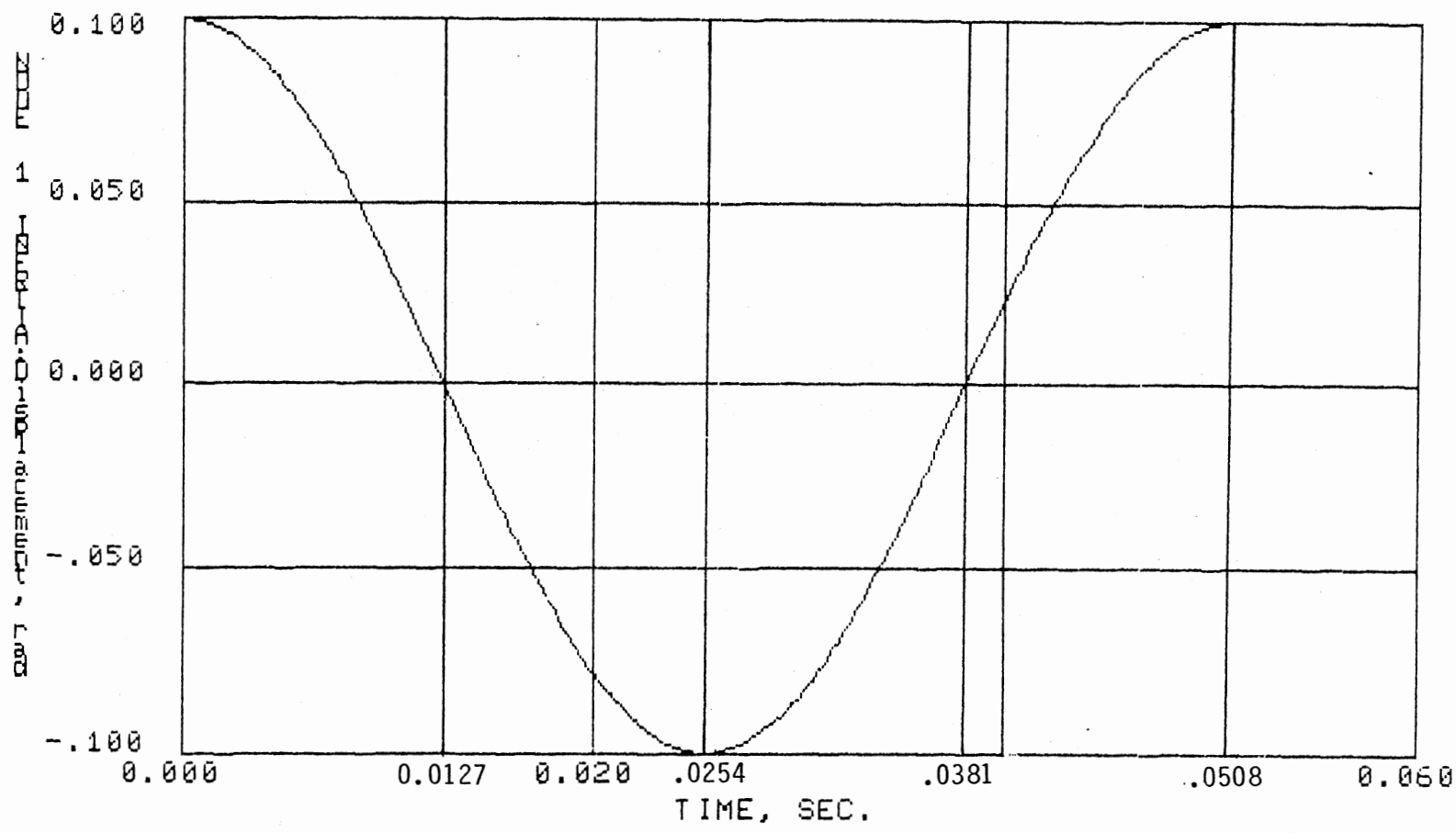
Initial Conditions:

Node 1 $x_{11} = 0.1000$
 $x_{12} = 0.0$
 Node 2 $x_{21} = 0.02353$
 $x_{22} = 0.0$
 Node 3 $x_{31} = -0.03449$
 $x_{32} = 0.0$

No external torques

Run Conditions:

Time step = 0.0002
 Start time = 0.0
 Run length = 0.0508



VERF01***RUN 1***28-JAN-88

Fig. 5.6. Integration Verification Output

TABLE 5.2
INPUT FOR VERIFICATION OF
IDEAL GEAR PAIR

Number of nodes: 2

Node and element description:

Node 1 - NO1, Passive
Elem 1 - EL3, Ideal Gear Pair
Node 2 - NO1, Passive

R-constants:

Node 1 $RN_{11} = 7.5E-03$
 $RN_{12} = 0.0$
Elem 1 $RE_{11} = 18E06$
 $RE_{12} = 1.6445$
 $RE_{13} = 3.2890$
Node 2 $RN_{21} = 15E-03$
 $RN_{22} = 0.0$

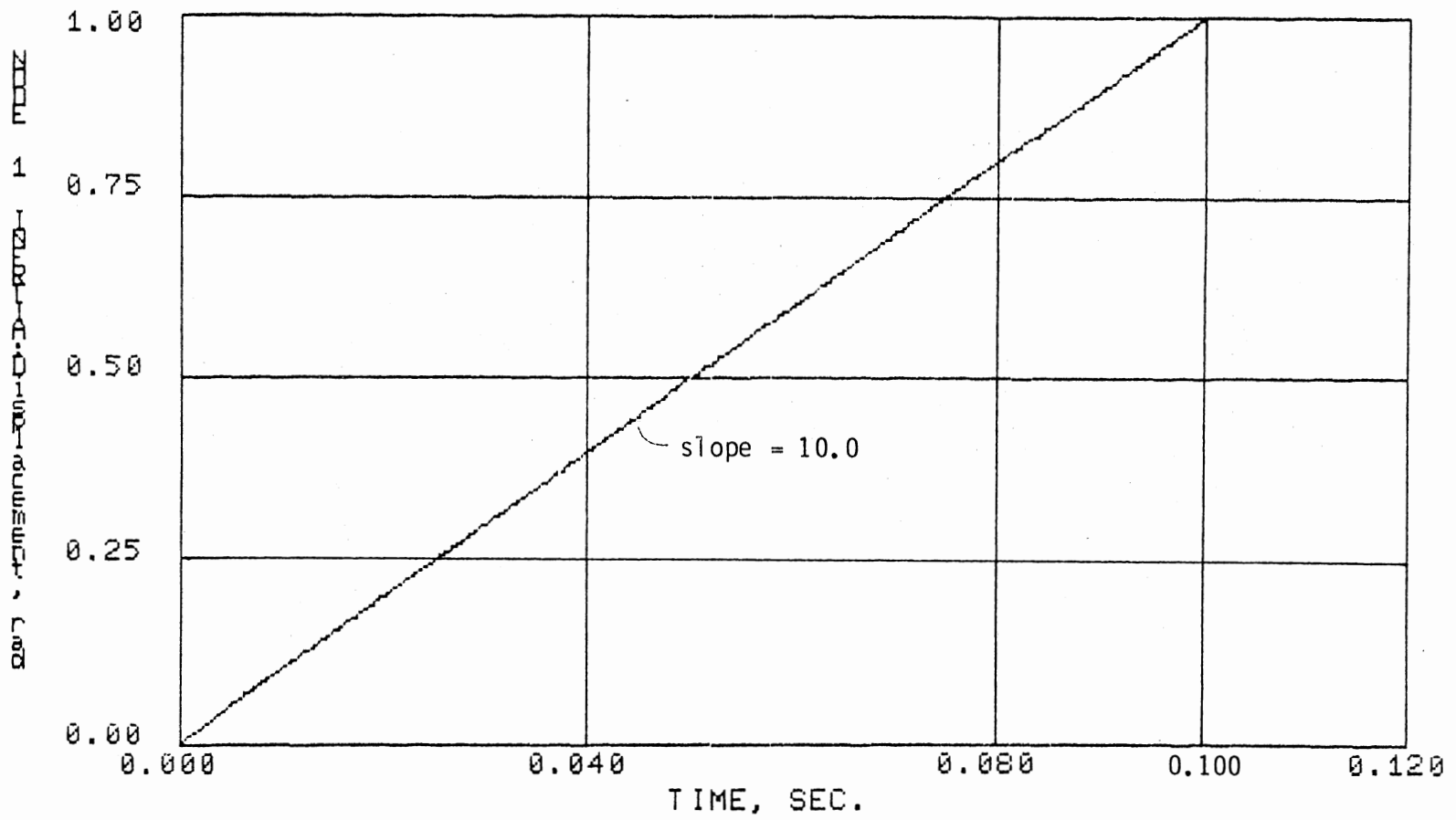
Initial Conditions:

Node 1 $x_{11} = 0.0$
 $x_{12} = 10.0$
Node 2 $x_{21} = 0.0$
 $x_{22} = 10.0$

No external torques

Run Conditions:

Time step = 0.0002
Start time = 0.0
Run length = 0.1



VERF02***RUN 1*** 28-JAN-8

Fig. 5.7. Gear Pair Verification Output

TABLE 5.3
 INPUT FOR VERIFICATION OF SPUR
 GEAR PAIR WITH BACKLASH

Number of nodes: 2

Node and element description:

Node 1 - N01, Passive
 Elem 1 - EL3, Spur Gear Pair with Backlash
 Node 2 - N01, Passive

R-constants:

Node 1 $RN_{11} = 7.537E-03$
 $RN_{12} = 0.0$
 Elem 1 $RE_{11} = 2.93E06$
 $RE_{12} = 1.6445$
 $RE_{13} = 1.6445$
 $RE_{14} = 28$
 $RE_{15} = 1.6380$
 $RE_{16} = 0.1838$
 $RE_{17} = 0.001$
 Node 2 $RN_{21} = 10.082$
 $RN_{22} = 0.0$

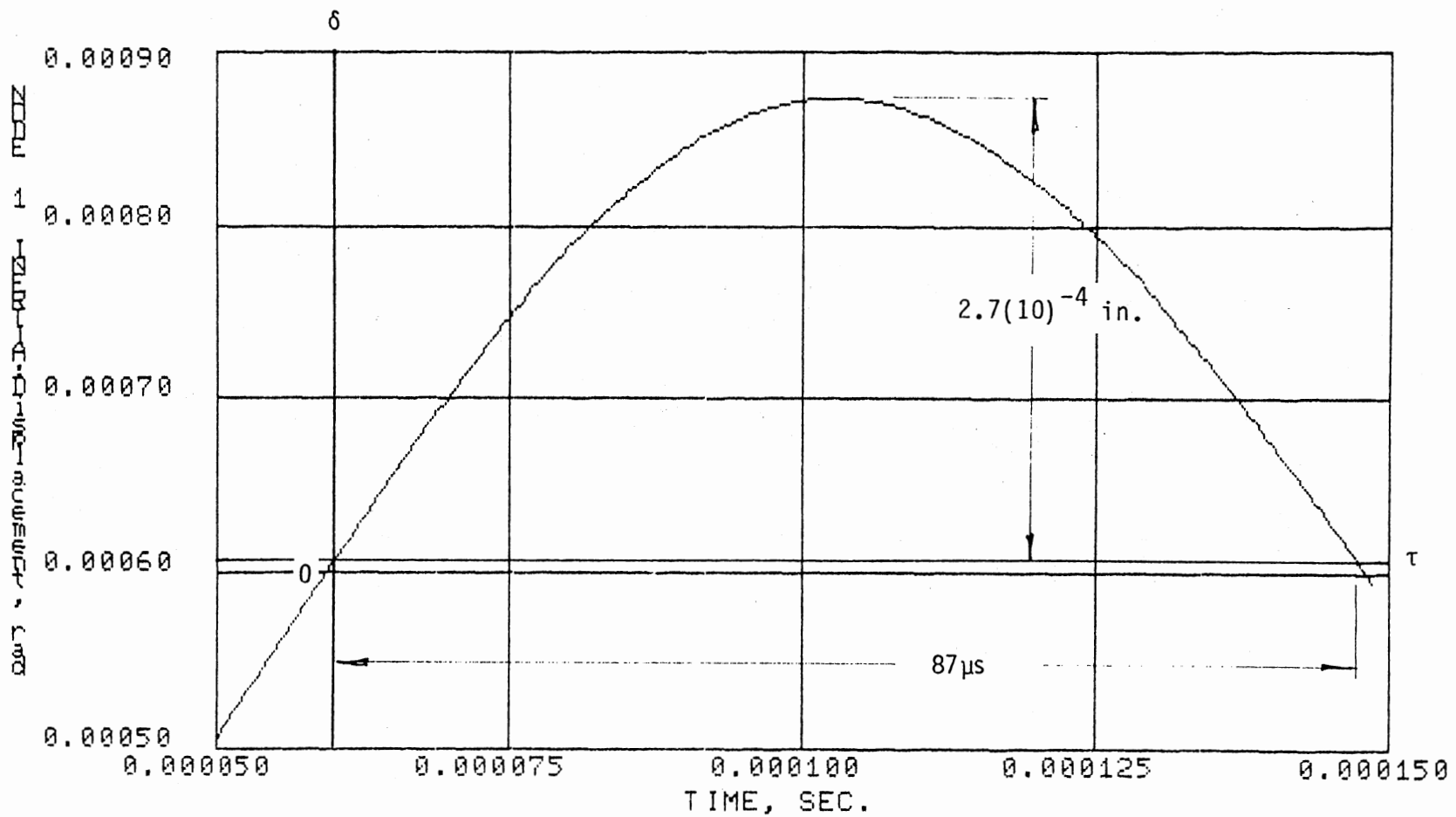
Initial Conditions:

Node 1 $x_{11} = 0.0$
 $x_{12} = 10.0$
 Node 2 $x_{21} = 0.0$
 $x_{22} = 0.0$

No external torques

Run Conditions:

Time step = $5.0E-07$
 Start time = 0.0
 Run length = $2.0E-04$



VERF03.SAU***RUN 1*** 9-FEB-88

Fig. 5.8. Spur Gear Pair with Backlash Verification Output

TABLE 5.4
INPUT FOR VERIFICATION OF
KEYED JOINT

Number of nodes: 2

Node and element description:
Node 1 - N01, Passive
Elem 1 - EL2, Keyed Joint
Node 2 - N01, Passive

R-constants:

Node 1 $RN_{11} = 7.537E-03$
 $RN_{12} = 0.0$
Elem 1 $RE_{11} = 2.6312$
 $RE_{12} = 0.001$
 $RE_{13} = 0.50$
 $RE_{14} = 0.3491$
 $RE_{15} = 4.000$
 $RE_{16} = -1.4562$
 $RE_{17} = 2.03E06$
Node 2 $RN_{21} = 10.082$
 $RN_{22} = 0.0$

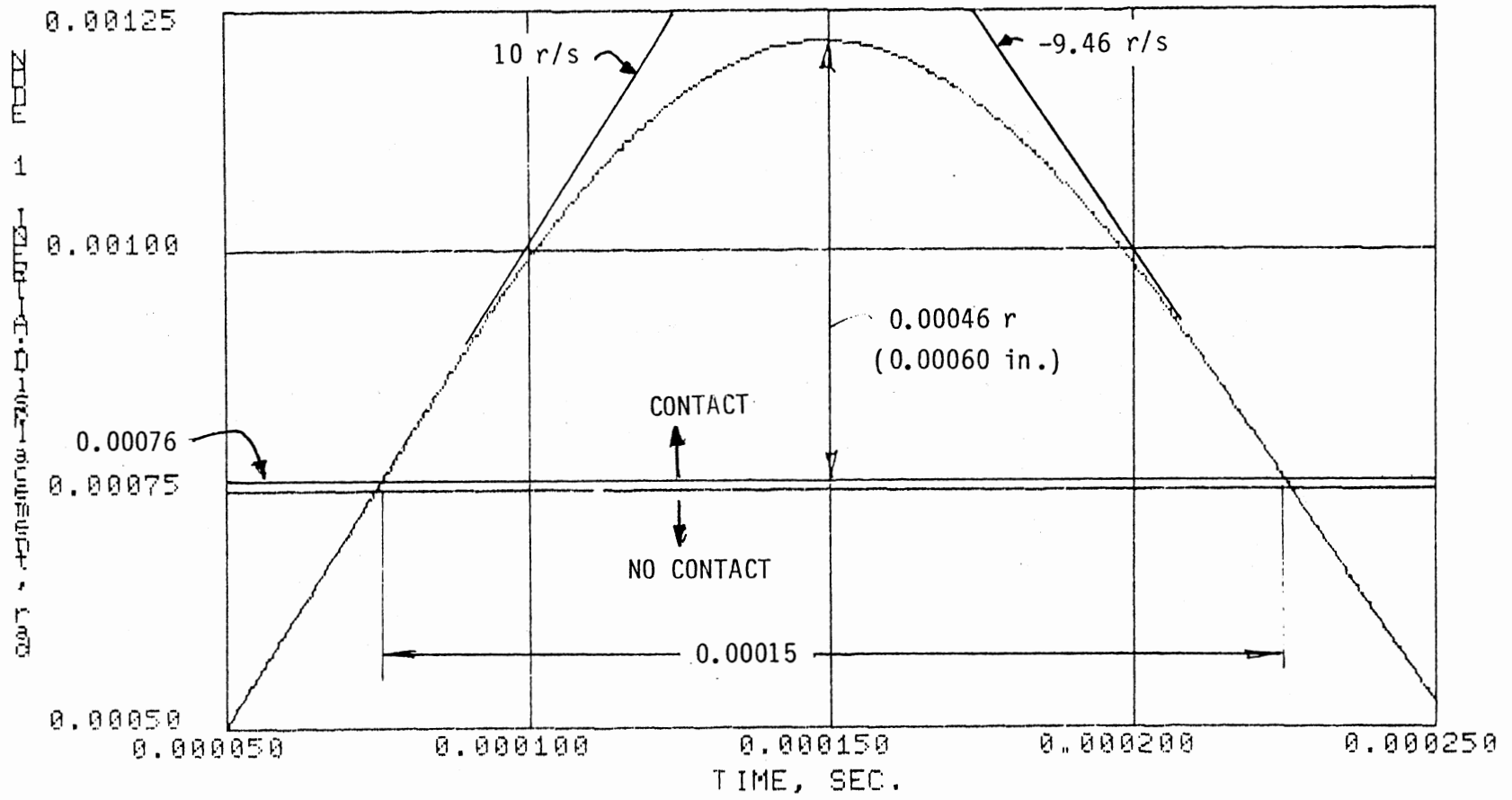
Initial Conditions:

Node 1 $x_{11} = 0.0$
 $x_{12} = 10.0$
Node 2 $x_{21} = 0.0$
 $x_{22} = 0.0$

No external torques

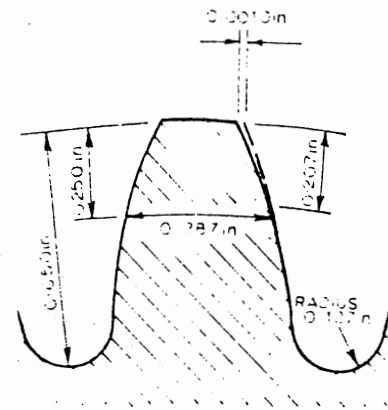
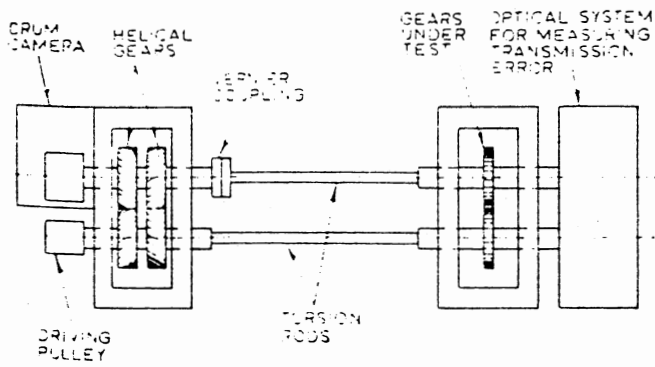
Run Conditions:

Time step = $5.0E-07$
Start time = 0.0
Run length = $3.0E-04$



VERF05***RUN 1***19-MAR-88

Fig. 5.9. Keyed Joint Verification Output



(a) Gear Test Rig

(b) Tooth Profile

Fig. 5.10. Gregory, Harris and Munro Experiment

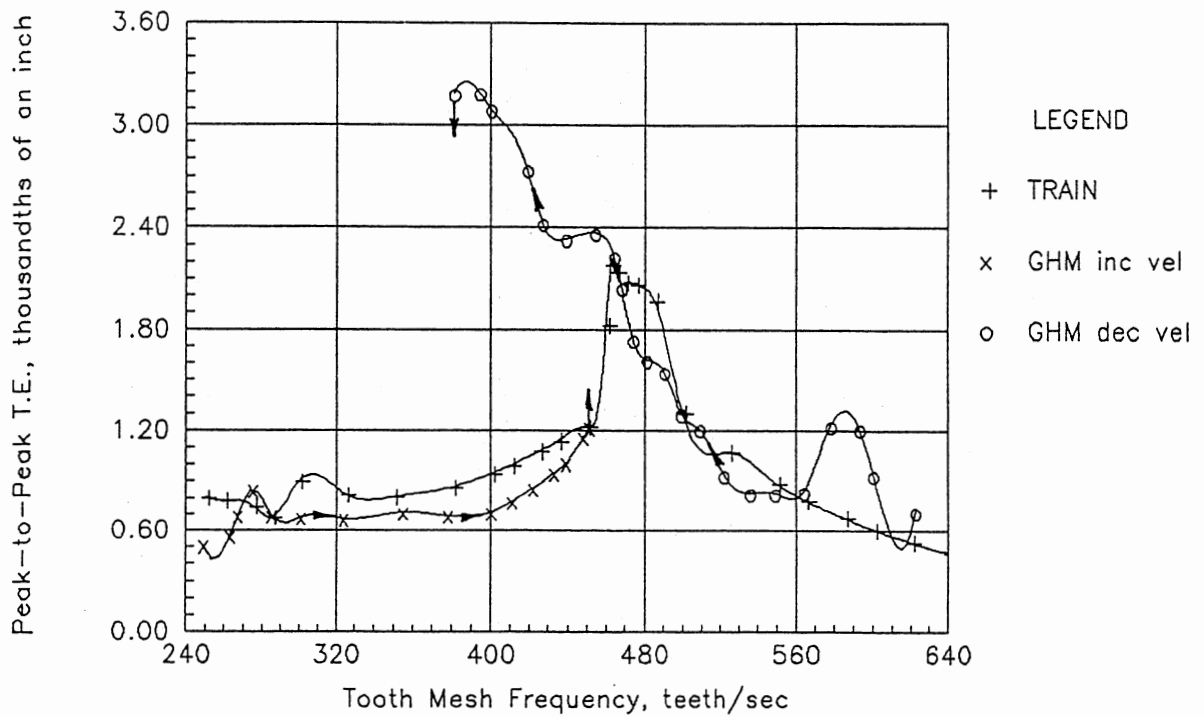


Fig. 5.11. Comparison Between TRAIN Results and Experiment

TABLE 5.5
 INPUT FOR VERIFICATION OF GREGORY,
 HARRIS AND MUNRO TEST

Number of nodes: 4

Node and element description:

Node 1 - N01, Passive
 Elem 1 - EL1, Shaft
 Node 2 - N01, Passive
 Elem 2 - EL3, Spur Gear Pair with Backlash
 Node 3 - N01, Passive
 Elem 3 - EL1, Shaft
 Node 4 - N01, Passive

R-constants:

Node 1 $RN_{11} = 100.0$
 $RN_{12} = 0.0$
 Elem 1 $RE_{11} = 32000$
 $RE_{12} = 0.0$
 Node 2 $RN_{21} = 0.987$
 $RN_{22} = 0.0$
 Elem 2 $RE_{21} = 234500$
 $RE_{22} = 3.7588$
 $RE_{23} = 3.7588$
 $RE_{24} = 32$
 $RE_{25} = 1.6676$
 $RE_{26} = 0.1637$
 $RE_{27} = 0.005$
 Node 3 $RN_{31} = 0.987$
 $RN_{32} = 0.0$
 Elem 3 $RE_{31} = 32000$
 $RE_{32} = 0.0$
 Node 4 $RN_{41} = 100.0$
 $RN_{42} = 0.0$

Initial Conditions:

Node 1 $x_{11} = -0.187847$
 $x_{12} = \text{varies}$
 Node 2 $x_{21} = -0.212810$
 $x_{22} = \text{varies}$
 Node 3 $x_{31} = -0.214283$
 $x_{32} = \text{varies}$
 Node 4 $x_{41} = -0.239246$
 $x_{42} = \text{varies}$

External torques:

Node 1 Constant velocity
 Node 4 798.8

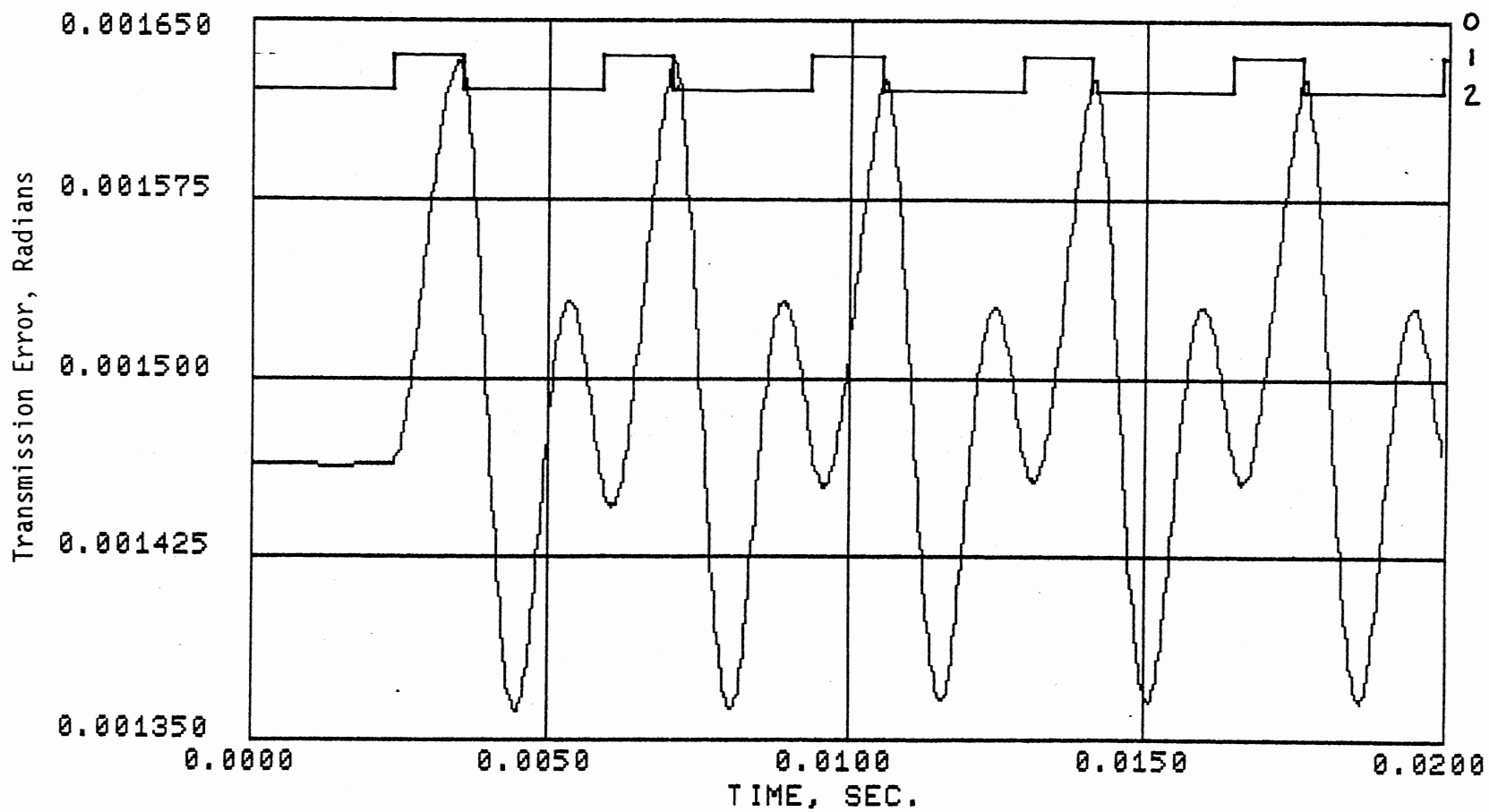
TABLE 5.5 (Continued)

Run Conditions:
Time step = 8.0E-06
Start time = 0.0
Run length = 0.0200

between the teeth.

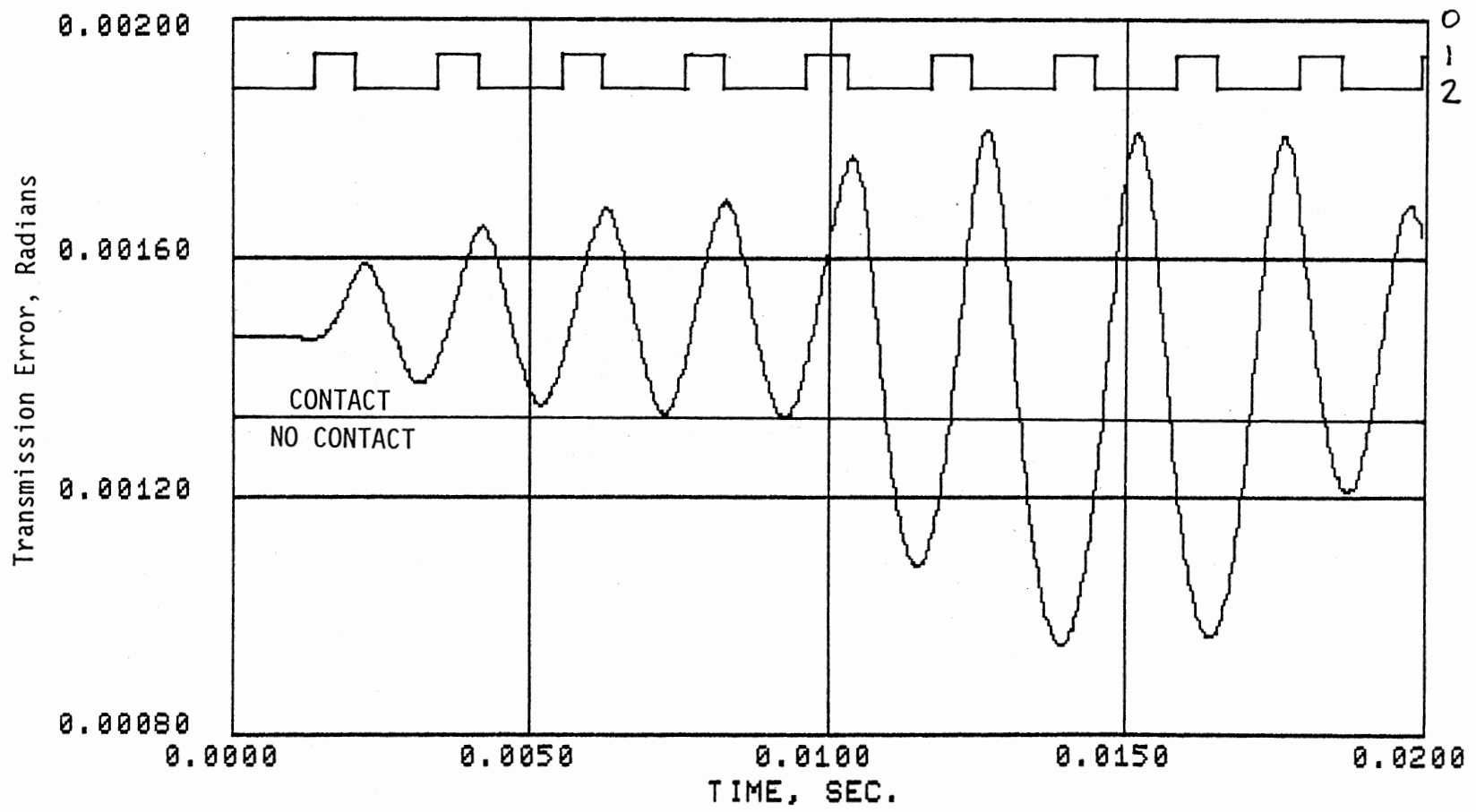
The typical response for speeds below the speed where tooth contact is first lost is shown in Figure 5.12. The tooth-mesh frequency for this plot is 285 teeth/s. The predominate response is once per tooth, but there is also a twice per tooth (570 Hz) response as well. This form of once- and twice per tooth response continues as speed increases until the critical speed of 460 teeth/s is reached. The response at a speed of 485 teeth/s is shown in Figure 5.13. Here there is a once per tooth response with growing amplitude. When the amplitude reaches the point where tooth separation occurs the response frequency changes and the amplitude grows more rapidly until the effect of the damping due to impact begins to return the amplitude to lower levels. Figure 5.14 shows a typical response at speeds above the critical range of 460 to 500 teeth/s. Here the response is uniformly once per tooth with a constant amplitude.

The TRAIN simulation agrees well with the experimental results except in the prediction of the magnitude of the jump on decreasing speed. The experiment showed a maximum peak-to-peak transmission error of about 0.00325 inch at a mesh frequency of about 385 teeth/s, while the simulation predicts a maximum of 0.0022 inch at 460 teeth/s. On the



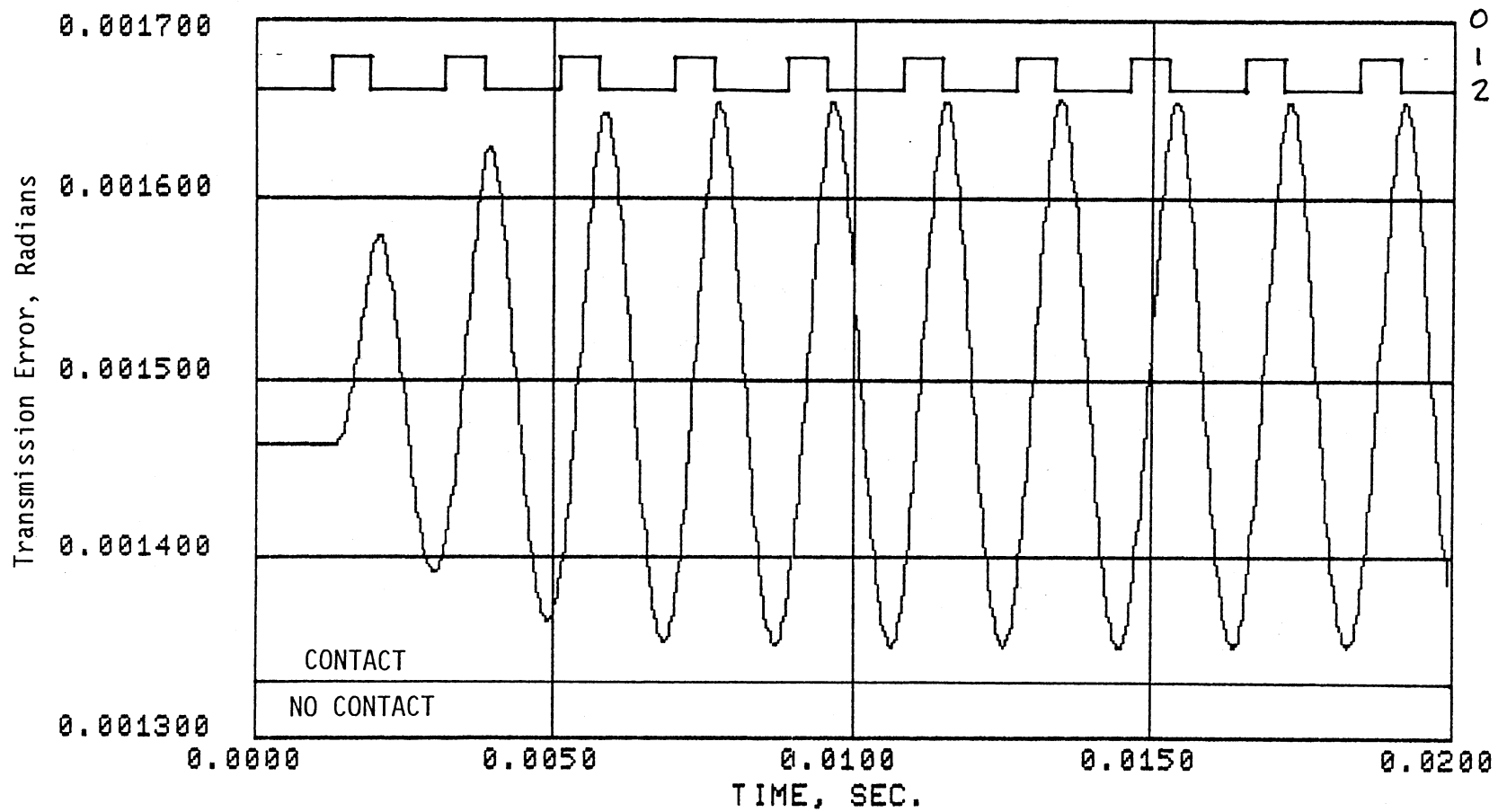
GREGORY, HARRIS & MUNRO***RUN285***20-MAY-89

Fig. 5.12. System Response, 285 Teeth/s



GREGORY, HARRIS & MUNRO***RUN485***20-MAY-89

Fig. 5.13. System Response, 485 Teeth/s



GREGORY, HARRIS & MUNRO***RUN525***20-MAY-89

Fig. 5.14. System Response, 525 Teeth/s

other hand, a system such as the one modeled would be designed to avoid speeds in the critical range. Outside of this range TRAIN will do a good job of predicting the dynamic loads on the system elements.

CHAPT VI

OTHER ELEMENT MODELS

6.1. Shaft Model

Shafts are modeled as massless visco-elastic elements. The stiffness is assumed to be constant over the span and internal damping is provided for. If a shaft has significant mass, it is accounted for in the nodes to which the shaft is attached. The shaft element is EL1 and is further described in Appendix H.

6.2. Helical Gear Pair

Helical gears are modeled in the same way as spur gears (see Chapter III) except for the way in which tooth mesh stiffness is determined. The tooth pair stiffness for spur gears is very nearly a binary function, i.e., the length of contact is either one or two times the face width (for gears with a contact ratio of two or less), the number being determined by the position of the contact point along the line of action. Because of the helical shape of the teeth, there is not an abrupt change in the length of contact on helical gears.

The contact ratio for a helical gear pair is the sum of two components: profile contact ratio, which is defined in the same way as it is for spur gears and is determined for transverse sections; and face, or axial, contact ratio. The face contact ratio is the number of base

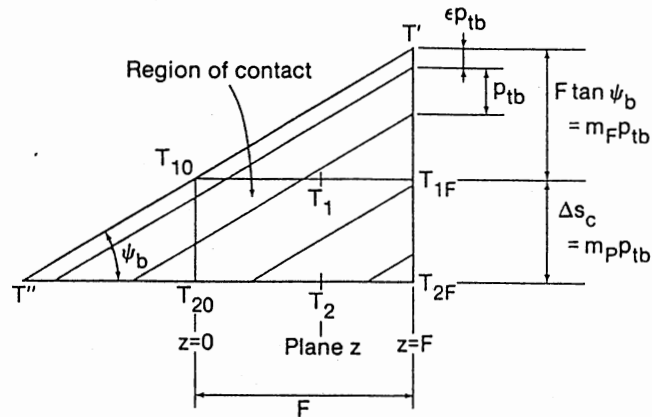


Fig. 6.1. The Plane of Action (from Colbourne, 1987)

pitches in the product of face width and the tangent of the base helix angle. The length of contact for a pair of helical gears is a function of the contact ratios, the base pitch and the base helix angle and does not vary as dramatically with tooth contact position as it does with spur gears. In fact, it can be shown that it is theoretically possible for the length of contact to be a constant if the face contact ratio is an integer.

The length of contact (the total length of the theoretical lines of contact between teeth in mesh) is given by Colbourne (1987) as

$$\begin{aligned}
 L_c = p_{tb} [& (n_{c\epsilon} + 1)(m_c - \epsilon - 0.5n_{c\epsilon}) \\
 & - (n_{F\epsilon} + 1)(m_F - \epsilon - 0.5n_{F\epsilon}) \\
 & - (n_{p\epsilon} + 1)(m_p - \epsilon - 0.5n_{p\epsilon})] / \sin \zeta_b \quad (6.1)
 \end{aligned}$$

where p_{tb} , m_c , m_F , m_p , and ζ_b are the transverse base pitch, total contact ratio, face contact ratio, profile contact ratio, and base helix angle respectively; and

$$n_{c\epsilon} = \text{int}(m_c - \epsilon)$$

$$n_{F\epsilon} = \text{int}(m_F - \epsilon)$$

$$n_{p\epsilon} = \text{int}(m_p - \epsilon)$$

and the operator $\text{int}(f)$ is the largest integer which is less than or equal to f . The value of L_c is always a minimum when the parameter ϵ is zero and a contact line passes through the upper corner T_{10} of the region of contact (see Figure 6.1.). And the value of L_c is a maximum when ϵ is equal to $[m_F - \text{int}(m_F)]$, and a contact line passes through the upper corner T_{1F} .

The mesh stiffness of the gear pair is the product of the length of contact and the stiffness per unit length which is generally taken to be $E/17.6$, where E is Young's modulus for the gear material (Quandt, 1986). The helical gear-pair element is described in Appendix H.

CHAPTER VII

SIMULATION OF A MULTI-CLEARANCE TRAIN

7.1. Description of System

A system similar to the experimental set-up of Gregory, Harris and Munro (1962) was chosen for simulational analysis. In fact, it is the same system that is described and simulated in section 5.2.5 with an additional gear pair added so that there are two elements with clearances. The second gear pair is identical to the first pair and is connected to the output of the first pair with a moderately stiff shaft.

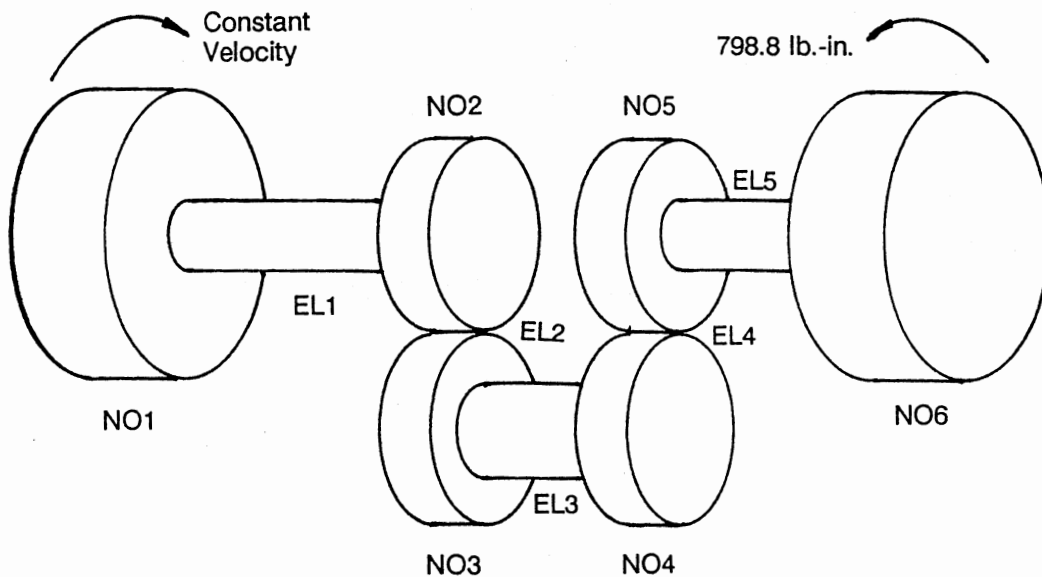


Fig. 7.1. Multi-Clearance System Diagram

TABLE 7.1
INPUT FOR MUTI-CLEARANCE
SIMULATION MODEL

Number of nodes: 6

Node and element description:

Node 1 - N01, Passive
 Elem 1 - EL1, Shaft
 Node 2 - N01, Passive
 Elem 2 - EL2, Spur Gear Pair w/Backlash
 Node 3 - N01, Passive
 Elem 3 - EL1, Shaft
 Node 4 - N01, Passive
 Elem 4 - EL2, Spur Gear Pair w/Backlash
 Node 5 - N01, Passive
 Elem 5 - EL1, Shaft
 Node 6 - N01, Passive

R-constants:

Node 1	$RN_{11} = 100.0$
	$RN_{12} = 0.0$
Elem 1	$RE_{11} = 50000$
	$RE_{12} = 0.0$
Node 2	$RN_{21} = 0.931$
	$RN_{22} = 0.0$
Elem 2	$RE_{21} = 500000$
	$RE_{22} = 3.7588$
	$RE_{23} = 3.7588$
	$RE_{24} = 32$
	$RE_{25} = 1.6676$
	$RE_{26} = 0.1637$
	$RE_{27} = 0.005$
Node 3	$RN_{31} = 0.931$
	$RN_{32} = 0.0$
Elem 3	$RE_{31} = 500000$
	$RE_{32} = 0.0$
Node 4	$RN_{41} = 0.931$
	$RN_{42} = 0.0$
Elem 4	$RE_{41} = 500000$
	$RE_{42} = 3.7588$
	$RE_{43} = 3.7588$
	$RE_{44} = 32$
	$RE_{45} = 1.6676$
	$RE_{46} = 0.1637$
	$RE_{47} = 0.005$
Node 5	$RN_{51} = 0.931$
	$RN_{52} = 0.0$
Elem 5	$RE_{51} = 50000$
	$RE_{52} = 0.0$
Node 6	$RN_{61} = 100.0$

TABLE 7.1 (Continued)

$$RN_{62} = 0.0$$

Initial Conditions:

Node 1	$x_{11} = -0.196834$
	$x_{12} = \text{varies}$
Node 2	$x_{21} = -0.212810$
	$x_{22} = \text{varies}$
Node 3	$x_{31} = -0.214203$
	$x_{32} = \text{varies}$
Node 4	$x_{41} = -0.215801$
	$x_{42} = \text{varies}$
Node 5	$x_{51} = -0.217194$
	$x_{52} = \text{varies}$
Node 6	$x_{61} = -0.233170$
	$x_{62} = \text{varies}$

External torques:

Node 1	Constant velocity
Node 4	798.8

Run Conditions:

Time step	= 2.5E-05
Start time	= 0.0
Run length	= 0.0200

A diagram of the system is shown in Figure 7.1 and the TRAIN input is given in Table 7.1.

The two gear pairs are connected, through very compliant shafts, to large inertias that form the two end nodes of the system. The input node rotates at constant velocity, regardless of the torque applied to it. The other end node has a load torque of 798.8 lb.-in. applied to it which causes an initial wind-up of the system that accounts for the nominal, or static, transmission error at each gear mesh. Thus, although the initial angular position of each node is different, the initial angular velocity of each node is the same for each run of the

simulation.

Separate analysis of the system as linear elements without backlash indicates that the system natural frequencies are 2.67, 26.2, 118, 621, and 632 Hz when both sets of gears are in single-pair contact.

7.2. Simulation Conditions

A series of 23 runs were made, varying the initial velocity for each one. The velocity is stated in terms of tooth mesh frequency which is directly related to the angular velocity and the number of teeth on a given gear. In this simulation all gears have the same number of teeth (32). The mesh frequency was varied from 260 to 640 teeth/sec (51.051 to 125.664 rad/sec). For each run, the relative displacement of each gear pair and the torque on the connecting shaft was plotted.

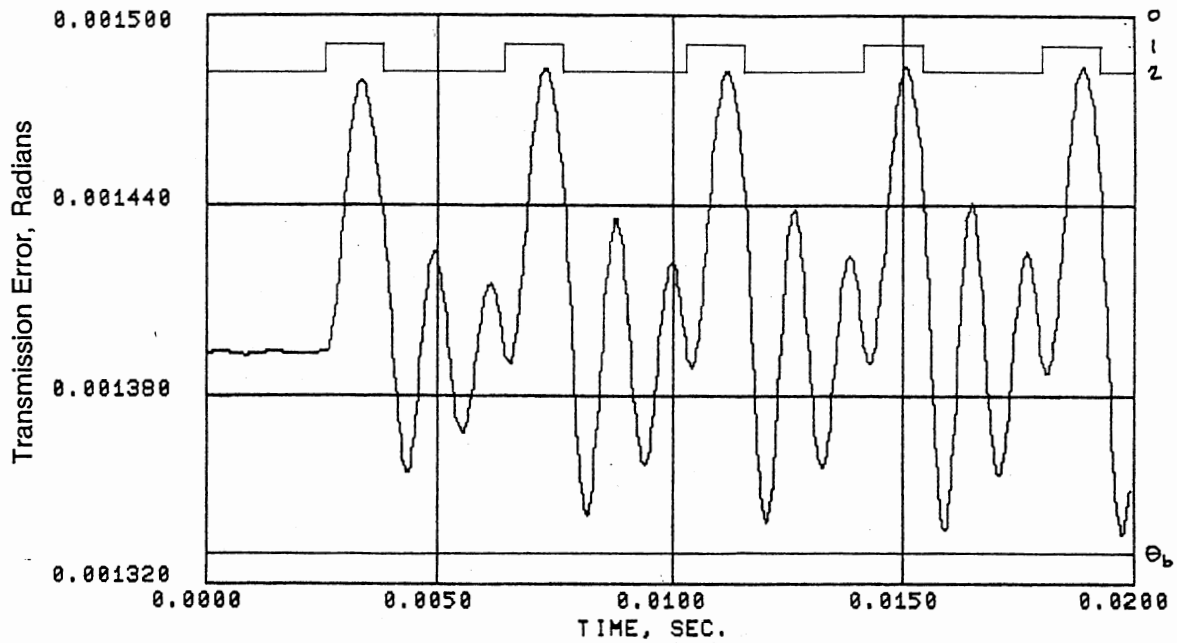
The relative displacement between a pair of kinematically perfect, rigid gears should remain zero as the gears turn. However, even gears that have no profile error will, because they are not rigid and because they have a variable length of contact, have a non-zero relative displacement. The relative displacement between a pair of gears has been defined as transmission error. Thus, any deviation of the position of a gear in mesh with another gear from the kinematically correct position is a measure of transmission error. In addition to error due to deformation and changes in length of contact, profile and other manufacturing errors are the cause of transmission error in gears. If there were no relative motion between the gears the torque on the connecting shaft would remain constant and be equal in magnitude to the load torque on the system of 798.8 lb.-in.

7.3. Simulation Results

The transmission error for each pair and the connecting shaft torque for a mesh frequency of 260 teeth/sec. are shown in Figures 7.2, 7.3 and 7.4, respectively. The plots of transmission error also contain plots of the number of pairs of teeth in contact that runs along the top of the transmission error plot. Notice that the scale (which is arbitrary) for the number of pairs in contact increases toward the bottom of the figure. The line which indicates the limit of contact between the gears is also shown on the transmission error plots and is labeled on the right-hand side as θ_0 . When the transmission error (relative displacement) falls below this line the gears lose contact. When the curve recrosses the line there is an impact between the gears. As can be seen, at a mesh frequency of 260 teeth/sec. there is no loss of contact for either gear pair.

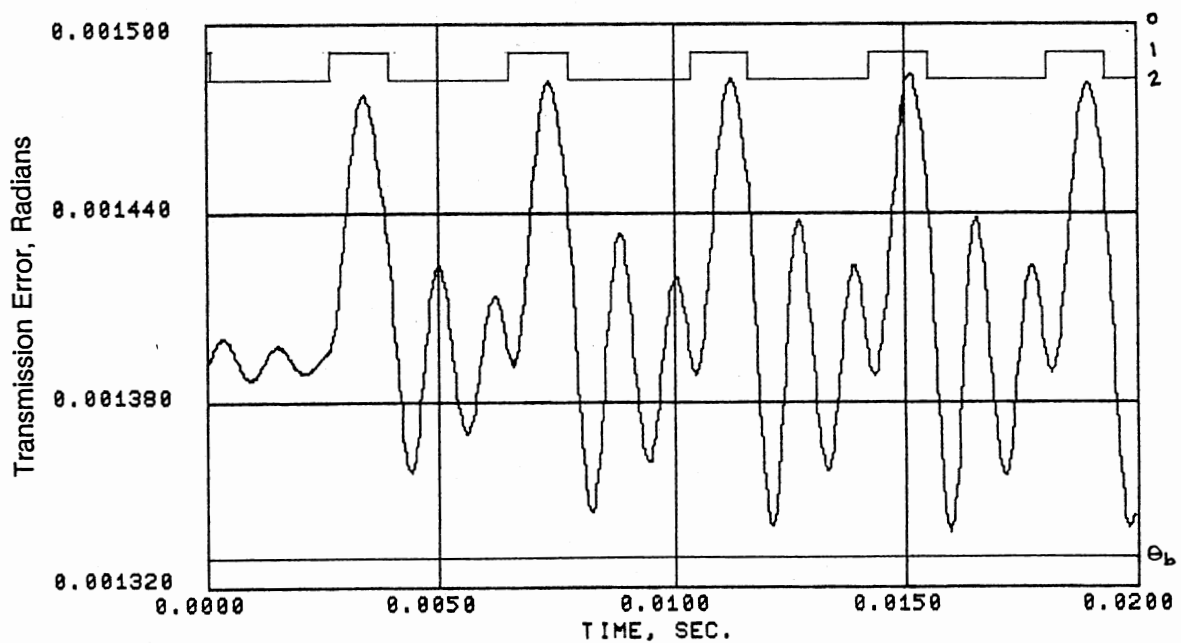
The response for both sets of gears is virtually identical, the only difference is a result of the fact that the first pair (Fig. 7.2) is initially in two-pair contact while the second pair (Fig. 7.3) is initially in single-pair contact. However, the change from one- to two-pair contact occurs very soon after the start of the simulation.

As the mesh frequency is increased (by speeding up the system) the gears remain in contact until the 330-340 teeth/sec. range. From this speed until about 480 teeth/sec. there is some loss of contact between mating gears. Figure 7.5 shows the response of the first pair at a mesh frequency of 400 teeth/sec. Notice that there is loss of contact on almost every cycle of transmission error. This has a damping effect on the motion which prevents even larger swings in relative displacement.



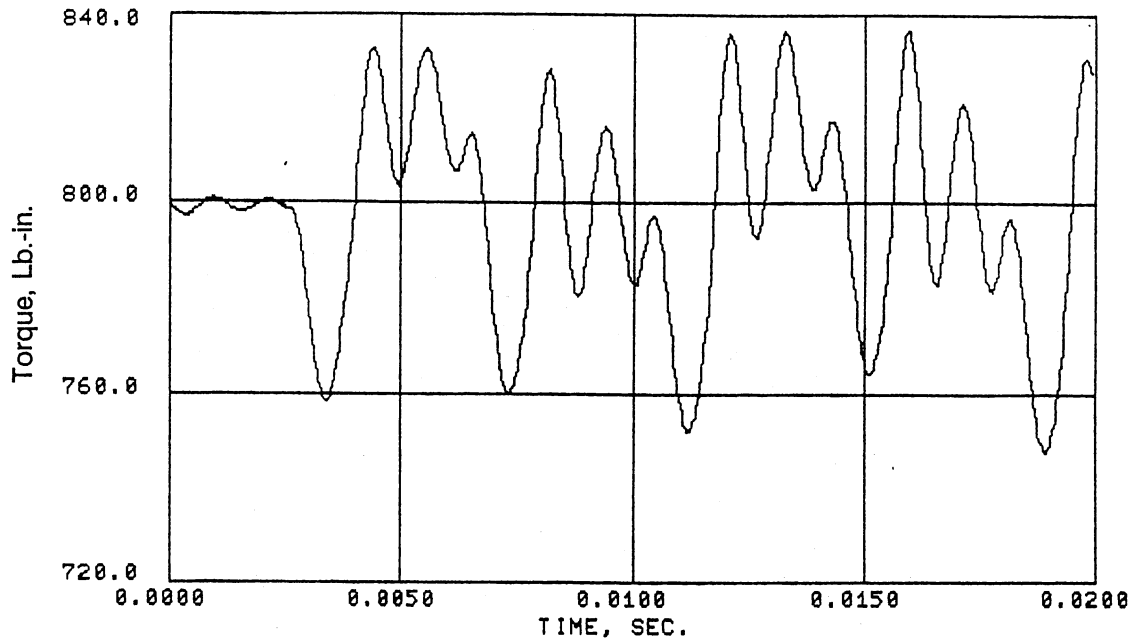
TWO CLEARANCE MODEL***RUN260***23-OCT-88

Fig. 7.2. Transmission Error, Nodes 2 & 3, 260 Teeth/Sec.



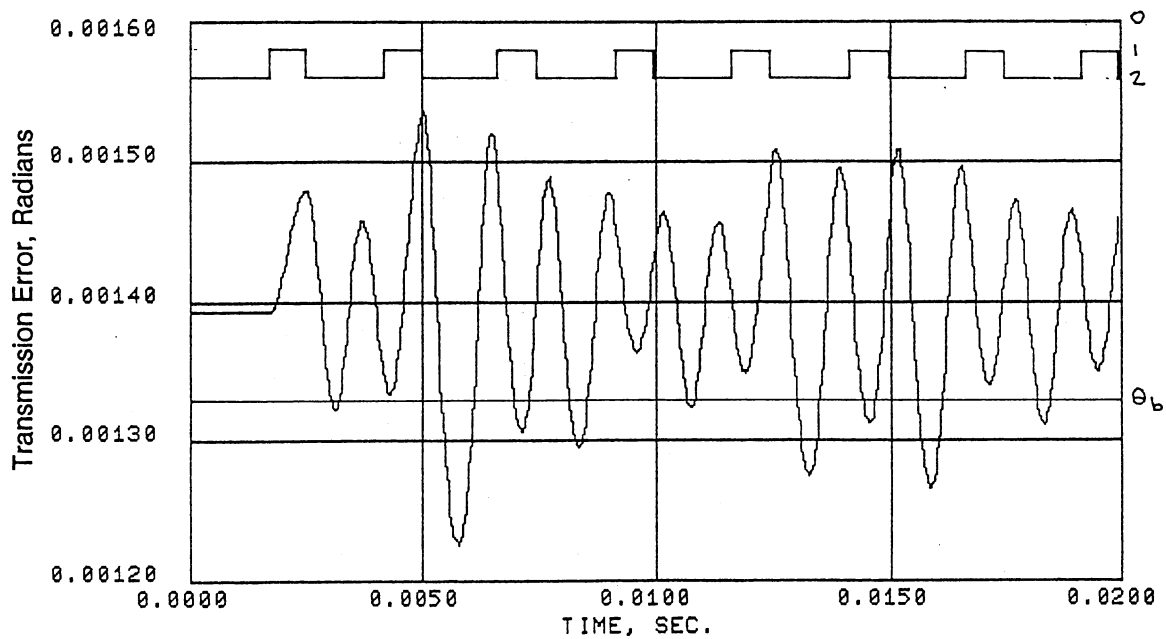
TWO CLEARANCE MODEL***RUN260***23-OCT-88

Fig. 7.3. Transmission Error, Nodes 4 & 5, 260 Teeth/Sec.



TWO CLEARANCE MODEL***RUN260***23-OCT-88

Fig. 7.4. Torque on Shaft EL3, 260 Teeth/Sec.



TWO CLEARANCE MODEL***RUN400***23-OCT-88

Fig. 7.5. Transmission Error, Nodes 2 & 3, 400 Teeth/Sec.

A comparison between the response of the first gear pair in this simulation (labeled as TWO CLEAR) with the only gear pair in the simulation of Section 5.2.5 (labeled as G, H & M) is shown in Figure 7.6. Here the peak-to-peak change in transmission error is plotted as a function of mesh frequency. There is no appreciable change in the peak-to-peak transmission error when a second gear pair (and a second clearance) is added to the system. However, it must be pointed out that, in this case, the second set had identical characteristics to the first and, its one-pair to two-pair change function was almost in phase with the first gear pair. Also shown in Figure 7.6 are the regions of continuous contact and intermittent contact.

The transmission error in the gears leads to torsional variations in the other elements of the drive system. The maximum, minimum and range torques on the shaft connecting the two gears is shown as a function of mesh frequency in Figure 7.7. Note that the nominal torque is the load torque of 798.8 lb.-in.

Finally, from the analysis of the linearized system without backlash, we would expect to find the greatest transmission error in the 600-640 teeth/sec. range. This is the case, but the response in the 340-380 teeth/sec. range was not predicted. This happens to be about three times the 118 Hz. frequency and might be explained as a response to that system frequency. It is also nearly one-half the frequency of the predominant response frequency and might be related to it.

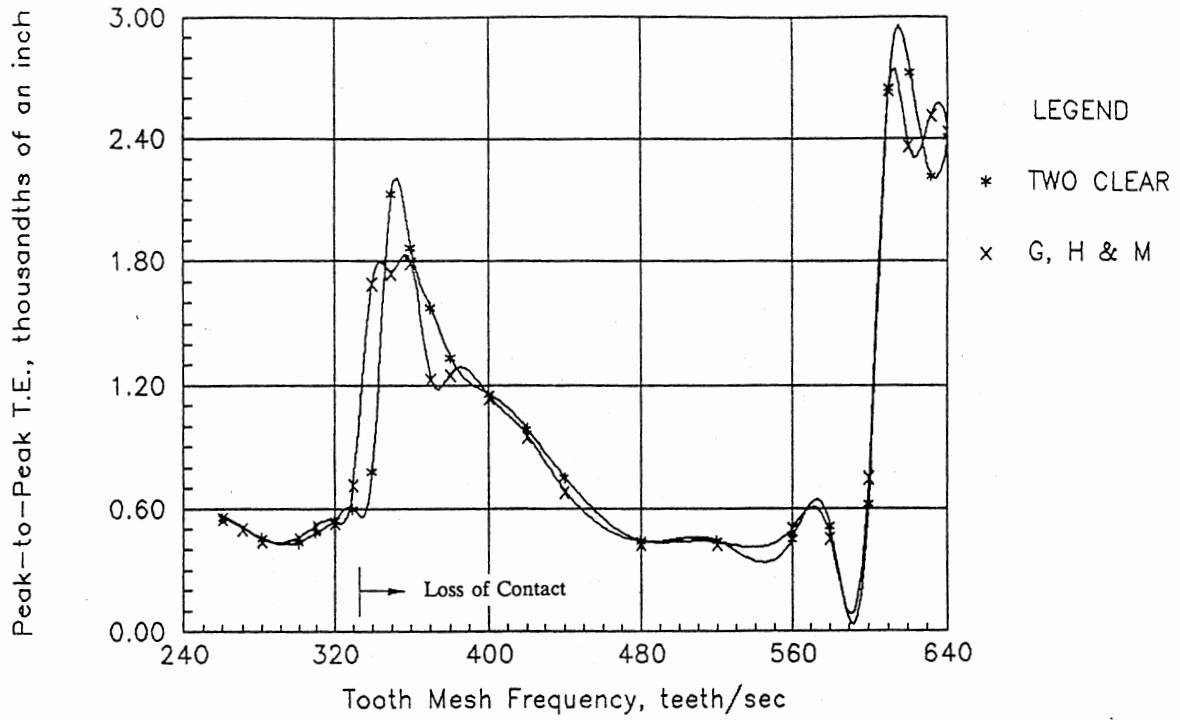


Fig. 7.6. Peak-To-Peak Transmission Error vs Mesh Frequency

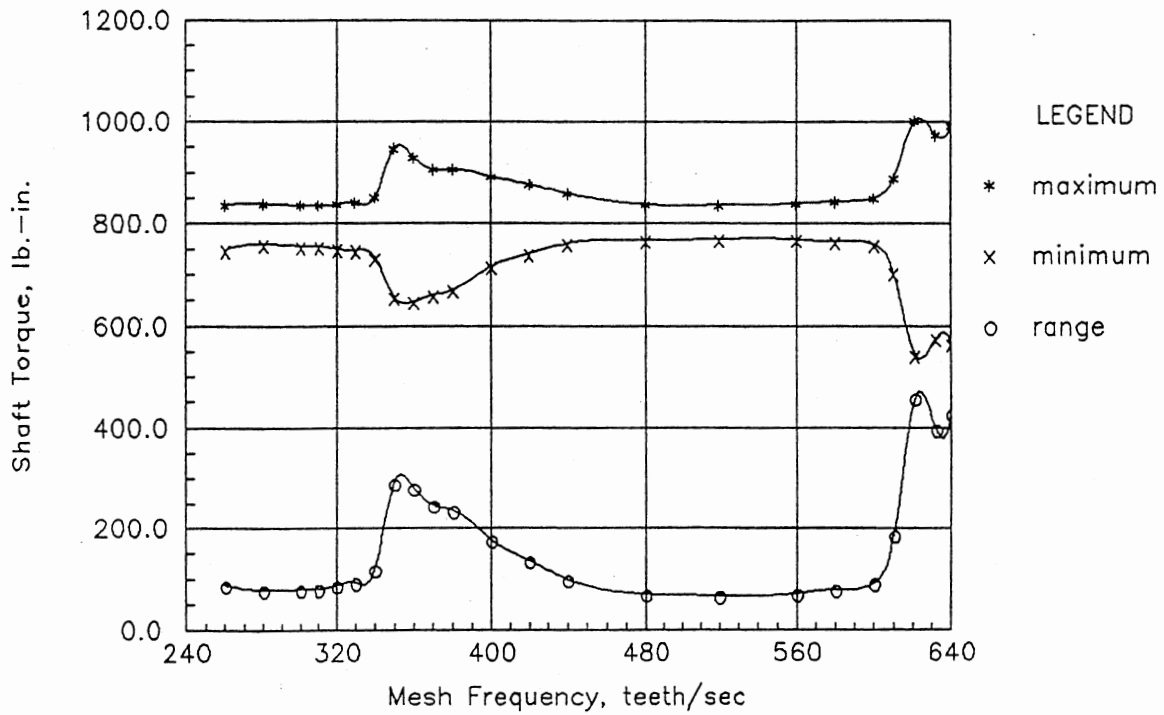


Fig. 7.7. Torque on Shaft EL3 vs Mesh Frequency

CHAPTER VIII

SUMMARY, CONCLUSIONS, AND RECOMMENDATIONS

8.1. Summary

The work described herein concerns a) the development of a general-purpose, interactive simulation program with graphical interface, b) the development of realistic, nonlinear mechanical elements (particularly the keyed joint), and c) the use of the program to simulate various mechanical systems.

Although not described in detail, the simulation program TRAIN (which is described in Chapter V) is a central part of the work. The design of the preprocessor, with its ability to accept any sequential arrangement of elements, and the graphic postprocessor utilize distinctive programming techniques that were developed by the author.

The two major mechanical elements developed are the spur/helical gear pair with backlash and the keyed joint. They are described in Chapters III and IV, respectively. The gear pair is based on the earlier work of Yang and Sun (1985) with additions in the area of change of tooth stiffness with position. The development of the keyed joint model is entirely new. The use of finite element modeling was very helpful in the development.

The use and results from TRAIN are found in Chapters V and VII. In Chapter V the various verification models are described and results are

given. Chapter VII is a description of a multi-clearance model and the results obtained when the system was simulated using TRAIN.

8.2. Conclusions

When the work was started, it was not at all clear that the user interface that was desired for the simulation program could be realized. Now that the goal is met, we can conclude that a simulation preprocessor that allows the user to build a model interactively in block diagram fashion without explicitly writing any system equations is feasible and desirable.

Repeated use of TRAIN by the author has shown it to be a versatile program useful for both transient and steady-state analysis of nonlinear systems.

A rotary, as opposed to an equivalent rectilinear, model is feasible and makes the interpretation of results easier.

A keyed joint can, and should, be modeled as a combination of hub, key and shaft components separated by clearances.

A method has been developed for the study of systems with multiple clearances although that has not been done to any extent in this work.

8.3. Recommendations

The recommendations made all relate to further work, and they are:

1. Add the ability to specify nonstandard tooth profiles to the spur and helical gear models. This will allow a more thorough comparison with the published work of Gregory, et al. (1962).
2. Conduct physical experiments to verify the keyed joint model predictions.

3. Develop models of other drive train elements such as worm gears.
4. Port the program to a microcomputer environment, making improvements in the user interface and the graphic output in the process.
5. Develop off-line programs that take as interactive input the user's description of system elements and produce as output the required constants for running TRAIN.

BIBLIOGRAPHY

- Allen, R. R., 1979, "Multiport Models for the Kinematic and Dynamic Analysis of Gear Power Transmissions," ASME, Journal of Mechanical Design, Vol. 101, No. 2, April, pp. 258-267
- Azar, R. C., 1974, "An Investigation of Impact Phenomenon in Geared Torsional Systems," (unpub. Ph.D. dissertation, Univ. of Massachusetts, Amherst, MA)
- Azar, R. C., and Crossley, F. R. E., 1975, "An Experimental Investigation of Impact Phenomenon in Spur Gear Systems," 4th World Congress
- Azar, R. C., and Crossley, F. R. E., 1977, "Digital Simulation of Impact Phenomenon in Spur Gear Systems," ASME, Journal of Engineering for Industry, Vol. 99, No. 3, Aug., pp. 792-798
- Bahgat, B. M., Osman, M. O. M., and Sankar, T. S., 1983, "On the Spur-Gear Dynamic Tooth-Load Under Consideration of System Elasticity and Tooth Involute Profile," ASME, Journal of Mechanisms, Transmissions, and Automation in Design, Vol. 105, Sept., pp. 302-309
- Barkan, P., 1964, "Impact," Mechanical Design and Systems Handbook. New York: McGraw Hill Book Co., Inc.
- Benton, M., and Seireg, A., 1978, "Simulation of Resonances and Instability Conditions in Pinion-Gear Systems," ASME, Journal of Mechanical Design, Vol. 100, No. 1, Jan., pp. 26-31
- Benton, M., and Seireg, A., 1981, "Factors Influencing Instability and Resonance in Geared Systems," ASME, Journal of Mechanical Design, Vol. 103, April, pp. 372-378
- Brach, R. M., 1981, "Moments Between Impacting Rigid Bodies," ASME, Journal of Mechanical Design, Vol. 103, Oct., pp. 812-817
- Budynas, R. G., 1977, Advanced Strength and Applied Stress Analysis. New York: McGraw Hill Book Co., Inc.
- Cardou, A., and Tordion, G. V., 1984, "Calculation of Spur Gear Tooth Flexibility by the Complex Potential Method," 84-DET-85, ASME, New York, NY
- Chakraborty, J., and Hunashikatti, H. G., 1974, "Determination of the Combined Mesh Stiffness of a Spur Gear Pair Under Load," 74-DET-39,

ASME, New York, NY

- Cipra, R. J., and Uicker, J. J., Jr., 1981a, "On the Dynamic Simulation of Large Nonlinear Mechanical Systems. Part 1: An Overview of the Simulation Technique," ASME, Journal of Mechanical Design, Vol. 103, Oct., pp. 849-856
- Cipra, R. J., and Uicker, J. J., Jr., 1981b, "On the Dynamic Simulation of Large Nonlinear Mechanical Systems. Part 2: The Time Integration Technique," ASME, Journal of Mechanical Design, Vol. 103, Oct., pp. 857-865.
- Colbourne, J. R., 1987, The Geometry of Involute Gears, New York: Springer-Verlag, pp. 491-502
- Cornell, R. W., 1981, "Compliance and Stress Sensitivity of Spur Gear Teeth," ASME, Journal of Mechanical Design, Vol. 103, April, pp. 447-459
- Deresiewicz, H., 1968, "A Note on Hertz's Theory of Impact," Acta Mechanica, Vol. 6, pp. 110-112
- Dubowsky, S., 1974, "On Predicting the Dynamic Effects of Clearances in Planar Mechanisms," ASME, Journal of Engineering for Industry, Vol. 96, No. 1, Feb., pp. 317-323
- Dubowsky, S., and Gardner, T. N., 1975, "Dynamic Interactions of Link Elasticity and Clearance Connections in Planar Mechanical Systems," ASME, Journal of Engineering in Industry, Vol. 97, No. 2, May, pp. 652-661
- Dubowsky, S., and Freudenstein, F., 1971, "Dynamic Analysis of Mechanical Systems With Clearances, Part 1: Formation of Dynamic Model; Part 2: Dynamic Response," ASME, Journal of Engineering for Industry, Vol. 93, No. 1, Feb., pp. 305-316
- Dubowsky, S., and Gardner, T. N., 1977, "Design and Analysis of Multilink Flexible Mechanisms With Multiple Clearance Connections," ASME, Journal of Engineering For Industry, Vol. 99, Series B, No. 1, Feb., pp. 88-96
- Dubowsky, S., and Moening, M. F., 1978, "An Experimental and Analytical Study of Impact Forces in Elastic Mechanical Systems with Clearances," Pergamon Press Ltd., Mechanism and Machine Theory, Vol. 13, pp. 451-465
- Dubowsky, S., Deck, J. F., and Costello, H., 1986, "The Dynamic Modeling of Flexible Spatial Machine Systems With Clearance Connections," 86-DET-62, ASME, New York, NY
- Dudley, D. W., 1984, Handbook of Practical Gear Design. 2nd Ed. New York: McGraw-Hill Book Co., Inc.
- Elkholy, A. H., 1984, "Tooth Load Sharing in High-Contact Ratio Spur

- Gears," 84-DET-65, ASME, New York, NY
- Furrow, R. W., and Mabie, H. H., 1970, "The Measurement of Static Deflection in Spur Gear Teeth," Pergamon Press, Journal of Mechanisms, Vol. 5, No. 2, pp. 147-168
- Gregory, R. W., Harris, S. L. and Munro, R. G., 1962, "Dynamic Behaviour of Spur Gears," Proceedings of the Institute of Mechanical Engineers, London, Vol. 178 Pt. 1 No. 8, pp. 207-226
- Gregory, R. W., Harris, S. L. and Munro, R. G., 1963, "Torsional Motions of a Pair of Spur Gears," Proceedings of the Institute of Mechanical Engineers, London, Vol. 178 Pt. 3F, pp. 166-173
- Hahn, W. F., 1969, "Study of Instantaneous Load to Which Gear Teeth are Subjected," (Unpub. Ph.D. dissertation, Univ. of Illinois, Urbana, IL)
- Haines, R. S., 1980, "Survey: 2-Dimensional Motion and Impact at Revolute Joints," Pergamon Press Ltd., Mechanism and Machine Theory, Vol. 15, pp. 361-370
- Harris, S. L., 1957, "Dynamic Loads on the Teeth of Spur Gears," Proceedings of the Institute of Mechanical Engineers, London, June, pp. 87-112
- Herbert, R. G., and McWhannell, D. C., 1977, "Shape and Frequency Composition of Pulses From an Impact Pair," ASME, Journal of Engineering for Industry, Vol. 99, Series B, Aug., pp. 513-518
- Huang, R. C., Haug, E. J., Jr., and Andrews, J. G., 1978, "Sensitivity Analysis and Optimal Design of a Mechanical System with Intermittent Motion," ASME, Journal of Mechanical Design, Vol. 100, No. 3, July, pp. 492-499
- Hunt, K. H., and Crossley, F. R. E., 1975, "Coefficient of Restitution Interpreted as Damping in Vibroimpact," ASME, Journal of Applied Mechanics, Vol. 97, Series E, No. 2, June, pp. 440-445
- Kashay, A. M., Voelker, F. C., and Smalley, A. J., 1972, "Dynamic Shock Phenomena in Rolling Mills," ASME, Journal of Engineering for Industry, May, pp. 647-659
- Kasuba, R., 1962, "An Analytical and Experimental Study of Dynamic Loads on Spur Gear Teeth," (Unpub. Ph.D. dissertation, Univ. of Illinois, Urbana, IL)
- Kasuba, R., and Evans, J. W., 1981, "An Extended Model for Determining Dynamic Loads in Spur Gearing," ASME, Journal of Mechanical Design, Vol. 103, No. 2, April, pp. 398-409
- Liu, T., and Lee, T. W., 1986, "Dynamics of An Overconstrained Shaft Coupling," 86-DET-7, ASME, New York, NY

- Mostofi, A., and Dadbin, A., 1986, "Impact Type Loading Mechanisms," 86-DET-170, ASME, New York, NY
- Okubo, H., Hoson, K., and Sakaki, K., 1968, "The Stress Concentration in Keyways when Torque is Transmitted Through Keys," *Experimental Mechanics*, Vol. 8, Aug., pp. 375-380
- Oledzki, A., 1980, "On the Modeling of Certain Mechanical Systems with a Hysteresis Loop," Pergamon Press Ltd., *Mechanism and Machine Theory*, Vol. 15, pp. 479-490
- Orthwein, W. C., 1975, "Keyway Stresses When Torsional Loading Is Applied by the Keys," *Experimental Mechanics*, Vol. 15, June, pp. 245-248
- Orthwein, W. C., 1979, "A New Key and Keyway Design," *ASME, Journal of Mechanical Design*, April, pp. 338-341
- Quandt, E., 1986, "Prediction of Mesh-Generated Gear System Vibrations," David Taylor Research Center, Annapolis, MD, DTNSRDC/PAS-86/3, p. 12
- Richardson, Herbert H., 1958, "Static and Dynamic Load, Stress, and Deflection Cycles in Spur-Gear Systems," (Unpub. Sc. D. dissertation, M.I.T., Cambridge, MA)
- Riven, E. I., 1986, "Design and Application Criteria for Connecting Couplings," *ASME, Journal of Mechanisms, Transmissions, and Automation in Design*, Vol. 108, No. 1, March, pp. 96-105
- Roark, R. J. and Young, W. C., 1975, Formulas for Stress and Strain. 5th Ed. New York: McGraw Hill Book Co., Inc.
- Seager, D. L., 1969, "Dynamic Behavior of Helical Gears," 60-VIBR-16, ASME, New York, NY
- Seireg, A., Shah, S. C. and Khazekhan, K., 1975, "Dynamic Stresses in Gear Teeth Under Conditions of Sustained Oscillations Through the Backlash," 4th World Congress on the Theory of Machines and Mechanisms, Sept., pp. 205-208
- Shigley, J. E. and Mitchell, L. D., 1983, Mechanical Engineering Design. 4th Ed. New York: McGraw-Hill.
- Timoshenko, S. P. and Goodier, J. N., 1970, Theory of Elasticity. 3rd Ed. New York: McGraw Hill Book Co., Inc.
- Townend, M. S., and Kerr, A. H., 1982, "Approximate Dynamics Using Hamilton's Principle, Including Applications to Non-Conservative and Constrained Systems," Pergamon Press Ltd., *Mechanism and Machine Theory*, Vol. 17, No. 3, pp. 213-220
- Veluswami, M. A., and Crossley, F. R. E., 1975, "Multiple Impacts of a Ball Between Two Plates, Part I-Some Experimental Observations;

- Part II-Mathematical Modeling," ASME, Journal of Engineering for Industry, Vol. 97, Series B, No. 3, Aug., pp. 820-835
- Wang, C. C., 1975, "Rotational Vibration with Backlash," (Unpub. Ph.D. dissertation, Univ. of Sheffield, England)
- Wang, C. C., 1978, "Rotational Vibration with Backlash - Part 1," ASME, Journal of Mechanical Design, Vol. 100, No. 2, April, pp. 363-373
- Wang, C. C., 1980, "On Derivation of Hertzian Impact Formula in the Geared Rotational System," 80-C2/DET-55, ASME, New York, NY
- Wang, C. C., 1981a, "Rotational Vibration with Backlash - Part 2," ASME, Journal of Mechanical Design, Vol. 103, No. 2, April, pp. 387-397
- Wang, C. C., 1981b, "Calculating Natural Frequencies with Extended Tuplin's Method," ASME, Journal of Mechanical Design, Vol. 103, April, pp. 379-386
- Wang, C. C., 1985, "On Analytical Evaluation of Gear Dynamic Factors Based on Rigid Body Dynamics," ASME, Journal of Mechanisms, Transmissions, and Automation in Design, Vol. 107, No. 2, Jun., pp. 301-311
- Wang, S. M., 1974, "Analysis of Nonlinear Transient Motion of a Geared Torsional System," ASME, Journal of Engineering for Industry, Vol. 96, No. 1, Feb., pp. 51-59
- Wang, S. M., and Morse, I. E., Jr., 1972, "Torsional Response of a Gear Train System," ASME, Journal of Engineering for Industry, Vol. 94, No. 2, May, pp. 583-594
- Weber, C., 1949, "The Deformations of Loaded Gears and the Effect on Their Load-Carrying Capacity," Report No. 3
- Willis, R. J., 1983, "Some Experiences with Computers in the Design of Geared Power Transmission Systems," IMACS, Modeling and Simulation in Engineering
- Winfrey, R. C., Anderson, R. V., and Gnilka, C. W., 1973, "Analysis of Elastic Machinery with Clearances," ASME, Journal of Engineering for Industry, Vol. 95, No. 3, Aug., pp. 695-703
- Yang, D. C. H., and Lin, J. Y., 1986, "Hertzian Damping, Tooth Friction and Bending Elasticity in Gear Impact Dynamics," 86-DET-64, ASME, New York, NY
- Yang, D. C. H., and Sun, Z. S., 1985, "A Rotary Model for Spur Gear Dynamics," ASME, Journal of Mechanisms, Transmissions, and Automation in Design, Vol. 107, No. 4, Dec., pp. 529-535

APPENDIX A

TOOTH MESH CONTACT ZONES

When a tooth first comes into contact with a tooth on the mating gear it will be in a zone of two-pair contact. Between that instant and the time when it ceases to make contact with the mating gear it will go through a zone of single-pair contact. The angle from the point of initial contact to the beginning of single-pair contact is

$2\pi(m_p - 1)/N$, while the angle from the point of initial contact to the end of single-pair contact is $2\pi/N$; where m_p is the contact ratio and N is the number of teeth on the gear. The width of the single-pair contact zone is $2\pi(2 - m_p)/N$, $1 \leq m_p \leq 2$.

These angles and other basic gear relationships are shown on Figure A.1. In this figure, the line marked "A" represents the beginning of contact for a pair of teeth. "P" is the point at which the teeth pass through the pitch point, and "B" is the end of contact for the pair. The angle, α , is the angle of approach. The number of teeth in contact is a periodic function with period $2\pi/N$, but the angular displacement of a gear ranges between 0 and 2π .

The value of c in equations 3.18 and 3.19 is found by the following procedure.

$$\text{Let } n = \text{INT}\left[\frac{\theta}{2\pi N}\right] \quad (\text{A.1})$$

where θ is the rotational displacement of the gear, and N is the number of teeth. Then, let $\theta' = \theta - n(2\pi/N)$. Now, several boundaries can be

defined. They are

$$\left. \begin{aligned}
 \theta_1' &= \pi(4m_p - 9) - \alpha \\
 \theta_2' &= -\alpha - \pi/2N \\
 \theta_3' &= \theta_1' + 2\pi/N \\
 \theta_4' &= \theta_2' + 2\pi/N \\
 \theta_5' &= \theta_3' + 2\pi/N \\
 \theta_6' &= \theta_4' + 2\pi/N
 \end{aligned} \right\} \quad (\text{A.2})$$

The following algorithm is used to define c .

If $\theta' < \theta_1'$ then

$$c = 2$$

Else if $\theta_1' \leq \theta' < \theta_2'$ then

$$c = 1$$

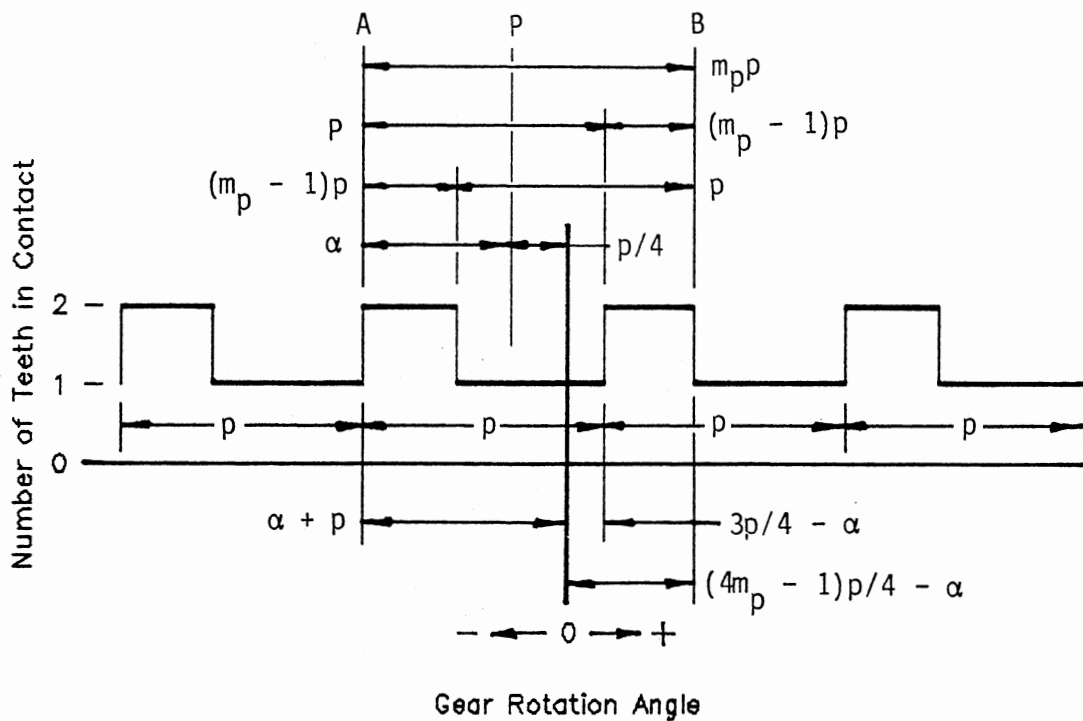


Fig. A.1. Number of Teeth in Contact

Else if $\theta_2' \leq \theta' < \theta_3'$ then

$c = 2$

Else if $\theta_3' \leq \theta' < \theta_4'$ then

$c = 1$

Else if $\theta_4' \leq \theta' < \theta_5'$ then

$c = 2$

Else if $\theta_5' \leq \theta' < \theta_6'$ then

$c = 1$

Else

$c = 2$

APPENDIX B

GEAR TOOTH DEFLECTION ANALYSIS

The following method was used to predict tooth deflection using the Timoshenko and Baud tapered beam.

First, determine L , h_0 and β for the tooth (see Figure 3.4 and equation (3.10)) as follows:

1. Establish a cartesian coordinate system with origin at the gear center and the x-axis coincident with the centerline of a tooth.
2. Define the following points on the tooth profile: P, at the pitch circle; Q, at the addendum circle (tip).
3. Pass a line through the points P and Q.
4. Define the intersection of this line with the x-axis as point R, and with the dedendum circle as point S.
5. Then

$$L = X_R - X_S \quad (B.1)$$

$$h_0 = 2Y_S \quad (B.2)$$

$$\beta = \tan^{-1}[(Y_P - Y_Q)/(X_Q - X_P)] \quad (B.3)$$

Next, determine the distance from the vertex (R) to the point of application of the load, a .

1. With respect to the coordinate system defined above, let the point on the tooth profile where the load is applied be C.

Then, if

R_C = distance from O to C

t_C = arc tooth thickness at C

α_C = angle subtended by half tooth thickness at C

ϕ_C = involute pressure angle at C

2. The distance, a , is

$$a = X_R - R_C \cos \alpha_C \quad (\text{B.4})$$

where

$$\alpha_C = t_C / (2R_C) \quad (\text{B.5})$$

$$\frac{t_C}{2R_C} = \frac{\pi}{2N} + \text{inv} \phi - \text{inv} \phi_C \quad (\text{B.6})$$

$$\phi_C = \cos^{-1}(R_B / R_C) \quad (\text{B.7})$$

ϕ = gear pressure angle

N = number of teeth on gear

R_B = base circle radius

Finally, derive the rotation angle, θ , and contact point radius, R_C , as a function of normalized distance along the line of action.

1. The independent variable is d_n . It is zero at the first point of contact, A, and is one at the end of contact, B. Thus,

$$0 \leq d_n \leq 1.$$

2. The absolute distance along the line of action is d . It is related to d_n by

$$d = d_n Z - u_1 \quad (\text{B.8})$$

thus,

$$-u_1 \leq d \leq u_2$$

where

$$z = u_1 + u_2 \quad (\text{B.9})$$

and is the length of action.

3. The line from the center of the gear to the point P on the tooth profile is the reference line for measuring rotation angles. The rotation angle, θ , is zero when the pair of teeth first contact. Thus, $0 \leq \theta \leq \alpha_1 + \beta_1$
4. Let α be the angle from the line of centers to the gear tooth reference line, then

$$\alpha = \alpha_1 - \theta \quad (\text{B.10})$$

and

$$\alpha = -d/R_B \quad (\text{B.11})$$

then, substituting (B.11) into (B.10) and solving for θ , gives

$$\theta = \alpha_1 + d/R_B \quad (\text{B.12})$$

5. Let the pressure angle of the contact point be ϕ_C , then

$$\phi_C = \tan^{-1}(\tan\phi - \alpha) \quad (\text{B.13})$$

$$R_C = R_B / \cos\phi_C \quad (\text{B.14})$$

APPENDIX C

PERTURBATION SOLUTION TO IMPACT EQUATION

With reference to equations (3.15), let

$$X = R_{b1}\theta_1/b - R_{b2}\theta_2/b - 1 \quad (C.1)$$

then

$$\dot{X} = R_{b1}\dot{\theta}_1/b - R_{b2}\dot{\theta}_2/b \quad (C.2)$$

and

$$\ddot{X} = R_{b1}\ddot{\theta}_1/b - R_{b2}\ddot{\theta}_2/b \quad (C.3)$$

Substituting equations (3.15) into (C.3),

$$\ddot{X} = \frac{R_{b1}T_1(t)}{J_1b} - \frac{R_{b2}T_2(t)}{J_2b} - \frac{1}{b}\left(\frac{R_{b1}^2}{J_1} + \frac{R_{b2}^2}{J_2}\right)[F(t) + G(t)] \quad (C.4)$$

For the conditions

$$F(t) = kxb$$

$$G(t) = Dx\dot{x}b^2$$

where k and D are constant, and

$$T_1(t) = T_2(t) = 0$$

we have

$$\ddot{X} + Db\left(\frac{R_{b1}^2}{J_1} + \frac{R_{b2}^2}{J_2}\right)X\dot{X} + k\left(\frac{R_{b1}^2}{J_1} + \frac{R_{b2}^2}{J_2}\right)X = 0 \quad (C.5)$$

Now, let

$$\omega_0^2 = k\left(\frac{R_{b1}^2}{J_1} + \frac{R_{b2}^2}{J_2}\right) \quad (C.6)$$

and

$$\tau = \omega_0 t \quad (C.7)$$

Then we can rewrite equation (C.5) as

$$\ddot{X} + Db\omega_0^2 \dot{X}X/k + \omega_0^2 X = 0 \quad (\text{C.8})$$

or, changing independent variables from t to τ ,

$$\omega_0^2 X'' + Db\omega_0^3 X'X/k + \omega_0^2 X = 0 \quad (\text{C.9})$$

which, in turn, can be rewritten as

$$X'' + X = -\frac{D\omega_0}{k} X'X \quad (\text{C.10})$$

If we let $-D\omega_0/k = \epsilon$, we have

$$X'' + X = \epsilon X'X \quad (\text{C.11})$$

Using the Lindstedt-Poincare' method, we seek a periodic solution of equation (C.11). Let

$$T = \omega\tau \quad (\text{C.12})$$

then we have

$$\omega^2 X'' + \epsilon\omega X'X + X = 0 \quad (\text{C.13})$$

where

$$X(T) = X_0(T) + \epsilon X_1(T) + \epsilon^2 X_2(T) + \dots \quad (\text{C.14})$$

and

$$\omega = \omega_0 + \epsilon\omega_1 + \epsilon^2\omega_2 + \dots \quad (\text{C.15})$$

For initial conditions, take

$$X_0(0) = 0, X_0'(0) = V$$

$$X_i(T + 2\pi) = X_i(T)$$

$$X_i(0) = 0, X_i'(0) = 0; i = 1, 2, 3, \dots$$

Then

$$X' = X_0' + \epsilon X_1' + \epsilon^2 X_2' + \dots$$

$$X'' = X_0'' + \epsilon X_1'' + \epsilon^2 X_2'' + \dots$$

and

$$X'X = X_0X_0' + \epsilon(X_0X_1' + X_1X_0') + \epsilon^2(X_0X_2' + X_1X_1' + X_2X_0') + \dots$$

$$\omega^2 = \omega_0^2 + 2\varepsilon\omega_0\omega_1 + \varepsilon^2(\omega_1^2 + 2\omega_0\omega_2) + \dots$$

Substituting these into equation (C.13) gives

$$\begin{aligned} & \omega^2 X_0'' + \varepsilon\omega^2 X_1'' + \varepsilon^2\omega^2 X_2'' + \\ & + \varepsilon\omega X_0 X_0' + \varepsilon^2\omega(X_0 X_1' + X_1 X_0') + \\ & X_0 + \varepsilon X_1 + \varepsilon^2 X_2 + \dots = 0 \end{aligned} \quad (\text{C.16})$$

Substituting for the ω terms

$$\begin{aligned} & \omega_0^2 X_0'' + \varepsilon 2\omega_0\omega_1 X_0'' + \varepsilon^2(\omega_1^2 + 2\omega_0\omega_2) X_0'' + \\ & + \varepsilon\omega_0^2 X_1'' + \varepsilon^2 2\omega_0\omega_1 X_1'' + \\ & + \varepsilon^2\omega_0^2 X_2'' + \\ & + \varepsilon\omega_0 X_0 X_0' + \varepsilon^2\omega_1 X_0 X_0' + \\ & + \varepsilon^2\omega_0(X_0 X_1' + X_1 X_0') + \\ & X_0 + \varepsilon X_1 + \varepsilon^2 X_2 + \dots = 0 \end{aligned} \quad (\text{C.17})$$

Setting the sum of the terms with like powers of ε equal to zero yields,

$$\varepsilon^0: \omega_0^2 X_0'' + X_0 = 0 \quad (\text{C.18})$$

$$\varepsilon^1: \omega_0^2 X_1'' + X_1 = -2\omega_0\omega_1 X_0'' - \omega_0 X_0 X_0' \quad (\text{C.19})$$

$$\begin{aligned} \varepsilon^2: \omega_0^2 X_2'' + X_2 = & -(\omega_1^2 + 2\omega_0\omega_2) X_0'' - 2\omega_0\omega_1 X_1'' \\ & -\omega_1 X_0 X_0' - \omega_0(X_0 X_1' + X_1 X_0') \end{aligned} \quad (\text{C.20})$$

We will find solutions, in turn, for equations (C.18), (C.19) and (C.20). Starting with (C.18)

Let $X_0 = V \sin T$, $X_0' = V \cos T$, if $\omega_0^2 = 1$

then $X_0'' = -V \sin T$

Using the results from the solution of (C.18), we proceed to (C.19),

where we have

$$\begin{aligned} X_1'' + X_1 &= 2\omega_1 V \sin T - V^2 \sin T \cos T \\ &= 2\omega_1 V \sin T - 0.5V^2 \sin 2T \end{aligned} \quad (C.21)$$

To remove the secular terms from (C.21), let $\omega_1 = 0$, then

$$X_1'' + X_1 = -0.5V^2 \sin 2T \quad (C.22)$$

which has the solution

$$X_1 = -(V^2/3) \sin T + (V^2/6) \sin 2T \quad (C.23)$$

Differentiating twice gives

$$X_1' = -(V^2/3) \cos T + (V^2/3) \cos 2T \quad (C.24)$$

$$X_1'' = (V^2/3) \sin T - (2V^2/3) \sin 2T \quad (C.25)$$

Substituting the above into (C.20) we have

$$X_2'' + X_2 = 2\omega_2 V \sin T - (V^3/6) [-0.5 \sin T - 2 \sin 2T + 1.5 \sin 3T] \quad (C.26)$$

To remove the secular terms, let

$$2\omega_2 V + V^3/12 = 0$$

$$\text{solving for } \omega_2, \omega_2 = -V^2/24 \quad (C.27)$$

Now, equation (C.26) becomes

$$X_2'' + X_2 = (V^3/12)(4 \sin 2T - 3 \sin 3T) \quad (C.28)$$

The solution for this equation is

$$X_2 = (V^2/288)(37 \sin T - 32 \sin 2T + 9 \sin 3T) \quad (C.29)$$

Substituting into equation (C.14), we have the total solution,

$$\begin{aligned} X(T) &= V \sin T + \epsilon(V^2/6)(-2 \sin T + \sin 2T) \\ &\quad + \epsilon^2(V^2/288)(37 \sin T - 32 \sin 2T + 9 \sin 3T) \\ &\quad + \dots \end{aligned} \quad (C.30)$$

where $T = \omega\tau$ and $\tau = \omega_0 t$

and $\omega = 1 - (V^2/24)$

but,
$$V = \frac{\dot{\delta}(0)}{b\omega\sqrt{k\left(\frac{R_{b1}^2}{J_1} + \frac{R_{b2}^2}{J_2}\right)}} = \frac{\dot{\delta}(0)}{b\omega\omega_0}$$

$$= c_1/\omega$$

Thus,

$$\omega = 1 - c_1^2/(24\omega^2) = 1 - c_2/\omega^2$$

or

$$\omega^3 - \omega^2 + c_2 = 0 \tag{C.31}$$

This equation can have one of three possible sets of roots, 1) 2 positive, real; 1 negative, real, 2) 1 positive; 2 imaginary, or 3) 1 negative; 2 imaginary. The equation is of the form

$$x^3 + bx^2 + cx + d = 0$$

where $b = -1$, $c = 0$, and $d = c_2$.

Let $x = y + 1/3$, then we have

$$y^3 + py + q = 0$$

where $p = -1/3$, and $q = c_2 - 2/27$.

Now let $y = z + 1/(9z)$, then we have

$$z^6 + qz^3 - p^3/27 = 0$$

Let

$$R = -(1/27)^2 + (c_2 - 2/27)^2/4$$

then

$$z^3 = -q/2 + \sqrt{R}$$

The roots of equation (C.31) are

$$\omega_1 = z_1 - 1/(9z_1) + 1/3$$

$$\omega_2 = z_2 - 1/(9z_2) + 1/3$$

$$\omega_3 = z_3 - 1/(9z_3) + 1/3$$

Now, using the numeric values of Appendix E, we can evaluate C_1 , C_2 and the other parameters to find the ω_i and the solution $X(T)$.

First, we have

$$C_2 = C_1^2/24 \quad (\text{C.32})$$

and

$$C_1 = \frac{\dot{\delta}(0)}{b\sqrt{k\left(\frac{R_{b1}^2}{J_1} + \frac{R_{b2}^2}{J_2}\right)}} \quad (\text{C.33})$$

The numerical values are

$$\dot{\delta}(0) = 16.445 \text{ in/s}$$

$$b = 0.001 \text{ in}$$

$$k = 18.03 \times 10^6 \text{ lb/in}$$

$$\left(\frac{R_{b1}^2}{J_1} + \frac{R_{b2}^2}{J_2}\right) = 359.082 \text{ in/lb/s}^2$$

Substituting into (C.32) and (C.33), we have $C_1 = 0.2044$ and $C_2 = 0.0017405$.

The value for C_2 is quite small compared with the $2/27$ term in the definition of q , above. However, solving for q , we have

$$q = 0.0017405 - 0.07407 = -0.072334$$

$$R = -(1/27)^2 + (-0.072334)/4$$

$$= -0.0000637$$

and $\sqrt{R} = \pm 0.0079816i$

$$Z^3 = 0.036167 + 0.0079816i$$

$$= 0.0079816(4.5313 + i)$$

$$= 0.0370373(\cos 12.445^\circ + i \sin 12.445^\circ)$$

The roots of Z are

$$Z_1 = 0.33246 + 0.02411i$$

$$Z_2 = -0.18711 + 0.27586i$$

$$Z_3 = -0.14535 - 0.29997i$$

Substituting into the equations for ω_i gives

$$\omega_1 = (0.33246)^2 + 0.33333 = 0.99825$$

$$\omega_2 = -(0.18711)^2 + 0.33333 = -0.04089$$

$$\omega_3 = -(0.14535)^2 + 0.33333 = 0.04263$$

Taking the positive values, we have

$$V = C_1/\omega = \begin{cases} 0.2044/0.99825 = 0.2048 \\ 0.2044/0.04263 = 4.7947 \end{cases}$$

We choose the value of ω closest to 1 since, if $C_2 = 0$, that would be the solution. Since C_2 is very small, we expect a solution for ω near unity. Then $\omega = 0.99825$ and $V = 0.2048$. Substituting into equation (C.30) we have

$$X(t) = 0.2048 \sin 80322t \\ + 0.004009(-2 \sin 80322t + \sin 160644t)$$

but $\delta(t) = bx(t)$, so the final solution to equation (3.28) is

$$\delta(t) = 0.0001968 \sin 80322t + 4.0009(10)^{-6} \sin 160644t$$

This equation is plotted in Figure 3.11.

APPENDIX D

DELTA SOLUTION

The Delta Method (Thomson, 1981) is a graphical method for solving the equation

$$x + f(\dot{x}, x, t) = 0 \quad (D.1)$$

For the case of impacting gear teeth, the equation to be solved is

$$x + c\epsilon D\dot{x}\dot{x} + c\epsilon Kx = 0 \quad (D.2)$$

If we let

$$c\epsilon K = \Omega^2 \quad (D.3)$$

$$\tau = \Omega t \quad (D.4)$$

and

$$y = dx/d\tau = x/\Omega \quad (D.5)$$

$$\delta = c\epsilon D\dot{x}\dot{x}/\Omega^2 \quad (D.6)$$

then substitution of equations (D.3) and (D.5) into (D.6) yields

$$\delta = D\Omega xy/K \quad (D.7)$$

Now, substituting equations (D.3), (D.4), (D.5) and (D.7) into (D.2), we have

$$\Omega^2 (d^2x/d\tau^2) + \Omega^2 \delta + \Omega^2 x = 0$$

which can be further simplified to

$$dy/dx = -(x+\delta)/y \quad (D.8)$$

Although δ is a function of y , x , and τ , for small changes in the variables it can be assumed constant. In this case, equation (D.8) can be integrated to give

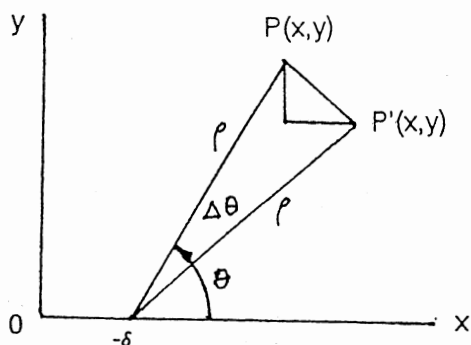


Fig. D.1. Graphical Interpretation of Equation (D.9)

$$(x+\delta)^2 + y^2 = r^2 \quad (\text{D.9})$$

Equation (D.9) describes a circle of radius r (the constant of integration) with center at $x = -\delta$ and $y = 0$. Thus, for small increments of τ , the solution corresponds to a small arc of a circle as shown in Figure D.1.

Although originally described as a graphical procedure, the successive determination of x and y for changes in τ can be calculated numerically. It can be shown (Thomson, 1981) that $d\theta = dx/y = d\tau$, where $d\theta$ is the angular rotation of the line CP in figure D.1. Furthermore, for small angles, we can represent the arc PP' by a straight line of length $rd\theta$. The $rd\theta$ is the hypotenuse of the right triangle whose vertical and horizontal sides are dy and dx , respectively. As seen in figure D.1, the angle between dy and $rd\theta$ is $\theta - d\theta/2$, where θ is the angle that the line CP makes with the x -axis. Thus, we have the relationships

$$\cos(\theta - d\theta/2) = dy / (rd\theta) \quad (\text{D.10})$$

$$\sin(\theta - d\theta/2) = dx / (rd\theta) \quad (\text{D.11})$$

By expanding the left-hand side of equations (D.10) and (D.11), and

solving for dy and dx , we have

$$dy = rd\theta[\cos\theta + d\theta(\sin\theta)/2] \quad (D.12)$$

$$dx = rd\theta[\sin\theta - d\theta(\cos\theta)/2] \quad (D.13)$$

But, $\cos\theta = (x+\delta)/r$ and $\sin\theta = y/r$, so

$$dy = -d\theta(x + \delta + d\theta/2) \quad (D.14)$$

and

$$dx = d\theta[y - d\theta(x+\delta)/2] \quad (D.15)$$

Using the dimensions given in Appendix E, we have

$$x(0) = 0$$

$$\dot{x}(0) = 16.445 \text{ in/s}$$

$$D = 1.285\text{E}+05 \text{ lb s}^2/\text{in}^2$$

$$K = 18.03\text{E}+06 \text{ lb/in}$$

$$\epsilon = 359.082 \text{ in/lb s}^2$$

$$\Omega = 80463 \text{ rad/s}$$

$$y(0) = 2.044\text{E}-04 \text{ in}$$

A small Pascal program was written to solve for x and y as a function of time, t . The results are plotted in figure 3.11.

APPENDIX E

GEAR DIMENSIONS FOR PERTURBATION AND DELTA EXAMPLES

E.1 Moment of Inertia

Consider the gear to be equivalent to a cylinder with radius, r_p , and length, F . Then,

$$V = \pi r_p^2 F \text{ in}^3$$

$$W = \rho V = \pi \rho r_p^2 F \text{ lb}$$

$$m = W/g = \pi \rho r_p^2 F/g \text{ lb-sec}^2/\text{in}$$

$$J = m r_p^2/2 \text{ lb sec}^2\text{in}$$

$$J = \frac{\pi \rho r_p^4 F}{2g}$$

$$= \frac{\pi(0.282)}{2(386)} r_p^4 F$$

$$= 1.148(10)^{-3} r_p^4 F \text{ lb sec}^2\text{in for steel}$$

E.2 Damping Coefficient

From equation (3.12)

$$D = \frac{6(1-e)}{[(2e-1)^2+3]} \cdot \frac{k}{V_i}$$

The relationship used for the perturbation solution for the coefficient

of restitution (see Goldsmith, 1960, Figure 166, p 258) is

$$e = 1 - 0.019 V_i^{0.48}$$

and the initial velocity is

$$V_i = |R_{b1}\dot{\theta}_1 - R_{b2}\dot{\theta}_2|$$

when

$$|R_{b1}\theta_1 - R_{b2}\theta_2| = b$$

E.3 Gear Dimensions

The following gear dimensions were used in the perturbation and delta example solutions:

$$N_1 = N_2 = 28, \quad P = 8, \quad \phi = 20^\circ, \quad F = 0.700 \text{ in}$$

from these

$$r_p = N_1/2P = 28/16 = 1.750 \text{ in}$$

$$a = 1/P = 0.125 \text{ in.}$$

$$R_o = r_p + a = 1.8750 \text{ in}$$

$$R_{b1} = R_{b2} = r_p \cos 20^\circ = 1.6445 \text{ in}$$

$$J_1 = 1.148(10)^{-3} (1.750)^4 (0.700)$$

$$= 7.537 \times 10^{-3} \text{ lb sec}^2 \text{ in}$$

$$k = 2.58(10)^7 (0.700) = 18.03 \times 10^6 \text{ lb/in}$$

Mass is added to the output shaft to make its undamped natural frequency 350 hz.

$$350 = \frac{1}{2\pi} \sqrt{\frac{k R_{b2}^2}{J_2}}$$

$$J_2 = \frac{KR_b^2}{(700\pi)^2} = \frac{(18.03 \times 10^6)(1,6445)^2}{(700\pi)^2}$$

$$= 10.082 \text{ lb sec}^2\text{in}$$

The length of action is

$$z = 2\sqrt{R_o^2 - R_b^2} - 2r_p \sin\phi$$

$$z = 2\sqrt{(1.875)^2 - (1.6445)^2} - 3.500 \sin 20^\circ$$

$$= 0.6043 \text{ in}$$

$$p_b = \pi \cos 20^\circ / 8 = 0.36902 \text{ in}$$

$$m_p = z / p_b = 1.6376$$

$$\alpha = \pi m_p / N$$

$$= \pi(1.6376) / 28 = 0.18374 \text{ rad}$$

APPENDIX F

PROGRAM DESCRIPTION FOR NUMERICAL SOLUTION
TO SPUR GEAR MODEL

```

PROGRAM GearSim;

CONST
  pi = 3.141592654;

TYPE
  StateVar = ARRAY[1..4] OF REAL;

VAR
  XK,XK1,X
  TimeStep,RunTime,Time,Vi,Baclash,Delta, : StateVar;
  T1,T2,TS,J1,J2,Ft,Gt,D,P,N1,N2,Face,
  r1,r2,Alpha,mc,k,rb1,rb2,phi           : REAL;
  I,J,C                                   : INTEGER;
  Contact,Impact,WriteFlag               : BOOLEAN;
  Out,Inp                                  : TEXT;
  FileName                                 : STRING[14];

{
*****
***** FUNCTIONS & PROCEDURES *****
*****
}

FUNCTION ArcCos(x:REAL):REAL;
{Returns the angle which is the inverse cosine of x.}

BEGIN
  ArcCos:=-ArcTan(x/SQRT(1.0-X*X))+pi/2.0;
END; {ArcCos}

FUNCTION Inertia(r,f:REAL):REAL;
{Returns the moment of inertia of a steel gear}

BEGIN
  Inertia:=1.148E-03*r*r*r*r*f;
END; {Inertia}

```

```
FUNCTION PitchRad(P,N:REAL):REAL;
{Returns the pitch radius of a gear}
```

```
BEGIN
  PitchRad:=N/(2.0*P);
END; {PitchRad}
```

```
FUNCTION Inv(phi:REAL):REAL;
{Returns the involute of an angle}
```

```
BEGIN
  Inv:=SIN(phi)/COS(phi)-phi
END; {Inv}
```

```
FUNCTION ContAng(phi,r1,r2,P:REAL):REAL;
{Returns the contact angle for a pair of teeth}
```

```
VAR
  a,b,d,ra,beta,ta,phia : REAL;
```

```
BEGIN
  a:=1.0/P
  b:=r2*COS(pi/2.0+phi);
  d:=b+SQRT(b*b+a*(2.0*r2+a));
  ra:=SQRT(d*d+r1*r1-2.0*d*r1*COS(pi/2.0-phi));
  beta:=ArcCos((ra*ra+r1*r1-d*d)/(2.0*ra*r1));
  phia:=ArcCos(r1*COS(phi)/ra);
  ta:=pi/(4.0*P*r1)+Inv(phi)-Inv(phia);
  ContAng:=beta+ta;
END; {ContAng}
```

```
FUNCTION Contratio(phi,r1,r2,P:REAL):REAL;
{Returns the contact ratio for a pair of gears}
```

```
VAR
  a,ro1,ro2,rb1,rb2,lab : REAL;
```

```
BEGIN
  a:=1.0/P;
  ro1:=r1+a;
  ro2:=r2+a;
  rb1:=r1*COS(phi);
  rb2:=r2*COS(phi);
  lab:=SQRT(ro1*ro1-rb1*rb1)+SQRT(ro2*ro2-rb2*rb2)-(r1+r2)*SIN(phi);
  Contratio:=lab*P/(pi*COS(phi));
END; {Contratio}
```



```

FUNCTION Mode(x:StateVar):INTEGER;
{Returns the number of teeth in contact and the contacting face.
 Positive values indicate contact on the forward face,negative
 values on the rear face.}

```

```

VAR

```

```

  N,I           : INTEGER;
  Delta,LoLimit,HiLimit : REAL;

```

```

BEGIN

```

```

  N:=TRUNC(N1*(X[1]+alpha)/(2.0*PI))+1;

```

```

  LoLimit:=2.0*pi*(N-2.0+mc)/N1-alpha;

```

```

  HiLimit:=2.0*pi*N/N1-alpha;

```

```

  Delta:=rb1*X[1]-rb2*X[3];

```

```

  IF Delta >= Baclash THEN

```

```

    BEGIN

```

```

      IF (X[1] > LoLimit) AND (X[1] < HiLimit) THEN

```

```

        Mode:=1

```

```

      ELSE

```

```

        MODE:=2;

```

```

    END;

```

```

  IF (Delta > -Baclash) AND (Delta < Baclash) THEN Mode:=0;

```

```

  IF Delta <= -Baclash THEN

```

```

    IF (X[1] > LoLimit) AND (X[1] < HiLimit) THEN

```

```

      Mode:=-2;

```

```

END; {Mode}

```

```

FUNCTION Damping:REAL;

```

```

{Evaluates the damping coefficient for the current impact event.}

```

```

VAR

```

```

  e : REAL;

```

```

BEGIN

```

```

  IF Vi > 0.0 THEN e:=1.0-0.019*EXP(0.48*LN(Vi)) ELSE e:=1.0;

```

```

  IF e < 1.0 THEN

```

```

    Damping:=6.0*k*(1.0-e)/((SQR(2.0*e-1.0)+3.0)*Vi)

```

```

  ELSE

```

```

    Damping:=0.0;

```

```

END; {Damping}

```

```

FUNCTION SGN(X:REAL):REAL;

```

```

{Returns +1.0 if X is positive or zero, else -1}

```

```

BEGIN

```

```

  IF X >=0.0 THEN

```

```

    SGN:=1.0

```

```

  ELSE

```

```

    SGN:=-1.0

```

```

END; {SGN}

```

```
FUNCTION F(I,C:INTEGER;X:StateVar;D:REAL):REAL;
{Evaluates the state equations that are being integrated by RK4}
```

```
VAR
```

```
  DelTab,RelDel,RelVel : REAL;
```

```
BEGIN
```

```
{ WRITELN('F: X[1]=' ,X[1]:8:6, ' X[3]=' ,X[3]:8:4);}
```

```
  RelDel:=rb1*X[1]-rb2*X[3];
```

```
  RelVel:=rb1*X[2]-rb2*X[4];
```

```
  DelTab:=ABS(RelDel)-Backlash;
```

```
  Ft:=k*DelTab;
```

```
{  Gt:=D*RelVel*DelTab*SGN(RelDel);}
```

```
  IF DelTab < 0.0 THEN
```

```
    BEGIN
```

```
      Ft:=0.0;
```

```
      Gt:=0.0;
```

```
    END;
```

```
  CASE I OF
```

```
    1 : F:=X[2];
```

```
    2 : F:=(T1-C*rb1*(Ft+Gt))/J1;
```

```
    3 : F:=X[4];
```

```
    4 : F:=(T2+C*rb2*(Ft+Gt))/J2;
```

```
  END;
```

```
END; {F}
```

```
PROCEDURE RK4;
```

```
{Fourth-order Runge Kutta integration routine.}
```

```
VAR
```

```
  Dummy : REAL;
```

```
  RC : ARRAY[1..4,1..4] OF REAL;
```

```
  I : INTEGER;
```

```
BEGIN
```

```
  FOR I:=1 TO 4 DO RC[I,1]:=F(I,C,XK,D)*TS;
```

```
  FOR I:=1 TO 4 DO X[I]:=XK[I]+0.5*RC[I,1];
```

```
  FOR I:=1 TO 4 DO RC[I,2]:=F(I,C,X,D)*TS;
```

```
  FOR I:=1 TO 4 DO X[I]:=XK[I]+0.5*RC[I,2];
```

```
  FOR I:=1 TO 4 DO RC[I,3]:=F(I,C,X,D)*TS;
```

```
  FOR I:=1 TO 4 DO X[I]:=XK[I]+RC[I,3];
```

```
  FOR I:=1 TO 4 DO RC[I,4]:=F(I,C,X,D)*TS;
```

```
  FOR I:=1 TO 4 DO XK1[I]:=XK[I]+
    (RC[I,1]+2.0*RC[I,2]+2.0*RC[I,3]+RC[I,4])/6.0;
```

```
  Dummy:=F(1,C,XK1,D);
```

```
END; {RK4}
```

```
PROCEDURE GetData;
{Sets up I/O files and reads the input data}
```

```
BEGIN
  ClrScr;
  WRITELN('Enter output file name');
  READLN(FileName);
  ASSIGN(Out,FileName);
  REWRITE(Out);
  ASSIGN(Inp,'gearsim.inp');
  RESET(Inp);
  ClrScr;
  FOR I:=1 TO 4 DO READLN(Inp,XK[I]);
  READLN(Inp,Baclash);
  READLN(Inp,TimeStep);
  READLN(Inp,RunTime);
  READLN(Inp,T1);
  READLN(Inp,T2);
  READLN(Inp,P);
  READLN(Inp,N1);
  READLN(Inp,N2);
  READLN(Inp,face);
  READLN(Inp,phi);
  CLOSE(Inp);
END; {GetData}
```

```
PROCEDURE Constants;
{Calculates gear constants from input data}
```

```
BEGIN
  phi:=pi*phi/180.0;
  r1:=PitchRad(P,N1);
  r2:=PitchRad(P,N2);
  rb1:=r1*COS(phi);
  rb2:=r2*COS(phi);
  alpha:=Contratio(phi,r1,r2,P);
  { alpha:=0.18374;}
  mc:=Contratio(phi,r1,r2,P);
  J1:=Inertia(r1,face);
  J2:=Inertia(r2,face);
  { J2:=10.082;}
  k:=25.76E06*face;
  WRITELN('phi=',phi:5:4,' r1=',r1:8:6,' r2=',r2:8:6,' rb1=',rb1:8:6);
  WRITELN('rb2=',rb2:8:6,' alpha=',alpha:5:4,' mc=',mc:8:6);
  WRITELN('J1=',J1:8:7,' J2=',J2:8:6,' k=',k:8:0);
END; {Constants}
```

```
PROCEDURE Initialize;
```

```
BEGIN
```

```
  Contact:=FALSE;
  Impact:=FALSE;
  WriteFlag:=TRUE
  Delta:=rb1*XK[1]-rb2*XK[3];
  Vi:=ABS(rb1*XK[2]-rb2*XK[4]);
  D:=Damping;
  Ft:=0.0;
  Gt:=0.0;
  Time:=0.0;
  TS:=TimeStep;
END; {Initialize}
```

```
{*****
*****          MAIN PROGRAM          *****
*****}
```

```
BEGIN {GearSim}
```

```
  GetData;
  Constants;
  Initialize;
  REPEAT
    IF WriteFlag THEN
      BEGIN
        WRITE(Out,Time:8:6,' ',SGN(Delta)*(ABS(Delta)-Baclash):8:6,' ',
              XK[2]:8:5);
        WRITE(Out,' ',XK[3]:8:6,' ',XK[4]:8:5);
        WRITELN(Out,' ',Ft:8:5,' ',Gt:8:5);
        WriteFlag:=FALSE;
      END;
    C:=Mode(XK);
    RK4;
    Delta:=rb1*XK[1]-rb2*XK[3];
    IF ((ABS(Delta) >= Baclash) AND (NOT Contact) AND (NOT Impact)) THEN
      BEGIN
        Impact:=TRUE;
        TS:=TimeStep/10.0;
      END
    ELSE
      BEGIN
        WriteFlag:=TRUE
        Time:=Time+TS;
        FOR J:=1 TO 4 DO XK[J]:=XK1[J];
        WRITE('t=',Time:8:6,' Delta=',Delta:8:6);
        WRITE(' Impact is ',Impact,' Contact is ',Contact);
        WRITELN(' C=',C:2,' VI=',VI:8:6);
        IF Contact AND (ABS(Delta) < Baclash) THEN
          BEGIN
            Impact:=FALSE;
```

```
    TS:=TimeStep;
    Contact:=FALSE;
  END;
  IF (ABS(Delta) >= Baclash) AND Impact AND NOT Contact THEN
  BEGIN
    Contact:=TRUE;
    Vi:=ABS(rb1*XK[2]-rb2*XK[4]);
    D:=Damping;
  END;
  END;
  UNTIL (Time > RunTime);
  CLOSE(Out);
  WRITELN('Simulation Complete');
END.
```

APPENDIX G

NODE LIBRARY

The available node types are defined below.

N01 - Passive Inertia

This node type is used for all nodes except motors, which, when used, must be located at position 1 only. Thus, for nodes 2 and up, only N01 may be used. N01 may also be used in position 1. The terms used in the state equations are defined in Figure G.1. The state equations are:

$$\dot{x}_{i1} = x_{i2} \quad (G.1)$$

$$\dot{x}_{i2} = (-d_i x_{i2} + T_i^L - T_i^R) / J_i \quad (G.2)$$

where x_{i1} , x_{i2} , T_i^L , T_i^R are the angular displacement, angular velocity, external torque on the left and right, respectively. The RN-constants (refer to 5.1.1.2.) are:

$$RN_{i1} = J_i, \text{ inertia, in } \text{lb s}^2/\text{rad}$$

$$RN_{i2} = d_i, \text{ external damping, in } \text{lb s}/\text{rad}$$

N02 - DC Motor

This node-type represents a constant field, variable armature, DC motor. It may only be used in position 1. The terms used in the state equations are defined in Figure G.2. The state equations are:

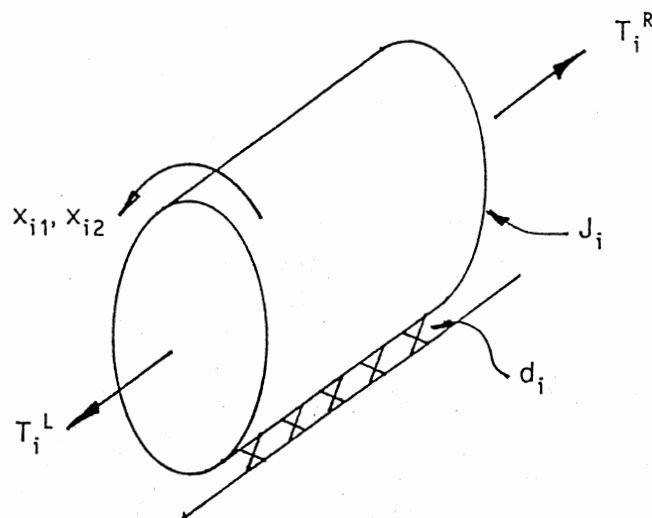


Fig. G.1. Passive Inertia

$$\dot{x}_{11} = x_{12} \quad (G.3)$$

$$\dot{x}_{12} = (-d x_{12} + \alpha x_{13} - T_1^R)/J \quad (G.4)$$

$$\dot{x}_{13} = (-R x_{13} - \alpha' x_{12} + e)/L \quad (G.5)$$

where x_{11} , x_{12} , x_{13} , e , and T_1^R are the angular displacement, angular velocity, armature current, armature voltage, and load torque, respectively. The RN-constants (refer to 5.1.1.2.) are:

$$RN_{11} = J, \text{ armature inertia, in } \text{lb s}^2/\text{rad}$$

$$RN_{12} = d, \text{ external damping, in } \text{lb s}/\text{rad}$$

$$RN_{13} = \alpha, \text{ motor parameter, in } \text{lb}/\text{amp}$$

$$RN_{14} = L, \text{ armature inductance, henry}$$

$$RN_{15} = R, \text{ armature resistance, ohm}$$

$$RN_{16} = \alpha', \text{ electrical equivalent of } \alpha, \text{ volt sec}$$

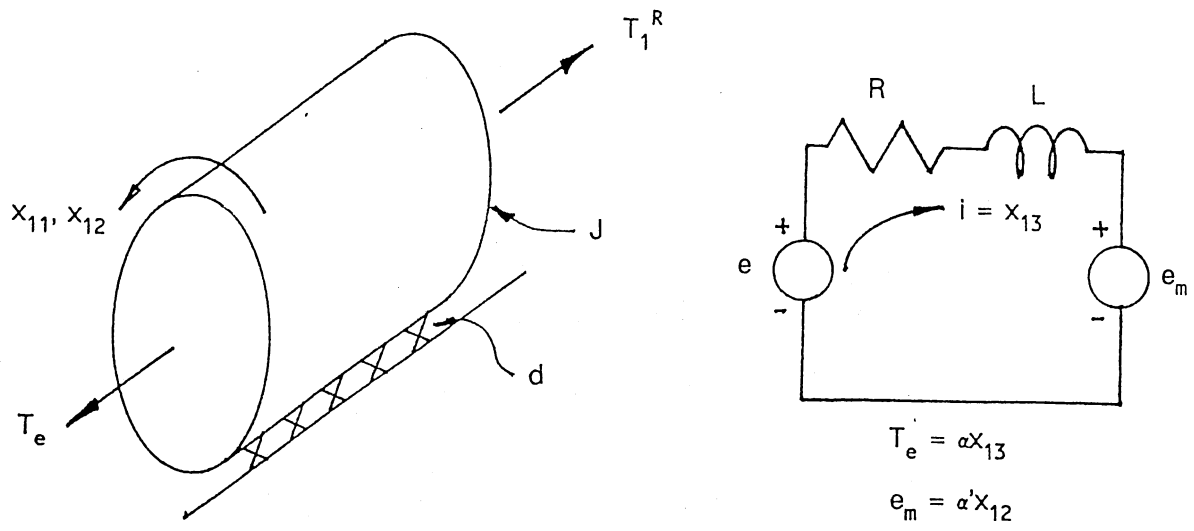


Fig. G.2. DC Motor

APPENDIX H

ELEMENT LIBRARY

The available element types are defined below.

EL1 - Shaft

This element is used to connect nodes directly with a linear, visco-elastic coupling. It provides for internal damping. The terms used in the torque equations are defined in Figure H.1. The torque equations are:

$$T_i^R = b_i(x_{i1} - x_{(i+1)1}) + d_i(x_{i2} - x_{(i+1)2}) \quad (H.1)$$

$$T_i^L = b_{i-1}(x_{(i-1)1} - x_i) + d_{i-1}(x_{(i-1)2} - x_{i2}) \quad (H.2)$$

Where j is the position number of the node for which the torque is being evaluated, and x_{11} and x_{12} are the angular displacement and angular velocity of the i th node, respectively. The RE-constants (refer to 5.1.1.2.) are:

$$RE_{11} = b_1, \text{ stiffness, lb in/rad}$$

$$RE_{12} = d_1, \text{ internal damping, lb in s/rad}$$

EL2 - Keyed Joint

This element is used to model a standard keyed joint. It includes nonlinear stiffness, clearance (backlash), and damping. The terms in the torque equation are defined in Figure H.2. The torque equations are

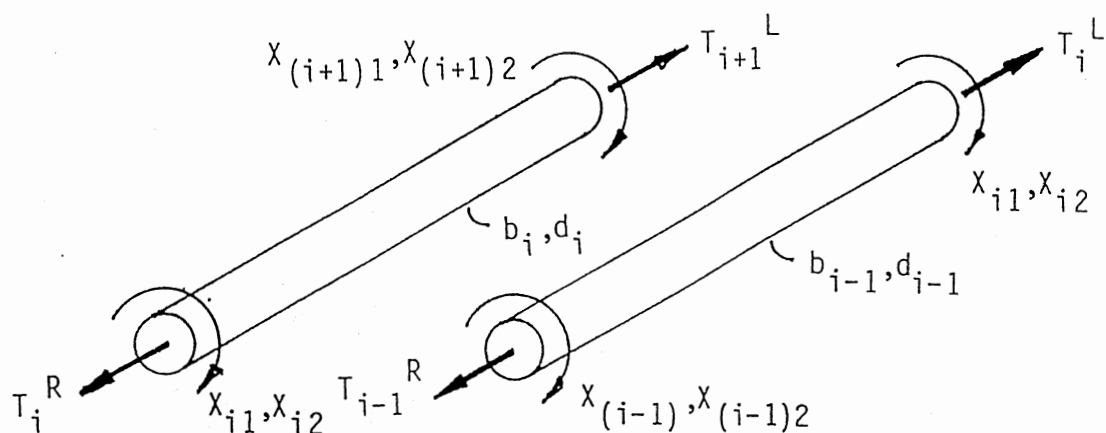


Figure H.1. Shaft Element

given separately for the right and left torque, and for the three possible conditions of contact, i.e., contact on the forward face, no contact, and contact on the rear face of the key. For the right torque, for

$$(i) \quad \delta_{ij} \geq 0$$

$$T_i^R = (k_i \delta_{ij} + D_i \delta_{ij} \dot{\delta}_{ij}) d_i / 2 \quad (H.3)$$

$$(ii) \quad -2b_i < \delta_{ij} < 0$$

$$T_i^R = 0 \quad (H.4)$$

$$(iii) \quad \delta_{ij} \leq -2b_i$$

$$T_i^R = [k_i (\delta_{ij} + 2b_i) + D_i (\delta_{ij} + 2b_i) \dot{\delta}_{ij}] d_i / 2 \quad (H.5)$$

where i is the position number of the node for which the torque is being evaluated, and

$$j = i + 1 \quad (H.6)$$

$$\delta_{ij} = (x_{i1} - x_{j1})d_i/2 - b_i \quad (\text{H.7})$$

$$\dot{\delta}_{ij} = (x_{i2} - x_{j2})d_i/2 \quad (\text{H.8})$$

For the left torque, for

$$(i) \quad \delta_{ij} \geq 0$$

$$T_i^L = (K_j \delta_{ij} + D_j \dot{\delta}_{ij})d_j/2 \quad (\text{H.9})$$

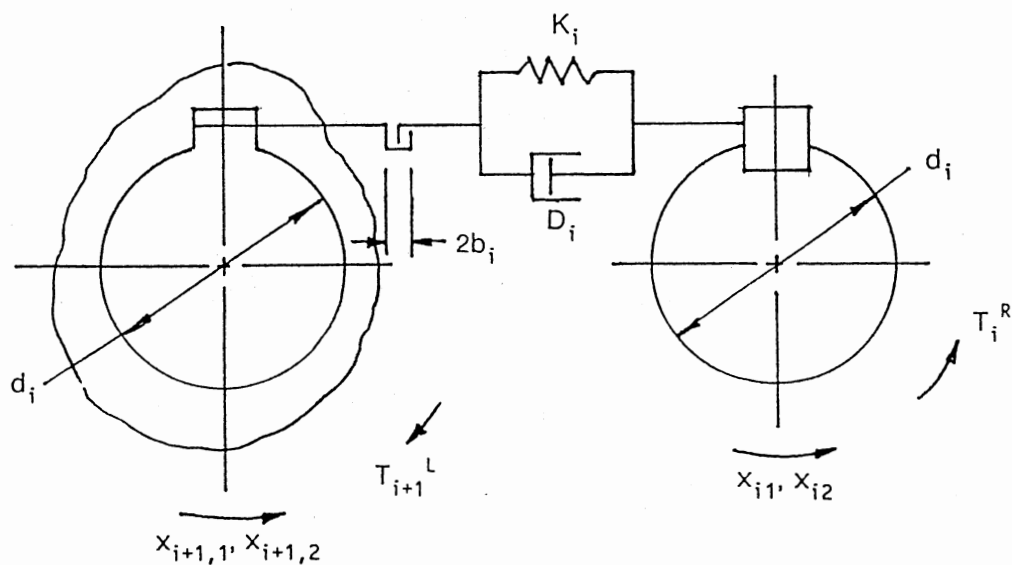
$$(ii) \quad -2b_j < \delta_{ij} < 0$$

$$T_i^L = 0 \quad (\text{H.10})$$

$$(iii) \quad \delta_{ij} \leq -2b_j$$

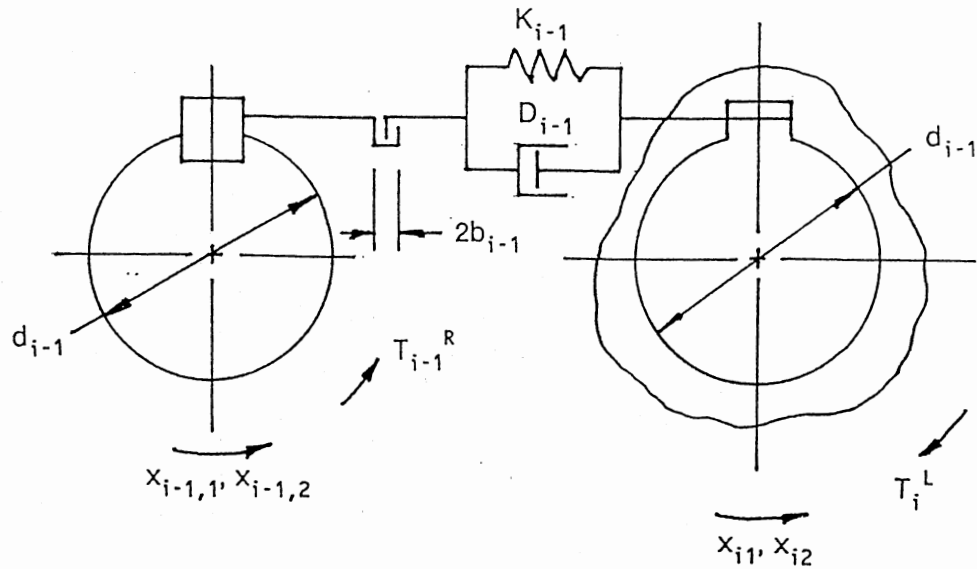
$$T_i^L = [K_j(\delta_{ij} + 2b_j) + D_j(\delta_{ij} + 2b_j)\dot{\delta}_{ij}]d_j/2 \quad (\text{H.11})$$

where i is the position number of the node for which the torque is being evaluated, and



(a) Right Torque

Figure H.2. Keyed Joint Element



(b) Left Torque

Figure H.2. Keyed Joint Element

$$j = i - 1 \quad (\text{H. 12})$$

$$\delta_{ij} = (x_{j1} - x_{i1})d_j/2 - b_j \quad (\text{H. 13})$$

$$\dot{\delta}_{ij} = (x_{j2} - x_{i2})d_j/2 \quad (\text{H. 14})$$

and x_{i1} and x_{i2} are the angular displacement and angular velocity, respectively. The RE-constants (refer to 5.1.1.2.) are:

$$RE_{11} = d_1, \text{ shaft diameter, in}$$

$$RE_{12} = b_1, \text{ half-clearance between hub and key, in}$$

See Chapter IV for a discussion of the nonlinear stiffness coefficient, k , and the damping coefficient, D .

EL3 - Ideal Gear Pair

This element is used to model a gear pair (spur or helical) for which there is no damping or backlash. Constant tooth stiffness is

included. The terms used in the torque equations are defined in Figure H.3. The torque equations are:

$$T_i^R = k_i (r_{i1} x_{i1} - r_{i2} x_{i2}) r_{i1} \quad (\text{H. 15})$$

$$T_i^L = k_{i-1} (r_{(i-1)1} x_{(i-1)1} - r_{(i-1)2} x_{i1}) r_{(i-1)2} \quad (\text{H. 16})$$

where i is the position number of the node for which the torque is being evaluated, and x_{i1} and x_{i2} are the angular displacement and angular velocity, respectively. The RE-constants (refer to 5.1.1.2.) are:

$$RE_{11} = k_1, \text{ tooth pair stiffness, lb/in}$$

$$RE_{12} = r_{11}, \text{ base circle radius (driver), in}$$

$$RE_{13} = r_{12}, \text{ base circle radius (driven), in}$$

EL4 - Spur Gear Pair With Backlash

This element is used to model a spur gear pair with backlash and impact damping. Mesh stiffness is a function of mesh angle and also depends on the number of teeth in contact. As in the case of EL3, this element is a torque amplifier. The terms used in the torque equations

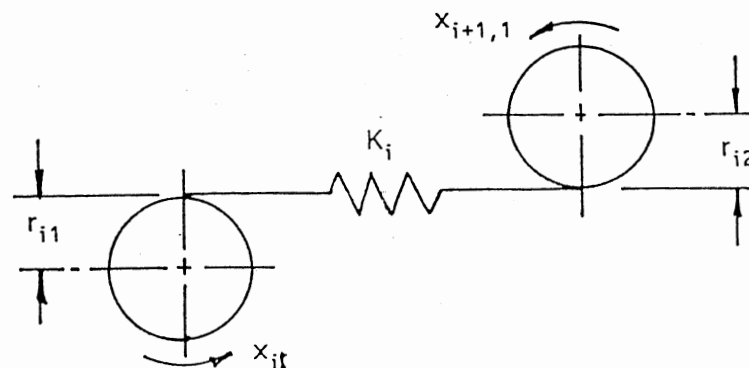


Figure H.3. Ideal Gear Pair Element

are defined in Figure H.4. The torque equations are given separately for the right and left torque, and for the three possible conditions of contact, i.e., contact on the forward face, no contact, and contact on the rear face of the tooth. For the right torque, for

$$(i) \quad \delta_{ij} \geq 0$$

$$T_i^R = C_i (k_i \delta_{ij} + D_i \delta_{ij} \dot{\delta}_{ij}) r_{i1} \quad (H.17)$$

$$(ii) \quad -2b_i < \delta_{ij} < 0$$

$$T_i^R = 0 \quad (H.18)$$

$$(iii) \quad \delta_{ij} \leq -2b_i$$

$$T_i^R = c_i (k_i \delta_{ij} + D_i \delta_{ij} \dot{\delta}_{ij}) r_{i1} \quad (H.19)$$

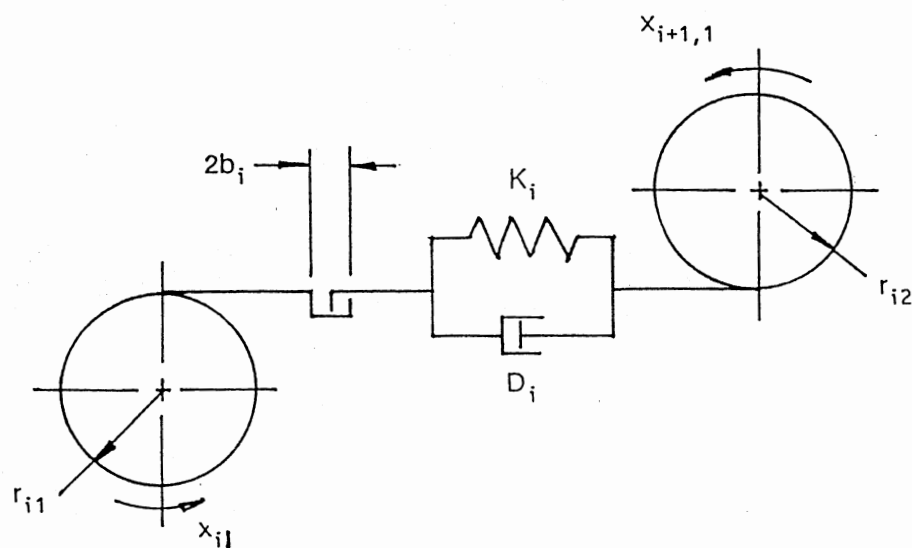


Figure H.4. Spur Gear Pair With Backlash Element

where i is the position number of the node for which the torque is being evaluated, and

$$j = i + 1 \quad (\text{H. 20})$$

$$\delta_{ij} = (r_{i1}x_{i1} - r_{i2}x_{j1}) - b_i \quad (\text{H. 21})$$

$$\dot{\delta}_{ij} = (r_{i1}\dot{x}_{i2} - r_{i2}\dot{x}_{j2}) \quad (\text{H. 22})$$

For the left torque, for

$$(i) \quad \delta_{ij} \geq 0$$

$$T_i^L = c_j(k_j\delta_{ij} + D_j\dot{\delta}_{ij})r_{j2} \quad (\text{H. 23})$$

$$(ii) \quad -2b_j < \delta_{ij} < 0$$

$$T_i^L = 0 \quad (\text{H. 24})$$

$$(iii) \quad \delta_{ij} \leq -2b_j$$

$$T_i^L = c_j(k_j\delta_{ij} + D_j\dot{\delta}_{ij})r_{j2} \quad (\text{H. 25})$$

where

$$j = i - 1 \quad (\text{H. 26})$$

$$\delta_{ij} = (r_{j2}x_{j1} - r_{j1}x_{i1}) - b_j \quad (\text{H. 27})$$

$$\dot{\delta}_{ij} = (r_{j2}\dot{x}_{j2} - r_{j1}\dot{x}_{i2}) \quad (\text{H. 28})$$

and x_{i1} and x_{i2} are the angular displacement and angular velocity, respectively. The parameter c_1 takes the values 0, ± 1 , or ± 2 , depending on the contact condition. See Chapter III for a discussion of the stiffness coefficient, k_1 , and the damping coefficient, D_1 . The RE-constants are:

$RE_{11} = N$, the number of teeth on the driver

$RE_{12} = r_{11}$, base circle radius (driver), in

$RE_{13} = r_{12}$, base circle radius (driven), in

$RE_{14} = m_p$, contact ratio

$RE_{15} = \alpha$, angle of approach, radians

$RE_{16} = b_1$, half-clearance between teeth, in

APPENDIX I

ADDING AN ELEMENT TYPE

When a new element type is to be added to TRAIN the data file TFILE01.DAT and the FORTRAN code for the functions LTRQ and RTRQ must be modified.

The data file TFILE01.DAT consists of a header, two node-type records and five element-type records. The header consists of the first four lines in the file. Line 2 contains the total number of nodes and elements currently defined (7) and line four contains the current number of elements defined (5). Both of these numbers must be incremented by one for each new element type added. The first line (field) in a node-type record contains the string NODE RECORD, and the first line in an element record contains the string ELEMENT RECORD. The number of lines (fields) in an element-type record is $n + 4$, where n is the number of RE-constants defined for the element. When adding a new element type to the end of TFILE01.DAT, use the same format as for the current elements, paying particular attention to the columns in which the data starts.

The functions LTRQ and RTRQ are evaluated for each integration step in the solution processor. There must be a torque equation defined in each of these subprograms for each element type that might be chosen by the user of TRAIN. In adding a new element to TRAIN, follow the format found in Appendix H and in the functions LTRQ and RTRQ. Then, add an additional case to the block IF statement and the appropriate FORTRAN

code to LTRQ and RTRQ. For example, the next element type number will be 6 and the following would be added at the end of block 0500:

```
ELSE IF(TYPE .EQ. 6) THEN  
  .  
  .  
  .  
ENDIF
```

The FORTRAN code for the torque equation would be placed between the ELSE IF line and the ENDIF line.

VITA

Thomas A. Cook

Candidate for the Degree of
Doctor of Philosophy

Thesis: SIMULATION OF DRIVE TRAINS WITH MULTIPLE CLEARANCES

Major Field: Mechanical Engineering

Biographical:

Personal Data: Born in Shanghai, China, May 13, 1933, the son of Jesse S. and Betty R. Cook. Married to B. Ruth Shook on May 9, 1955.

Education: Graduated from Washington-Lee High School in Arlington, Virginia, in January, 1951; received Bachelor of Science in Mechanical Engineering Degree from the Massachusetts Institute of Technology in June, 1959; received Master of Science in Mechanical Engineering from the University of Arkansas in May, 1981; completed requirements for the Doctor of Philosophy Degree at Oklahoma State University in July, 1989.

Professional Experience: Spacecraft Development Engineer, Jet Propulsion Laboratory, 1959-1961; Chief Engineer, TAD, Inc, 1961-1962; Senior Consulting Engineer, United Shoe Machinery Co., 1962-1966; Vice President, TAD, Inc., 1966-1967; President, TAD Products Corp., 1968-1970; President, COMPRINT, 1971-1978; Quality Control Manager, Citation Manufacturing Co., 1978-1979; Graduate Assitant, Mechanical Engineering Department, University of Arkansas, 1979-1980; Engineering Specialist, Daisy Manufacturing Co., 1980; Instructor, Mechanical Engineering Department, University of Arkansas, 1981-1983; Lecturer, School of Mechanical & Aerospace Engineering, Oklahoma State University, 1983-1988; Associate Professor, Mechanical & Aerospace Engineering Department, School of Engineering, Mercer University, September, 1989, to present.